

**Photochemical Activation of Tetraalkylammonium Cations
by Hexachloroplatinate(IV)**

Imelda Hotmarisi Silalahi

PhD

University of York

Chemistry

March 2017

Abstract

Unexpectedly, a Zeise's salt analogue, the dinuclear, butadiene-bridged complex, *trans*- $\eta^2:\eta^2$ -1,3-butadiene-bis(trichloroplatinate(II)) was isolated when $[\text{AuCl}_4]^-$ and $[\text{PtCl}_4]^{2-}$ were reacted together in the presence of the tetrabutylammonium cation. Early observations ruled out the involvement of the gold(III) species in generating the butadiene directly, but it was found to be acting as an oxidising agent facilitating conversion of $[\text{Pt}^{\text{II}}\text{Cl}_4]^{2-}$ to $[\text{Pt}^{\text{IV}}\text{Cl}_6]^{2-}$, which turned out to be a key observation. Further studies identified the source of the C₄ fragment of butadiene as the tetrabutylammonium cation, suggesting a C–H activation, perhaps *via* some Shilov chemistry, linked perhaps to a Hofmann-like elimination. The reaction is photochemical and proceeds directly from $(\text{NBu}_4)_2[\text{PtCl}_6]$ in the total absence of gold. A computational study and related literature precedent regarding the excited state of $[\text{PtCl}_6]^{2-}$ showed the formation of Pt^{III} as well as chlorine radicals, revealing the possibility for radical induction of the reaction. Indeed, Pt^{III} and N-based radicals were found in the electron paramagnetic spectroscopy (EPR) spectrum of an irradiated frozen solution. Given the extrusion of a butadiene fragment from the tetrabutylammonium cation, the possible involvement of Hofmann elimination mechanism was considered. One possibility would be the elimination of butene in the first step with concomitant reduction to Pt^{II} leading to a butene analogues of Zeise's salt, which could then react further to give the observed product. However, this possibility was not supported by the observed unreactivity of $[\text{PtCl}_3(\text{butene})]^-$ (butene = 1-butene or 2-butene) under the prevailing reaction conditions. This led to the proposal of an intermediate complex in which $(\text{Bu}_3\text{N}(\text{butene}))^+$ is π -bound to $[\text{PtCl}_3]^-$, which was supported by mass spectrometric evidence from a photochemical study. The same reaction was carried out with the $[\text{PtCl}_6]^{2-}$ salt of other tetraalkylammonium cations (NPr_4^+ and NPe_4^+) and alkene-Pt^{II} complexes were again found with NPe_4^+ salts but not with NPr_4^+ salts. All of these results and observation were collected together to propose an outline mechanism for the reaction.

In a totally separate piece of work, some examples of polycatenar 2,5-diphenylpyridine ligands (LH) were prepared and bound to palladium(II) to give complexes with an orthometallated 2-phenylpyridine and an acac co-ligand – $[\text{Pd}(\text{L})(\text{acac})]$. These are analogous to related Pt^{II} complexes prepared in the group which were found to be liquid-crystalline and emissive. While some liquid-crystalline examples were prepared, none of the complexes showed evidence for room-temperature triplet emission, which can be a feature of palladium congeners. However, in the related platinum chemistry it was observed that on formation of the complexes with three alkyloxy groups on the metallating phenyl ring, there was a Pt-promoted C–O bond cleavage. The milder conditions required for formation of the palladium meant that the same C–O bond cleavage was not observed here.

Table of Contents

Abstract	ii
Table of Contents	iii
List of Schemes	viii
List of Figures	xiii
List of Tables	xx
Acknowledgements	xxiii
Author's Declaration	xxiv
Chapter One: C–H Activation Chemistry	1
1.1. Introduction.....	1
1.2. C–H Bond Functionalisation	4
1.2.1. Concerted Oxidative Addition	4
1.2.2. Stepwise Oxidative Addition	6
1.2.3. Electrophilic Activation and Functionalisation.....	7
1.2.4. Concerted Metallation–Deprotonation (CMD).....	7
1.3. Examples of C–H Activation Chemistry.....	9
1.3.1. Rhodium complexes	9
1.3.2. Ruthenium Complexes	14
1.3.3. Gold Complexes.....	16
1.3.4. Palladium Complexes	18
1.4. Shilov Chemistry and Electrophilic C–H Activation.....	21
1.4.1. Shilov Chemistry.....	21
1.4.2. Electrophilic C–H Activation.....	26
1.5. Photochemistry of Chloroplatinate Complexes	29

1.6. Hofmann Elimination	36
1.7. The Platinum Complex: <i>trans-η²:η²-1,3-butadiene-bis(trichloroplatinate(II))</i>	39

Chapter Two: Mechanistic Investigation of Tetrabutylammonium Activation by Hexachloroplatinate(IV) Complex..... 43

2.1. Introduction.....	43
2.2. Results	45
2.2.1. Activation of Tetrabutylammonium Cation: Formation of 1,3-butadiene-platinum(II) Complex (I).....	45
2.2.1.1. Reaction of [ⁿ Bu ₄ N] ₂ [PtCl ₄] with [ⁿ Bu ₄ N] [AuCl ₄]	46
2.2.1.2. Reaction of (ⁿ Bu ₄ N) ⁺ with [PtCl ₆] ²⁻	47
2.2.1.3. The Characterisation of 1,3-butadiene-platinum(II) Complex, I.....	48
2.2.1.4. Quantum Chemical Calculation of Geometries and Energies of Different Conformers of Complex I.....	65
2.2.2. Mechanistic Investigation of the Activation of (ⁿ Bu ₄ N) ⁺ cation by [PtCl ₆] ²⁻ Complex	67
2.2.2.1. Photochemistry of [ⁿ Bu ₄ N] ₂ [PtCl ₆].....	72
2.2.2.2. Theoretical Calculation on the Excited States of [PtCl ₆] ²⁻ Complex.....	77
2.2.2.3. Identification of paramagnetic species.....	79
2.2.2.4. Attempt to quantify platinum species in the mixture during the photolysis of [ⁿ BuN ⁺] ₂ [PtCl ₆].....	82
2.2.2.5. Monitoring the photoreaction of (NBu ₄) ₂ [PtCl ₆] using ¹⁹⁵ Pt NMR spectroscopy	87
2.2.2.6. The analysis of the reaction mixture of [ⁿ Bu ₄ N] ₂ [PtCl ₆] after photolysis....	94
2.2.2.7. Analogous Reactions	104
2.2.2.8. Investigation of the Second Activation of (ⁿ Bu ₄ N) ⁺ cation.	125
2.2.2.9. Investigation of the role of [PtCl ₄] ²⁻ in the activation of the (ⁿ Bu ₄ N) ⁺ cation	136
2.3. Discussion.....	140
2.4. Conclusion	146

Chapter Three: Synthesis, the Liquid-crystalline and the Luminescence Properties of Polycatenar-diphenylpyridine Complexes of Palladium(II) 147

3.1. Introduction to Emissive Metallomesogens	147
---	-----

3.1.1. Liquid Crystals	147
3.1.1.1. Thermotropic Liquid Crystals	148
3.1.1.2. Polycatenar Mesogens	152
3.1.2. Emissive Metallomesogens of the Group 10 Elements (M = Pd ^{II} , Pt ^{II}).....	156
3.2. Results and Discussion	167
3.2.1. Introduction	167
3.2.2. Synthesis	170
3.2.2.1. Synthesis of Ligands	170
3.2.2.2. Synthesis of the Polycatenar Palladium(II) Complexes.	171
3.2.2.3. The Observation of Regioselective C–O Cleavage in the Platinum(II) Complexes of the Polycatenar-diphenylpyridine Ligand.	176
3.2.3. Liquid Crystal Properties of the Ligands and Complexes	178
3.2.4. Small Angle X-ray Scattering of Complexes XIV (1) and XIV (2)	181
3.2.5. Photophysical Properties of the Complexes.....	183
3.3. Conclusion	186
Chapter Four: Experimental Methods	188
4.1. Instrumentation	188
NMR Spectroscopy	188
Far-Infrared	188
UV-Visible and Luminescence Spectroscopy	188
Mass Spectrometry (MS).....	189
Elemental Analysis.....	189
Gas Chromatography-Mass Spectroscopy (GC-MS).....	189
Electron Paramagnetic Resonance Spectroscopy	190
UV-Mass Spectrometry	190
Small-Angle X-ray Scattering (SAXS).....	190
Differential Scanning Calorimetry (DSC) and Polarised Optical Microscopy (POM)....	190
4.2. Materials	191

Purification of Solvents and Reagents	191
4.3. Methods for Investigation of Photochemical Activation of Tetraalkylammonium by Hexachloroplatinate(IV) Complex.	191
1. Preparation of Tetrabutylammonium Hexachloroplatinate(IV)	191
2. Preparation of Tetrabutylammonium Tetrachloroplatinate(II)	192
3. Preparation of Tetraethylammonium Hexachloroplatinate(IV)	192
4. Preparation of Tetrapropylammonium Hexachloroplatinate(IV)	193
5. Preparation of Tetrapropylammonium Tetrachloroplatinate(II)	193
6. Preparation of Tetrapentylammonium Hexachloroplatinate(IV)	193
7. Preparation of Tetrapentylammonium Tetrachloroplatinate(II)	193
8. Preparation of Tributylammonium Salts.....	194
9. Preparation of Bis(triphenylphosphine)iminium Hexachloroplatinate(IV).....	195
10. Preparation of Tetrabutylphosphonium Hexachloroplatinate(IV).....	195
11. Preparation of Tetrabutylammonium Hexachlorodiplatinate(II), (NBu ₄) ₂ [Pt ₂ Cl ₆].	196
12. Thermal Reaction of Tetraalkylammonium Hexachloroplatinate(IV) under Ambient Illumination	196
13. Photoreactions of Tetrabutylammonium Hexachloroplatinate(IV).....	198
14. Photolysis of Analogous Hexachloroplatinate(IV) Complexes	199
15. Synthesis of Trichloro(<i>η</i> ² -butene)platinate(II) Complexes, III	199
16. EPR experiments	201
17. Irradiation of [PtCl ₃ (butene)] ⁻ complexes under varied conditions.	203
4.4. Method for Synthesis, the Liquid-crystalline and the Luminescence Properties of Polycatenar-diphenylpyridine Complexes of Palladium(II)	203
4.4.1. Synthesis of Ligands	203
4.4.1.1. Tricatenar diphenylpyridine derivatives	203
4.4.1.2. Tetracatenar diphenylpyridine derivatives.....	207
4.4.1.3. Hexacatenar diphenylpyridine derivatives	210
4.4.2. Palladium Complexes	213
Na(acac).H ₂ O	213
[Pd(acac)(2,5-bis(4-(dodecyloxy)phenyl)pyridine)], XIV (1)	214
[Pd(acac)(2-(4-dodecyloxyphenyl)-5(3,4-didodecyloxyphenyl)pyridine)], XIV (2)	215
[Pd(acac)(2,5-Bis(3,4-bis(dodecyloxy)phenyl)pyridine)], XIV (3)	216
[Pd(acac)(2,5-Bis(3,4,5-tris(dodecyloxy)phenyl)pyridine)], XIV (4)	217

Appendices.....	219
Appendix 1: The ^{195}Pt NMR data for platinum complexes.....	219
Appendix 2: The $^{195}\text{Pt}\{^1\text{H}\}$ NMR spectra of $\text{K}_2[\text{PtCl}_6]$ in D_2O (top) and after one-hour irradiation (below).	220
Appendix 3: The 2D (^{15}N - ^1H) NMR spectra of NBu_3	220
Appendix 4: The 2D (^{15}N - ^1H) NMR spectra of HNBu_3Cl in d_6 -acetone	221
Appendix 5: The 2D (^{15}N - ^1H) NMR spectra of $(\text{NBu}_4)_2[\text{PtCl}_6]$ in d_6 -acetone	221
Appendix 6: The ^1H NMR spectra of the mixture of $(\text{PPN})(\text{PtCl}_3(1\text{-butene}))$ and $(\text{PPN})_2[\text{PtCl}_6]$ in CD_2Cl_2 on the heating in the dark condition.	222
Appendix 7: The $^{31}\text{P}\{^1\text{H}\}$ NMR spectrum of photoreaction mixture of $(\text{PBu}_4)_2[\text{PtCl}_6]$ recorded in d_6 -acetone.	223
Appendix 8: The $^{195}\text{Pt}\{^1\text{H}\}$ NMR spectra of photoreaction mixture of $(\text{PBu}_4)_2[\text{PtCl}_6]$ recorded in d_6 -acetone.	223
Appendix 9: ^1H NMR spectrum of 2-(4-dodecyloxyphenyl)-5(3,4-didodecyloxyphenyl)pyridine, V (2) , in CDCl_3	224
Appendix 10: ^1H NMR spectrum of 2,5-Bis(3,4-bis(dodecyloxyphenyl)pyridine, V (3) , in CDCl_3	225
Appendix 11: ^1H NMR spectrum of 2,5-Bis(3,4,5-tris(dodecyloxyphenyl)pyridine, V (4) , in CDCl_3	226
Appendix 12: ^1H NMR spectrum of complex XIV (1) in CD_2Cl_2	227
Appendix 13: ^1H NMR spectrum of complex XIV (2) in CDCl_3	228
Appendix 14: ^1H NMR spectrum of complex XIV (3) in CDCl_3	229
Appendix 15: ^1H NMR spectrum of complex XIV (4) in CDCl_3	230
Appendix 16: ^1H NMR spectrum of the chloro-bridged dimer palladium complex, (XIII (3)) in CDCl_3	231
Abbreviations.....	232
References.....	235

List of Schemes

Scheme 1: The reaction of $[\text{Ru}^{\text{II}}\text{Cl}_2(\text{dppe})_2]$ with naphthalene reported by Chatt and Davidson. ⁹	2
Scheme 2: Oxidation addition of hydrogen to an iridium(I) complex, reported by Vaska and DiLuzio. ¹⁰	2
Scheme 3: Catalytic hydrogenation of olefins and alkynes mediated by $[\text{RhCl}(\text{PPh}_3)_3]$ -Wilkinson- in benzene or chloroform at 25 °C. ¹¹	3
Scheme 4: H/D exchange reaction in Shilov system, reported by Shilov and co-workers. ¹²	3
Scheme 5: Activation of methane in Shilov system, reported by Shilov and co-workers. ¹²	4
Scheme 6: General pathway of concerted oxidative addition. ¹³	4
Scheme 7: The C–H insertion of iridium(I) complex through concerted oxidative addition as reported by Bergman and co-workers. ¹³	5
Scheme 8: The C–H activation of neopentane on the complex of $[\text{Ir}(\eta^5\text{-C}_5\text{Me}_5)(\text{CO})_2]$, reported by Graham and co-workers. ¹⁷	5
Scheme 9: C–H activation of benzene in $[\text{Lu}(\eta^5\text{-C}_5\text{Me}_5)\text{H}]$ complex, reported by Watson and co-workers. ¹⁸	5
Scheme 10: An example of stepwise oxidative addition of aromatic ketones catalysed by $[\text{Ru}(\text{H})_2(\text{CO})(\text{PPh}_3)_3]$, reported by Murai and co-workers. ¹⁹	6
Scheme 11: Proposed mechanism of stepwise oxidative addition of aromatic ketones catalysed by $[\text{Ru}(\text{H})_2(\text{CO})(\text{PPh}_3)_3]$, reported by Matsubara <i>et al.</i> ²⁰	6
Scheme 12: The deprotonation mechanism via an assisted intramolecular (upper) or assisted intermolecular (lower) or unassisted (middle) pathways. ²⁹	8
Scheme 13: The oxidative coupling of benzoquinoline with 1,3-dimethoxybenzene catalysed by the palladium(II) complex proceeds through the CMD mechanism which site selective depends on the anion, reported by Sanhueza <i>et al.</i> ³³	9
Scheme 14: General pathways of C–H insertion of hydrocarbons into the rhodium catalyst directed by functional groups. ³⁵	10

Scheme 15: The C–H alkylation of phenyl pyridine using rhodium catalyst, $[\text{RhCl}(\text{C}_8\text{H}_{14})_2]_2$, in the presence of tricyclophosphine, reported by Lim and Kang, 1994. ³⁹	11
Scheme 16: The proposed mechanism of the C–H alkylation of 2-phenylpyridine using rhodium catalyst, reported by Lim and Kang, 1994. ³⁹	11
Scheme 17: The reaction of ortho-alkylation of ketimines with olefin catalysed by Wilkinson’s catalyst whereas the reaction of aldimines does not proceed as reported by Jun <i>et al.</i> ⁴¹	12
Scheme 18: The proposed mechanism of the intramolecular olefin coupling catalysed by Wilkinson’s catalyst as reported by Fujii <i>et al.</i> ⁴²	13
Scheme 19: The photo-dimerisation reaction of methyl propionate catalysed by $[\text{RhCl}(\text{CO})(\text{PMe}_3)_2]$, reported by Sakakura <i>et al.</i> ⁴³	13
Scheme 20: The proposed mechanism of the photo-dimerisation of methyl propionate catalysed by $[\text{RhCl}(\text{CO})(\text{PMe}_3)_2]$, reported by Sakakura <i>et al.</i> ⁴³	14
Scheme 21: Direct arylation of 2-pyridylbenzene catalysed by $[\text{RuCl}_2(\text{C}_6\text{H}_6)]_2$ as reported by Oi <i>et al.</i> ⁴⁴	15
Scheme 22: The proposed mechanism of arylation of phenylpyridines using phenyl halides catalysed by ruthenium(II) complex, reported by Arockiam, <i>et al.</i> ³⁴	15
Scheme 23: The reaction mechanism of alkynes addition with methanol catalysed by $[\text{Au}(\text{CH}_3)(\text{PPh}_3)]$, reported by Teles <i>et al.</i> ⁴⁸	17
Scheme 24: Oxidative addition of R-X (R = Ar, X = I, Br) to gold(I) as reported by Bourissou and co-workers. ⁵⁰	17
Scheme 25: The oxidative addition of a $[(\text{NHC})\text{-Au}^{\text{I}}\text{-Cl}]$ complex by biphenylene resulting in a stable biphenyl-gold(III) complex, reported by Toste and co-workers. ⁵⁴	18
Scheme 26: Molecular structure of palladium(II) complex coordinating with CH reported by Maitlis and co-workers. ⁵⁵	19
Scheme 27: Olefination of arenes catalysed by palladium(II) complex in $\text{Pd}^{\text{II}}/\text{Pd}^0$ catalytic cycle reported by Moritani and Fujiwara. ⁵⁷	19
Scheme 28: Directed ortho olefination of benzoic acid reported by Miura <i>et al.</i> ⁶⁰	20

Scheme 29: Functionalisation Mechanism of Cyclopalladated Complex through 1) Reductive Elimination ($\text{Pd}^{\text{II}}/\text{Pd}^0$ Catalytic Cycle), 2) Electrophilic Cleavage: a) Direct, b) One-Electron Oxidation, c) Two-Electron Oxidation. FG = functional group. ⁶²	21
Scheme 30: The proposed mechanism of methane activation in the Shilov's system. ¹²	22
Scheme 31: The oxidation of methane catalysed by platinum(II) complex reported by Periana and co-workers. ²⁴	24
Scheme 32: The postulated mechanism of methane functionalisation reported by Periana and co-workers. ²⁴	24
Scheme 33: Ethane activation reaction under Periana-Catalityca system reported by Periana and co-workers. ⁶⁵	25
Scheme 34: The mechanism of ethane activation and functionalisation using the Periana-catalytica system. ⁶⁵	26
Scheme 35: The exchange reaction of $[\text{PtCl}_6]^{2-}$ with Cl^- catalysed by Pt^{III} species reported by Rich and Taube. ⁶⁷	29
Scheme 36: The exchange reaction of $[\text{PtCl}_4]^{2-}$ with Cl^- catalysed by Pt^{III} species reported by Rich and Taube. ⁶⁷	30
Scheme 37: Transformation of alcohols catalysed by $[\text{PtCl}_6]^{2-}$ under irradiation reported by Cameron and Bocarsly. ⁶⁸	31
Scheme 38: Oxidation reaction of $[\text{Pt}^{\text{III}}\text{Cl}_5]^{2-}$ by CuCl_2 in catalytic formation of alcohols reported by Cameron and Bocarsly. ⁶⁸	31
Scheme 39: Transformation of (a) ethanol and (b) 2-propanol in the presence of $[\text{PtCl}_6]^{2-}$ under irradiation reported by Cameron and Bocarsly. ⁶⁹	32
Scheme 40: The reduction of $[\text{PtCl}_4]^{2-}$ in alcohols reported by Cameron and Bocarsly. ⁶⁹	32
Scheme 41: Photoreaction of an alkane in the presence of aqueous hexachloroplatinate(IV) solution reported by Shulpin and co-workers. ⁷⁵	33
Scheme 42: The photoreaction of organotin and organogermanium compounds with $[\text{PtCl}_6]^{2-}$ reported by Shulpin and co workers. ⁷⁹	34

Scheme 43: Proposed mechanism of the formation of σ -alkyl-platinum(IV) on the irradiation of alkanes with $[\text{PtCl}_6]^{2-}$ present reported by Shulpin and co-workers. ⁷⁹	34
Scheme 44: The mechanism proposed by Shul'pin for the photoreaction of $[\text{PtCl}_6]^{2-}$ with aromatic compounds. ⁸²	35
Scheme 45: General pathway of Hofmann elimination reaction.....	36
Scheme 46: Hofmann elimination reaction of tetrapropylammonium fluoride in a non-aqueous system reported by Harmon <i>et al.</i> ⁸³	36
Scheme 47: Hofmann elimination of NBu_4^+ in a solution containing cis-dichlorobis(triethylphosphine)platinum(II) complex reported by Davies <i>et al.</i> ⁸⁸	37
Scheme 48: Hofmann elimination of tetrabutylammonium cation initiated by a radical reported by Wrzyszczyński <i>et al.</i> ⁸⁹	38
Scheme 49: The reaction of $[(\text{PPh}_3)_4\text{Pd}]$ with $(\text{NBu}_4)(\text{CN})$ in a presence of water reported by Erhardt <i>et al.</i> ⁹⁰	38
Scheme 50: The theoretically proposed mechanism of Hoffman elimination taking place in the reaction of $[(\text{PPh}_3)_4\text{Pd}]$ with $(\text{NBu}_4)(\text{CN})$ modelled by the quaternary ammonium $(\text{EtNMe}_3)^+$ cation, reported by Erhardt <i>et al.</i> ⁹⁰	39
Scheme 51: The reaction of $[\text{Pd}(\text{PPh}_3)_4]$ with $(\text{NBu}_4)(\text{CN})$ in an absence of water reported by Erhardt <i>et al.</i> ⁹⁰	39
Scheme 52: The synthesis of the butadiene complex, $(\text{NBu}_4)_2[\text{Pt}_2\text{Cl}_6(\mu\text{-C}_4\text{H}_6)]$ from the chlorobridge complex, $(\text{NBu}_4)_2[\text{Pt}_2\text{Cl}_6]$ reported by Briggs <i>et al.</i> ⁹⁹	41
Scheme 53: The synthesis of the butadiene complex, $[\text{Pt}_2\text{Cl}_4(\text{PR}_3)_2(\mu\text{-C}_4\text{H}_6)]$ from the chlorobridge complex, $[\text{Pt}_2\text{Cl}_4(\text{PR}_3)_2]$ reported by Briggs <i>et al.</i> ⁹⁹ ..	41
Scheme 54: The formation of the butadiene-platinum(II) complex (I) (with the X-ray structure) from the mixture of $[\text{PtCl}_4]^{2-}$ and $[\text{AuCl}_4]^-$ salts with $(\text{NBu}_4)^+$ cation.	44
Scheme 55: The suggested structure of the intermediate compound (I.A) appeared at -2570 ppm on the $^{195}\text{Pt}\{^1\text{H}\}$ NMR spectra.	101
Scheme 56: Proposed molecular structures of compounds resulted in the photolysis of $[\text{Pe}_4\text{N}]_2[\text{PtCl}_6]$	108

Scheme 57: The reaction showing a formation of allylic-platinum complex from propene-platinum dimer as reported by Mann <i>et al.</i> ¹²⁹	124
Scheme 58: A proposed mechanism the formation of platinum(II) complex to form η^1, η^3 - μ -allyl-platinum(II) complex via sequential deprotonation of η^2 -propene-platinum(II) complex as reported by Bandoli <i>et al.</i> ¹³⁰ ...	125
Scheme 59: The de-coordination of (η^2 -1-butene)-trichloroplatinate(II) anion under light in CD ₂ Cl ₂ solution.	129
Scheme 60: Photolysis reaction of cis-2-butene in the gas phase as reported by Cundall <i>et al.</i> and Chesick <i>et al.</i> ^{131, 132}	133
Scheme 61: The proposed reaction to form the N-based radical in irradiation of [nBu ₄ N] ₂ [PtCl ₆].....	143
Scheme 62: A proposed mechanism of photochemical activation of tetrabutylammonium cation by hexachloroplatinate(IV) complex... 145	
Scheme 63: Preparation of the platinum(II)-acac complexes of the diphenylpyridine ligands by Prokhorov. Conditions: (vii) CH ₃ COOH, reflux, overnight; (viii) K(acac).H ₂ O, under reflux in: a. ethoxyethanol; b. CHCl ₃ / EtOH.....	169
Scheme 64: Preparation of the polycatenar-diphenylpyridine ligands. Conditions: (i) MeOH, reflux, 17 h; (ii) Et ₂ O; (iii) NaHCO ₃ , EtOH/CH ₃ COOH, 120 °C, 7 h; (iv) o-xylene, 200 °C, overnight; (v) 200 °C, 5 h; (vi) DMF, K ₂ CO ₃ , 100 °C, 12 h.....	171
Scheme 65: Preparation of the palladium-acac complexes of the diphenylpyridine ligands. Conditions: (vii) CH ₃ COOH, reflux, overnight; (viii) reagent: Na(acac).H ₂ O in a. acetone, reflux; b. CHCl ₃ / EtOH, reflux.....	172
Scheme 66: The reaction of the phenyl pyridine ligands with K ₂ [PtCl ₄] leading to –O–C bond cleavage observed by Prokhorov. Reaction conditions: reagent: K(acac).H ₂ O in CHCl ₃ / EtOH, under reflux.	177
Scheme 67: The proposed pathway of ether cleavage occurred in the cycloplatination of the diphenylpyridines ligand in acetic acid.	178

List of Figures

Figure 1: Diagrams illustrating two different ways in which electrophilicity affects the total energy as well as reaction rate on activation and functionalisation of alkane. (Image reproduced from the paper reported by Hashiguchi <i>et al.</i>) ²⁸	27
Figure 2: The structure of the butadiene-platinum(II) complex reported by a) Jonassen; ⁹⁴ b) Chatt; ⁹⁵ c) Grogan and Nakamoto; ⁹⁷ and d) Adam. ⁹⁸ ..	40
Figure 3: The single crystal structure of $[(\mu\text{-C}_4\text{H}_6)\text{Pt}_2\text{Cl}_6]^{2-}$ in three different views.	49
Figure 4: The butadiene conformers on coordination to two platinum(II) centres.	50
Figure 5: The ^1H NMR (500 MHz) spectrum of I recorded in CD_2Cl_2 at 298 K.....	53
Figure 6: The ^1H NMR spectrum (500 MHz) of I recorded in d_6 -acetone at 298 K..	54
Figure 7: The ^1H - ^1H COSY spectra (500 MHz) of I recorded in CD_2Cl_2 at 298 K.....	55
Figure 8: The ^1H - ^1H COSY spectra (500 MHz) of I recorded in d_6 -acetone at 298 K	56
Figure 9: The ^1H NMR spectra of complex I stored in d_6 -acetone for 17 days (top) and that of its fresh solution (bottom).	58
Figure 10: The ^1H NMR spectra of the complex I stored in CD_2Cl_2 for 17 days (top) and that of its fresh solution (bottom).	59
Figure 11: The ^1H NMR spectra of the complex I stored in CDCl_3 for 17 days (top) and that of its fresh solution (bottom).	60
Figure 12: The ^1H NMR spectra of the complex I in d_6 -acetone at temperature variations (top: 318 K, bottom: 298K).	60
Figure 13: The ^1H NMR spectra of the complex I in CDCl_3 at temperature variations (top: 328 K, bottom: 298 K)	61
Figure 14: $^{195}\text{Pt}\{^1\text{H}\}$ NMR spectrum (107 MHz) of the complex I in d_6 -acetone at 298 K.	63
Figure 15: 2D ^{195}Pt - ^1H NMR spectra (107 MHz) of the complex I in d_6 -acetone at 298 K	64
Figure 16: The conformers of platinum(II)-1,3-butadiene complexes.....	65
Figure 17: The optimised geometries of conformers I. 1 – I.3 using M06/def2-TZVPP.	66

Figure 18: The evolution of ^{195}Pt NMR spectrum of $[\text{nBu}_4\text{N}]_2[\text{PtCl}_6]$ in d_6 -acetone at 323 K under ambient light.	69
Figure 19: Evolution of platinum species on photolysis of $[\text{nBu}_4\text{N}]_2[\text{PtCl}_6]$ in d_6 -acetone at 323 K under ambient light, a) in area spanning – 950 to – 1850 ppm, b) in olefin area spanning – 2050 to – 2950 ppm.....	70
Figure 20: The ^1H -NMR spectrum (500 MHz; with enlargement of a new signal at 4.35 ppm) of the reaction mixture of $[\text{nBu}_4\text{N}]_2[\text{PtCl}_6]$ in d_6 -acetone under heating and ambient light.	71
Figure 21: The ^2D NMR spectrum (76.8 MHz) of thermal reaction under ambient light mixture of $[\text{nBu}_4\text{N}]_2[\text{PtCl}_6]$ in d_6 -acetone, with enlargement of signals at 4.8 and 5.7 ppm. *observed on ^1H NMR spectrum, + only appeared on $^2\text{D}\{^1\text{H}\}$ NMR spectrum.	71
Figure 22: The UV spectra of acetone and $[\text{nBu}_4\text{N}]_2[\text{PtCl}_6]$ in acetone	73
Figure 23: The ^1H NMR spectra of complex I on irradiation in d_6 -acetone.	75
Figure 24: The UV spectra of the chloroplatinate complexes in acetone.....	76
Figure 25: The UV spectra of the chloroplatinate complexes in dichloromethane.	76
Figure 26: The electronic spectra of $[\text{PtCl}_6]^{2-}$ from the experimental method and the calculation along with the visualisation of electron density difference between the ground state and the excited state associated with the states of S_{31} (207 nm) and S_{22} (324 nm) (note: yellow: increasing of electron density and blue: decreasing of electron density compared to the ground state).	78
Figure 27: Electron density difference between the ground state (S_0) and the T_1 state calculated for $[\text{PtCl}_6]^{2-}$ in relaxed T_1 state geometry (note: yellow: increasing of electron density and blue: decreasing of electron density compared to the ground state).....	79
Figure 28: The EPR spectrum of $[\text{nBu}_4\text{N}]_2[\text{PtCl}_6]$ on irradiation for 20 minutes in dichloromethane at 120 K. a) on wide range, b) enlargement in the organic area and c) Et_3N^+ as reported in ref. ¹²²	81
Figure 29: Graph showing integration of peaks in vary of pulse delay, D_1 , for $[\text{nBu}_4\text{N}]_2[\text{PtCl}_6]$, $[\text{nBu}_4\text{N}]_2[\text{PtCl}_4]$, and $[\text{nBu}_4\text{N}]_2[\eta^2\text{-Cl}_3\text{Pt}(\text{C}_6\text{H}_6)\text{-}\eta^2\text{-PtCl}_3]$ in d_6 -acetone solutions.	84
Figure 30: Calibration curves of $[\text{nBu}_4\text{N}]_2[\text{PtCl}_6]$ (a) and $[\text{nBu}_4\text{N}]_2[\text{PtCl}_4]$ (b) showing correlations of integral peaks recorded from $^{195}\text{Pt}\{^1\text{H}\}$ NMR	

	experiments with complexes concentration in solutions of in d ₆ -acetone.....	86
Figure 31:	¹⁹⁵ Pt{ ¹ H} NMR spectra of a mixture of [ⁿ Bu ₄ N] ₂ [PtCl ₆], [ⁿ Bu ₄ N] ₂ [PtCl ₄], [ⁿ Bu ₄ N] ₂ [(PtCl ₃) ₂ (C ₄ H ₆)] in d ₆ -acetone recorded at 64.52 MHz for ¹⁹⁵ Pt nucleus (¹ H = 300 MHz).....	87
Figure 32:	Evolution of platinum species on photolysis of [ⁿ Bu ₄ N] ₂ [PtCl ₆] in d ₆ -acetone. In area spanning a) 650 to – 250 ppm b)– 950 to – 1850 ppm, c) olefin area: –2050 to – 2950 ppm.	90
Figure 33:	Evolution of platinum species on photolysis of [ⁿ Bu ₄ N] ₂ [PtCl ₆] in CD ₂ Cl ₂ . In area spanning a) 650 to – 250 ppm b)– 950 to – 1850 ppm, c) olefin area: – 2050 to – 2950 ppm.....	92
Figure 34:	Graphs showing the consumption of [ⁿ Bu ₄ N] ₂ [PtCl ₆] during the irradiation under different conditions.	93
Figure 35:	¹ H-NMR spectra of H ⁿ Bu ₃ NCl, ⁿ Bu ₃ N, and ⁿ Bu ₄ NCl in d ₆ -acetone.....	96
Figure 36:	The 2D- ¹⁵ N- ¹ H NMR spectra of the mixture of photolysed [ⁿ Bu ₄ N] ₂ [PtCl ₆] under UV light, recorded in d ₆ -acetone.	97
Figure 37:	Photofragment spectra of [HNBu ₃] ⁺ (m/z 186), [(ⁿ Bu ₄ N) ₂ Cl] ⁺ (m/z 520), [(ⁿ Bu ₄ N) ₂ Cl[(ⁿ Bu ₃ N(C ₄ H ₇)PtCl ₃)] ⁺ (m/z 1061) and [(ⁿ Bu ₄ N) ₃ [PtCl ₄]] ⁺ (m/z 1064)	98
Figure 38:	The 2D-(¹ H- ¹⁹⁵ Pt)-NMR spectra of the reaction mixture of [ⁿ Bu ₄ N] ₂ [PtCl ₆] in acetone photolysed thermally under ambient light, recorded in d ₆ -acetone at 298 K; left: the 1D- ¹⁹⁵ Pt{ ¹ H} NMR spectrum showing the peaks at – 2570 and – 2567 ppm.....	102
Figure 39:	The low-VT ¹⁹⁵ Pt{ ¹ H} NMR spectra of the mixture of [ⁿ Bu ₄ N] ₂ [PtCl ₆] in d ₆ -acetone after photolysis.	104
Figure 40:	The ¹ H NMR spectrum of the [ⁿ Pe ₄ N] ₂ [PtCl ₆] mixture in acetone after 24 hours of heating under reflux and ambient light.	109
Figure 41:	The ¹ H NMR spectrum of the photoreaction mixture of [ⁿ Pe ₄ N] ₂ [PtCl ₆] in acetone recorded in d ₆ -acetone at 298 K, with expansion of the region containing hydrogen resonances from bound alkene.	110
Figure 42:	The ¹⁹⁵ Pt NMR spectra of the photoreaction mixture of [ⁿ Pe ₄ N] ₂ [PtCl ₆] in acetone recorded in d ₆ -acetone at 298 K.....	110

Figure 43: The ^1H - ^1H COSY spectra of the $[\text{Pe}_4\text{N}]_2[\text{PtCl}_6]$ mixture in acetone after 48 hours of heating under reflux and ambient light.	111
Figure 44: The 2D- $(^{195}\text{Pt}-^1\text{H})$ NMR spectra of the photoreaction mixture of $[\text{Pe}_4\text{N}]_2[\text{PtCl}_6]$ in acetone recorded in d_6 -acetone at 298 K.....	112
Figure 45: The 2D- $^{195}\text{Pt}-^1\text{H}$ NMR spectra of the $[\text{Pe}_4\text{N}]_2[\text{PtCl}_6]$ mixture in acetone after 48 hours of heating under reflux and ambient light.....	113
Figure 46: The in situ-photo-EPR spectra of $[\text{Pe}_4\text{N}]_2[\text{PtCl}_6]$ compared with $[\text{Bu}_4\text{N}]_2[\text{PtCl}_6]$ recorded in dichloromethane at 120 K showing a) platinum(III) radical and b) organic <i>N</i> -based radical.	114
Figure 47: The optimised geometry of pentadiene conformers at M06/def2-TZVPP level of theory.....	116
Figure 48: The ^1H NMR spectrum of the mixture of photolysis of $[\text{Pr}_4\text{N}]_2[\text{PtCl}_6]$ in acetone, recorded in d_6 -acetone. The chemical shifts at 1.02, 1.88 and 3.54 are corresponded with propyl protons; the signals at 4.42 and 4.35 ppm shown in the enlargement spectrum were found to correlate with a ^{195}Pt chemical shift in olefin-Pt ^{II} area in 2D- $^{195}\text{Pt}-^1\text{H}$ NMR spectra.	119
Figure 49: The $^{195}\text{Pt}\{^1\text{H}\}$ NMR spectra of the mixture of $[\text{Pr}_4\text{N}]_2[\text{PtCl}_6]$ photolysis in acetone recorded in d_6 -acetone at 298 K. (cross: unknown signal; asteriks: olefin-Pt(II) signals).....	120
Figure 50: The in situ-photo-EPR spectra of $[\text{Pr}_4\text{N}]_2[\text{PtCl}_6]$ compared with $(\text{Bu}_4\text{N})_2[\text{PtCl}_6]$ recorded in dichloromethane at 120 K showing: a) platinum(III) radical and b) organic <i>N</i> -based radical.	120
Figure 51: The 2D- $^{195}\text{Pt}-^1\text{H}$ NMR spectra of the mixture of photolysis of $[\text{Pr}_4\text{N}]_2[\text{PtCl}_6]$ in acetone recorded in d_6 -acetone at 298.....	122
Figure 52: The ^{195}Pt NMR spectra of the $[\text{Pr}_4\text{N}]_2[\text{PtCl}_6]$ mixture in acetone on heating for 48 hours under reflux and ambient light recorded in CD_2Cl_2 at 295 K.	123
Figure 53: The ^1H NMR spectra of the $[\text{Bu}_4\text{N}][\text{PtCl}_3(1\text{-butene})]$, III.1 , in d_6 -acetone on the irradiation under UV light.....	127
Figure 54: The $^{195}\text{Pt}\{^1\text{H}\}$ NMR spectra of the $[\text{Bu}_4\text{N}][\text{PtCl}_3(1\text{-butene})]$, III.1 , in d_6 -acetone on the irradiation under UV light.....	127
Figure 55: The ^1H NMR spectra of the mixture of $[\text{PPN}][\text{PtCl}_3(1\text{-butene})]$, III.2 and $[\text{PPN}]_2[\text{PtCl}_6]$ in CD_2Cl_2 on the irradiation under UV light. (asteriks mark	

	new signals proposed as resulting from decomposition of 1-butene.	130
Figure 56:	The ^{195}Pt NMR spectra of the mixture of $[\text{PPN}][\text{PtCl}_3(1\text{-butene})]$, III.2 , and $[\text{PPN}]_2[\text{PtCl}_6]$ in CD_2Cl_2 on the irradiation under UV light.....	131
Figure 57:	The ^1H NMR spectra of the mixture of $[\text{PPN}][\text{PtCl}_3(2\text{-butene})]$, IV , and $[\text{PPN}]_2[\text{PtCl}_6]$ in CD_2Cl_2 during the irradiation. (asteriks mark new signals proposed as resulting from decomposition of 2-butene.....	134
Figure 58:	The 2D- ^{195}Pt - ^1H NMR spectra of the mixture of $[\text{PPN}][\text{PtCl}_3(2\text{-butene})]$, IV , and $[\text{PPN}]_2[\text{PtCl}_6]$ in CD_2Cl_2 after the irradiation for 120 minutes.	135
Figure 59:	The $[\text{PPN}]_2[\text{PtCl}_6]$ signal on the $^{195}\text{Pt}\{^1\text{H}\}$ NMR spectra during the irradiation of the mixture of $[\text{PPN}][\text{PtCl}_3(2\text{-butene})]$ and $[\text{PPN}]_2[\text{PtCl}_6]$ in CD_2Cl_2	135
Figure 60:	The EPR spectrum of the mixture of III.2 and $[\text{PPN}]_2[\text{PtCl}_6]$ in dichloromethane at 120 K under the UV irradiation for 25 minutes, compared with the spectrum of $[\text{nBu}_4\text{N}]_2[\text{PtCl}_6]$ (left); expansion on the organic region (right).	136
Figure 61:	The percentage of $[\text{PtCl}_6]^{2-}$ recorded during photoreactions in variable moles of $[\text{PtCl}_4]^{2-}$	138
Figure 62:	The photochemical in-situ EPR spectra of $[\text{nBu}_4\text{N}]_2[\text{PtCl}_4]$ in CH_2Cl_2 at 120 K compared to that of $[\text{nBu}_4\text{N}]_2[\text{PtCl}_6]$	139
Figure 65:	The structure of cholesteryl benzoate. ¹³⁵	148
Figure 66:	A general molecular structure of calamitic mesogens. ¹³⁵	149
Figure 67:	A picture of molecular arrangement in nematic phase. ⁵⁹	150
Figure 68:	A diagram of the chiral nematic phase. ⁵⁹	150
Figure 69:	Diagrams of a) Smectic A, b) Smectic C, and c) Smectic B (viewed from above and from the side) phases. ⁵⁹	151
Figure 70:	A general structure of disc-like mesogens. ⁵⁹	151
Figure 71:	A diagram of the columnar phase. ⁵⁹	152
Figure 72:	The description of tetracatenar mesogen in (A) symmetrical system and (B) unsymmetrical system.	153

Figure 73:	Molecular structure of silver(I) complex of the symmetrical polycatenar-alkoxystilbazole. ¹⁴³	154
Figure 74:	The molecular structure of the symmetrical polycatenar-palladium(II) mesogens (74). ¹⁴³	155
Figure 75:	An illustration of the formation of SmC phase on the tetracatenar mesogens. ¹⁴³	156
Figure 76:	Molecular structure of the metallomesogens based on platinum and palladium metals synthesised by Hegmann et al. ¹⁵²	157
Figure 77:	Molecular structures of the emissive metallomesogens of platinum(II) complexed with biphenylpyridine ligand derivatives. ^{147, 153}	159
Figure 78:	The molecular structure of polarised emissive platinum(II) mesogens on the basis of phenylpyridine ligand derivatives. ¹⁵⁴	160
Figure 79:	The molecular structure of emissive platinum(II) mesogens based on 1,3-dibipyridylbenzene ligand derivatives (82, 83) ¹⁴⁶ and the parent complex (84). ¹⁵⁵	161
Figure 80:	The molecular structure of emissive metallomesogens of the platinum(II) complexes of pyridyl pyrazolate ligands. ¹⁵⁶	162
Figure 81:	The molecular structure of emissive metallomesogens of the platinum(II) complexes of isoquinoline pyrazolate ligands. ¹⁵⁷	163
Figure 82:	The molecular structure of the luminescent σ -alkynyl platinum(II) terpyridine complexes. ¹⁵⁹	164
Figure 83:	The molecular structure of the emissive metallomesogens of Nile-Red-palladium(II) derivatives. ^{160, 161}	165
Figure 84:	The molecular structure of emissive mesomorphic allyl-palladium(II) complexes with 1-pyridyl-3-pyridiniumyl-1,3-diketonate co-ligand. ¹⁶²	166
Figure 83:	The molecular structure of metallomesogens palladium(II) complexes of Schiff base ligands with co-ligand of N-benzoyl thiourea. ¹⁶³	167
Figure 86:	The molecular structure of emissive and mesomorphic palladium(II) complexes of Schiff base ligands with co-ligand of N-benzoyl thiourea. ¹⁶⁴	167
Figure 87:	Posibble molecular structure of dichloro-bridged-tetracatenar-palladium(II) complex.	173

Figure 88:	The ¹ H-NMR spectra of the tetracatenar-palladium(II) dimer complex (top) and the ligand (bottom) in the aromatic area.	174
Figure 89:	¹ H-NMR spectra of tetracatenar-phenylpyridine-palladium(II) complex (top) and the ligand (bottom) in CDCl ₃	176
Figure 90:	Optical micrographs (on cooling) of the (a) SmC phase of the tricatener ligand (V (2)) and (b) SmA phase of the tricatener-palladium(II) complex (XIV (2)).	180
Figure 91:	Two-dimensional small angle X-ray scattering patterns obtained for complex XIV (1) : (a) in isotropic phase (T = 255 °C); (b) in the Smectic A phase (T = 222 °C) and (c) in crystal phase (T = 127 °C).	181
Figure 92:	Two dimensional-small angle X-ray scattering patterns obtained for the complex XIV (2) : (a) in isotropic phase at (T = 149 °C); (b) in the Smectic A phase (T = 116 °C) and (c) in crystal phase (T = 55 °C).	181
Figure 93:	The small-angle X-ray scattering pattern of complex XIV (1) in the SmA state (T = 205 °C)	182
Figure 94:	The small-angle X-ray scattering pattern of complex XIV (2) in the SmA state (T = 105 °C)	182
Figure 95:	The absorption spectra of polycatenar ligands in dichloromethane solution at room temperature.	184
Figure 96:	The absorption spectra of polycatenar palladium(II) complexes in dichloromethane solution at room temperature.	184
Figure 97:	The absorption spectra of polycatenar ligands and palladium(II) complexes in dichloromethane solution at room temperature.	185

List of Tables

Table 1: Bond lengths and angle data of $[\text{Pt}_2\text{Cl}_6(\text{C}_4\text{H}_6)]^{2-}$ compared to the data reported by Adam <i>et al.</i> ⁹⁸	50
Table 2: Chemical shifts (δ) and coupling constant (J) of the butadiene protons recorded in CD_2Cl_2 at 295 K. * defined from H_x resonance.....	52
Table 3: The energies and Gibbs free energies of conformers I.1 – I.3 calculated at the B3LYP/def2-TZVPP level of theory. The relative energies and Gibbs free energies of conformer I.2 and I.3 relative to conformer I.1 are also shown.	66
Table 4: Key bond distances and angles of the geometries of the complexes optimised at the M06/def2-TZVPP level of theory and from the crystal structure of conformer I.1	67
Table 5: Molar absorptivity of chloroplatinate complexes in different solvents and wavelengths.	75
Table 6: Chemical shifts of ^{195}Pt with correlated protons observed on 2D-HMQC- ^{195}Pt - ^1H NMR spectrum of photoreaction mixture of $[\text{Bu}_4\text{N}]_2[\text{PtCl}_6]$ in acetone.	100
Table 7: Chemical shifts of ^{195}Pt with correlated protons observed on 2D-HMQC- ^{195}Pt - ^1H NMR spectrum the mixture of $[\text{Pe}_4\text{N}]_2[\text{PtCl}_6]$ in acetone after photolysis. *irradiation under $h\nu > 305$ nm at room temperature, **irradiation under ambient light and heating under reflux.	107
Table 8: Theoretical conformers of platinum(II)-pentadiene complex; the chloro ligands were removed to simplify the structures.....	115
Table 9: The relative energies of conformers of pentadiene-platinum(II) complexes.	116
Table 10: Thermal behaviour of the ligands observed by POM and DSC.	180
Table 11: Thermal behaviour of the complexes observed by POM and DSC.	180
Table 12: Photophysical Properties of Palladium Complexes in CH_2Cl_2 Solution at 298 K.	185
Table 13: Photophysical Properties of Ligands in CH_2Cl_2 Solution at 298 K.	186
Table 14: Amount of starting materials for the photolysis of analogous hexachloroplatinate(IV) complexes.....	199

Table 15: Parameters of EPR experiments and observed g value in vary of samples.
..... 202

Table 16: Descriptions quantities of starting materials used and conditions of
reactions. 203

Acknowledgements

Praise to God for granting me the opportunity and strength to take this PhD study. While it has been a very challenging journey, I feel greatly grateful for having invaluable supports from various individuals.

My heartfelt gratitude goes to my supervisor, Duncan Bruce, on his willingness, time and his support in guiding and helping me continuously during my period of the study, especially during my writing time. Same appreciation goes to Jason Lynam who took the time to kindly supervise me and Julia in our second year.

To the Directorate General for Higher Education, Ministry of Research, Technology and Higher Education, Indonesia, for the sponsor and also to Department of Chemistry, Faculty of Mathematics and Science, Tanjungpura University, Kalimantan Barat, Indonesia.

My sincere thank to Pedro M. Aguiar and Heather Fish for their huge assistances in using NMR instrument, to Victor Chechik and Philip Groves for helps in the analysis of EPR and its discussion, Caroline Dessent and Edward Matthews for helps in photodissociation spectroscopy, Barbara Procacci and Naser Jasim who help in photolysis, Laurence Abbott for assistance in using the emission lifetime instrument, as well as Julia Sarju for help in GC-MS analysis. Thanks to Marsel Shafikov and Linda Mcallister who have done the quantum chemical calculations. For series of analysis, great appreciation is for, Graeme Mcallister for elemental analysis, Karl Heaton for mass spectrometry analysis, also Adrian Whitwood for conducting the Single-XRD and Alessio for carrying out the SAXS experiments.

Thank for Rachel, Alice and Sharon at the Graduate Office, whose administrative assistance is equally important in supporting my study as a PhD student.

Thank you very much for all labmates, who I cannot mention one by one, in the laboratory of Materials during 2012-2015 period. You all made lab times comfortable and enjoyable.

Thank to Indonesian friends who made my time in York feels so much like home; for my best friends, Julia Sarju and Dian Ekowati, who are always there to help, support and cherish me. I love you.

For my Mom, I cannot thank enough for your continuous love and pray. For my beloved brothers and sisters, Ulida, Triana, Valerie, Judika, Sahala, Elida, Verawaty and Josepina, thank you very much for supporting me all the time, especially during the period of this study. I love you all.

Author's Declaration

I declare that the work presented in this thesis is my own work unless otherwise stated or indicated by References. This work has not been presented for an award at this, or any other, University. The calculation of geometries and energies of the Pt-butadiene complex was conducted by Linda Mcallister, TDDFT calculations for hexachloroplatinate(IV) complex and geometries for Pt-pentadiene were carried out by Marsel Shafikov. All sources are acknowledged as References.

Chapter One: C–H Activation Chemistry

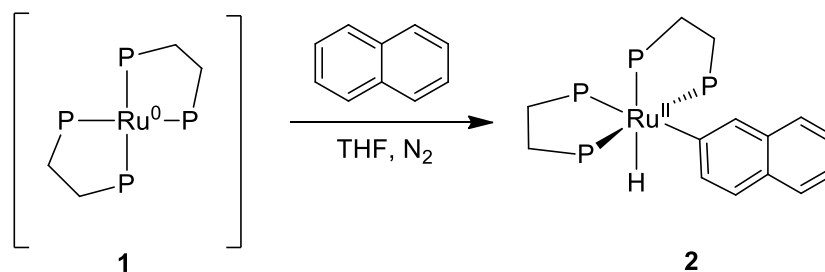
1.1. Introduction

Petroleum remains the main source of hydrocarbon used to produce materials, chemicals and energy. To reduce the dependency on this non-renewable resource, one of the strategies is to use more efficient methods so that less feedstock is required thus the search for efficient hydrocarbon activation and functionalisation under mild conditions with cleaner processing is still ongoing.¹⁻⁵

The carbon-hydrogen bond is strong thermodynamically and hence difficult to cleave heterolytically or homolytically. The homolytic C–H bond dissociation energy of H₃C–H, for instance, is 435 kJ mol⁻¹ compared to the C–O bond of H₃C–OH which is 383 kJ mol⁻¹ and the C–C bond of H₃C–CH₃ which is 368 kJ mol⁻¹.⁶ On energetic grounds alone, homolytic C–H activation presents an issue of selectivity and perhaps further reaction of the activated product, which may contain bonds such as C–C, C–O whose strength is lower than that of C–H. So there are two noticeable issues: selectivity and yield. Using transition-metal complexes to cleave C–H bonds catalytically has been applied in the selective preparation of products from hydrocarbons. The approach of C–H activation is different mechanistically from the homolytic pathway.⁷ Important considerations of the utilisation of the complexes are the choice of metal and ligand design. Ligands should be able to provide an active coordination site to facilitate the C–H activation, whereas metals are expected to have a variety of oxidation states available for the reaction.

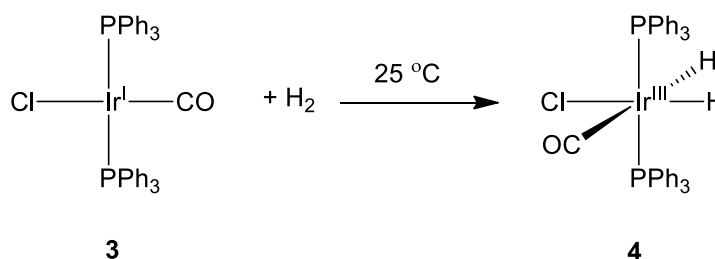
Transformation of hydrocarbons mediated by metal complexes generally takes place in two steps: (i) activation of the alkane where the metal complex inserts into C–H bond to form C–M, commonly *via* an oxidative addition pathway forming an activated metal-alkyl compound and (ii) functionalisation of the activated moiety to result in products and release of the metal complex.⁸

Chatt and Davidson first reported a C–H insertion involving an oxidative addition pathway in 1965. An addition of aromatic hydrocarbons such as naphthalene into a solution of $[\text{Ru}^{\text{II}}\text{Cl}_2(\text{dppe})_2]$ in THF gives a C–H activation product (**2**) *via* formation of an intermediate active species, $[\text{Ru}^0(\text{dppe})_2]$ (**1**) resulting from a reduction of $[\text{Ru}^{\text{II}}\text{Cl}_2(\text{dppe})_2]$ in a presence of tertiary phosphine. This active species then activates the C–H bond of naphthalene (Scheme 1).⁹



Scheme 1: The reaction of $[\text{Ru}^{\text{II}}\text{Cl}_2(\text{dppe})_2]$ with naphthalene reported by Chatt and Davidson.⁹

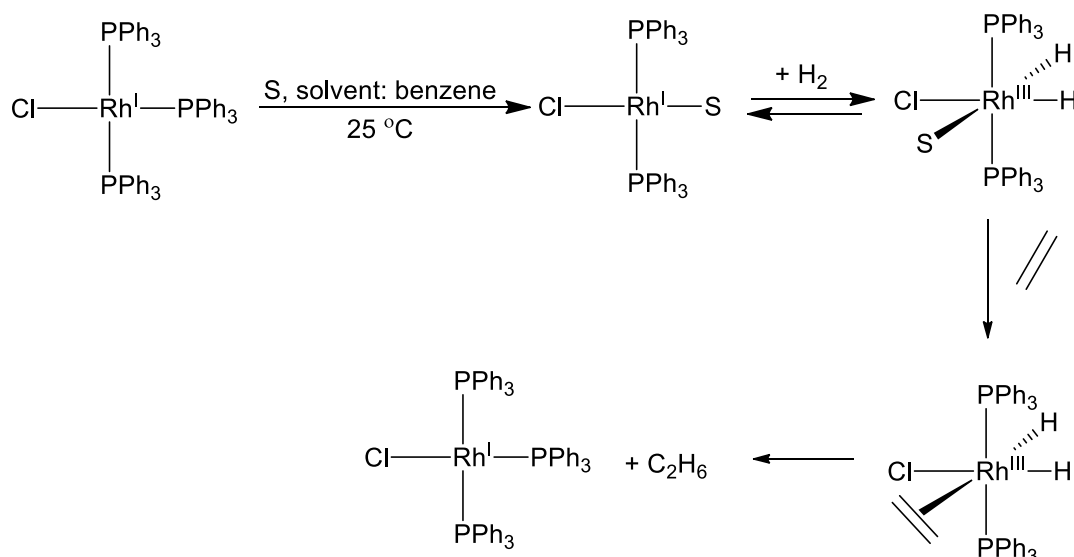
Earlier, Vaska had reported an example of oxidative addition in a reaction of H_2 with a square-planar iridium(I) complex, $[\text{Ir}^{\text{I}}\text{Cl}(\text{CO})(\text{PPh}_3)_2]$ (**3**) to give the octahedral, iridium(III) complex, $[\text{Ir}^{\text{III}}\text{Cl}(\text{H})_2(\text{CO})(\text{PPh}_3)_2]$ (**4**) (Scheme 2).¹⁰ This reaction was H–H activation, but it is relevant on the basis of bond strength as the C–H bond is comparable to H–H bond, thus the hydride coordination to the iridium(I) complex suggests that C–H activation through oxidative addition might be possible.



Scheme 2: Oxidation addition of hydrogen to an iridium(I) complex, reported by Vaska and DiLuzio.¹⁰

At around the same time, Wilkinson and co-workers reported the catalytic hydrogenation of olefins and alkynes mediated by the rhodium complexes,

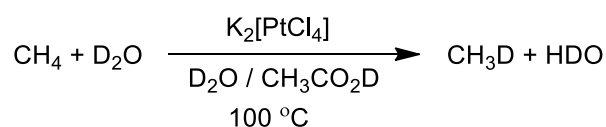
$[\text{Rh}^{\text{I}}\text{Cl}(\text{PPh}_3)_2(\text{S})]$ and $[\text{Rh}^{\text{III}}\text{Cl}(\text{H})_2(\text{PPh}_3)_2(\text{S})]$ (S = solvent: benzene or chloroform), demonstrating an oxidative addition / reductive elimination cycle (Scheme 3).¹¹



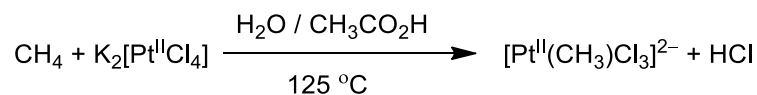
Scheme 3: Catalytic hydrogenation of olefins and alkynes mediated by $[\text{RhCl}(\text{PPh}_3)_3]$ -Wilkinson- in benzene or chloroform at 25 °C.¹¹

Metals in their lowest oxidation states, often with a d^{10} electronic configuration, are stabilised by electron-poor ligands whose unfilled orbitals overlap well, and have the correct symmetry and similar energy for interaction with the d^{10} orbitals of metal. This combination can lead to ligand addition to the complex with concomitant oxidation of the metal centre.

In another early example of C–H activation; Shilov reported H/D exchange catalysed by $[\text{PtCl}_4]^{2-}$ (Scheme 4) and followed this by further reports concerning activation and functionalisation of methane in a $[\text{PtCl}_4]^{2-}/[\text{PtCl}_6]^{2-}$ system giving methanol and methyl chloride (Scheme 5).¹²



Scheme 4: H/D exchange reaction in Shilov system, reported by Shilov and co-workers.¹²



Scheme 5: Activation of methane in Shilov system, reported by Shilov and co-workers.¹²

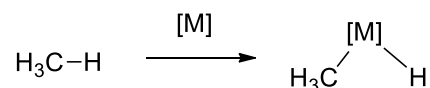
C–H activation has since been developed and utilised in the synthesis of many molecules such as pharmaceuticals and petrochemicals, agrochemicals and solvents. A summary of the role of metal complexes in C–H activation will be presenting after a discussion of C–H functionalisation.

1.2. C–H Bond Functionalisation

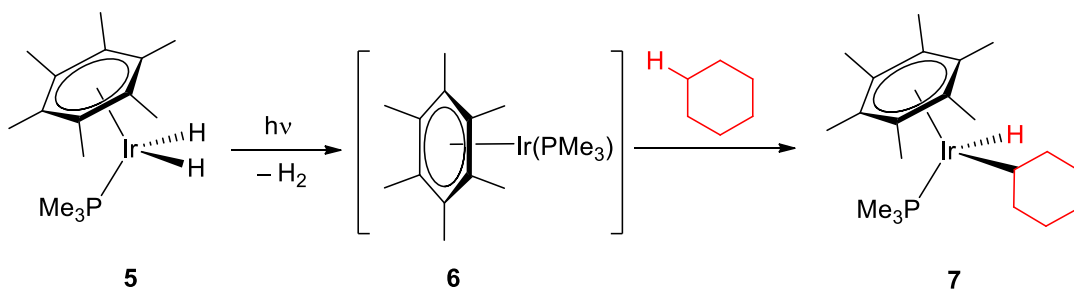
Functionalisation of C–H bonds can be classified into four major classes based on how the C–H bond is activated by the transition metal catalyst.^{4, 5} These are concerted oxidative addition, stepwise oxidative addition, electrophilic activation and functionalisation, and concerted metallation-deprotonation, which are discussed briefly below.

1.2.1. Concerted Oxidative Addition

In concerted oxidative addition, a low-valent transition metal inserts into a C–H bond with oxidation of the metal (Scheme 6).¹³⁻¹⁶ The example demonstrating this pathway is alkane activation by an iridium(I) complex (**6**) generated *in situ* by irradiation from an iridium(III) precursor (**5**) (Scheme 7).¹³

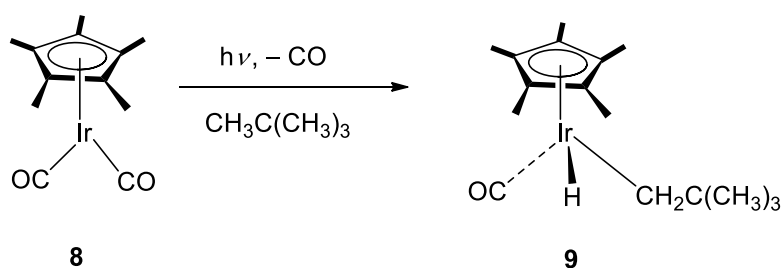


Scheme 6: General pathway of concerted oxidative addition.¹³



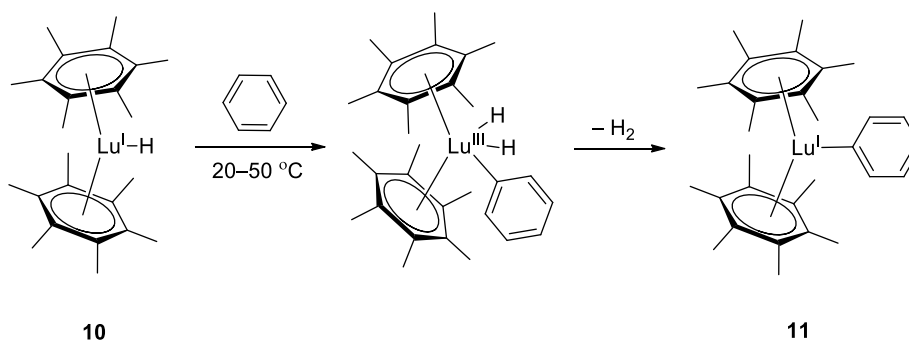
Scheme 7: The C–H insertion of iridium(I) complex through concerted oxidative addition as reported by Bergman and co-workers.¹³

In 1982, Graham and co-workers also reported an activation of neopentane and cyclohexane on the similar complex of iridium(I) *via* the same pathway (Scheme 8).¹⁷



Scheme 8: The C–H activation of neopentane on the complex of $[\text{Ir}(\eta^5\text{-C}_5\text{Me}_5)(\text{CO})_2]$, reported by Graham and co-workers.¹⁷

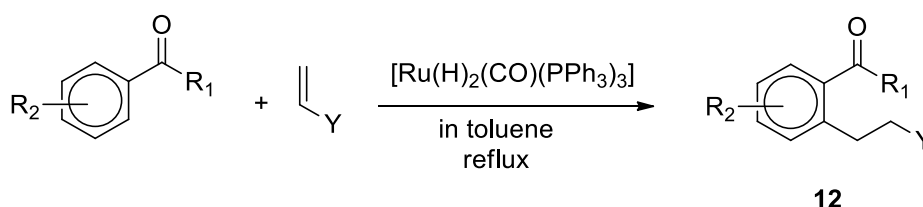
Simultaneously, Watson reported a C–H activation of benzene using a complex of lutetium(I) (**10**) under mild conditions suggesting the concerted oxidative addition pathway (Scheme 9).¹⁸



Scheme 9: C–H activation of benzene in $[\text{Lu}(\eta^5\text{-C}_5\text{Me}_5)\text{H}]$ complex, reported by Watson and co-workers.¹⁸

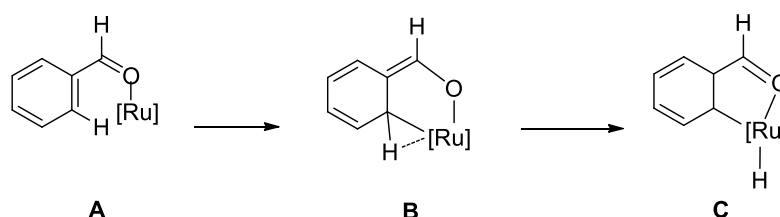
1.2.2. Stepwise Oxidative Addition

In stepwise oxidative addition C–H bond activation begins with nucleophilic attack of the metal at an electron-deficient carbon then hydrogen from the carbon atom migrates to the metal centre. This functionalisation is mediated by low-valent transition metals; for example, *ortho*-selective addition of aromatic ketones to a double bond of olefins catalysed by $[\text{Ru}(\text{H})_2(\text{CO})(\text{PPh}_3)_3]$ results in a C–H/olefin coupling product (**12**) (Scheme 10).¹⁹



Scheme 10: An example of stepwise oxidative addition of aromatic ketones catalysed by $[\text{Ru}(\text{H})_2(\text{CO})(\text{PPh}_3)_3]$, reported by Murai and co-workers.¹⁹

A study of the mechanism of the reaction experimentally as well as theoretically demonstrated that C–H activation on the aromatic ketone is promoted by the carbonyl functional group where the active species, the low-valent transition metal (**A**) coordinates to the carbonyl oxygen while increasing the oxidation state of the metal by two with an agostic interaction to the *ortho* hydrogen atom (**B**). It then is followed by migration of hydrogen at the *ortho* position to the metal centre (**C**) (Scheme 11).^{20, 21} This mechanism contributes to the selectivity of C–H activation at *ortho* positions where the closest C–H bond to the metal centre is activated preferentially as dictated by oxygen coordination.²⁰



Scheme 11: Proposed mechanism of stepwise oxidative addition of aromatic ketones catalysed by $[\text{Ru}(\text{H})_2(\text{CO})(\text{PPh}_3)_3]$, reported by Matsubara *et al.*²⁰

1.2.3. Electrophilic Activation and Functionalisation

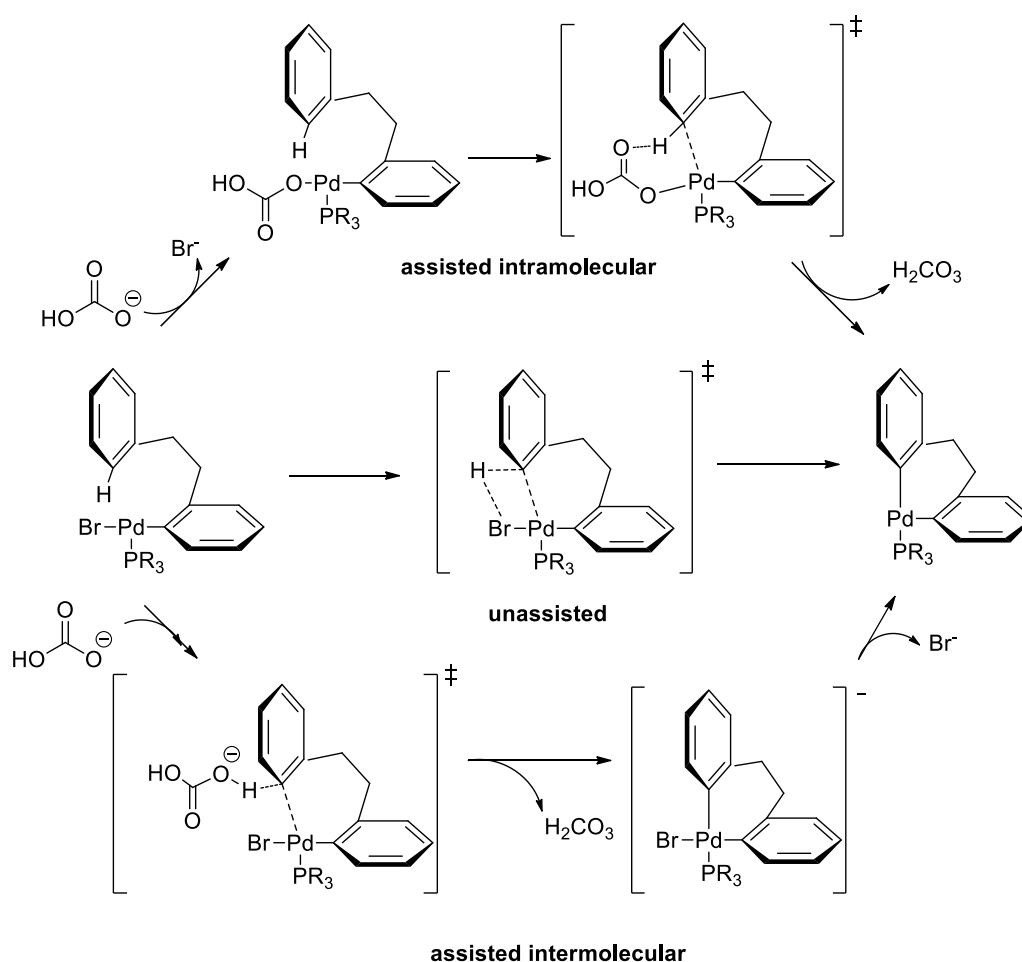
This was recognised first in methane activation catalysed by $[\text{PtCl}_4]^{2-}$ in acidic aqueous media in the presence of $[\text{PtCl}_6]^{2-}$ giving methanol or methyl chloride as reported by Shilov in 1972.²² The activation is believed to follow an electrophilic pathway where electrophilic metals seek out an electron-rich C–H bond. Although it was not fully understood at that time, the authors proposed a mechanism that consisted of three parts, namely C–H insertion to the catalyst, $[\text{PtCl}_4]^{2-}$ resulting in an alkyl-Pt^{II} species; oxidation of the alkyl-Pt^{II} moiety by $[\text{PtCl}_6]^{2-}$ giving an alkyl-Pt^{IV} complex and then functionalisation of the alkyl-Pt^{IV} complex through nucleophilic attack yielding methanol or methyl chloride while releasing the Pt^{II} catalyst (Scheme 30). Occasionally, the reaction of higher alkanes yielded the corresponded alkene through a β -H abstraction pathway. This system became known as Shilov chemistry.^{16, 23-26} The proposed mechanism, especially the insertion and oxidation steps, was debatable and studies to understand the mechanism as well as to make the system catalytic have been carried out by researchers such as Bercaw and co-workers²⁷; Periana and co-workers.²⁴ This will be discussed in more detail later in Section 1.4.

Lately, C–H activation and functionalisation in cationic main group systems, such as thallium(III), and lead(IV) have been reported. It was observed that $[\text{Tl}(\text{OOCF}_3)_3]$ as well as $[\text{Pb}(\text{OOCF}_3)_4]$ activate methane, ethane, and propane stoichiometrically in trifluoroacetic acid, yielding the corresponding ester of the hydrocarbon. A study of the mechanism carried out suggested the activation also proceeds through an electrophilic pathway giving metal-alkyl moiety as intermediate.²⁸

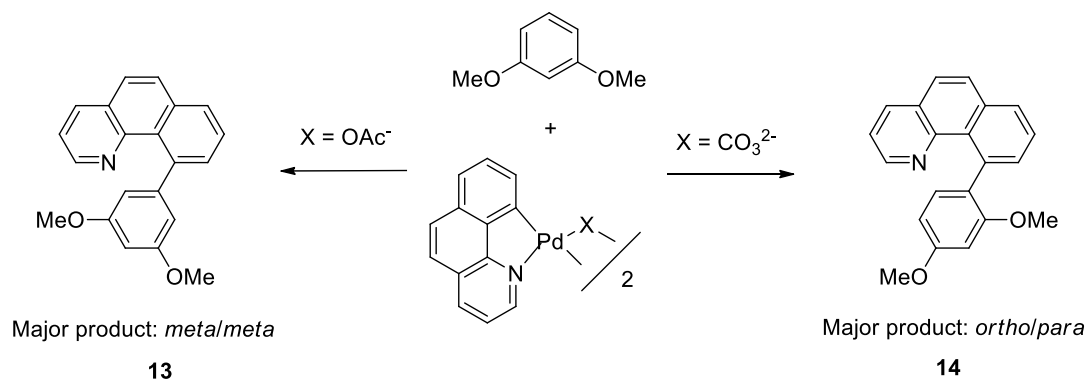
1.2.4. Concerted Metallation–Deprotonation (CMD)

In this mechanism, C–H bond functionalisation is initiated through proton abstraction from the hydrocarbon by a base while metal insertion is taking place. The mechanism involves simultaneous and selective C–H bond cleavage and deprotonation by base, such as carbonate, acetate or related basic ligand, whereas

products result from reductive elimination of the transformed moiety.²⁹⁻³⁴ For example, regioselective intramolecular arylation of substituted bromobenzyl diarylmethanes catalysed by a palladium complex in the presence of K_2CO_3 proceeds through simultaneous proton abstraction and metal insertion. The deprotonation can proceed *via* an assisted intramolecular or assisted intermolecular or assisted pathway (Scheme 12). The selectivity is directed by electron-withdrawing substituents *ortho* to the reacting site on the aromatic ring.²⁹ The same mechanism was also observed in a site-selective, oxidative coupling of benzoquinoline with 1,3-dimethoxybenzene; the selectivity depends on the base (Scheme 13).³³



Scheme 12: The deprotonation mechanism *via* an assisted intramolecular (upper) or assisted intermolecular (lower) or unassisted (middle) pathways.²⁹



Scheme 13: The oxidative coupling of benzoquinoline with 1,3-dimethoxybenzene catalysed by the palladium(II) complex proceeds through the CMD mechanism which site selective depends on the anion, reported by Sanhueza *et al.*³³

1.3. Examples of C–H Activation Chemistry

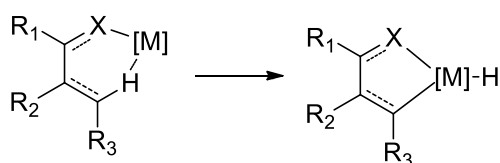
As mentioned earlier, the studies of C–H activation at metal complexes and its application to chemical synthesis have developed quickly. Homolytic C–H cleavage commonly requires harsh conditions to overcome C–H bond strength; however methods involving transition-metal complexes have proceeded under mild conditions demonstrating the significant role of transition-metal. Here are some examples of metal complex reactions.

1.3.1. Rhodium complexes

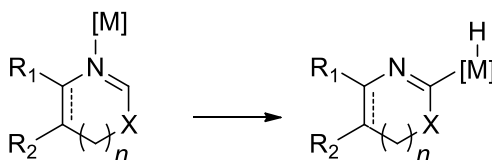
Rhodium complexes have been known to catalyse regioselective C–C bond formation *via* functionalisation of activated C–H bonds. The reactions are: alkylation of olefins, arenes and *N*-heterocycles, alkenylation of olefins and arenes, and arylation of arenes as well as *N*-heterocycles. The rhodium catalyst has also been modified to fit the reactions and to obtain desired products therefore the rhodium catalyst system has been widely utilised in organic synthesis; the reports were reviewed.³⁵⁻³⁸ Wilkinson's catalyst appears to be the best choice for C–H activation of substrates of pyridine derivatives.^{37, 38} The pyridyl group is the key for the pre-coordination onto the metal centre initiating intramolecular as well as intermolecular C–H activation and directing *ortho*-selectivity.

The activation commonly is started from coordination of the functional group to the metal centre. Then the coordinated intermediate complex can undergo C–H insertion on two different pathways based on the way the functional groups behaved. The group can either chelate the metal centre leading to metallacycle formation or can undergo C–H insertion without metallacyclisation where the functional group stabilises the formation of metal-carbon at an approximate position. In the metallacyclic pathway, the chelation helps the C–H activation and directs the functionalisation at a selective position which in a majority of known reactions is at *ortho* position (Scheme 14).³⁵

1. Chelation-assisted C–H activation



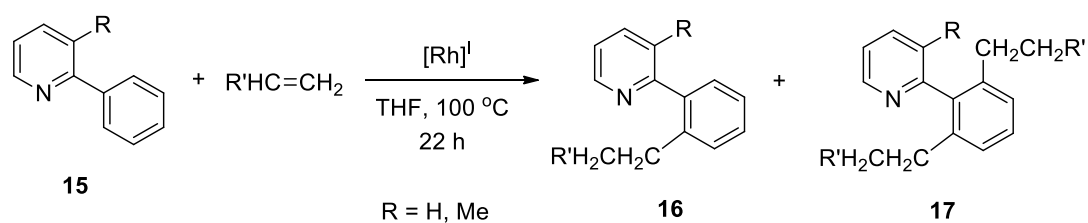
2. C–H Activation of *N*-heterocycles



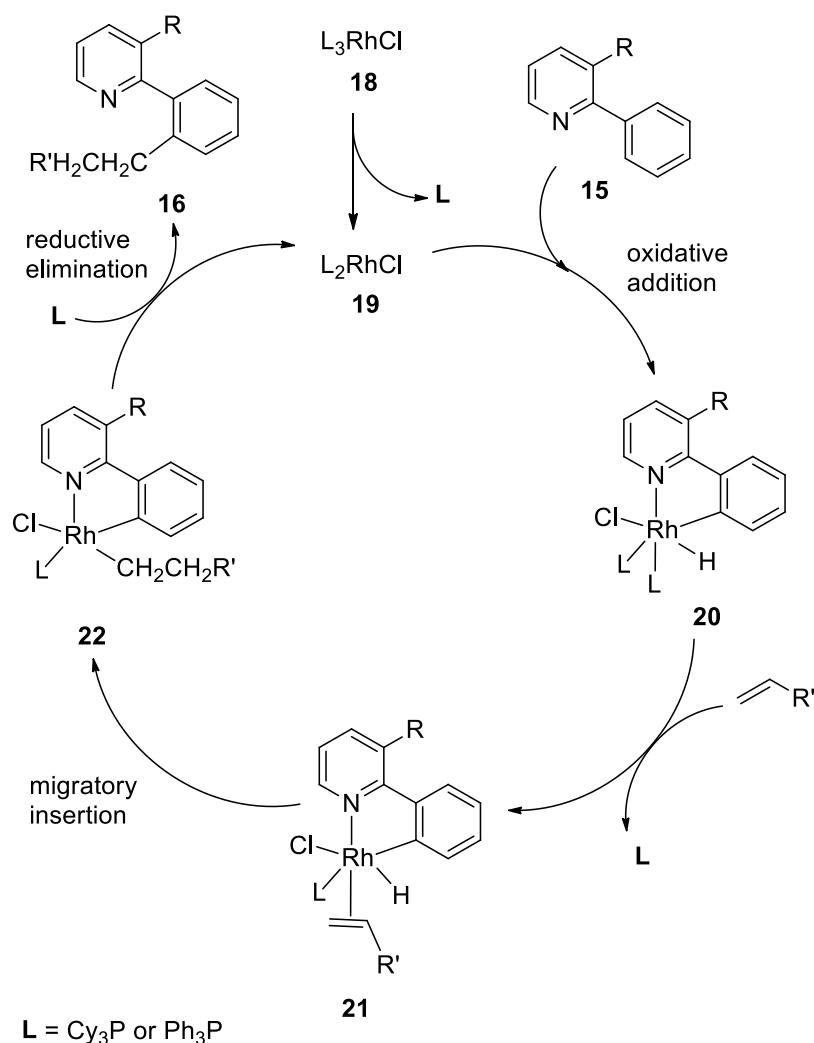
Scheme 14: General pathways of C–H insertion of hydrocarbons into the rhodium catalyst directed by functional groups.³⁵

Lim and Kang reported a C–H alkylation of phenylpyridines (**15**) using the dimeric rhodium catalyst, di- μ -chlorobis(cyclooctadiene)-dirhodium(I), ([RhCl(C₈H₁₄)₂]₂), in the presence of tricyclohexylphosphine, involving the chelation-assisted pathway (Scheme 15). The alkylation occurs selectively at an *ortho* position of the phenyl ring directed by a pyridyl group. A mechanistic study suggests that the nitrogen group binds to rhodium then activates the *ortho*-C–H bond of the phenyl group to form a five-membered metallacyclic ring intermediate with a hydride bound to rhodium (**20**). Then an olefin coordinates to the intermediate complex followed by a migratory insertion to give an alkyl-rhodium complex (**22**). Reductive elimination of the alkyl moiety releases the rhodium catalyst while the alkylated product (**16**) is

obtained (Scheme 16).³⁹ Further investigations made by the same authors showed both electronic and steric effects contribute to both the reactivity and selectivity.⁴⁰



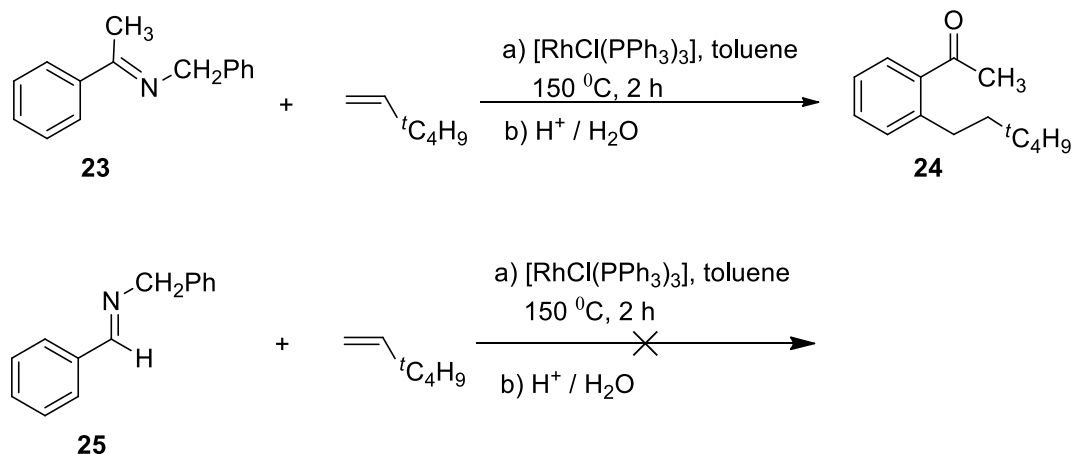
Scheme 15: The C–H alkylation of phenyl pyridine using rhodium catalyst, $[\text{RhCl}(\text{C}_8\text{H}_{14})_2]_2$, in the presence of tricyclophosphine, reported by Lim and Kang, 1994.³⁹



Scheme 16: The proposed mechanism of the C–H alkylation of 2-phenylpyridine using rhodium catalyst, reported by Lim and Kang, 1994.³⁹

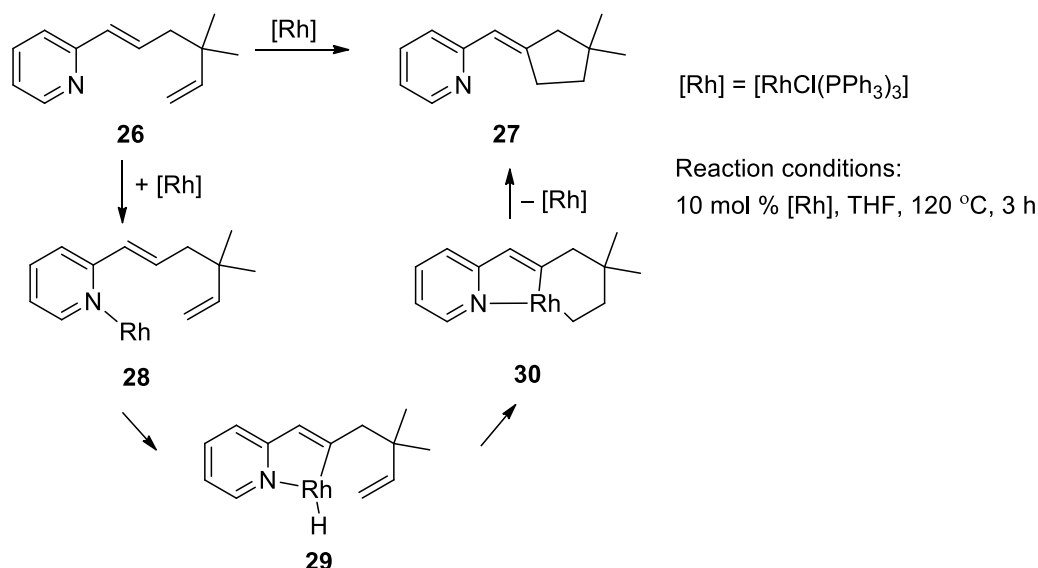
Jun and co-workers in 2000 reported that *ortho*-alkylation of ketimines with olefins catalysed by Wilkinson's catalyst proceeds successfully through a chelation-

assisted route provided by the substrates. However, under the same conditions, alkylation of aldimines fails, as in the absence of the alkyl groups, the chelation is sterically unfavourable (Scheme 17). Instead, the alkylation proceeds in an assistance of pyridine derivatives, namely 2-amino-3-picoline, by taking place a hydroacylation of aldimines prior to the alkylation.⁴¹



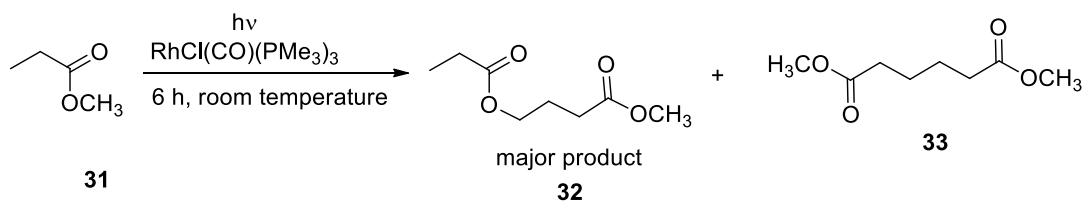
Scheme 17: The reaction of *ortho*-alkylation of ketimines with olefin catalysed by Wilkinson's catalyst whereas the reaction of aldimines does not proceed as reported by Jun *et al.*⁴¹

Intramolecular olefin coupling of pyridyl-substituted 1,5-dienes catalysed by Wilkinson's catalyst was also reported. A proposed mechanism describing the activation of pyridyl-substituted 1,5-dienes is drawn in Scheme 18. The activation is initiated by pyridyl coordination to give **28**, followed by the C–H activation at the vinylic position giving intermediate **29**. This activation promotes the intramolecular insertion of the terminal double bond to result in metallacycle **30**. Reductive elimination of **30** releases the catalyst and generating product **27**.⁴²

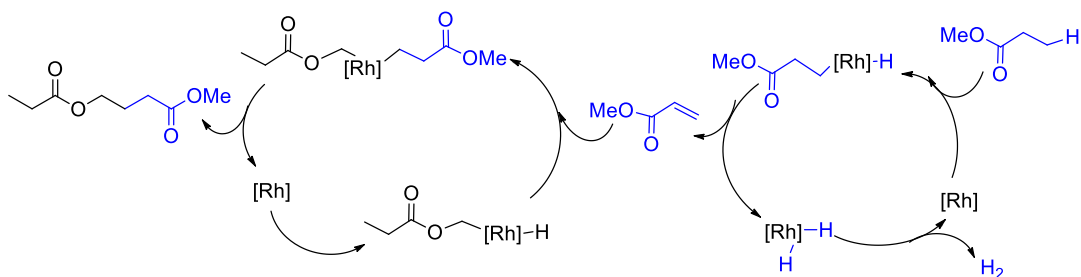


Scheme 18: The proposed mechanism of the intramolecular olefin coupling catalysed by Wilkinson's catalyst as reported by Fujii *et al.*⁴²

The rhodium(I) complex, $[RhCl(CO)(PMe_3)_2]$ was found to catalyse dehydrogenation of methyl propionate under irradiation, at room temperature to afford a head-to-tail dimerisation product of methyl 4-propionyloxybutyrate with a small amount of dimethyl adipate at room temperature (Scheme 19). The photo-dehydrogenation presumably generates methyl acrylate which is proposed to be an intermediate substrate in the rhodium-catalysed alkylation of methyl propionate (Scheme 20).⁴³ The reaction demonstrated the ability of the rhodium complex to insert into the C–H bonds at different positions namely methyl attached to the oxygen atom and the terminal carbon of the propyl chain in addition to the olefin insertion during the dimerisation.



Scheme 19: The photo-dimerisation reaction of methyl propionate catalysed by $[RhCl(CO)(PMe_3)_2]$, reported by Sakakura *et al.*⁴³



Scheme 20: The proposed mechanism of the photo-dimerisation of methyl propionate catalysed by $[\text{RhCl}(\text{CO})(\text{PMe}_3)_2]$, reported by Sakakura *et al.*⁴³

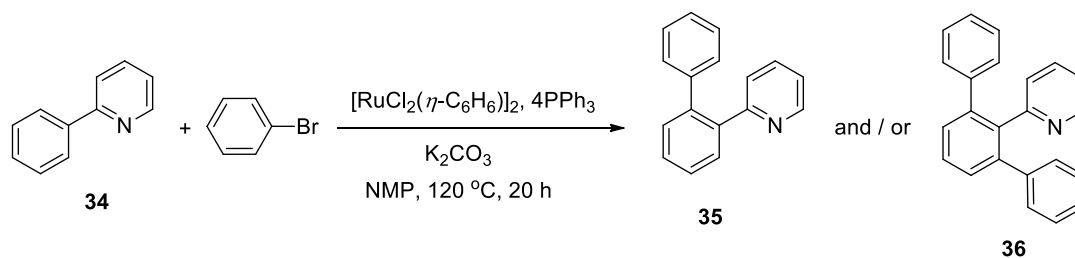
There have been many studies conducted to employ rhodium complexes to carry out synthesis of organic molecules as well as to accommodate controlled selectivity by providing steric hindrance or appropriate geometry in which mechanistic studies guide the developments.³⁵

1.3.2. Ruthenium Complexes

Seeking a slightly cheaper metal alternative, researchers have been motivated to develop methodology using ruthenium complexes. This follows a key early example reported by the Murai, Chatani and Kakiuchi group on formation of C–C bonds from a reaction of aromatic compounds with olefin catalysed by the ruthenium(II) complex, $[\text{Ru}(\text{H})_2(\text{CO})(\text{PPh}_3)_3]$ where the precursor is the ruthenium(0) complex, $[\text{Ru}(\text{CO})(\text{PPh}_3)_3]$. (Scheme 10).¹⁹

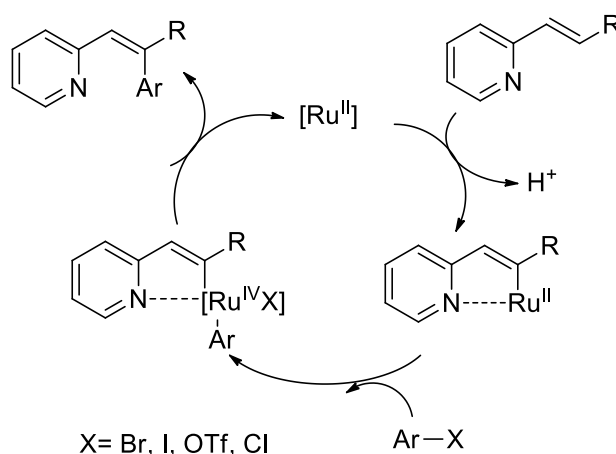
Furthermore, a reaction using a more stable precursor, the ruthenium(II) complex, $[\text{RuCl}_2(\text{C}_6\text{H}_6)]_2$ was reported to catalyse a direct *ortho*-arylation of 2-pyridylbenzene using aryl halides in the presence of K_2CO_3 and NMP (*N*-methylpyrrolidinone). The reaction of substituted 2-pyridylarenes with one equivalent of bromobenzene results in monoarylated product mixed with a diarylated product. The exclusive second arylation occurs when an excess (three equivalent) of bromobenzene is reacted with the substrate, demonstrating a steric hindrance (Scheme 21).^{44, 45} Oi and co-workers extended a scope of bromobenzenes to those containing electron-donating group as well as electron-withdrawing group, and 2-bromonaphthalene; the arylation reactions afford coupled product.⁴⁶ With a variety of directing groups

such as imidazoles, and thiazoles, the reactions are also taken place with good yields.⁴⁷ Using other ruthenium(II) catalyst precursors, such as $[\text{RuCl}_2(\text{PPh}_3)_3]$, and $[\text{RuCl}_2(\text{COD})]_n/4 \text{ PPh}_3$, the reaction shows similar activity.³⁴



Scheme 21: Direct arylation of 2-pyridylbenzene catalysed by $[\text{RuCl}_2(\text{C}_6\text{H}_6)_2]_2$ as reported by Oi *et al.*⁴⁴

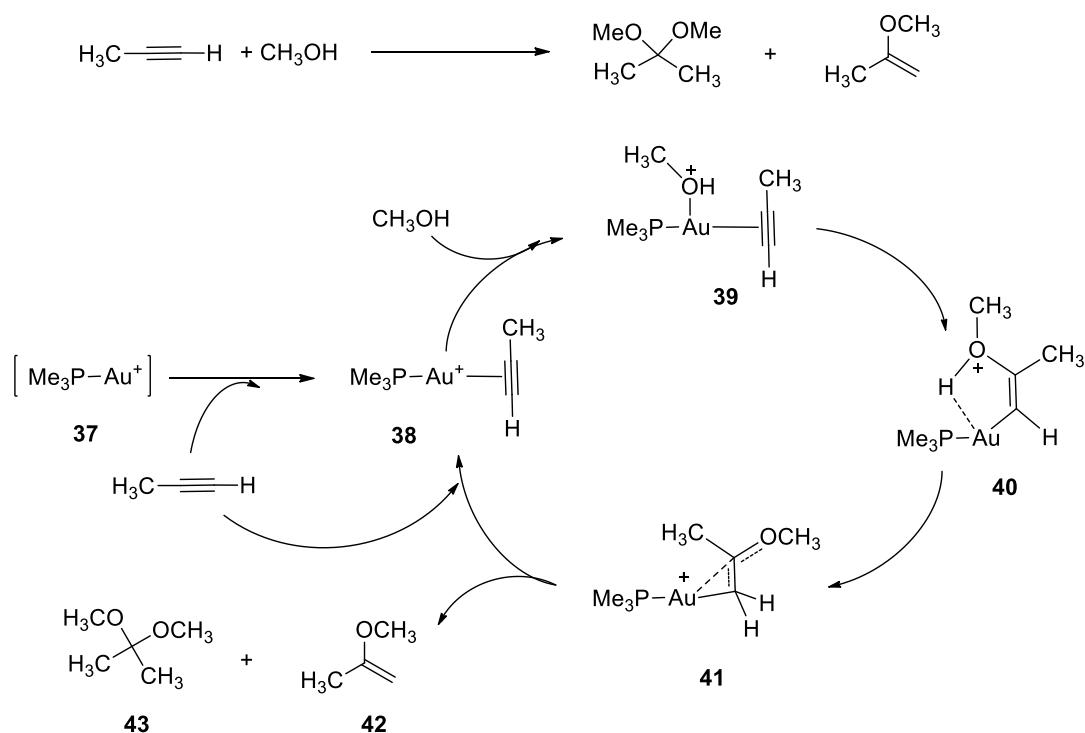
A proposed mechanism for the arylation of phenylpyridine derivatives is shown in Scheme 22. The first step is coordination of ruthenium to the substrates *via* a deprotonation, assisted by a base, with coordination of the pyridyl group into the metal centre. Then the second step is oxidative addition of the ruthenium(II) complex to a ruthenium(IV) complex while an insertion of phenyl halide onto the metal centre. Reductive elimination of the complex gives an arylation product and regenerates the catalyst.³⁴ In terms of the C–H activation assisted by a base on the proton abstraction, appears to be mechanistically similar to the pathway by palladium(II) complexes in C–C bond formation.²⁹⁻³³



Scheme 22: The proposed mechanism of arylation of phenylpyridines using phenyl halides catalysed by ruthenium(II) complex, reported by Arockiam, *et al.*³⁴

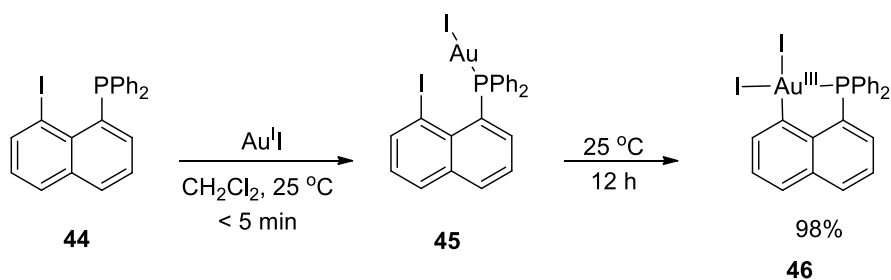
1.3.3. Gold Complexes

The role of gold in organometallic reactions was widely established only in the late 1990s after discovery of the carbophilic properties of gold(I). This property was recognised when a reaction of alkynes with methanol afforded dimethoxy alkane in the presence of gold(I) demonstrating an activation and functionalisation of C–C π -bonds (Scheme 23).⁴⁸ The reaction had been earlier observed using gold(III), Na[AuCl₄] but the metal quickly reduced to inactive gold(0)⁴⁹ whereas in the gold(I) system, [Au(CH₃)(PPh₃)] with CH₃SO₃H, the catalyst was found to be very efficient without the reduction of gold. In the system, it is observed that ligands, acid, and the anion play important roles in the catalytic activity. Supported by ³¹P NMR spectroscopy and *ab initio* calculations, a reaction mechanism was proposed (Scheme 23). The cycle begins with coordination of the metal centre to the alkyne followed by associative coordination of oxygen to the gold(I)-propyne complex (**38**) to result in the intermediate **39** which rearranged to form compound **40**. 1,3-Hydrogen migration (deprotonation-re-protonation) gives compound **41** and the products (**42** and **43**) is obtained by ligand exchange to release the catalyst back into the system.⁴⁸



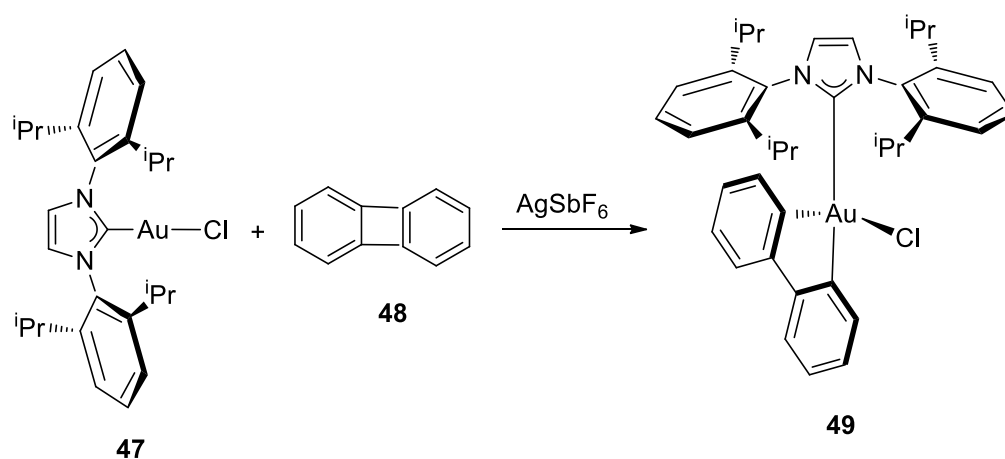
Scheme 23: The reaction mechanism of alkynes addition with methanol catalysed by $[\text{Au}(\text{CH}_3)(\text{PPh}_3)]$, reported by Teles *et al.*⁴⁸

More recently, reactions demonstrating the ability of gold(I) complexes to undergo a spontaneous oxidative addition were reported.⁵⁰ The reaction is assisted by a chelating phosphine ligand which spontaneously coordinated to the gold centre which then underwent an R–X insertion (R= aryl, X= I, Br) *via* oxidative addition (Scheme 24). The potential of the phosphine ligands to direct the coordination of gold(I) was reported previously by the same group and becomes an inspiration for such reactions involving the phosphine-directed oxidative addition to gold(I) in R–X activation.^{51, 52}



Scheme 24: Oxidative addition of R–X (R = Ar, X = I, Br) to gold(I) as reported by Bourissou and co-workers.⁵⁰

Subsequently in 2015, Teles,⁵³ mentioned a breakthrough in gold chemistry where an unusual substrate, biphenylene (**48**), inserts a [(NHC)-Au^I-Cl] complex (**47**) *via* an oxidative addition to result in a stable biphenyl-gold(III) complex (**49**) (Scheme 25).⁵⁴ Both, the substrates and the gold(I) complex play significant roles in the oxidative addition reaction. The gold(I) complex is energetically and geometrically prepared for an easy oxidative addition as it is coordinatively unsaturated and there is the bite angle of a chelating ligand. The substrate, biphenylene, can be employed as a precursor of benzene. Thus, the energy of hydrogenation of biphenylene to biphenyl is high (235 kJ mol⁻¹) but the enthalpy of hydrogenation of biphenyl to form two moles of benzene is less than 1 kJ mol⁻¹, so that once the biphenyl is generated, the formation of benzene through hydrogenation will be favoured energetically. This demonstrates that biphenyl derivatives may be a good precursor for benzene substrates. Additionally, oxidative addition of the gold(I) by biphenylene generates a stable complex which does not undergo a subsequent reductive elimination.⁵³

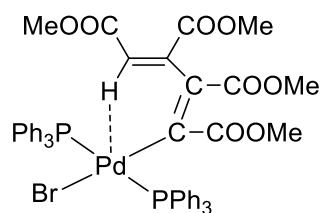


Scheme 25: The oxidative addition of a [(NHC)-Au^I-Cl] complex by biphenylene resulting in a stable biphenyl-gold(III) complex, reported by Toste and co-workers.⁵⁴

1.3.4. Palladium Complexes

The C–H activation using palladium complexes was perhaps first realised when some palladium complexes bound through a C–H agostic interaction to C–H, *e.g.*,

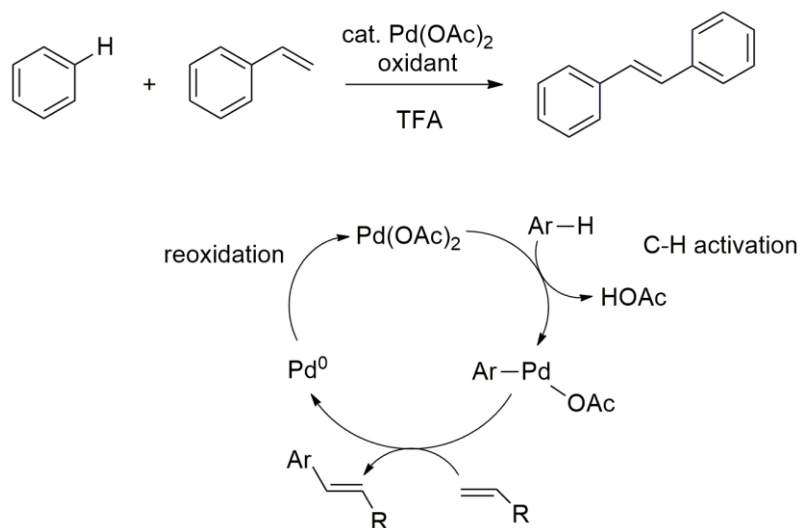
complex **50**, were isolated and crystallographic analysed.⁵⁵ The CH group was then established as a ligand to a transition metal and was considered to undergo an oxidative addition of C–H bonds to a metal.⁵⁶



50

Scheme 26: Molecular structure of palladium(II) complex coordinating with CH reported by Maitlis and co-workers.⁵⁵

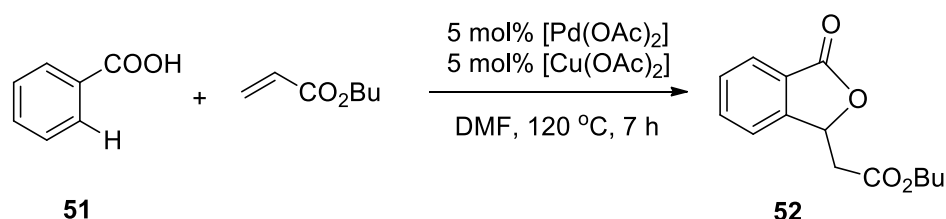
One of the earliest examples of C–H activation involving the palladium complex is the activation of benzene by $[\text{Pd}(\text{OAc})_2]$ followed by alkene insertion and β -hydride elimination to result in olefinated arene derivatives (Scheme 27).⁵⁷ The requirement for a large excess of the substrate and the lack of regioselective control limits the scope and applicability of this reaction.



Scheme 27: Olefination of arenes catalysed by palladium(II) complex in $\text{Pd}^{\text{II}}/\text{Pd}^0$ catalytic cycle reported by Moritani and Fujiwara.⁵⁷

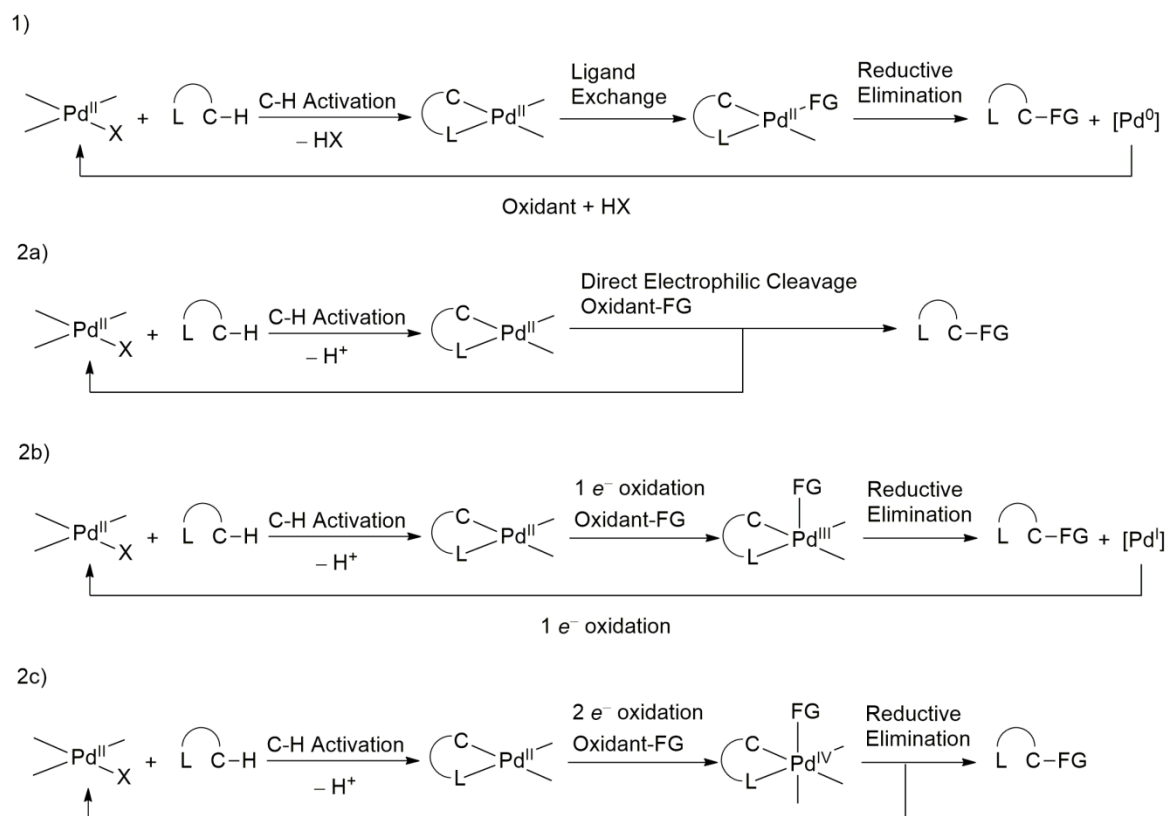
A similar method using benzoic acid as a substrate (Scheme 28) demonstrated an *ortho*-selective and effective reaction suggesting an important role of the acyl functional group to direct regioselectivity. The authors investigated the reaction

with a wider range of substrates containing nitrogen and oxygen atoms such as *N*-(arylsulfonyl) derivatives, naphthoic acid, and benzoic acid to prove that the reaction is promoted by acidic directing groups to initiate *ortho*-palladation in which C–H insertion occurs at the *ortho* position towards the directing group, to result in palladated complexes.⁵⁸⁻⁶⁰ That observation is one the inspirations for further development in achieving regioselective reactions involving palladium catalysts.⁶¹



Scheme 28: Directed *ortho* olefination of benzoic acid reported by Miura *et al.*⁶⁰

The palladated complexes can then be functionalised *via* two different pathways (Scheme 29). Firstly, the functionalisation can take place through a reductive process, either a reaction of reductive elimination, β -hydride elimination or deprotonation to afford products and Pd⁰. The palladium(0) is then re-oxidised to the palladium(II) catalyst. Secondly, the functionalisation might involve an electrophilic reagent. The reaction can proceed through direct electrophilic cleavage of the Pd–C bond in which the oxidation state of the metal centre does not change and the catalyst is regenerated directly without a further oxidation step while products are obtained. The functionalisation can also take place by a one-electron or a two-electron oxidation of the intermediate palladacycle complex. Products are obtained through a reductive elimination.⁶²



Scheme 29: Functionalisation Mechanism of Cyclopalladated Complex through 1) Reductive Elimination ($\text{Pd}^{\text{II}}/\text{Pd}^0$ Catalytic Cycle), 2) Electrophilic Cleavage: a) Direct, b) One-Electron Oxidation, c) Two-Electron Oxidation. FG = functional group.⁶²

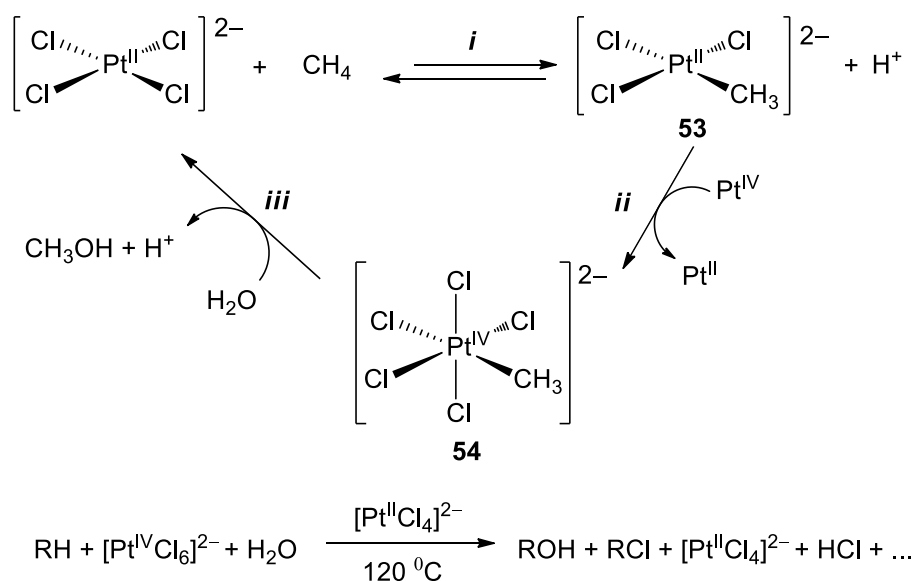
1.4. Shilov Chemistry and Electrophilic C–H Activation

1.4.1. Shilov Chemistry

The first discovery demonstrating C–H activation in a homogenous system using a platinum complex was when Garnett and Hodges, in the 1960s, observed a H/D exchange of aromatic hydrocarbons in a system of $\text{CH}_3\text{COOD}/\text{D}_2\text{O}$ and $\text{K}_2[\text{Pt}^{\text{II}}\text{Cl}_4]^{2-}$ or $\text{Na}_2[\text{Pt}^{\text{II}}\text{Cl}_4]^{2-}$.⁶³ The isotope exchange is a diagnostic experiment of the carbon–hydrogen insertion.

Inspired by this observation, Shilov and co-workers carried out and reported the H/D exchange of alkanes under the similar conditions. Furthermore, work revealing the C–H activation and functionalisation of methane under the same conditions in

the presence of $[\text{PtCl}_6]^{2-}$ was reported.¹² After carrying out a mechanistic study regarding the H/D exchange and the methane activation, Shilov and co-workers proposed a mechanism comprising three parts that described the reaction as a catalytic cycle (Scheme 30). Firstly, there is C–H insertion into an active species of platinum, $[\text{Pt}^{\text{II}}\text{Cl}_4]^{2-}$ to give the alkyl-platinum(II) complex **53** (Scheme 30, *i*). The active species was proposed to be generated under aqueous acidic conditions; the second part involved an oxidation of the alkyl-platinum(II) moiety to the alkyl-platinum(IV) complex **54** where the oxidising agent in this system is $[\text{PtCl}_6]^{2-}$ (Scheme 30, *ii*); the last part is a functionalisation of the activated alkyl-platinum(IV) *via* nucleophilic attack by H_2O or HCl to give the major products as methanol or methyl chloride while releasing the $[\text{PtCl}_4]^{2-}$ catalyst (Scheme 30, *iii*).¹²



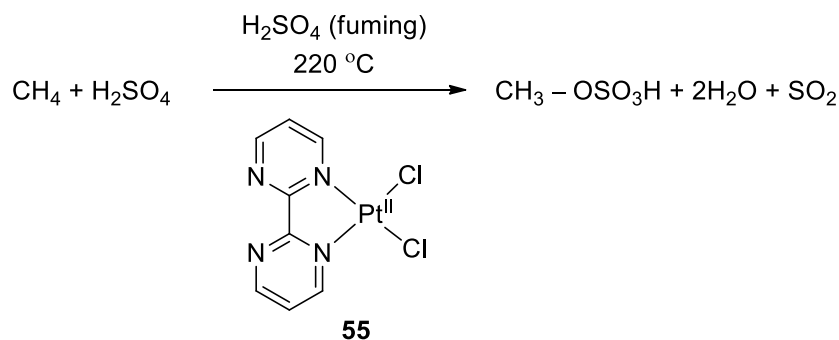
Scheme 30: The proposed mechanism of methane activation in the Shilov's system.¹²

Bercaw and co-workers have further studied the mechanism proposed by Shilov.²⁷ In the first step, although the mechanism is still not entirely understood, it is suggested that the C–H insertion involves an electrophilic activation where the alkane σ -coordinates to the platinum centre along with a direct loss of proton.^{7, 26,}

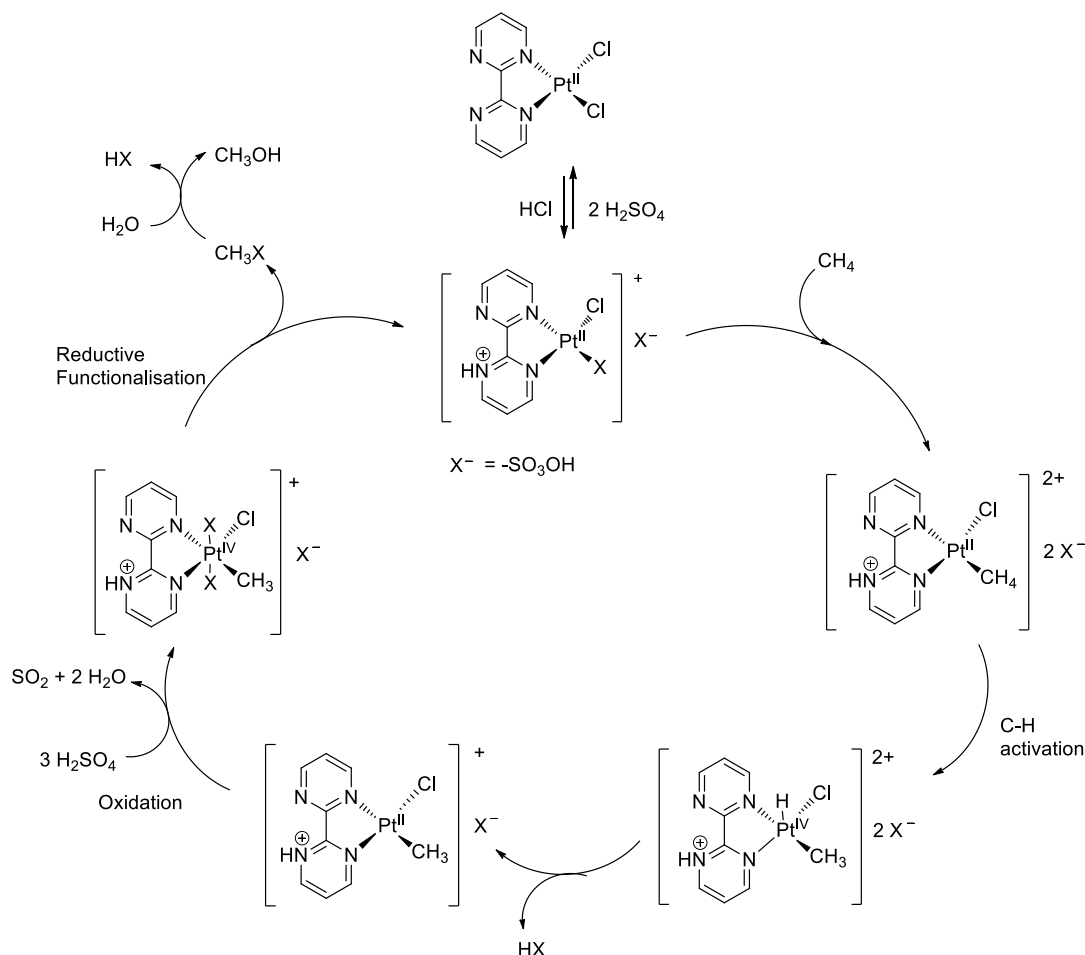
27, 64

While the first part, the C–H insertion, remained unclear, Bercaw's group succeeded in providing further detail about the second and the third parts. Thus, in the third part, it is believed that the functionalisation of the methyl–platinum(IV) moiety occurred *via* nucleophilic attack by water at the Pt–C bonds, confirming the mechanism proposed by Shilov. In the second part, the oxidation, an experiment using ^{195}Pt -isotope enrichment demonstrated that the formation of Pt^{IV} –alkyl from Pt^{II} –alkyl intermediate proceeded through an electron transfer rather than an alkyl transfer. This implies that $[\text{PtCl}_6]^{2-}$ was only a simple oxidising agent which can be replaced by other oxidants.²⁷ Attempts to search for an alternative for the oxidants have been reported.^{24, 27}

Linked with the Shilov's system, Periana and co-workers have reported an efficient approach to activation and functionalisation of alkanes by utilisation of concentrated sulfuric acid as the oxidant, replacing the $[\text{PtCl}_6]^{2-}$, and modification of the platinum(II) catalyst so that is viable in the strong acid condition under heating and is soluble in sulfuric acid.²⁴ The complex of $[\text{PtCl}_2(\text{NH}_3)_2]$ (both isomers, *trans* and *cis*) was found to be soluble in H_2SO_4 and capable of catalysing the functionalisation of CH_4 producing CH_3OH . However, the catalyst is unstable as precipitation of PtCl_2 was observed, which contributed to a low turnover (less than 20). To tackle the stability issue, a platinum complex with chelating *N*-ligands (**54**) was made and found to activate CH_4 effectively with high yield (Scheme 31). The complex stability stems from an oxidative dissolution of Pt^0 by H_2SO_4 facilitated by the 2,2'-bipyrimidine ligand as an uncoordinated nitrogen becomes protonated in the acid medium. In fact, the complex is still stable under the reaction conditions, contributing to the high catalytic activity and implying the important role of the bipyrimidine ligand. This system is known as the Periana-Catalytica System.⁷ The postulated mechanism resembles the Shilov system (Scheme 32), the difference being that the methyl-platinum(II) complex is oxidised by sulfuric acid instead of $[\text{PtCl}_6]^{2-}$, followed by the reductive functionalisation to afford methyl bisulfate. The bisulfate group protects the ester from further oxidation.²⁴



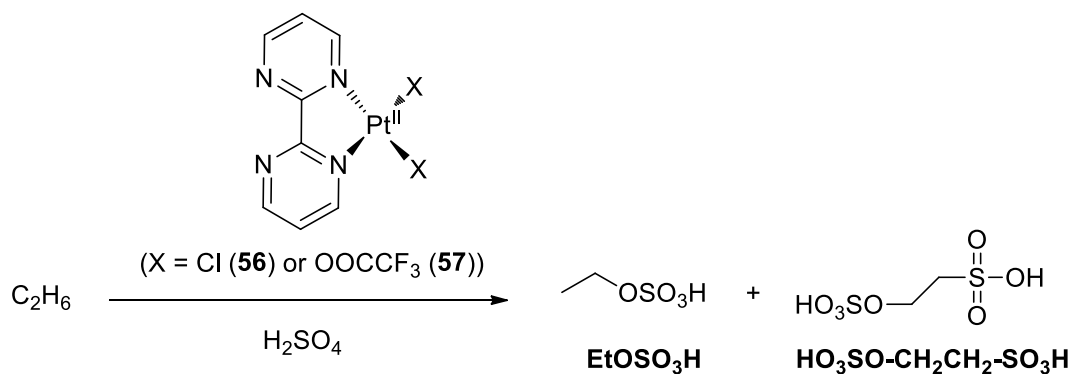
Scheme 31: The oxidation of methane catalysed by platinum(II) complex reported by Periana and co-workers.²⁴



Scheme 32: The postulated mechanism of methane functionalisation reported by Periana and co-workers.²⁴

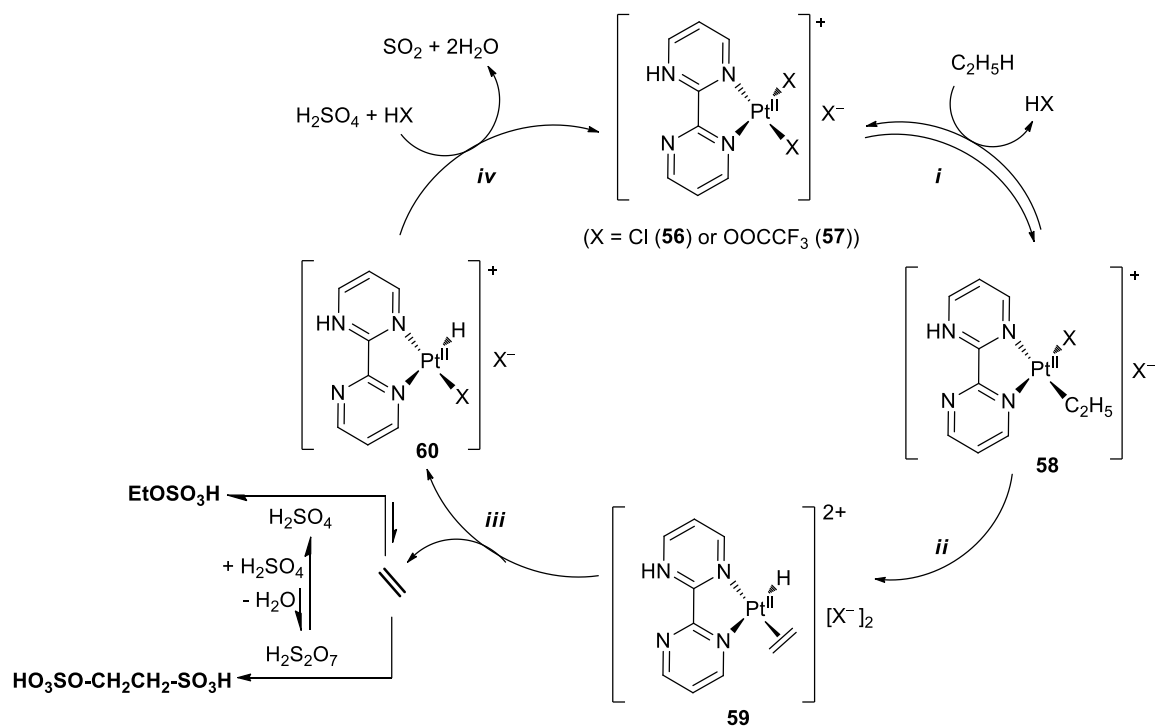
Using the Periana-Catalytica system, ethane was activated and functionalised to result selectively in ethyl bisulfate, EtOSO_3H . Further functionalisation of the ethyl bisulfate apparently gave the final product, the bisulfate ester of isethionic acid ($\text{HO}_3\text{SO}-\text{CH}_2\text{CH}_2-\text{SO}_3\text{H}$) (Scheme 33) instead of the bis-bisulfate ester of ethylene

glycol ($\text{HO}_3\text{SO}-\text{CH}_2\text{CH}_2-\text{OSO}_3\text{H}$), which was an expected product if the mechanism would followed the mechanism of methane functionalisation.⁶⁵ This implies that the ethane chemistry is not entirely the same as that of methane.



Scheme 33: Ethane activation reaction under Periana-Catalityca system reported by Periana and co-workers.⁶⁵

A mechanistic study demonstrates that in the ethane functionalisation, a fast β -hydride elimination of **58** takes place to form **59** which then giving ethylene and an intermediate Pt^{II} -hydride (**60**). The intermediate is oxidised by sulfuric acid to release the Pt^{II} catalyst. In the sulfuric acid solution, ethylene sulfonation occurred to give the final product (Scheme 34).⁶⁵



Scheme 34: The mechanism of ethane activation and functionalisation using the Periana-catalytica system.⁶⁵

1.4.2. Electrophilic C–H Activation

Shilov's system and the Periana-Catalytica system propose an electrophilic C–H activation. The Periana group explains more detail about the activation.²⁸ The electrophilic C–H activation using M–X transition metal complexes principally involves two steps: alkane (R–H) coordination to the complexes resulting in an $[M(R-H)]^+$ and X^- species, followed by a C–H bond cleavage of the intermediate complex to yield a M–R complex. Diagrams describing the net energy of those two steps that correlate the rate of reaction with the electrophilicity of metal complexes are shown in Figure 1.²⁸

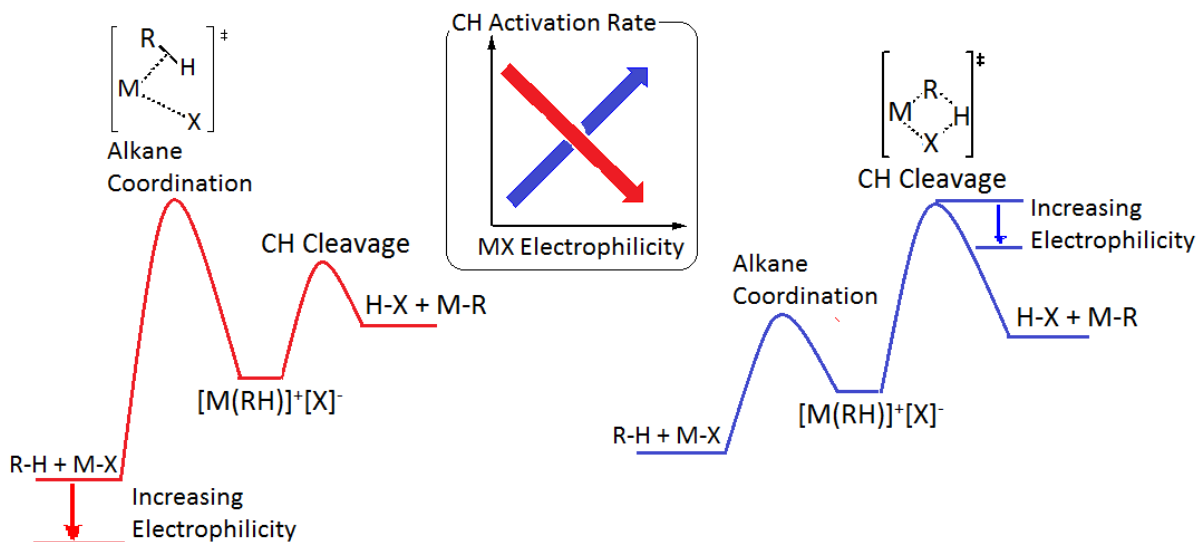


Figure 1: Diagrams illustrating two different ways in which electrophilicity affects the total energy as well as reaction rate on activation and functionalisation of alkane. (Image reproduced from the paper reported by Hashiguchi *et al.*)²⁸

The rate-limiting step of the overall reaction can be either the alkane coordination or the C–H bond cleavage. The red reaction profile shows the case when the rate-limiting step of the reaction is the C–H bond cleavage and the increase in metal electrophilicity stabilises the transition state energy. This scene will lead to a decrease of the overall reaction rate. Conversely, the blue diagram shows the alkane coordination as rate-limiting. The increase in metal electrophilicity stabilises the transition state energy of the alkane coordination step, increasing the overall reaction rate.²⁸ Although the authors earlier believed that the energy profile of electrophilic C–H activation only followed the former pathway, studies and observations made by Periana and co-workers demonstrated that electrophilic activation could also follow the latter scenario where increasing the electrophilicity improved the rate C–H activation.²⁸ In the Periana-Catalytica system, using $[PtCl_2(bpy)]$ in concentrated sulfuric acid for activation of methane, alkane coordination is suggested to be rate-limiting. Therefore, the reaction in superacid solvent, such as concentrated sulfuric acid, proceeds well as the acid will help the C–H bond cleavage step, but the reaction is halted in a weaker acid. The inhibition in the weaker acid (HX) solvent is a result of a competition of R–H with the anion, a

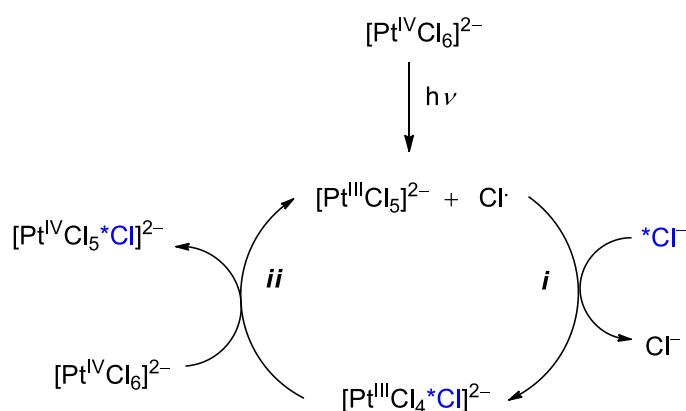
strong nucleophile, X^- , towards coordination to the electrophilic metal centre. But once the coordination is achieved, the C–H cleavage step will proceed quickly giving the activated alkyl metal moiety.

Conversely, it was reported that main-group cations, thallium(III), $Tl(OOCCF_3)_3$, and lead(IV), $Pb(OOCCF_3)_4$, selectively activate and functionalise methane, ethane and propane to give the corresponding alkyl trifluoroacetate esters in high yields. The reaction proceeds in non-superacidic solvents such as methane sulfonic acid contrarily to the reaction using the platinum bipyrimidine complex, yet the diagnostic radical pathway, which would give C–C cleavage as well as side product formation, was not observed in the reactions.²⁸ The alkane coordination to the electrophilic main group metals is fast, yet the strongly nucleophile species in the weak acid medium is not a competitor to the alkanes. Therefore, the energy profile of the main-group system seems to follow the blue diagram (Figure 1) where the rate-limiting step is the C–H bond cleavage. Moreover, this study demonstrates that on using highly electrophile metals, the transition state energy of the C–H bond cleavage step will be reduced so that the overall energy will be lower, contributing to the high rate of reaction.

Back to the activation of ethane in the Periana-Catalytica system, observations showed that the functionalisation rate of ethane (C–H bond cleavage step) was much higher than that of methane.⁶⁵ As now the C–H bond cleavage in the functionalisation proceeds faster, the rate-limiting step of the overall reaction is alkane coordination following the blue scenario shown in Figure 1. Therefore, the metal electrophilicity is important in the overall rate reaction of higher alkanes. These observations support the efficient activation and functionalisation of higher alkanes using the main-group metals which accommodate the electrophilic C–H activation requirements which are higher alkane and more electrophilic metals. Favourable interaction of alkanes with main group metals (M^+X^-) can be explained by using the HSAB concept. Soft acids, the electrophiles, d^{10} main group will make a strong bond M–C with soft bases, R–H, driving C–H cleavage and releasing H–X.⁶⁶

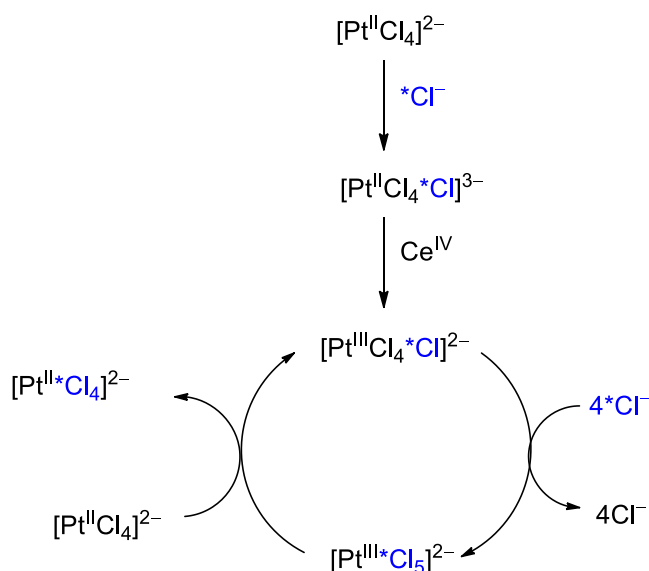
1.5. Photochemistry of Chloroplatinate Complexes

The photochemistry of the tetrachloroplatinate(II) and hexachloroplatinate(IV) anions has been reported.⁶⁷⁻⁷³ Taube and Rich reported photo-properties of $[\text{PtCl}_4]^{2-}$ and $[\text{PtCl}_6]^{2-}$ observed in an isotopic labelling experiment.⁶⁷ Under irradiation (open window on a sunny day) in an aqueous solution of HNO_3 and NaCl at 25°C , a chlorine exchange occurs between $[\text{PtCl}_6]^{2-}$ with Cl^- in the solution. It was reported that the exchange is also observed under dark conditions but with only 20% of the exchange compared to a complete exchange when the reaction was carried out under light, suggesting a photo-enhanced reaction. In the presence of reducing agents such as $[\text{Fe}(\text{CN})_6]^{2-}$, and $[\text{IrCl}_6]^{2-}$, the reaction is halted, thus demonstrating a chain reaction type. The reaction is also inhibited by Cl_2 , ruling out the possibility of elemental chlorine as a catalyst. Therefore, the reaction is believed to be catalysed by a radical suggesting a paramagnetic Pt^{III} species generated from the irradiation of $[\text{PtCl}_6]^{2-}$. A proposed mechanism is shown in Scheme 35.⁶⁷ The initiation step generates the catalyst, $[\text{Pt}^{\text{III}}\text{Cl}_5]^{2-}$, and a chlorine radical followed by a chloride ion substitution (Scheme 35, *i*). The propagation step proceeds after the generation of the catalyst, Pt^{III} , while the exchange of $[\text{PtCl}_6]^{2-}$ with the chloride ion is taking place. The chloride exchange step involves an inner-sphere electron transfer.⁷⁴



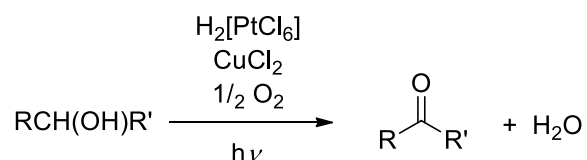
Scheme 35: The exchange reaction of $[\text{PtCl}_6]^{2-}$ with Cl^- catalysed by Pt^{III} species reported by Rich and Taube.⁶⁷

The photochemistry of $[\text{PtCl}_4]^{2-}$ appears to be quite different from that of $[\text{PtCl}_6]^{2-}$. Thus, when $[\text{PtCl}_4]^{2-}$ is illuminated under the same conditions as $[\text{PtCl}_6]^{2-}$, an exchange reaction takes place slowly but addition of an oxidant, Ce^{IV} , induces the reaction (Scheme 36). It was proposed that the initiation step proceeds through a one-electron oxidation of Pt^{II} by Ce^{IV} generating Ce^{III} and the active species Pt^{III} . Further steps proceed on the same basis as that of the $[\text{PtCl}_6]^{2-}$ reaction.⁶⁷ The observations imply that $[\text{PtCl}_4]^{2-}$ is not an effective precursor for the paramagnetic species, Pt^{III} , under light.



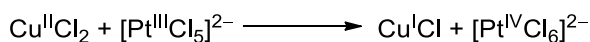
Scheme 36: The exchange reaction of $[\text{PtCl}_4]^{2-}$ with Cl^- catalysed by Pt^{III} species reported by Rich and Taube.⁶⁷

Furthermore, oxidation of alcohols to afford aldehyde and ketone products in the presence of $\text{H}_2[\text{PtCl}_6]$ under irradiation was reported (Scheme 37).⁶⁸ The reaction is catalytic where $\text{H}_2[\text{PtCl}_6]$ is the precursor to generate a photo-catalyst, Pt^{III} species. The catalytic reaction required co-catalysts, CuCl_2 and O_2 , for regeneration of the precursor, as in the absence of the co-catalysts the organoplatinum product was obtained stoichiometrically ending the catalytic cycle. It was also reported that the reaction is hampered in the absence of $\text{H}_2[\text{PtCl}_6]$ even though CuCl_2 and/or O_2 are added to the reaction.⁶⁸



Scheme 37: Transformation of alcohols catalysed by $[\text{PtCl}_6]^{2-}$ under irradiation reported by Cameron and Bocarsly.⁶⁸

Experimental results suggest the photoreaction of alcohols undergoes a chain-type reaction. The fact that CuCl_2 is unable to oxidise $[\text{PtCl}_4]^{2-}$ to $[\text{PtCl}_6]^{2-}$, excludes the possible role of the Pt^{II} and leads to the idea of the existence of Pt^{III} as Taube and Henry⁶⁷ reported earlier. Thus the CuCl_2 is proposed to be the charge-transfer mediator by one-electron oxidation of Pt^{III} to Pt^{IV} , while reduction of Cu^{II} to Cu^{I} allows the reaction to take place in a catalytic cycle (Scheme 38).

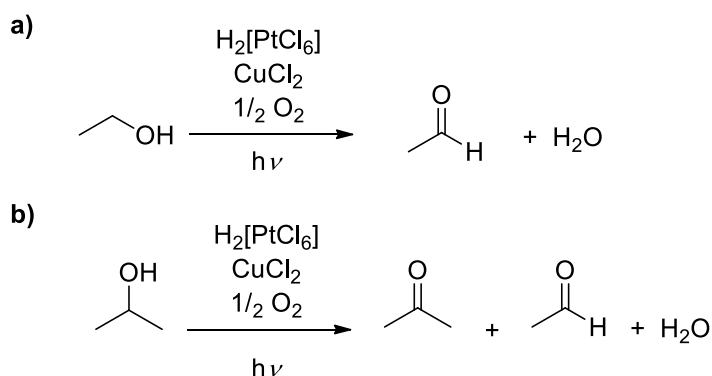


Scheme 38: Oxidation reaction of $[\text{Pt}^{\text{III}}\text{Cl}_5]^{2-}$ by CuCl_2 in catalytic formation of alcohols reported by Cameron and Bocarsly.⁶⁸

Furthermore, a diagnostic result of the chain-type reaction is also reported when irradiation of different types of alcohols is carried out. For example, when 2-propanol is irradiated, acetone is generated as expected but a small amount of acetaldehyde is also obtained indicating an occurrence of C–C cleavage which attests to the radical reaction leading to a loss of methyl which was unexpected (Scheme 39).⁶⁸ Conceptually, there should be prior formation of an oxygen-based free radical that leads to generation of methyl radical to result in the acetaldehyde. Moreover, when a bulky alcohol is treated under the reaction conditions, the rate is slower than that of the less bulky implying a steric hindrance effect on the reaction.⁶⁸ Therefore, it is suggested that coordination of the alcohols to the platinum complex takes place during the reaction.

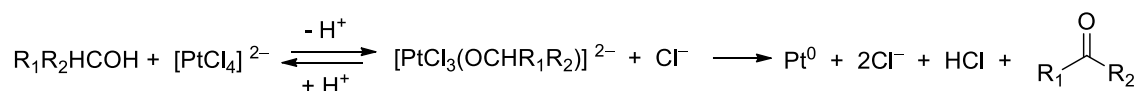
In a short, those observations, made by Cameron and co-workers,⁶⁸ demonstrate $[\text{PtCl}_6]^{2-}$ as a source of platinum(III) under light that is capable of catalysing the transformation of alcohols. A radical pathway is followed during the reaction but the initial activation pathway of alcohols is still uncertain and can either involve

radicals or can proceed through coordination of the alcohol onto the active platinum(III) complex.



Scheme 39: Transformation of (a) ethanol and (b) 2-propanol in the presence of $[\text{PtCl}_6]^{2-}$ under irradiation reported by Cameron and Bocarsly.⁶⁹

Further studies by Cameron and co-workers⁶⁹ show that $[\text{PtCl}_6]^{2-}$ can act as an inhibitor of a photoreduction of $[\text{PtCl}_4]^{2-}$ to Pt^0 in ethanol.⁶⁹ The role suggests the generation of platinum(III) that catalyses a chloride exchange with $[\text{PtCl}_4]^{2-}$ ⁶⁷ which will compete with the reduction of $[\text{PtCl}_4]^{2-}$. In the dark, $\text{K}_2[\text{PtCl}_4]$ was reduced to platinum(0) metal in ethanol to give 97% yield of acetone. The reaction proceeds through ligation of ethanol to the platinum complex followed by a β -hydride elimination to give Pt^0 and acetone (Scheme 40).⁶⁹

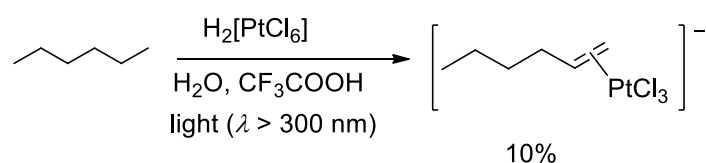


Scheme 40: The reduction of $[\text{PtCl}_4]^{2-}$ in alcohols reported by Cameron and Bocarsly.⁶⁹

A set of experiments to study solvent participation in the photoactivation of $[\text{PtCl}_6]^{2-}$ were reported.⁷⁰ Under light with a metal present, solvent can act as a substrate undergoing charge transfer to solvent (CTTS) states and becoming an active species.⁷⁰ The CTTS state denotes an electron excitation from the metal complex to an appropriate orbital of the solvent molecule. The state commonly occurs in the UV region, thus for example, when a photoreaction does not proceed under visible light but proceeds under UV irradiation, the CTTS state can be

responsible for the reaction. Monreal, *et.al* reported the photoreduction of $(\text{Bu}_4\text{N})_2[\text{PtCl}_6]$ in CHCl_3 under 297 nm light and attributed the reaction to a metal-centred process.⁷¹ The involvement of chloroform was suggested but definite evidence to distinguish the metal-centred state from the solvent state was not provided.

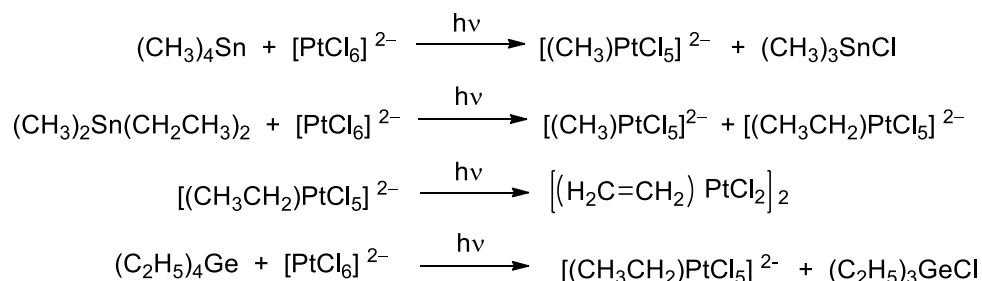
An extension of the role of $[\text{PtCl}_6]^{2-}$ under light was reported by Shul'pin in an activation of alkanes.⁷⁵ Reaction conditions are similar to the Shilov system but it is photochemical at room temperature with an absence of $[\text{PtCl}_4]^{2-}$. For example, irradiation of hexane with hexachloroplatinate(IV) affords hexene coordinated *via* a π -bond to a reduced platinum(II) complex (Scheme 41).⁷⁵ It suggests a C–H activation that appears to be followed by a β -hydride elimination and reductive elimination giving the alkene product coordinated to Pt^{II} .



Scheme 41: Photoreaction of an alkane in the presence of aqueous hexachloroplatinate(IV) solution reported by Shulpin and co-workers.⁷⁵

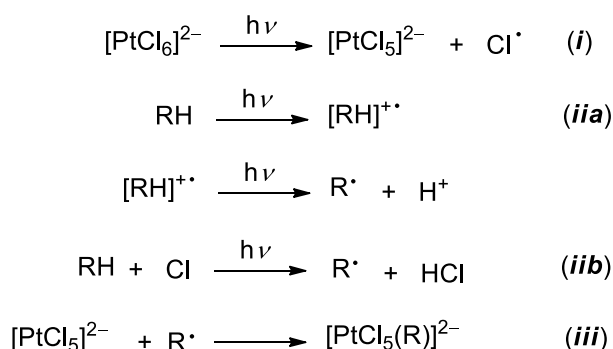
Mechanistic results regarding the photoactivation of alkanes using $[\text{PtCl}_6]^{2-}$ were reported by Shul'pin and co-workers.⁷⁶⁻⁷⁸ The paramagnetic, platinum(III) species is detected in the reaction using electron paramagnetic resonance (EPR) spectroscopy where a g value of about 2.40 was found, which is common for transition metal radicals.⁷⁹ The same peak is also observed when acetone is irradiated with $[\text{PtCl}_6]^{2-}$ present.⁷⁸ Moreover, a σ -alkyl-platinum(IV) complex was synthesised separately from a photoreaction of $[\text{PtCl}_6]^{2-}$ with metal tetraalkyls of Sn and Ge (Scheme 42), which was stable enough to be detected by nuclear magnetic resonance (NMR) spectroscopy. The reaction takes place through an electron substitution mechanism with involvement of an electron transfer from the tetraalkyl metal to the platinum(IV) complex. Further photolysis of the σ -alkyl-

platinum(IV) complex affords the π -alkene-platinum(II) complex (Scheme 42).⁷⁹ Similarly, the authors assumed that the formation of the π -alkene-platinum(II) complex in the irradiation of alkane with $[\text{PtCl}_6]^{2-}$ may proceed *via* the σ -alkyl-platinum(IV) intermediate.⁷⁹



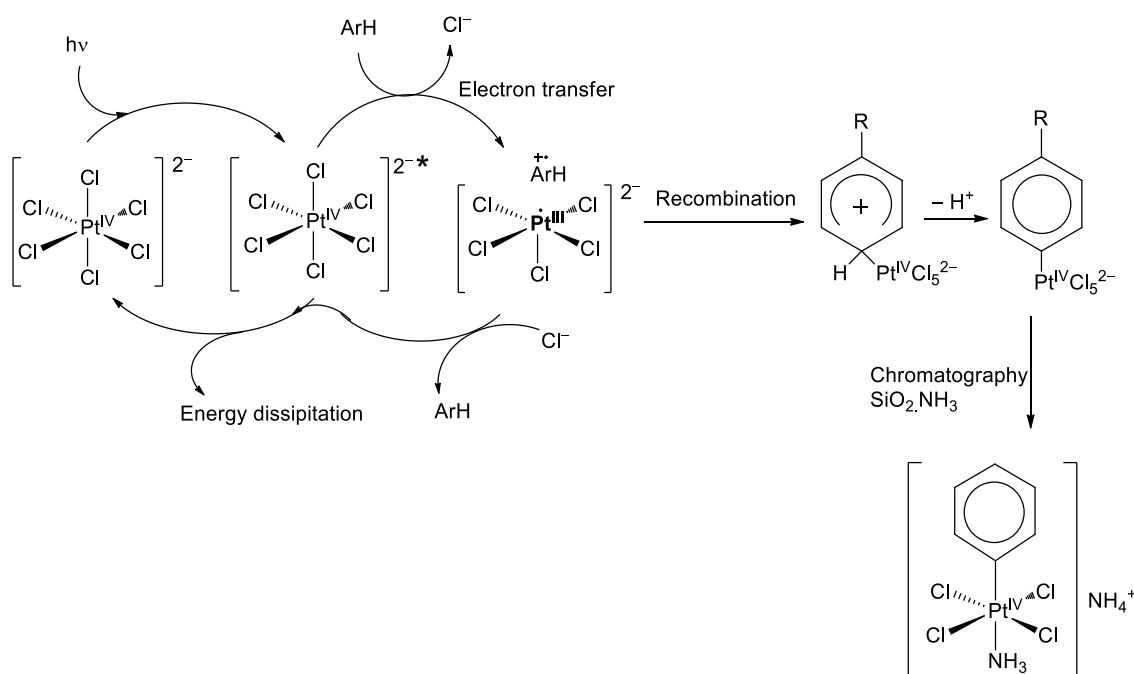
Scheme 42: The photoreaction of organotin and organogermanium compounds with $[\text{PtCl}_6]^{2-}$ reported by Shulpin and co workers.⁷⁹

Therefore, Shul'pin and co-workers proposed a mechanism for the photoactivation of alkanes in the presence of $[\text{PtCl}_6]^{2-}$.⁷⁹ There are two main parts: *i*) the formation of the σ -alkyl-platinum(IV), and *ii*) β -hydrogen elimination of the σ -alkyl-platinum(IV) moiety to give the corresponding π -alkene-platinum(II) complex. The first part can consist of two steps as described in Scheme 43, generation of Pt^{III} radical and chlorine radical from irradiation of $[\text{PtCl}_6]^{2-}$ (*i*). Formation of the organic radical can be either initiated by light (*ii*a) or a proton abstraction by the chlorine radical resulting in an alkyl radical (*ii*b). The next step is combination of the platinum and the organic radicals giving the alkyl-platinum(IV) intermediate (*iii*).



Scheme 43: Proposed mechanism of the formation of σ -alkyl-platinum(IV) on the irradiation of alkanes with $[\text{PtCl}_6]^{2-}$ present reported by Shulpin and co workers.⁷⁹

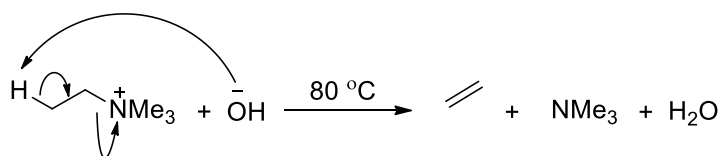
Hexachloroplatinic(IV) acid, $\text{H}_2[\text{PtCl}_6]$ also reacts with arenes in aqueous CF_3COOH to give a σ -aryl platinum(IV) complexes, a process known as the 'Shul'pin reaction'. The product is isolated as $[\text{NH}_4][\sigma\text{-ArPtCl}_4(\text{NH}_3)]$ by running the reaction mixture through silica loaded with ammonia. This reaction not only takes place thermally by heating at $40 - 70^\circ\text{C}$, but also by light promotion under visible light as well as gamma-irradiation.^{80, 81} When the hexachloroplatinate(IV) complex dissolves in the organic solvent, the reaction also proceeds in the absence of water and acid. For example, $[\text{NBu}_4]_2[\text{PtCl}_6]$, which is soluble in solvents with a wide range of polarity from water to chloroform, reacts with aromatic compounds, namely anisole, ethyl phenyl ether, diphenyl ether and benzene, in CH_2Cl_2 under light to produce the related σ -aryl-platinum(IV) complexes. It suggests that the reaction proceeds by electrophilic substitution with the participation of electron transfer from arenes to the Pt(IV) (Scheme 44).⁸²



Scheme 44: The mechanism proposed by Shul'pin for the photoreaction of $[\text{PtCl}_6]^{2-}$ with aromatic compounds.⁸²

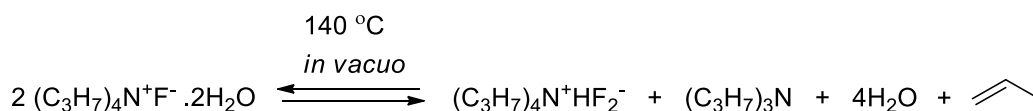
1.6. Hofmann Elimination

The degradation of tetraalkylammonium to afford the corresponding alkenes and trialkylamine has been observed.⁸³⁻⁸⁸ The degradation is initiated by a base which deprotonates an acidic proton bound to a β -carbon of the quaternary alkyl ammonium, followed by an elimination of alkene and releasing of a leaving group, tertiary amine. The reaction is known as the Hofmann Elimination. For example, reaction of ethyl trimethylammonium cation with hydroxide anion at 80 °C resulted in the formation of ethene and trimethylamine (Scheme 45).



Scheme 45: General pathway of Hofmann elimination reaction.

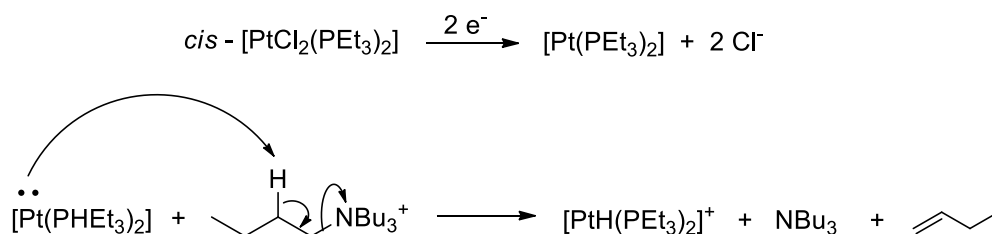
The reaction proceeds using both aqueous and non-aqueous bases.⁸³⁻⁸⁷ In non-aqueous base for instance, when strictly anhydrous tetrapropylammonium fluoride is heated *in vacuo*, the reaction gives rise to propene, tripropylamine, and tetrapropylammonium hydrogen difluoride (Scheme 46).⁸³ In the absence of water, fluoride ion becomes a strong base and efficiently abstracts the acidic proton from the tetraalkylammonium cation so that the Hofmann elimination takes place along with a formation of bifluoride anion that is stable thermodynamically.^{83, 84}



Scheme 46: Hofmann elimination reaction of tetrapropylammonium fluoride in a non-aqueous system reported by Harmon *et al.*⁸³

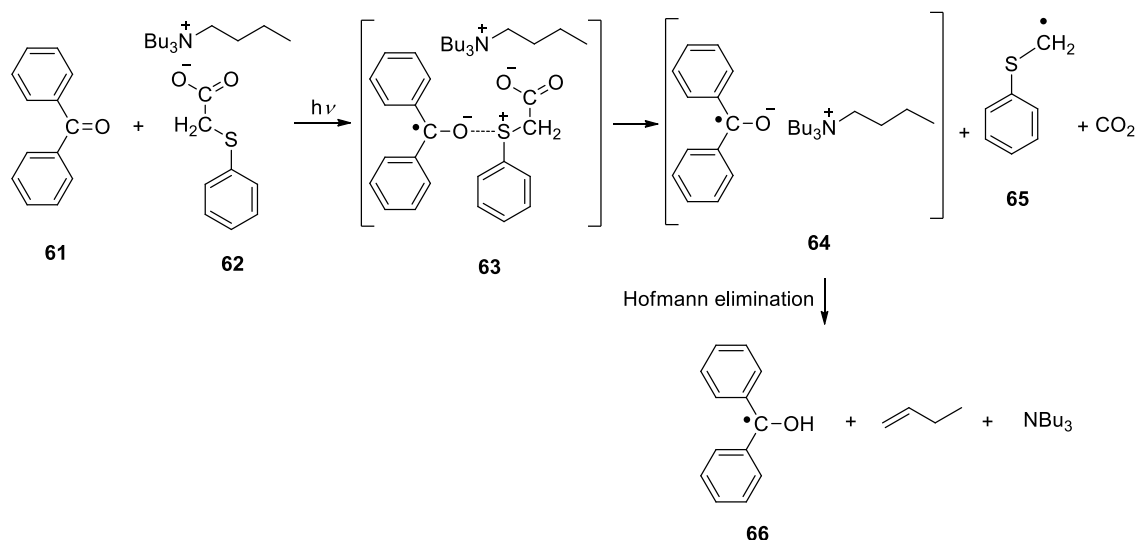
The Hofmann elimination can also be initiated by radicals as well as platinum complexes. Davies reported that Hoffman elimination takes place during an electrolysis process in a solution of acetonitrile/benzene containing $(\text{NBu}_4)\text{ClO}_4$ in a presence of *cis*-dichlorobis(triethylphosphine)platinum(II).⁸⁸ A proposed

mechanism given in Scheme 47 shows that, in the electrolysis, the platinum(II) complex is reduced to platinum(0), $[\text{Pt}(\text{PEt}_3)_2]$. The reduced platinum(0) complex plays a role as the base abstracting a proton from the β -carbon of the tetrabutylammonium cation to form a hydrido platinum(II) complex and affording butene and tributylamine.



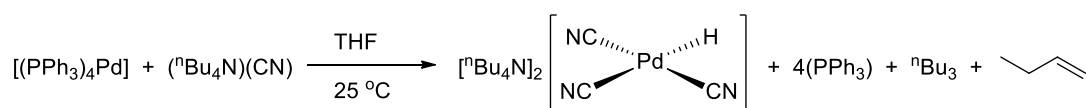
Scheme 47: Hofmann elimination of NBu_4^+ in a solution containing *cis*-dichlorobis(triethylphosphine)platinum(II) complex reported by Davies *et al.*⁸⁸

Furthermore, a radical anion was reported to act as a base in the Hofmann elimination of tetrabutylammonium cation.⁸⁹ It was observed when a mixture of benzophenone (**61**) and phenylthioacetate with tetrabutylammonium counter cation (**62**) was irradiated (Scheme 48). Under the irradiation, the sulfur atom of the phenylthioacetate transfers an electron to benzophenone generating a radical anion of benzophenone with the thioacetate cation (**63**). Then a decarboxylation occurs giving an α -alkylthio-type radical (**65**) and releasing the benzophenone radical anion (**64**). Hofmann elimination of the tetrabutylammonium cation then takes over initiated by the radical anion as the base.

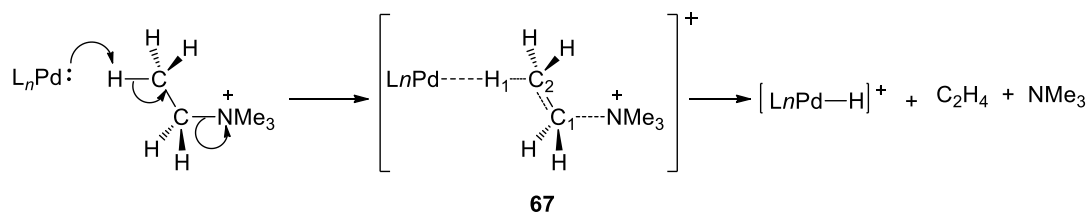


Scheme 48: Hofmann elimination of tetrabutylammonium cation initiated by a radical reported by Wrzyszczyński *et al.*⁸⁹

Furthermore, a reaction of palladium(0) complex, $[\text{Pd}(\text{PPh}_3)_4]$ with $(\text{NBu}_4)(\text{CN})$ undergoes a Hofmann elimination in a presence of water while in an absence of water, a different pathway takes place. In the presence of water, CN^- is immediately hydrolysed generating HCN and OH^- . The HCN conducts an oxidative addition of the $[\text{Pd}(\text{PPh}_3)_4]$ to result in $[(\text{CN})_3\text{PdH}]^{2-}$ whereas OH^- becomes an active base to initiate Hofmann elimination of NBu_4^+ generating 1-butene and NBu_3 (Scheme 49).⁹⁰ A theoretical study suggests the reaction takes place through concerted C–N and C–H bond activations as indicated by a change of bond distance between the corresponded atoms. The calculations show that, in a transition state (**67**), the distance of $\text{Pd}\cdots\text{H1}$ atoms is closer indicating an interaction between the palladium complex with the C–H bond, whereas the $\text{N}\cdots\text{C1}$ distance is elongated and the C1–C2 bond length is shortened, indicating a C=C double bond formation with the activation of C–N bond (Scheme 50).⁹⁰

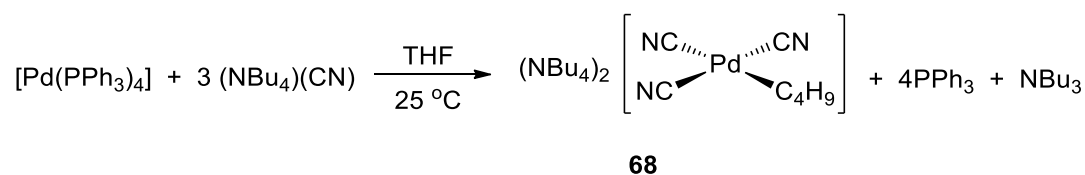


Scheme 49: The reaction of $[(\text{PPh}_3)_4\text{Pd}]$ with $(\text{NBu}_4)(\text{CN})$ in a presence of water reported by Erhardt *et al.*⁹⁰



Scheme 50: The theoretically proposed mechanism of Hoffman elimination taking place in the reaction of $[(PPh_3)_4Pd]$ with $(NBu_4)(CN)$ modelled by the quaternary ammonium $(EtNMe_3)^+$ cation, reported by Erhardt *et al.*⁹⁰

However, in anhydrous conditions, the reaction of $[Pd(PPh_3)_4]$ with $(NBu_4)(CN)$ in low-polar solvents proceeds by ligand dissociation to afford tetrabutylammonium salts of mixed of cyano phosphine Pd(0) anions which are suggested to be in tight ion pairs as commonly experienced by quaternary ammonium compound. The reaction results in $[(CN)_3PdBu]^{2-}$ and NBu_3 suggesting oxidative addition of the butyl-carbon to the palladium centre and activation of a C–N bond that is preceded by a collapse of the ion. Theoretical and experimental investigation presumes that the mechanism involves an S_N2-C-N oxidative addition and once the product, $[(CN)_3PdBu]^{2-}$ complex (**68**) forms, it does not experience a β -elimination (Scheme 51).



Scheme 51: The reaction of $[Pd(PPh_3)_4]$ with $(NBu_4)(CN)$ in an absence of water reported by Erhardt *et al.*⁹⁰

1.7. The Platinum Complex: *trans*- $\eta^2:\eta^2$ -1,3-butadiene-bis(trichloroplatinate(II))

The dinuclear butadiene–platinum(II) complex, $K_2[Pt_2Cl_6(C_4H_6)]$, was first prepared⁹¹ in order to investigate the nature of olefin coordination to metals. The

studies originated with the work of Zeise in 1831⁹² who successfully isolated a stable salt containing an anionic complex of platinum coordinated to ethene - the well-known Zeise's salt, $K[Pt(C_2H_4)Cl_3]$ from heating ethanol with $K_2[PtCl_4]$. The butadiene-platinum(II) complex was made⁹¹ by allowing butadiene gas to react with $K_2[PtCl_4]$ in aqueous HCl, a similar method to preparations of other olefin-platinum(II) complexes may be employed.⁹³

A structural interpretation using infrared spectroscopy proposed that the complex consists of butadiene which is a bridge bound to two platinum centres (Figure 2a).⁹⁴ Chatt, Johnson and Shaw proposed a structure similar to a structure of $[Fe(CO)_3(\eta^4-C_4H_6)]$, where the two platinum metals bound to all C-C bonds in the butadiene which are of equal length in a *cis*-planar arrangement (Figure 2b).⁹⁵ By using infrared spectroscopy and comparing the results with Zeise's salt⁹⁶, Grogan and Nakamoto suggested that the butadiene has a *trans*-planar arrangement having a centre of symmetry at the midpoint of the C-C bond, appearing like two Zeise's complex linked by the centre of symmetry (Figure 2c).⁹⁷ Later, Adam and co-workers reported crystallographic data of the butadiene complex resembling the interpretation suggested by Grogan and Nakamoto. The butadiene molecule was *trans*-planar while the two terminal C-C bonds π -bound to the two platinum metals and the central C-C bond was approximately a double bond based on the bond length data (Figure 2d).⁹⁸

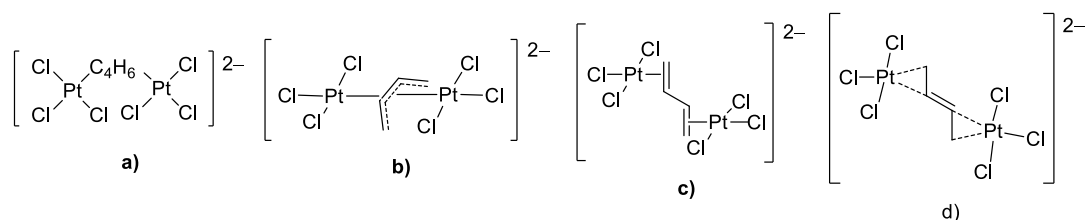
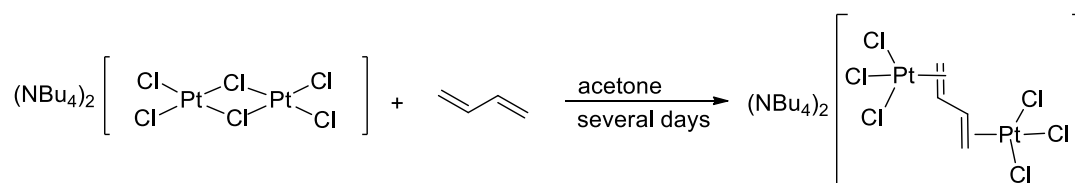


Figure 2: The structure of the butadiene-platinum(II) complex reported by a) Jonassen;⁹⁴ b) Chatt;⁹⁵ c) Grogan and Nakamoto;⁹⁷ and d) Adam.⁹⁸

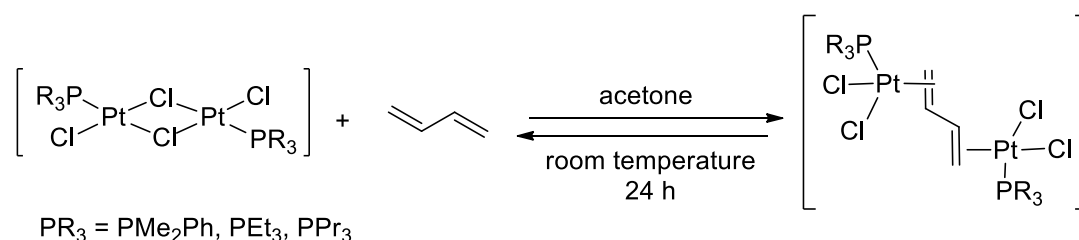
The dinuclear complex, $(NBu_4)_2[Pt_2X_6(\mu-C_4H_6)]$ ($X = Cl$ or Br) can be formed by placing the dinuclear, chloro-bridge complex, $(NBu_4)_2[Pt_2X_6]$ in acetone under a

1,3-butadiene atmosphere for several days, crystallised from acetone-diethyl ether afforded more than 80% yield (Scheme 52).⁹⁹



Scheme 52: The synthesis of the butadiene complex, (NBu₄)₂[Pt₂Cl₆(μ-C₄H₆)] from the chloro-bridge complex, (NBu₄)₂[Pt₂Cl₆] reported by Briggs *et al.*⁹⁹

Similarly, butadiene-platinum(II) complexes with a variety of ligands, [Pt₂Cl₄(PR₃)₂(μ-C₄H₆)] are also obtained from reactions of chloro-bridge complexes, [Pt₂Cl₄(PR₃)₂] (PR₃ = PMe₂Ph, PEt₃, or PPr₃) with 1,3-butadiene gas in acetone for several days (Scheme 53).⁹⁹ The structure of [Pt₂Cl₄(PMe₂Ph)₂(μ-C₄H₆)] is defined by using X-ray diffraction where the butadiene is in a *transoid* configuration while the two [PtCl₂(PMe₂Ph)] are coordinated to the two double bonds from the opposite sides of the butadiene. The butadiene-platinum(II) complex undergoes a reversible, slow isomerisation to form the corresponding *cis* complex at around room temperature while allowing the complex, [Pt₂Cl₄(PPr₃)₂(μ-C₄H₆)] to stand in a solution at 20 °C for 24 hours resulted in a loss of the butadiene ligand to give back the bridged complex [Pt₂Cl₄(PPr₃)₂].⁹⁹



Scheme 53: The synthesis of the butadiene complex, [Pt₂Cl₄(PR₃)₂(μ-C₄H₆)] from the chloro-bridge complex, [Pt₂Cl₄(PR₃)₂] reported by Briggs *et al.*⁹⁹

In the Bruce group a Zeise's salt analogue, the dinuclear, butadiene-bridged complex, *trans*-η²:η²-1,3-butadiene-bis(trichloroplatinate(II)) was isolated from a mixture of NBu₄⁺, [PtCl₄]²⁻ and [AuCl₄]⁻. Thus, while the complex itself and related species are known, its formation from NBu₄⁺, [PtCl₄]²⁻ and [AuCl₄]⁻ is at best

unexpected. An investigation of this reaction forms the basis for the major part of the work in this thesis.

Chapter Two: Mechanistic Investigation of Tetrabutylammonium Activation by Hexachloroplatinate(IV) Complex

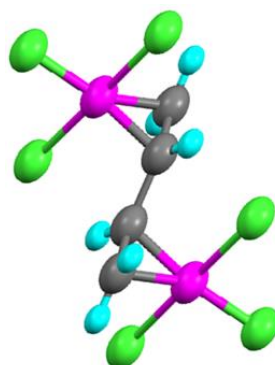
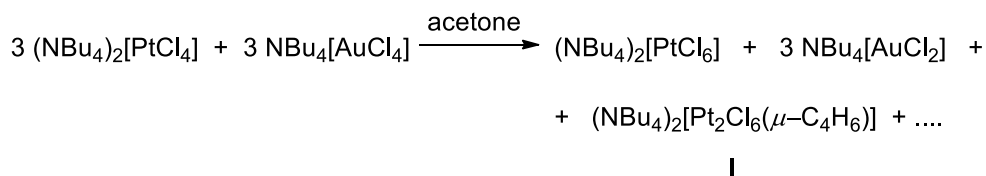
2.1. Introduction

As part of studies directed to the preparation of nanoparticle-doped, mesoporous silicas, we reported on the preparation of MCM-41 derivatives prepared by true liquid crystal templating and using two different metal precursors.^{100, 101} In one case, PtCo nanoparticles were formed inside the pores and were shown to exhibit a ferromagnetic response, although more detailed analysis revealed the nanoparticles to show a wide range of compositions.¹⁰² In then thinking about well-defined, heterobimetallic precursors that might lead to bimetallic nanoparticles of, defined composition, uniformly, we reported on the preparation of the mixed-metal, heterobinuclear anion $[\text{Cl}_2\text{Pd}(\mu\text{-Cl})_2\text{PtCl}_2]^{2-}$, obtained by reaction of $[\text{PtCl}_4]^{2-}$ and $[\text{PdCl}_4]^{2-}$ as their $[\text{K}(18\text{-crown-6})]^+$ salts. The solid obtained was shown to contain $[\text{Pd}_2\text{Cl}_6]^{2-}$, $[\text{Pt}_2\text{Cl}_6]^{2-}$ and $[\text{Cl}_2\text{Pd}(\mu\text{-Cl})_2\text{PtCl}_2]^{2-}$, the heterobinuclear target being obtained as about 25% of what turned out to be an inseparable mixture.¹⁰³

On the same basis, efforts to make the analogous bimetallic complexes consisting of platinum and gold were also made. A reaction of potassium tetrachloroplatinate(II) with potassium tetrachloroaurate(III) in aqueous solution was carried out but it appeared that instead of the formation of the bimetallic complexes, products of a reduction-oxidation reaction were observed where Pt^{II} was oxidised to Pt^{IV} with Au^{III} being reduced to Au^{I} . The reaction was repeated by manipulating the $\text{Pt}^{\text{II}} : \text{Au}^{\text{III}}$ ratio but the corresponding bimetallic complex remained elusive. When the reaction was performed at the 3:2 ratio of $\text{Pt}^{\text{II}} : \text{Au}^{\text{III}}$, metallic gold(0) was found in addition to the platinum(IV) and gold(I) complexes.

As part of the isolation process, tetrabutylammonium chloride, $^n\text{Bu}_4\text{NCl}$ was added to the reaction mixture and the material was allowed to stand in acetone at room

temperature during crystallisation. To precipitate the chlorometallate anion, an orange crystalline solid was isolated and assigned to be $[\text{}^n\text{Bu}_4\text{N}]_2[\text{PtCl}_6]$, but along with the platinum(IV) complex, a yellow crystalline solid was also obtained and on one occasion a single crystal of the compound was isolated. The single crystal X-ray data revealed an unexpected compound, a Zeise's salt analogue, the dinuclear, butadiene-bridged complex, *trans*- $\eta^2:\eta^2$ -1,3-butadiene-bis(trichloroplatinate(II)) in which *trans*-1,3-butadiene is coordinated at each double bond by a trichloroplatinate(II) fragment; two ${}^n\text{Bu}_4\text{N}^+$ were also present as cation (I). The reaction of $[\text{PtCl}_4]^{2-}$ with $[\text{AuCl}_4]^-$ as ${}^n\text{Bu}_4\text{N}^+$ salts in acetone was then conducted and the butadiene-platinum(II) complex was obtained by this route, too.¹⁰⁴ The stoichiometric reaction drawn in Scheme 54 was not yet balanced with side-products such as the butyl residue and the rest of chloride ions, thus it is designated by adding dots. Attempts to investigate the fate of the butyl remainder were carried out and the discussion is given in Section 2.2.2.6.



Scheme 54: The formation of the butadiene-platinum(II) complex (I) (with the X-ray structure) from the mixture of $[\text{PtCl}_4]^{2-}$ and $[\text{AuCl}_4]^-$ salts with $(\text{NBu}_4)^+$ cation.

Zeise's salt analogues, which are π -bound olefin complexes of platinum(II) are usually prepared by allowing the olefins (*e.g.* ethene, 1-butene, 2-butene) to react with $[\text{PtCl}_4]^{2-}$ in aqueous acidic solution. The complexes can also be obtained

through ligand substitution with the desired olefin under moderate conditions.^{105,}

106

The formation of butadiene from the reaction mixture was totally unexpected. The original starting materials did not contain a hydrocarbon source, until the addition of tetrabutylammonium chloride and acetone solvent required for the isolation step. Tetrabutylammonium chloride was intended to precipitate the $[\text{PtCl}_6]^{2-}$ anion whereas acetone was utilised to purify the $[\text{nBu}_4\text{N}]_2[\text{PtCl}_6]$. Therefore, it was suggested that the potential source of the butadiene was tetrabutylammonium cation, and that a C–H activation should occur at some point during the isolation step. Thus, there were mechanistic questions to be answered, namely: *i*) what activated the tetrabutylammonium cation; was it $[\text{PtCl}_4]^{2-}$ or $[\text{AuCl}_4]^-$ or the redox products: $[\text{PtCl}_6]^{2-}$ or $[\text{AuCl}_2]^-$ or some combination of the starting materials? *ii*) did acetone participate on the activation; was it the source or a mediator or only a spectator that can be replaced by other solvents? *iii*) why did the tetrabutylammonium cation undergo the activation in the system and could the analogous alkyl (*e.g.* tetrapropylammonium cation and tetrapentylammonium) or analogous cation (*e.g.* tetrabutylphosphonium) undergo the reaction? To answer those questions, some studies and experiments have been done and reported in the further sections.

The research objective is to investigate the formation of the butadiene-platinum(II) complex.

2.2. Results

2.2.1. Activation of Tetrabutylammonium Cation: Formation of 1,3-butadiene-platinum(II) Complex (I)

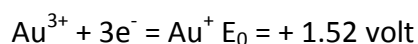
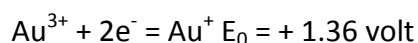
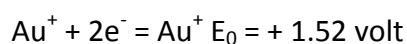
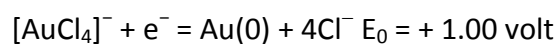
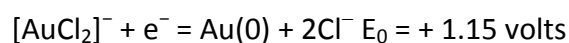
In this section, the experimental results as well as discussions will be presented regarding the first research question mentioned earlier, ‘what activates

tetrabutylammonium cation? '. The section begins with the reaction done by Sethi¹⁰⁴ and ends with the characterisation of the butadiene-platinum(II) complex.

2.2.1.1. Reaction of [ⁿBu₄N]₂[PtCl₄] with [ⁿBu₄N] [AuCl₄]

The reaction of [ⁿBu₄N]₂[PtCl₄] with [ⁿBu₄N][AuCl₄] in a 1:1 ratio in acetone was repeated at room temperature for 48 hours under a nitrogen atmosphere. The reaction gave the oxidation product [ⁿBu₄N]₂[PtCl₆] and the unexpected product, complex I, which was obtained in about 10% yield in dry acetone while only about 1% yield was obtained when reagent grade acetone was used. The suggestion arose that the gold(III) was acting simply as an oxidant since in the reaction of platinum(II) with gold(III) in different ratios, Pt^{IV} was spontaneously observed. If this were true, then formation of the butadiene complex may be possible directly from Pt^{IV}.

Halide complexes of gold(I) and gold(III) are powerful oxidants, easily reduced by mild reducing agents to metallic gold(0) due to their large, positive value of the standard reduction potential (E₀). For example, many naturally occurring reductants such as thiols, thioesters, and disulfides reduce gold(III) to gold(I) and gold(0) under biological conditions.¹⁰⁷



To prove the suggestion, a reaction using only the oxidation product, $[\text{PtCl}_6]^{2-}$ was carried out. Thus, tetrabutylammonium hexachloroplatinate(IV) in acetone was heated under reflux and the complex **I** was isolated. The observation supported the assertion that the gold was simply an oxidising agent leading to the formation of $[\text{PtCl}_6]^{2-}$ from which the Pt^{II} alkene complex formed.

A further mechanistic question then appeared namely; how Pt^{IV} activated the tetrabutylammonium cation which was assumed to be the source of the butadiene. As suggested in Chapter 1, the main complexes involved in the Shilov C–H activation system are $[\text{PtCl}_4]^{2-}$ and $[\text{PtCl}_6]^{2-}$, and these appear to be related to the chemistry of the butadiene-platinum(II) formation. Experiments to study the mechanism, in particular to follow the platinum species involved using $^{195}\text{Pt}\{^1\text{H}\}$ NMR spectroscopy in the reaction mixture, have been conducted and are presented in Section 2.2.2.

2.2.1.2. Reaction of $(^n\text{Bu}_4\text{N})^+$ with $[\text{PtCl}_6]^{2-}$

After the finding that formation of complex **I** occurred in the presence of only $[\text{PtCl}_6]^{2-}$, experiments to optimise the reaction conditions and also to show a role of acetone were designed. As a starting point, $[^n\text{Bu}_4\text{N}]_2[\text{PtCl}_6]$ was heated under reflux in acetone for five days. Every 24 hours, a sample of the mixture was taken, and then concentrated through rotary evaporation before precipitating with diethyl ether. The samples were characterised using ^1H and $^{195}\text{Pt}\{^1\text{H}\}$ NMR spectroscopy. Preliminary results showed total consumption of $[\text{PtCl}_6]^{2-}$ within 48 hours, demonstrated by the disappearance of $[\text{PtCl}_6]^{2-}$ peak in the $^{195}\text{Pt}\{^1\text{H}\}$ NMR spectra at 377 ppm. Meanwhile, a resonance at -1418 in the $^{195}\text{Pt}\{^1\text{H}\}$ NMR spectrum demonstrated that $[\text{PtCl}_4]^{2-}$ was found in the reaction mixture.

Reaction of $(^n\text{Bu}_4\text{N})^+$ with $[\text{PtCl}_6]^{2-}$ to form complex **I** proceeded in dry acetone as well as in reagent grade acetone yet the yield was about ten times as high in dry acetone. It is known that ligand substitution by water in metal complexes occurs commonly¹⁰⁸ thus it was suggested that the ligand substitution could compete

with the reaction. The ligand substitution of chloride by water was observed by $^{195}\text{Pt}\{^1\text{H}\}$ NMR spectroscopy. When a ^{195}Pt spectrum of a fresh solution of $\text{K}_2[\text{PtCl}_6]$ in D_2O was recorded a peak at 6 ppm was seen, but when the solution was re-recorded after one hour irradiation, a new peak at about 506 ppm was observed assigned to $[\text{PtCl}_5(\text{H}_2\text{O})]^{109}$ (Appendix 2). Therefore, subsequent reactions were carried under dry conditions and under reflux for 48 hours. When the reaction was repeated under the optimised condition, the product was obtained in about 68% yield.

To ensure $[\text{PtCl}_6]^{2-}$ played a key role in the reaction, $^n\text{Bu}_4\text{NCl}$ was heated under reflux in acetone, but no change was observed in the ^1H NMR spectrum.

To understand if there was a role for acetone, the reaction was conducted in alternative solvents. In dichloromethane, the reaction also proceeded to give the butadiene-platinum(II) complex in 14% yield, lower than that in acetone. The reaction in butanone also afforded the complex **I** where the yield obtained was 57% which is similar to the yield in acetone and within 24 h of reaction, the $[\text{PtCl}_6]^{2-}$ had been consumed. But why under the same conditions, was the yield of **I** obtained in acetone and butanone better than that in dichloromethane? It was not entirely understood yet, but one conclusive fact is that acetone clearly is not the source of the C4 fragment as the product was isolated from the reaction in dichloromethane.

2.2.1.3. The Characterisation of 1,3-butadiene-platinum(II) Complex, I

Complex **I**, a pale yellow, crystalline solid, was best obtained using the following procedure. After reaction, the mixture was concentrated to dryness in a rotary evaporator, and was then re-dissolved in a small amount of acetone. Diethyl ether was then added until a point where precipitation commenced. The resulting solid was collected and the supernatant was again precipitated with ether. The procedure was conducted several times to obtain the maximum amount of product, which reached 68% with respect to the initial mass of $[\text{Bu}_4\text{N}]_2[\text{PtCl}_6]$.

Elemental analysis confirmed the product as $[\text{Bu}_4\text{N}]_2[\text{Pt}_2\text{Cl}_6(\text{C}_4\text{H}_6)]$, the butadiene-platinate(II) complex with tetrabutylammonium as the counter cation.

a. Single crystal X-ray diffraction

Crystal data for $\text{C}_{36}\text{H}_{78}\text{Cl}_6\text{N}_2\text{Pt}_2$ ($M = 1141.88 \text{ g mol}^{-1}$): monoclinic, space group $P2_1/n$ (no. 14), $a = 13.1677(5) \text{ \AA}$, $b = 12.8495(6) \text{ \AA}$, $c = 13.3831(7) \text{ \AA}$, $\beta = 98.427(4)^\circ$, $V = 2239.95(18) \text{ \AA}^3$, $Z = 2$, $T = 109.9(4) \text{ K}$, $\mu (\text{MoK}\alpha) = 6.622 \text{ mm}^{-1}$, $D_{\text{calc}} = 1.693 \text{ g/cm}^3$, 11858 reflections measured ($6.918^\circ \leq 2\theta \leq 59.992^\circ$), 6514 unique ($R_{\text{int}} = 0.0382$, $R_{\text{sigma}} = 0.0619$) which were used as the starting geometry employed for all calculations involving this species. The final R_1 was 0.0360 ($I > 2\sigma(I)$) and wR_2 was 0.0791 (all data).

The crystal structure (Figure 3) demonstrated clearly that the butadiene adopts a planar geometry showing a *s-trans* conformation, while two $[\text{PtCl}_3]^-$ are coordinated to the diene from the opposite faces with bond angles of C2-C1-Pt1 of $73.5(3)^\circ$; C1-C2-Pt1 of $68.5(3)^\circ$ and the torsion angle for Pt1-C1-C2-C2' is $103.0(6)^\circ$. As mentioned in Chapter 1, Adam *et al.*⁹⁸ reported the crystal data for the same anion, where the counter cation was $(\text{EtMe}_3\text{N})^+$. There is a reasonable agreement between the data they reported and the data collected from the complex described here (Table 1). As discussed below, there is more than one conformer found in solution, but the one shown here was obtained consistently on several occasions.

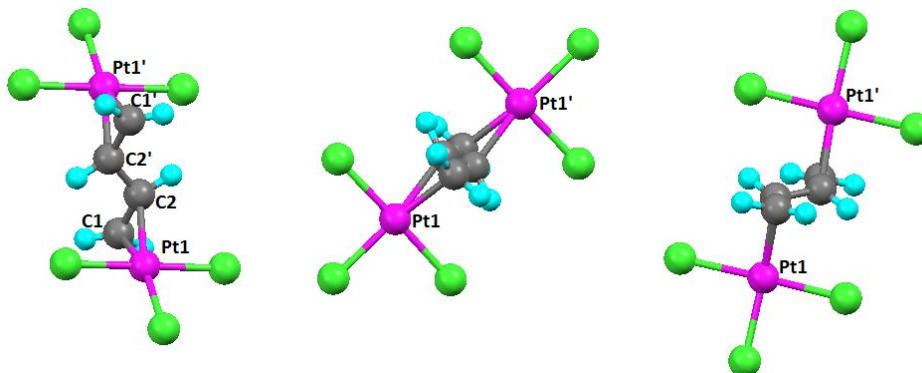


Figure 3: The single crystal structure of $[(\mu\text{-C}_4\text{H}_6)\text{Pt}_2\text{Cl}_6]^{2-}$ in three different views.

Table 1: Bond lengths and angle data of $[\text{Pt}_2\text{Cl}_6(\text{C}_4\text{H}_6)]^{2-}$ compared to the data reported by Adam *et al.*⁹⁸

Description	$[\text{EtMe}_2\text{N}]_2[\text{Pt}_2\text{Cl}_6(\text{C}_4\text{H}_6)]^{98}$	$[\text{nBu}_4\text{N}]_2[\text{Pt}_2\text{Cl}_6(\text{C}_4\text{H}_6)]$
Pt-Cl <i>cis</i> to diene	2.32(1), 2.29(1) Å	2.3045(12), 2.2901(12) Å
Pt-Cl <i>trans</i> to diene	2.29(1) Å	2.3016(11) Å
C1-C2	1.51(3) Å	1.403(7) Å
C2-C2'	1.36(3) Å	1.453(10) Å
Pt1-C1	2.20(3) Å	2.119(5) Å
Pt1-C2	2.18(2) Å	2.184(5) Å
Pt1-C2C1 centroid	2.05 Å	2.034 Å
C-C-C	118(2) °	122.3(6) °

b. ^1H NMR spectroscopy of the isolated product, **I**

The NMR spectra of **I** were acquired using the ^1H , $^{195}\text{Pt}\{^1\text{H}\}$, and $^{15}\text{N}\{^1\text{H}\}$ nuclei and employing one-dimensional as well as two-dimensional methods. The ^1H NMR spectrum and the 2D- ^1H - ^1H COSY spectra of the product are shown in Figure 5, and Figure 7, representing three conformers (which are shown in Figure 4) of the 1,3-butadiene complex. The conformers, are **I.1**: the 1,3-butadiene is *s-trans* while the platinum centres coordinate from opposite sides of the diene, so it is called anti-*trans*-1,3-butadiene-platinum(II); **I.2**: the 1,3-butadiene is *s-trans* and the orientation the two platinum centres coordinate to the same side of the diene so it is called *syn-trans*-1,3-butadiene-platinum(II) and **I.3**: the 1,3-butadiene is *s-cis* and the two platinum centres are bound to the diene from the opposite side named *anti-cis*-1,3-butadiene-platinum(II) (Figure 4).

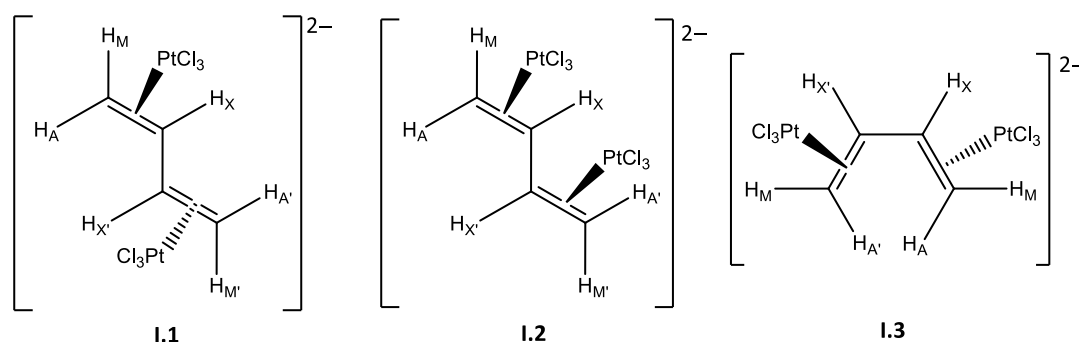


Figure 4: The butadiene conformers on coordination to two platinum(II) centres.

The *trans* isomer can be distinguished from *cis* isomer based on the magnitude of the coupling constant. Commonly, a *trans* coupling constant across a double bond is larger than the equivalent *cis* coupling.¹¹⁰ The 1,3-butadiene should be considered to be a three-spin system, and can be classified as an AA'MM'XX' spin-system – *i.e.* three parts of magnetically inequivalent spins (Figure 4).

The 2D-¹H-¹H COSY NMR spectra showed the resonances at 4.8 and 4.4 ppm to have correlations to the resonance at 5.6 ppm. To simplify the number of the chemical shifts, this set of peaks is labelled temporarily as X. The second set which appeared at 5.8, 4.3 and 4.1 ppm is labelled as Y and the last label is given as Z from which the chemical shifts are 6.3, 5.7 and 5.4 ppm.

In set X, the resonance at 4.8 ppm was a doublet of doublets with $J = 12.7$ Hz and 1.2 Hz, while this resonance at 4.4 ppm was a doublet of doublets with $J = 7.1$ Hz and 1.2 Hz. These were assigned as A,A' and M,M', respectively, so that the 12.7 Hz coupling represent *trans* $^3J_{AX}$ while the 7.1 Hz coupling is a *cis* $^3J_{MX}$. The 1.2 Hz coupling is $^2J_{AM}$ attributed to geminal protons. The resonance at 5.6 ppm then represent X,X', but is a complex second order multiplet thus it is not possible to determine the coupling constant from the multiplicity. The concept is used for the set Y and set Z in assigning the peaks to whether the proton is A,A', M,M' or X,X'.

In set Z, the signal at 6.3 ppm appears as an apparent doublet of triplets with a doublet coupling of 17.2 Hz and a triplet coupling of 10.4 Hz. The large doublet is assigned as $^3J_{HAX}$ while the triplet arises from assuming that $^3J_{HXM} = ^3J_{HXX'} = 10.4$ Hz, appearing as a virtual triplet. Therefore, the set Z is assigned to be the *anti-cis* conformer (**I.3**). The chemical shifts of set Y are displayed more clearly in d₆-acetone due to the absence of resonances of Z in acetone solution (Figure 6). However, in CD₂Cl₂, all the conformers are seen so that one of the chemical shifts of set Z overlaps with one of the signal in Y (at 5.8 ppm) complicating the elucidation. Therefore, to assign the conformer of Y, the spectrum recorded in d₆-acetone was used. In Y, as shown in Figure 6, the peak at 5.8 ppm looked like a

doublet of doublets but due to second-order effect, the pattern also appeared like two doublets of doublets. The multiplicity can result from couplings of the proton to two protons with different coupling magnitudes which are also seen in the doublets at 4.3 ppm with ${}^3J_{\text{HH}} = 7.6$ Hz and at 4.1 ppm with ${}^3J_{\text{HH}} = 13.2$ Hz. Therefore the coupling of 7.6 Hz represents ${}^3J_{\text{XM}}$ while the coupling of 13.2 Hz is ${}^3J_{\text{XA}}$. However, the ${}^3J_{\text{XX'}}$ coupling can not be measured due to the complex multiplicity, so which conformer this set describes cannot be determined from ${}^3J_{\text{XX'}}$, although the choice is either conformer **I.1** or conformer **I.2**. If structural stability is taken into account, represented by the population of the conformer in the ${}^1\text{H}$ NMR spectrum, then conformer **I.1** would be more structurally favourable than the conformer **I.2**, so that Y, which is the least populated, is assigned for the conformer **I.2** while X represents conformer **I.1**.

The proton chemical shifts, their multiplicity and coupling constants are tabulated in Table 2.

Table 2: Chemical shifts (δ) and coupling constant (J) of the butadiene protons recorded in CD_2Cl_2 at 295 K. * defined from H_X resonance.

Description	I.1	I.2	I.3
$\delta(\text{H}_\text{X}, \text{H}_\text{X'})$	5.6 ppm	5.8 ppm	6.3 ppm
$\delta(\text{H}_\text{A}, \text{H}_\text{A'})$	4.8 ppm	4.3 ppm	5.7 ppm
$\delta(\text{H}_\text{M}, \text{H}_\text{M'})$	4.4 ppm	4.1 ppm	5.4 ppm
${}^3J(\text{H}_\text{X}, \text{H}_\text{X'})$	-	-	10.4 Hz*
${}^3J(\text{H}_\text{A}, \text{H}_\text{X}) = {}^3J(\text{H}_\text{A'}, \text{H}_\text{X'})$	12.8 Hz	13.2 Hz	17.2 Hz*
${}^3J(\text{H}_\text{M}, \text{H}_\text{X}) = {}^3J(\text{H}_\text{M'}, \text{H}_\text{X'})$	7.1 Hz	7.6 Hz	10.4 Hz*
${}^2J(\text{H}_\text{A}, \text{H}_\text{M}) = {}^2J(\text{H}_\text{A'}, \text{H}_\text{M'})$	1.2 Hz	Unobserved	-
${}^2J(\text{Pt}-\text{H}_\text{A})$	60 Hz	Unobserved	Unobserved
${}^2J(\text{Pt}-\text{H}_\text{M})$	65 Hz	Unobserved	Unobserved

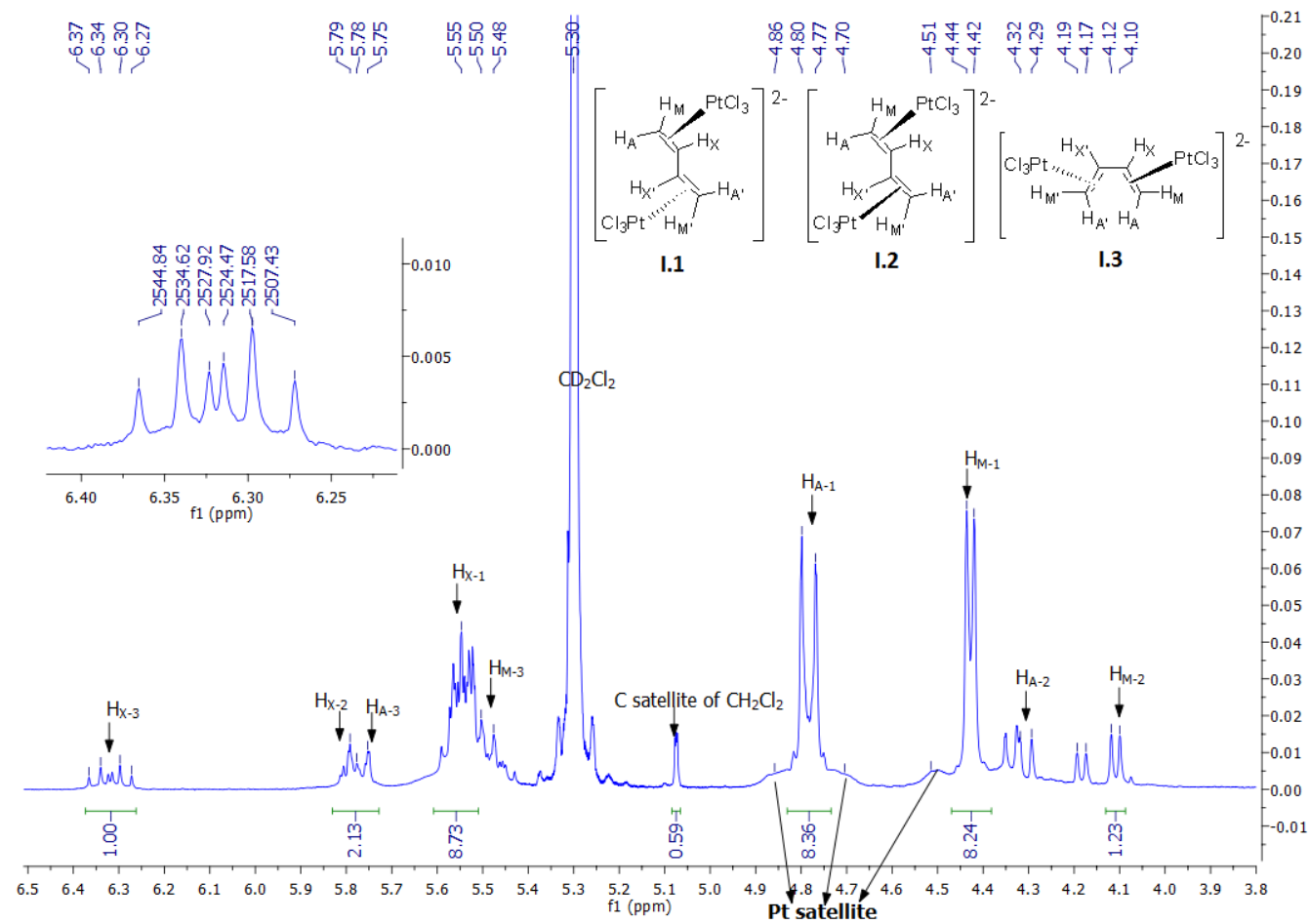


Figure 5: The ^1H NMR (500 MHz) spectrum of I recorded in CD_2Cl_2 at 298 K.

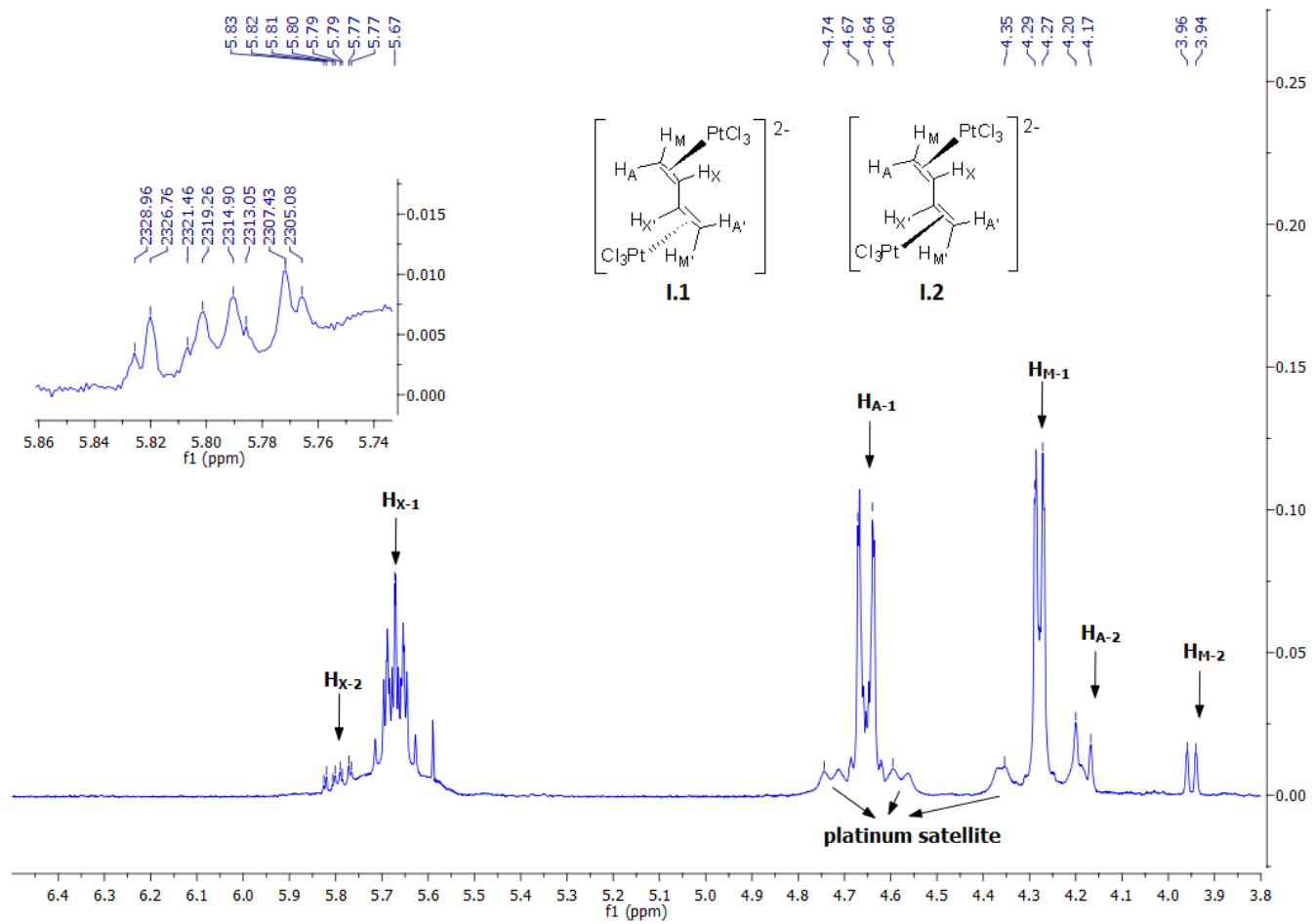


Figure 6: The ^1H NMR spectrum (500 MHz) of I recorded in d_6 -acetone at 298 K

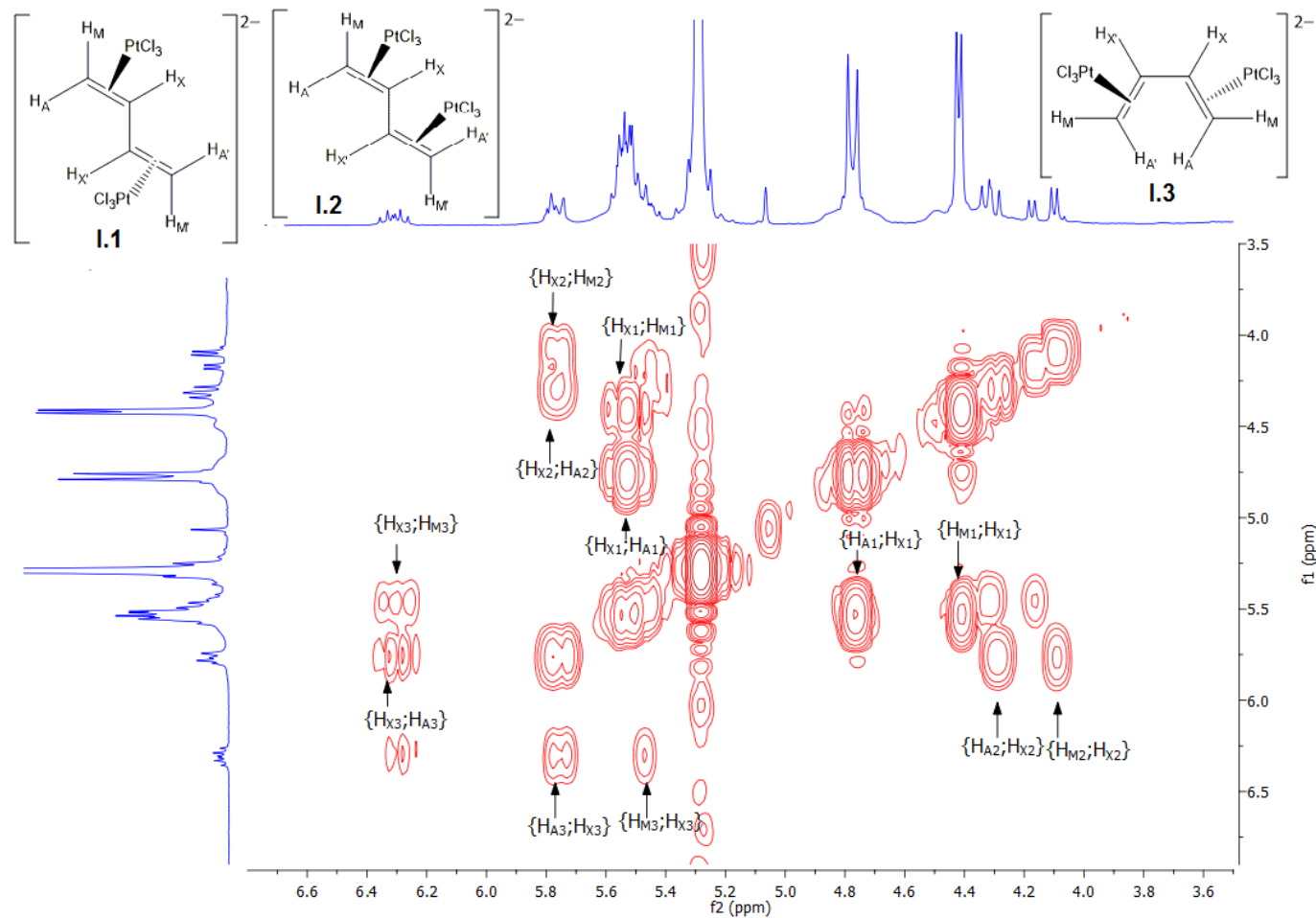


Figure 7: The ^1H - ^1H COSY spectra (500 MHz) of I recorded in CD_2Cl_2 at 298 K

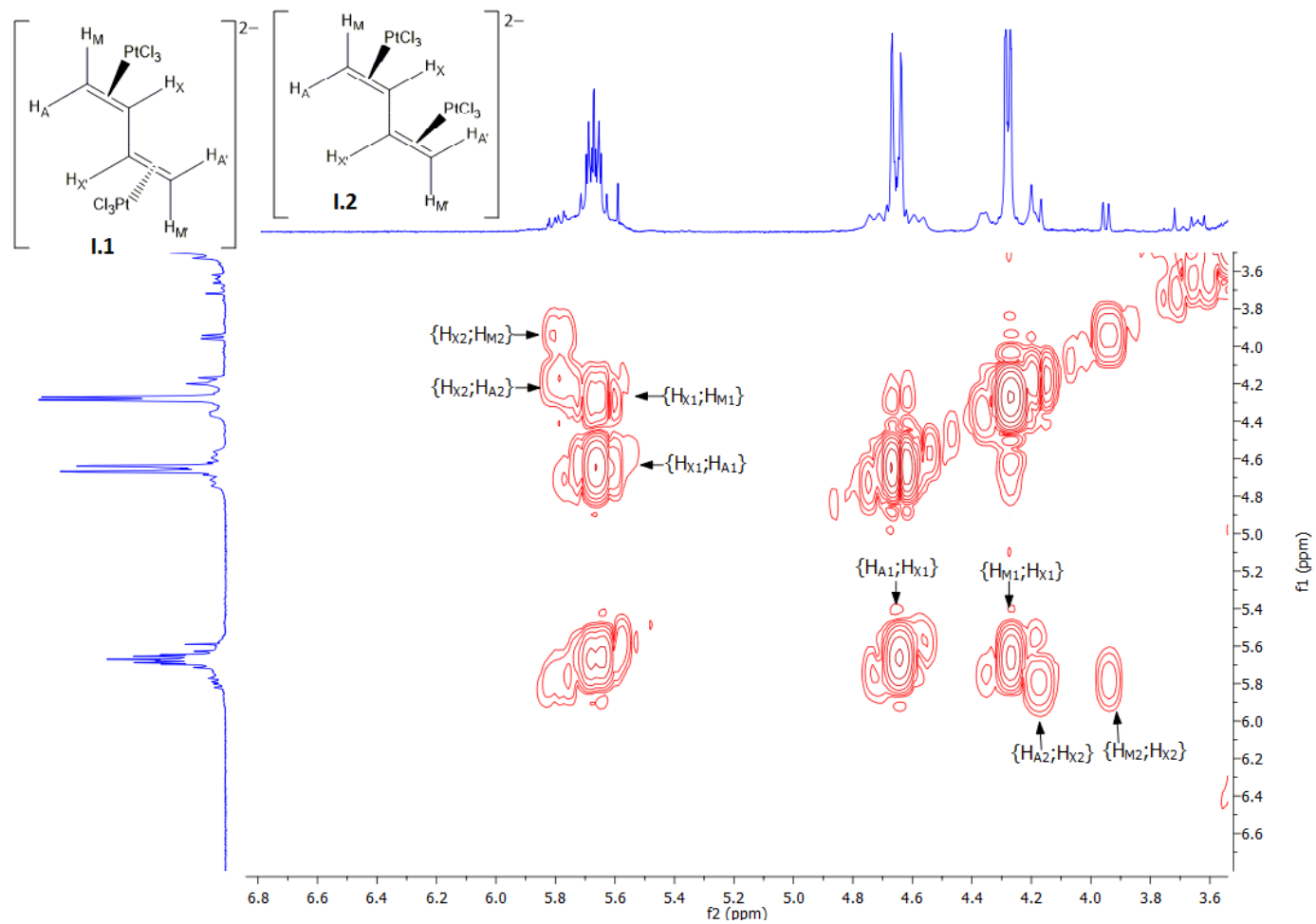


Figure 8: The ^1H - ^1H COSY spectra (500 MHz) of I recorded in d_6 -acetone at 298 K

The ^1H NMR spectrum also showed the platinum satellite of the butadiene protons H_A and H_M with $^2J_{\text{PtH}}$ of 60 and 65 Hz (Table 2). The analogous complex, Zeise's salt, $(\text{NBu}_4)[\text{PtCl}_3(\text{C}_2\text{H}_4)]$ was reported to show a platinum satellite in the ^1H NMR spectrum recorded at 299.78 MHz. In $\text{CD}_3\text{OD}/\text{CH}_3\text{OH}$ the $^2J_{\text{PtH}}$ is 64.9 Hz and in CDCl_3 it is 66.0 Hz.¹⁰⁵ The magnitudes are similar to the coupling constant seen in the butadiene-platinum(II) complex. The satellite was only observed at the proton chemical shifts of conformer **I.1**. The intensity was very low because of the low abundance of ^{195}Pt (33.8%). It was observed from the product dissolved in d_6 -acetone, CD_2Cl_2 and CDCl_3 at lower spectrometer frequencies (400 MHz and 500 MHz), but was not observed at 700 MHz due to a chemical shift anisotropy. Platinum satellites often are not visible as a contribution of the chemical shift anisotropy and the possibility to see the satellites decreases on an increase of the magnetic field of the spectrometer as the rate of relaxation increases.¹¹¹

The ^1H NMR spectrum showed that **I.1** is the most abundant, from 79 – 97%, depending on solvents. Calculations to investigate the energy of the 1,3-butadiene-platinum(II) conformers have been conducted and are presented in Section 2.2.1.4.

The relative conformer abundance shown by ^1H NMR spectroscopy was different when the butadiene-platinum(II) complex was dissolved in different solvents, namely d_6 -acetone (Figure 9), CD_2Cl_2 (Figure 10) and CDCl_3 (Figure 11). In all solvents used, the *anti-trans* conformer (**I.1**) was the main species observed in solution alongside a smaller amount of the *syn-trans* conformer (**I.2**). None of the *anti-cis* conformer (**I.3**) was seen in the fresh solution. All solutions were prepared from the same solid sample. The ratio of **I.1**:**I.2** was greatest in d_6 -acetone at 97:3 and the least in CDCl_3 at 79:21, while in CD_2Cl_2 it was 90:10. Solvents appears to contribute to the population of the conformers in which the polar solvent such as acetone (relative polarity = 0.355) stabilised the *anti-trans*- conformer (**I.1**) while the less polar solvent, chloroform (relative polarity = 0.259), destabilised it.

When stored in the dark for 17 days, the spectra in all solvents changed and the *cis-anti* conformer (**1.3**) appeared. The ratios of **1.1**:**1.2**:**1.3** in the different solvents were: d₆-acetone 88:4:8, CD₂Cl₂ 89:10:1, and CDCl₃ 79:19:2. Allowing the complex to stand for some time caused an interaction of the complex with the solvent that led to isomerisation. Heating a fresh solution of the complex to 45 °C in d₆-acetone and to 55 °C in CDCl₃ did lead to some broadening of the signals but the chemical shift did not change implying that isomerisation was not occurring.

It has reported that K₂[Pt₂Cl₆(C₄H₆)] was unusually stable compared to other olefin-platinum(II) complexes at room temperature, but when it was heated up to 80 °C, a decomposition was observed giving butadiene, chlorine, and metallic platinum.⁹⁴

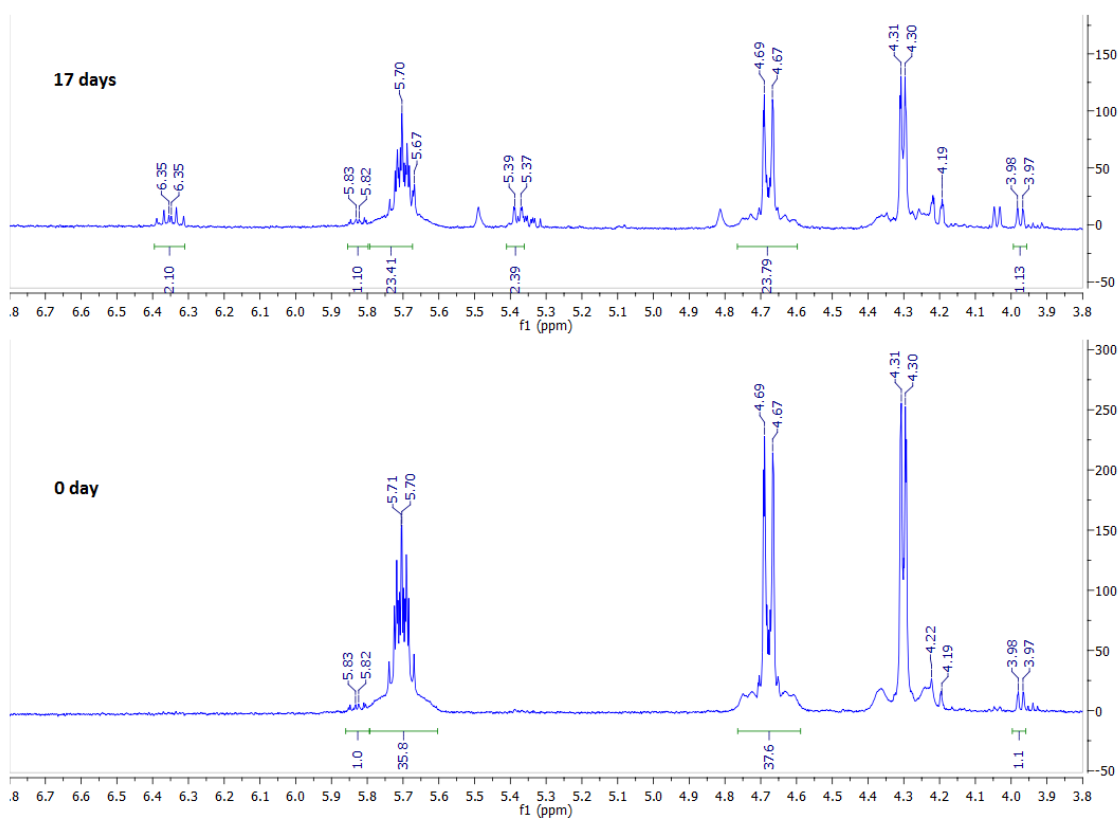


Figure 9: The ¹H NMR spectra (500 MHz) of complex I stored in d₆-acetone for 17 days (top) and that of its fresh solution (bottom).

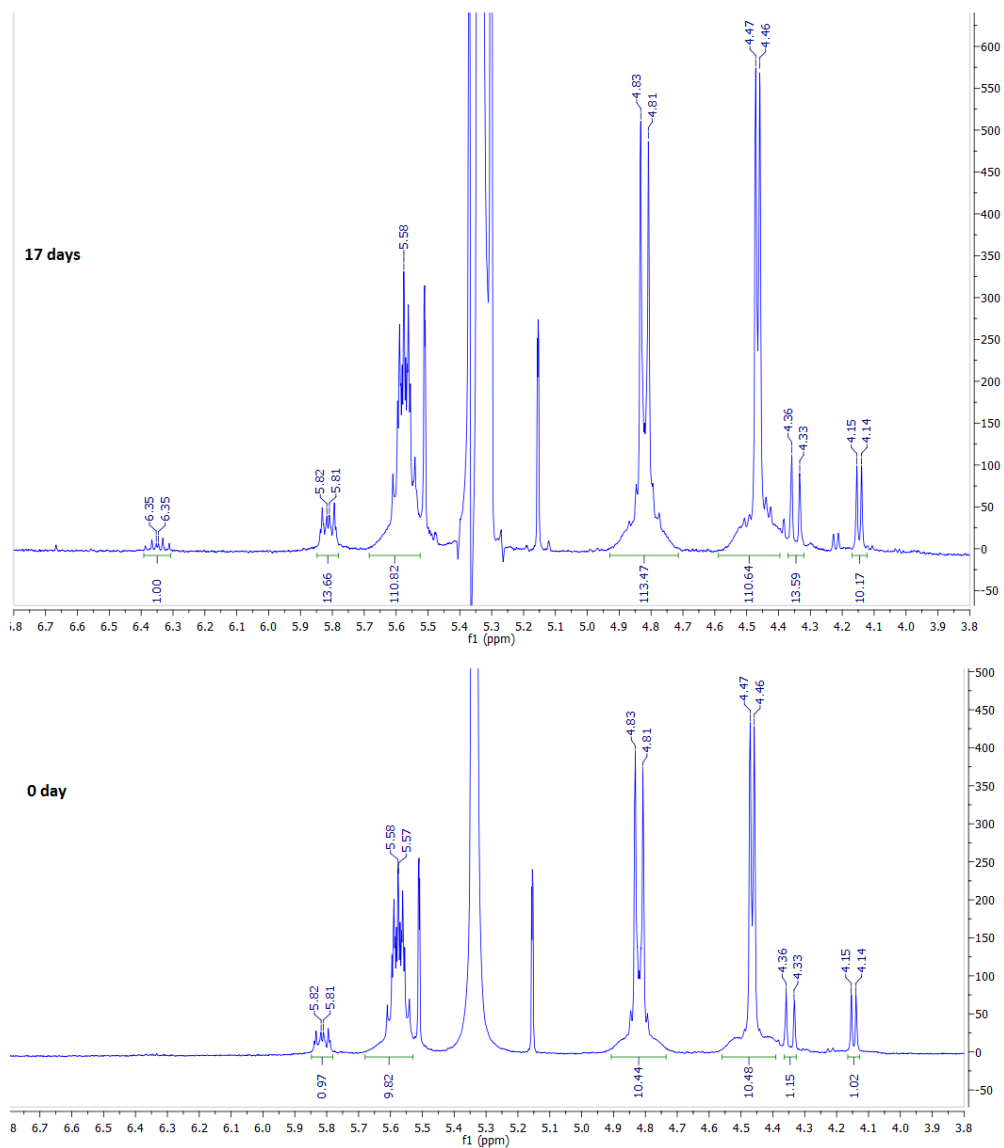


Figure 10: The ¹H NMR spectra (500 MHz) of the complex I stored in CD₂Cl₂ for 17 days (top) and that of its fresh solution (bottom).

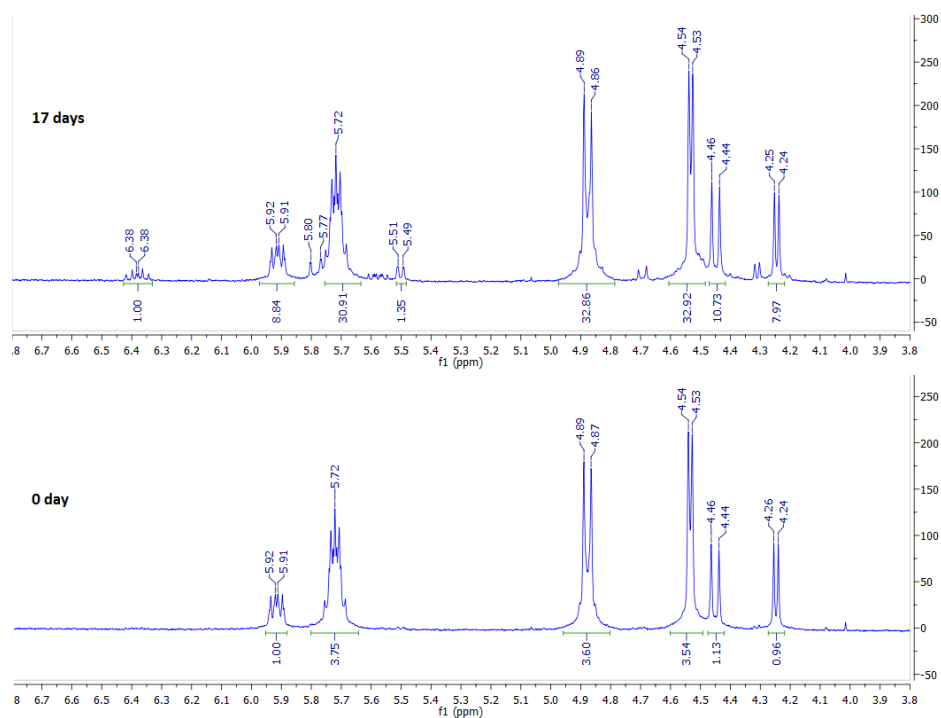


Figure 11: The ^1H NMR spectra (400 MHz) of the complex I stored in CDCl_3 for 17 days (top) and that of its fresh solution (bottom).

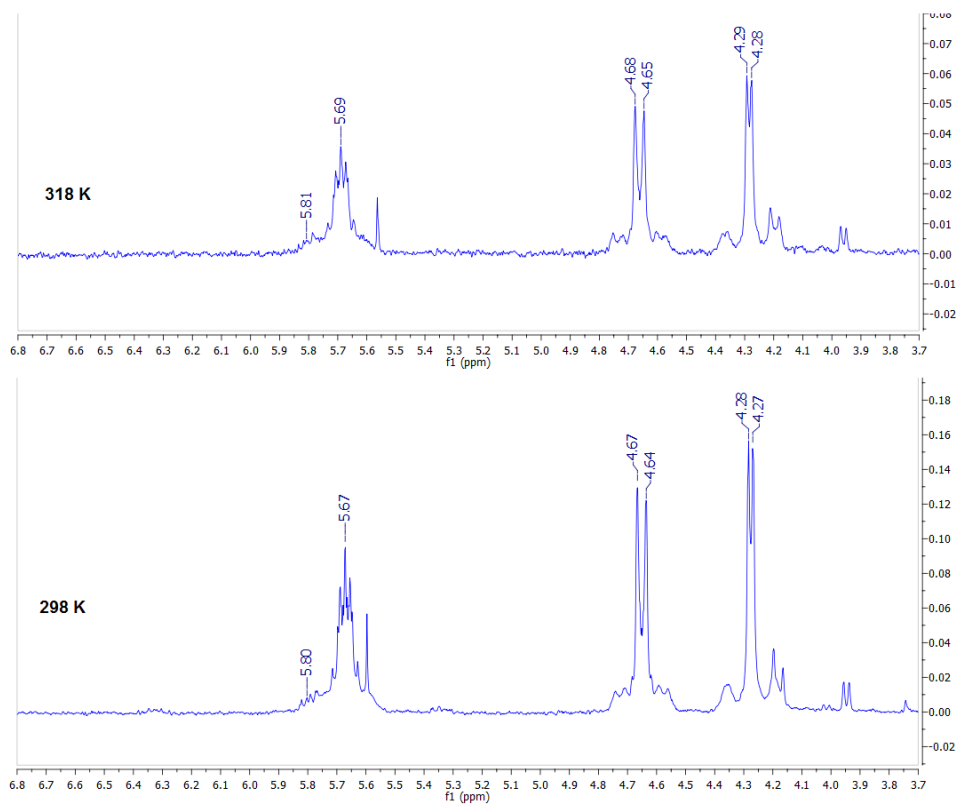


Figure 12: The ^1H NMR spectra (400 MHz) of the complex I in d_6 -acetone at temperature variations (top: 318 K, bottom: 298K).

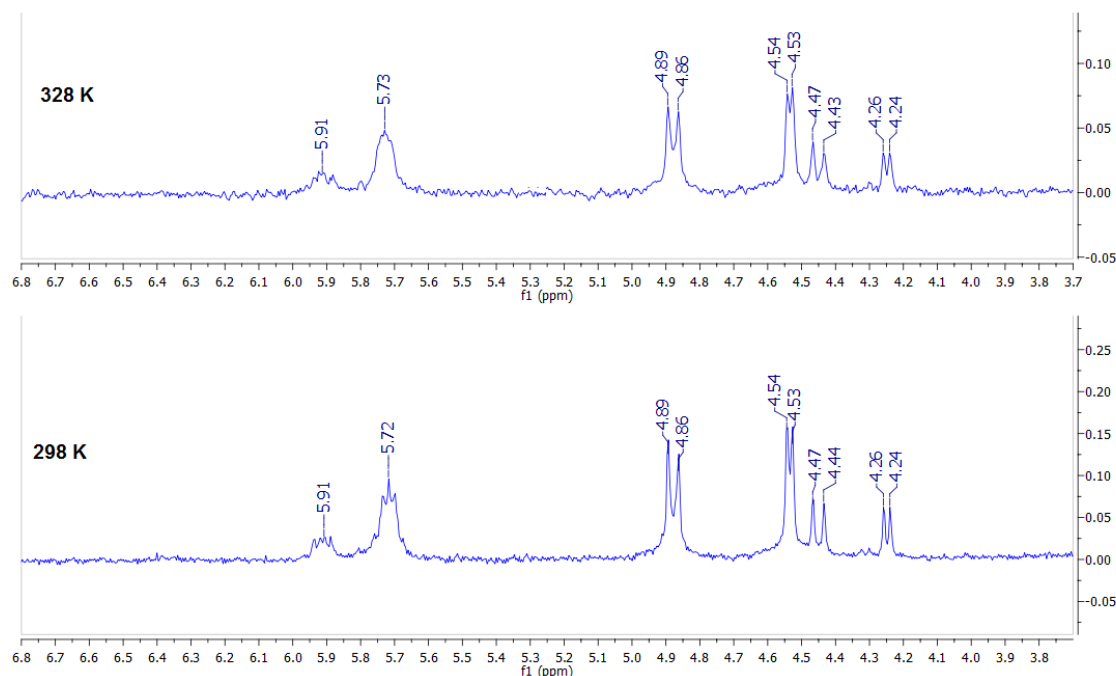


Figure 13: The ^1H NMR spectra (400 MHz) of the complex I in CDCl_3 at temperature variations (top: 328 K, bottom: 298 K)

c. $^{195}\text{Pt}\{^1\text{H}\}$ NMR spectroscopy of the isolated product, I

$^{195}\text{Pt}\{^1\text{H}\}$ NMR spectroscopy has also been used successfully to identify the platinum species. The NMR-active, isotope ^{195}Pt with nuclear spin, $I = \frac{1}{2}$ has an abundance of 33.8%, with a sensitivity of $\sim 10^{-4}$ relative to ^1H . It is known that the ^{195}Pt resonance depends significantly on the oxidation number of the platinum species and the counter ion as well as temperature and deuterated solvent used to record the spectra.¹¹² For example the chemical shifts of $[\text{PtCl}_6]^{2-}$ in water can be altered up to 1.1 ppm per degree temperature change which corresponds to 94 Hz K^{-1} at a frequency of 87.91 MHz, while by changing the solvent from H_2O to D_2O the chemical shift can be altered by 11 ppm.¹¹³ The range of the total chemical shift is wide from -6000 to $+7000$ ppm. Commonly, the chemical shift of a solution of $\text{K}_2[\text{PtCl}_6]$ in D_2O is the reference (zero ppm).¹¹¹

In this research, one-dimensional $^{195}\text{Pt}\{^1\text{H}\}$ NMR as well as two-dimensional (2D) $^{195}\text{Pt}\text{-}^1\text{H}$ techniques were used to identify the platinum species in the reaction

mixture, to follow changes during the reaction, as well as to identify the isolated product. The 2D- ^{195}Pt - ^1H experiments were carried out using the Heteronuclear Multiple Quantum Correlation (HMQC) method which exploits correlations between proton and platinum separated by more than one-bond (usually two or three). During the experiment, direct one-bond correlations are suppressed. Correlations are shown by the appearance of cross-peaks, and the intensity depends on the coupling constant.

The $^{195}\text{Pt}\{^1\text{H}\}$ and 2D- ^{195}Pt - ^1H (HMQC) NMR spectra of the isolated product in d_6 -acetone at 298 K were acquired and are shown in Figure 14 and Figure 15. The $^{195}\text{Pt}\{^1\text{H}\}$ NMR spectrum clearly showed a signal at -2521 ppm, while the two-dimensional spectra revealed another signal at -2591 ppm. The chemical shift at -2521 ppm correlated to the proton peaks at 5.6, 4.6 and 4.4 ppm thus it was assigned to the platinum in conformer **I.1** while the signal at -2591 ppm had correlations to the protons at 5.8, 4.3 and 4.1 ppm that corresponded to the platinum in conformer **I.2**. The shifts were expected as olefin-platinum(II) complexes usually appear in the range of -2370 to -3640 ppm.¹¹⁴ The ^{195}Pt chemical shift of the Zeise's salt was also reported in the range of -2791 to -2743 ppm depending on the cation and the solvent used.^{105, 114, 115}

To conclude, the complex **I** was identified by employing ^{195}Pt NMR spectroscopy which showed the resonances of the two conformers, **I.1** at -2521 ppm and **I.2** at -2591 ppm which are in accordance with chemical shifts of related and known olefin-platinum(II).¹¹²

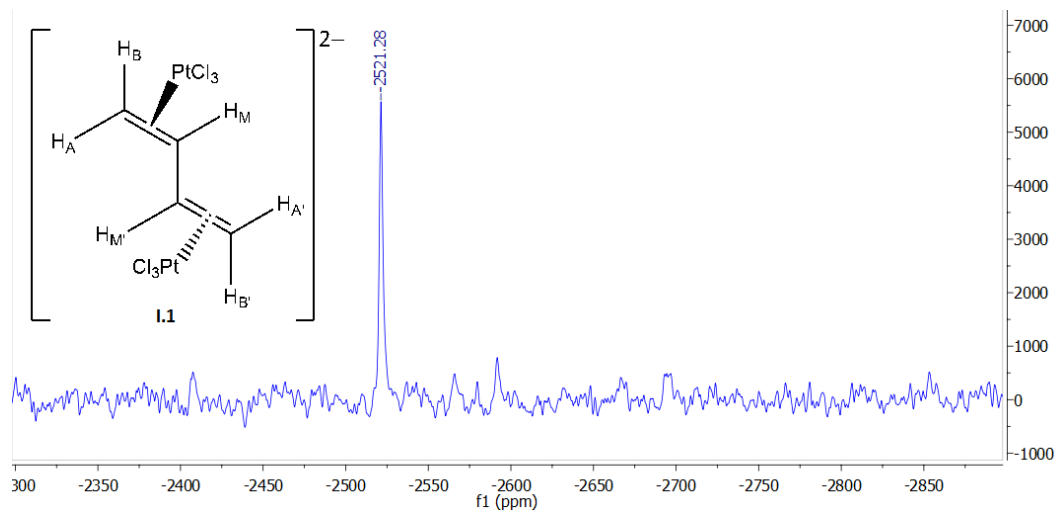


Figure 14: $^{195}\text{Pt}\{^1\text{H}\}$ NMR spectrum (107 MHz) of the complex I in d_6 -acetone at 298 K.

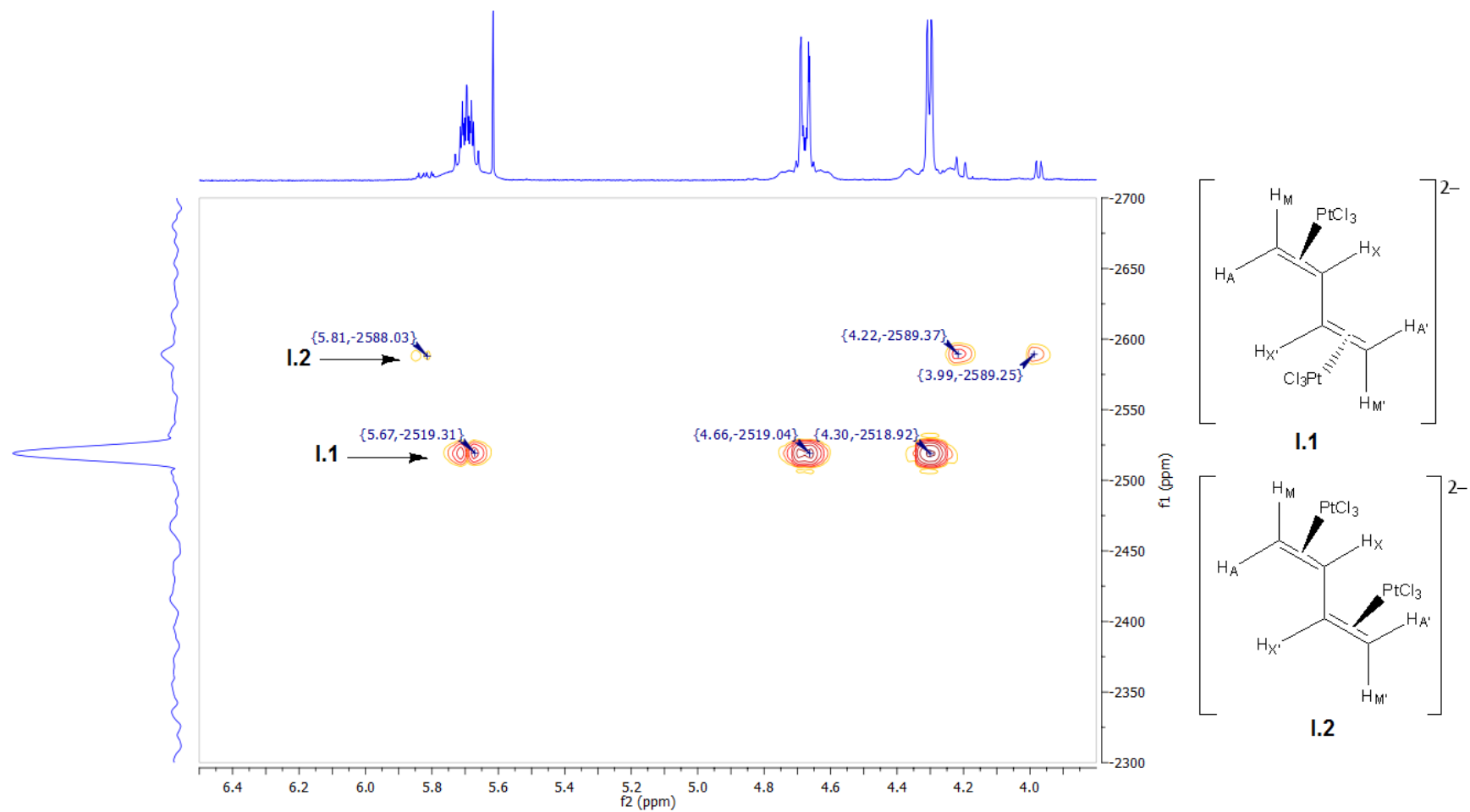


Figure 15: 2D ^{195}Pt - ^1H NMR spectra (107 MHz) of the complex I in d_6 -acetone at 298 K

2.2.1.4. Quantum Chemical Calculation of Geometries and Energies of Different Conformers of Complex I

Quantum chemical calculations of the $[(\mu\text{-C}_4\text{H}_6)(\text{PtCl}_3)_2]^{2-}$ complexes carried out by Linda McAllister were performed in Gaussian 09, revision D.01 using the DFT methods.¹¹⁶ Free butadiene has two conformers, namely *s-trans* and *s-cis*, whereas the platinum atoms can coordinate to the two carbon-carbon double bonds from the same or different sides. Therefore, in principle, there can be four conformers for the butadiene-platinum(II) complex, which are shown in Figure 16 and named *anti-trans*- (**I.1**), *syn-trans*- (**I.2**), *anti-cis*- (**I.3**), and *syn-cis*- (**I.4**). The geometries and relative energies of the conformers have been optimised and investigated.

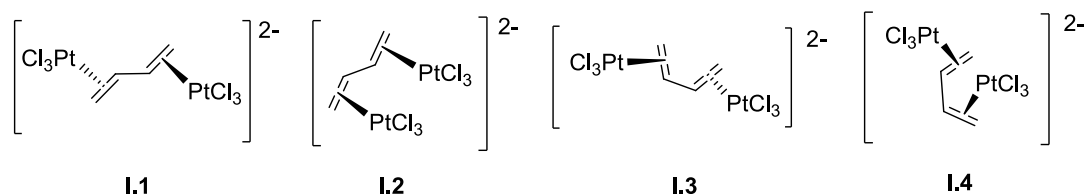


Figure 16: The conformers of platinum(II)-1,3-butadiene complexes

Geometry optimisation was done at the M06/def2-TZVPP level of theory with an effective core potential (ECP) used for platinum.¹¹⁷⁻¹¹⁹ In order to ensure that the optimised geometries corresponded to local minima on the respective potential energy surfaces, vibrational frequencies were calculated. Additional single point energy and vibrational frequency calculations were carried out at the B3LYP/def2-TZVPP level of theory to obtain the energies and Gibbs free energies of the conformers.¹²⁰

The geometries of conformers **I.1** – **I.3** (Figure 17) were optimised successfully at M06/def2-TZVPP level of theory. The *syn-cis*-conformer (**I.4**) was found to be the symmetrical structure of **I.1** as during the geometry optimisation, the rotation of the central C–C bond resulting in the conformer **I.1** (*anti-trans*).

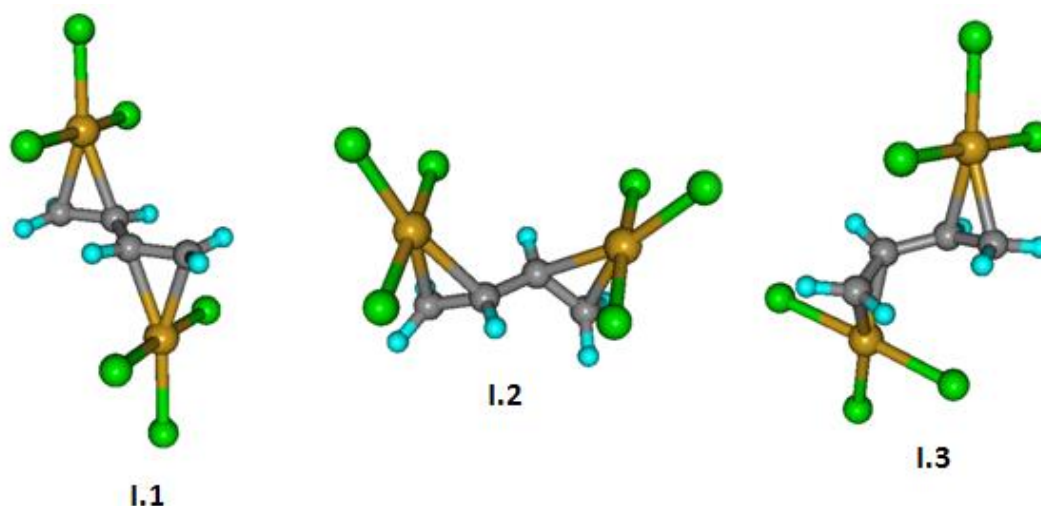


Figure 17: The optimised geometries of conformers I. 1 – I.3 using M06/def2-TZVPP.

Energy optimisation of the complexes carried out at the B3LYP/def2-TZVPP level of theory suggested that conformer **I.1** is the most stable and that the conformer **I.2** was the least stable (Table 3). These energy calculations reflect a gas phase situation and it is of interest that they do not match the relative abundances determined from experiment. Thus, as mentioned above, in CD_2Cl_2 the relative order is **I.1** > **I.2** > **I.3**, while in d_6 -acetone it is **I.1** > **I.2**, and **I.3** is not seen that showing solvation leads to a different order from gas-phase calculation. The theoretical energy Gibbs differences of the conformers are large thus by associating the values with equilibrium constant (K), the concentration of conformer **I.2** ($\Delta G = 54.79 \text{ kJ mol}^{-1}$) is expected to be very small (or almost nothing) compared to the conformer **I.1**. The fact that **I.2** exists in the solutions showing the important effect of solvation to compound **I**.

Table 3: The energies and Gibbs free energies of conformers **I.1** – **I.3** calculated at the B3LYP/def2-TZVPP level of theory. The relative energies and Gibbs free energies of conformer **I.2** and **I.3** relative to conformer **I.1** are also shown.

Conformer	$E / \text{kJ mol}^{-1}$	$\Delta E / \text{kJ mol}^{-1}$	$G / \text{kJ mol}^{-1}$	$\Delta G / \text{kJ mol}^{-1}$
I.1	-8287735.053		-8287617.136	
I.2	-8287769.201	34.1	-8287562.345	55
I.3	-8287727.325	7.73	-8287608.624	8

The key bond lengths and angles in the optimised geometries are given in Table 4. Parameters for the crystal structure of the *trans*-butadiene complex with [PtCl₃]⁻ groups bound to opposite faces were included for comparison with calculations.

Table 4: Key bond distances and angles of the geometries of the complexes optimised at the M06/def2-TZVPP level of theory and from the crystal structure of conformer **I.1**.

Conformer	r(Pt-C=C) / Å	r(C=C) / Å	r(C-C) / Å	a(C=C-C) / °	Torsion (C=C-C=C) / °
I.1 (Crystal structure)	2.068	1.423	1.464	120.7	180.0
I.1 (Calculation)	2.101	1.393	1.465	123.2	180.0
I.2	2.083	1.400	1.473	120.5	110.7
I.3	2.089	1.390	1.469	126.0	13.59

There was a reasonable agreement between the crystal structure and calculated parameters for conformer **I.1** suggesting that the level of theory used was suitable for these complexes. In conformers **I.2** and **I.3**, the dihedral angle between the four carbon atoms deviates from that expected of *trans*- and *cis*-butadiene respectively.

2.2.2. Mechanistic Investigation of the Activation of (ⁿBu₄N)⁺ cation by [PtCl₆]²⁻ Complex

To study the mechanism of the reaction between (ⁿBu₄N)⁺ and [PtCl₆]²⁻, several strategies were used. These included monitoring the reaction using ¹⁹⁵Pt{¹H} NMR spectroscopy and conducting the same reaction using tetraalkylammonium cations of different chain length as well as a different central atom for the cation.

In the first case, ¹⁹⁵Pt-NMR spectroscopy was utilised to follow the change in platinum species observed. Previously, ¹⁹⁵Pt{¹H} NMR spectrum of the reaction mixture had shown the appearance of [PtCl₄]²⁻, thus the ¹⁹⁵Pt{¹H} NMR experiments were set up so that the platinum chemical shift range covered hexachloroplatinate(IV) from 650 to -250 ppm; tetrachloroplatinate(II) from -950 to -1850 ppm and the olefin-platinum(II) product from -2250 to -3150 ppm. The

chemical shift ranges were chosen having collected spectra from well-defined analogues. The chemical shifts of selected platinum complexes are presented in Appendix 1. The chemical shift of hexachloroplatinate(IV) in d_6 -acetone was usually observed at about 370 – 380 ppm while in CD_2Cl_2 it appeared in the range of 215 ppm to 235 ppm. Tetrachloroplatinate(II) is more sensitive to changes in the cation and solvents because it is a square planar complex, and so the platinum of d_{z^2} orbital is more easily accessed, thus affecting the nuclear properties. The chemical shift of $[PtCl_4]^{2-}$ varied from –1400 to –1470 ppm in d_6 -acetone at 298 K and from –1490 to –1550 in CD_2Cl_2 in 295 K. The resonance of olefin-platinum(II) species are normally observed at about –2370 to –3640 ppm.¹¹²

The evolution of the platinum on the reaction of tetrabutylammonium cation with hexachloroplatinate(IV) in d_6 -acetone at 50 °C was monitored *in situ* by using $^{195}Pt\{^1H\}$ NMR spectroscopy. Integration of the peak of $[PtCl_6]^{2-}$ during the reaction was used to show the change. Those integrations were processed in a same way before comparing. The reaction was carried out in a sealed Young's NMR tube in the heated NMR probe which was dark. $^{195}Pt\{^1H\}$ and 1H NMR spectra were recorded every two hours for 18 hours.

The $^{195}Pt\{^1H\}$ NMR spectra of a reaction mixture during the heating showed no change in the integration of hexachloroplatinate(IV) species during the reaction. Also, no peaks appeared in the areas expected corresponding to the tetrachloroplatinate(II) and the olefin-platinum(II) complex. This NMR result demonstrated the hexachloroplatinate(IV) remains unchanged in the dark implying the importance of light on the reaction.

To evaluate the effect of light on the reaction, the experiment was repeated under ambient lighting conditions. The sample was heated at 50 °C in an oil bath then the spectra were recorded at intervals. Under ambient light condition, the integration of hexachloroplatinate(IV) decreased over time (Figure 18), while the signals associated with tetrachloroplatinate(II) and olefin-platinum(II) appeared and their

integration increased over the reaction time (Figure 19). However, the appearance of the olefin signals was unclear in the ^1H NMR spectrum of the reaction mixture (Figure 20). A weak signal was seen at 4.35 ppm which corresponded to an olefin chemical shift. On the enlargement of the spectrum, a triplet (1:1:1) peak with a coupling constant of 2.41 Hz which is consistent with a proton coupled to deuterium was observed. A $^2\text{D}\{^1\text{H}\}$ NMR experiment was carried out to confirm this assignment (Figure 21). The signal at 4.35 ppm was again appeared in the $^2\text{D}\{^1\text{H}\}$ NMR spectrum implying a partial deuteration and additionally, weak peaks at 4.8 and 5.7 ppm were also observed. These observations thus indicated the formation of the olefin derivatives which is a diagnostic sign of C–H activation.

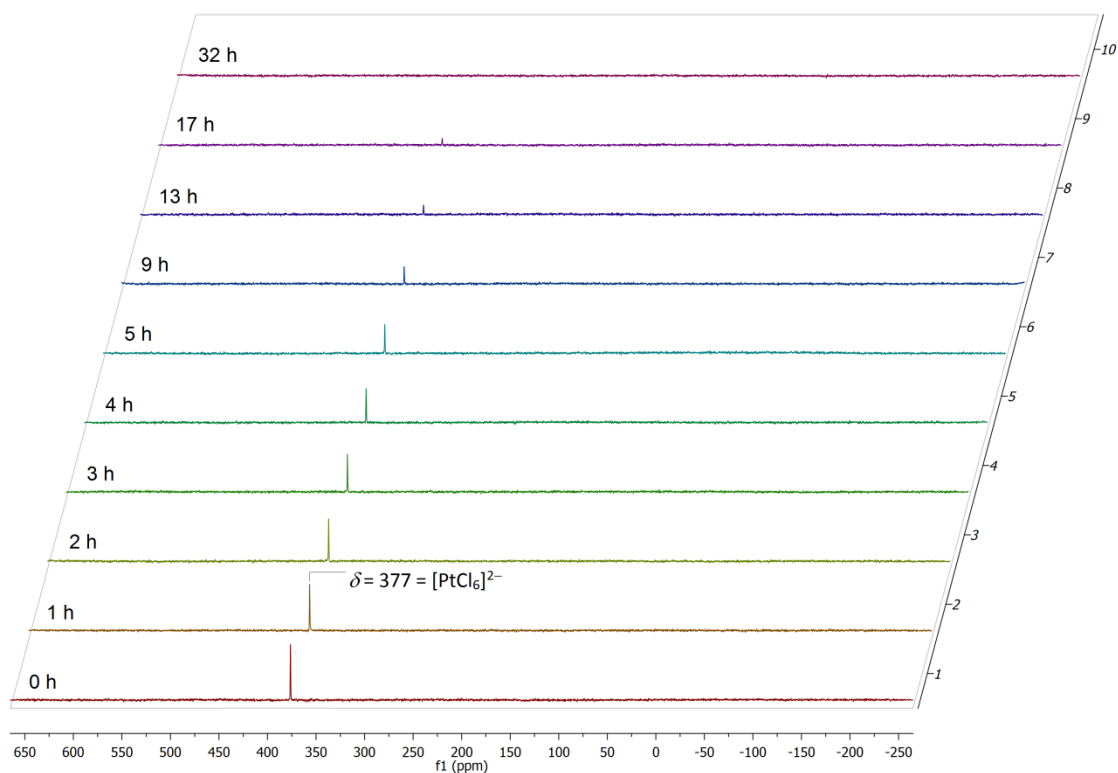


Figure 18: The evolution of $^{195}\text{Pt}\{^1\text{H}\}$ NMR spectrum (107 MHz) of $[\text{nBu}_4\text{N}]_2[\text{PtCl}_6]$ in d_6 -acetone at 323 K under ambient light.

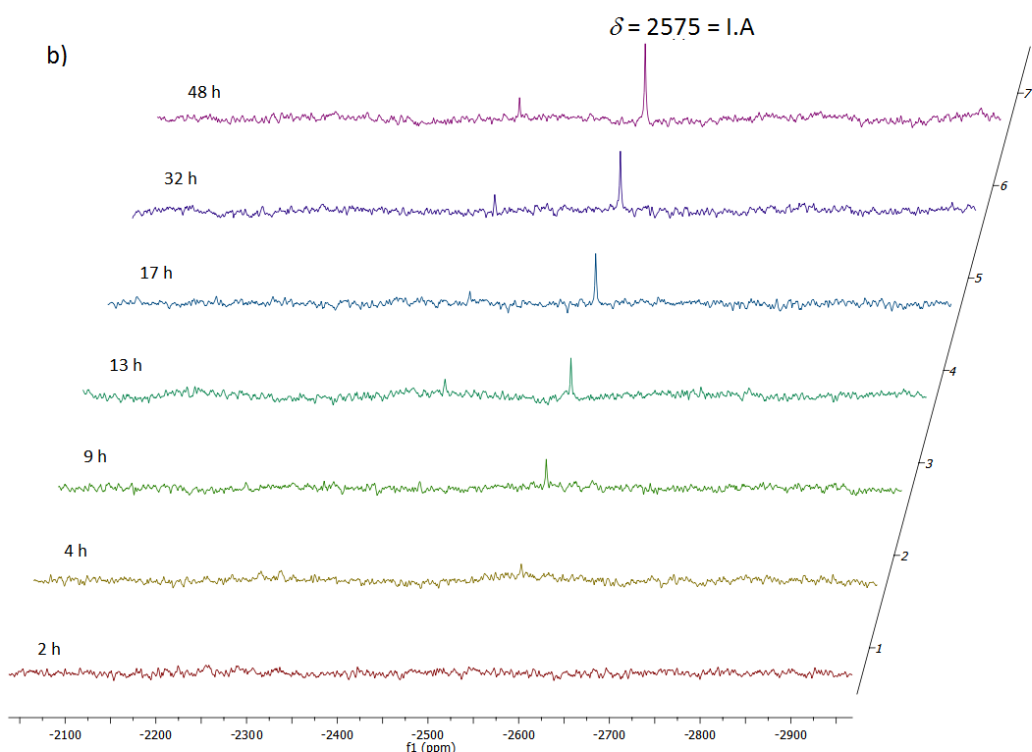
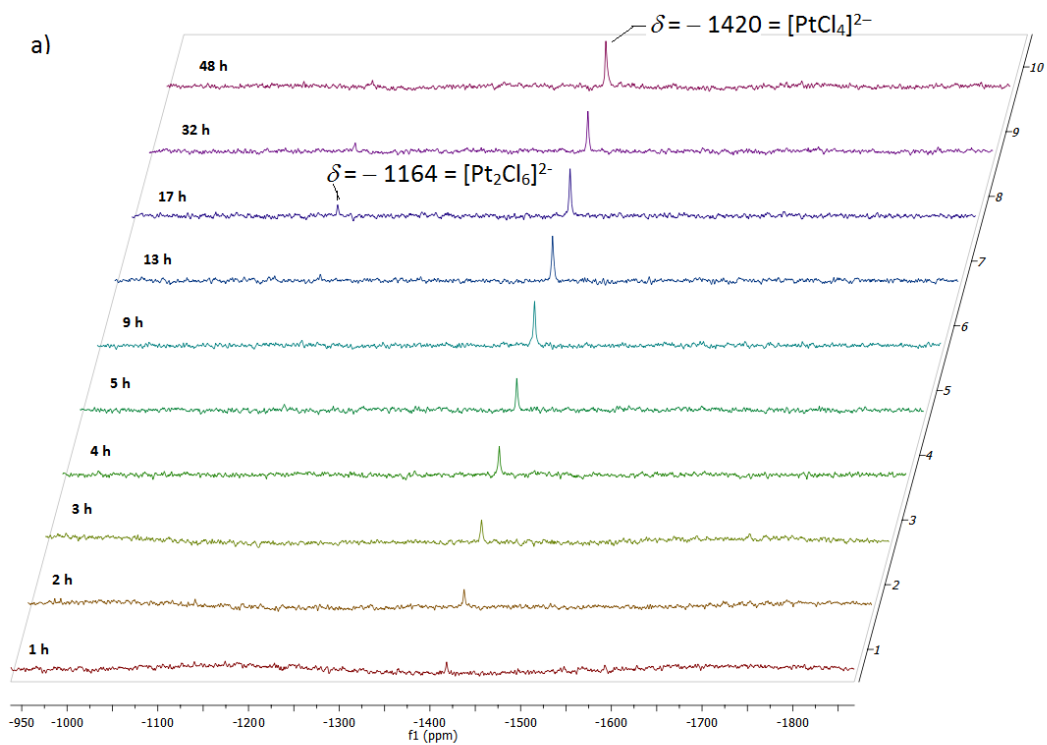


Figure 19: Evolution of platinum species on photolysis of $[\text{nBu}_4\text{N}]_2[\text{PtCl}_6]$ in d_6 -acetone at 323 K under ambient light, in $^{195}\text{Pt}\{^1\text{H}\}$ NMR spectra (107 MHz) in area spanning a) – 950 to – 1850 ppm, b – 2050 to – 2950 ppm.

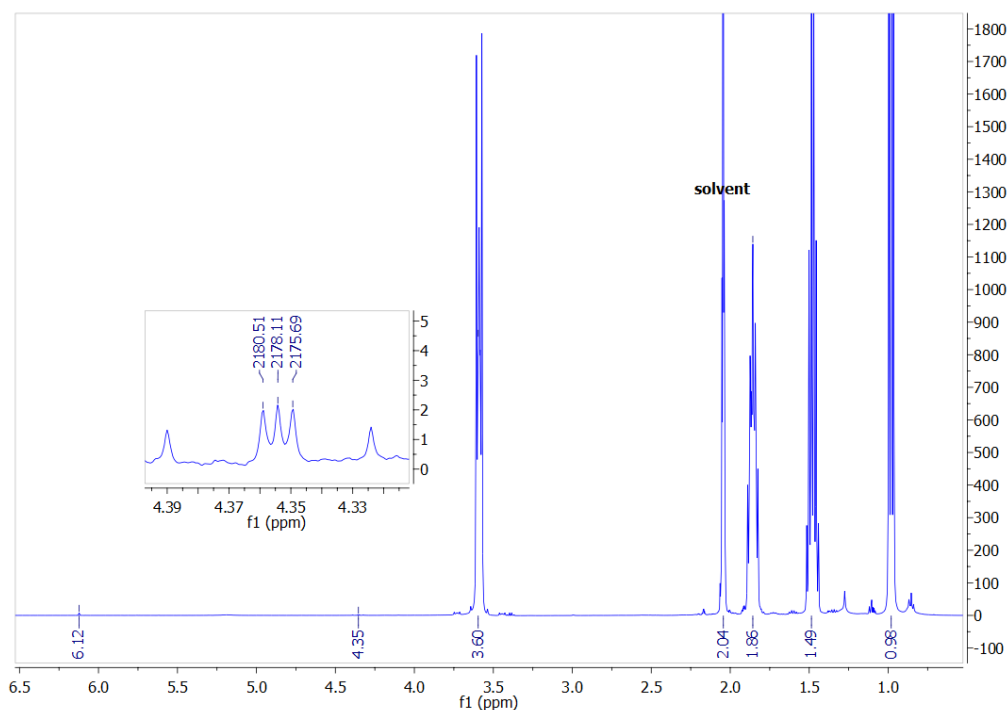


Figure 20: The ^1H -NMR spectrum (500 MHz; with enlargement of a new signal at 4.35 ppm) of the reaction mixture of $[\text{nBu}_4\text{N}]_2[\text{PtCl}_6]$ in d_6 -acetone under heating and ambient light.

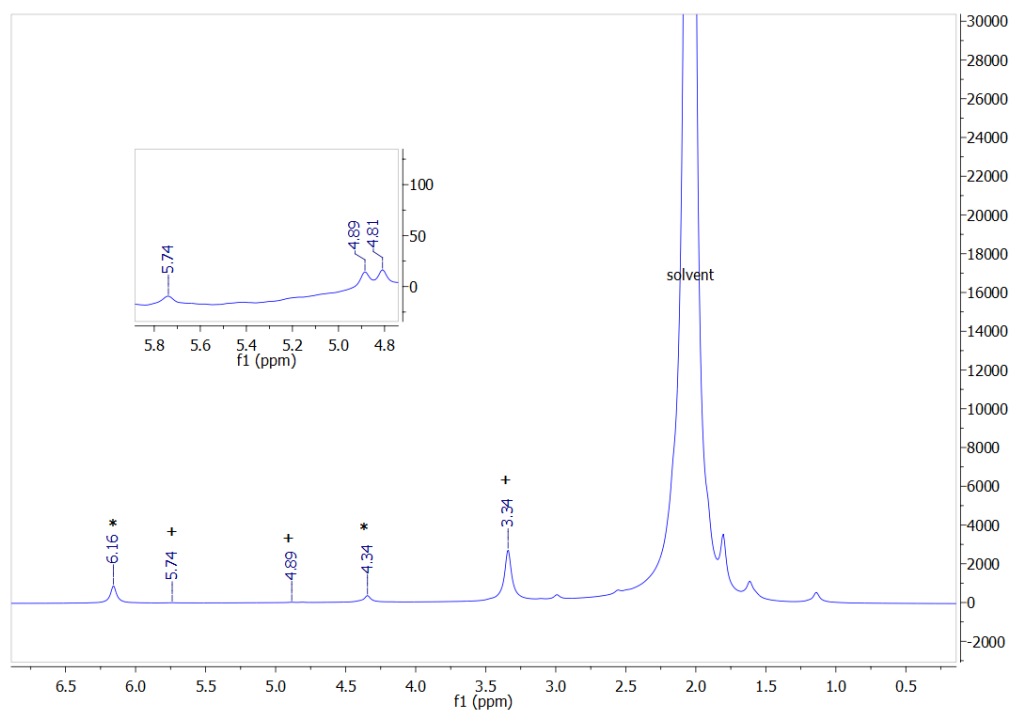


Figure 21: The ^2D NMR spectrum (76.8 MHz) of thermal reaction under ambient light mixture of $[\text{nBu}_4\text{N}]_2[\text{PtCl}_6]$ in d_6 -acetone, with enlargement of signals at 4.8 and 5.7 ppm. *observed on ^1H NMR spectrum, + only appeared on $^2\text{D}\{^1\text{H}\}$ NMR spectrum.

Furthermore, the reaction of ${}^n\text{Bu}_4\text{N}^+$ with $[\text{PtCl}_6]^{2-}$ in acetone under reflux for 48 hours was repeated but rigorously in the dark in a set of amber coated glass apparatus. The ${}^1\text{H}$ and ${}^{195}\text{Pt}\{{}^1\text{H}\}$ NMR analysis demonstrated no reaction. Conversely, when the solution of tetrabutylammonium hexachloroplatinate(IV) was illuminated under ambient light at room temperature, the hexachloroplatinate(IV) was consumed and the olefin compound was formed.

Thus it is shown that $[{}^n\text{Bu}_4\text{N}]_2[\text{PtCl}_6]$ is inert under purely thermal conditions, but that in the presence of light, $[\text{PtCl}_6]^{2-}$ is consumed and $[\text{PtCl}_4]^{2-}$ appears^{67-69, 71-73, 121} along with Pt^{II} -olefin complexes. Furthermore, when carried out under illumination with ambient light under reflux in d_6 -acetone, there was evidence of deuterium incorporation into the butyl of $({}^n\text{Bu}_4\text{N})^+$ cation implying a viable C–H activation process and the H/D exchange with the solvent.

2.2.2.1. Photochemistry of $[{}^n\text{Bu}_4\text{N}]_2[\text{PtCl}_6]$

Shul'pin and co-workers reported the reaction of hydrocarbons with $[\text{PtCl}_6]^{2-}$ under irradiation as well as thermally⁷⁵⁻⁷⁸ but the importance of light in the activation of ${}^n\text{Bu}_4\text{N}^+$ cation was unexpected. Therefore, the photochemistry of $[{}^n\text{Bu}_4\text{N}]_2[\text{PtCl}_6]$ was studied and to begin, UV-vis spectra of the chloroplatinate anions were recorded, followed by irradiation under a variety of wavelengths to determine the wavelength necessary to activate $[\text{PtCl}_6]^{2-}$ in the formation of the butadiene-platinum(II) complex.

A UV-vis spectrum (Figure 22) of a solution of tetrabutylammonium hexachloroplatinate(IV) in acetone showed an absorption with $\lambda_{\text{max}} = 324$ nm with a shoulder at about 370 nm; a weak, longer wavelength absorption was also seen at 470 nm. The UV-vis spectrum of pure acetone is shown for reference. To define the viable wavelength responsible for the activation of $({}^n\text{Bu}_4\text{N})^+$ by $[\text{PtCl}_6]^{2-}$ photolysis of the complex in acetone at a variety of wavelengths was carried out. Using the UV-vis spectra as a guide, the irradiations were conducted at each of 495, 435, 345 and 305 nm for 10 minutes. The ${}^{195}\text{Pt}\{{}^1\text{H}\}$ NMR spectra

demonstrated consumption of $[\text{}^n\text{Bu}_4\text{N}]_2[\text{PtCl}_6]$ on irradiation at wavelengths shorter than 495 nm, with higher rates at 345 and 305 nm where 45% conversion was obtained compared to only about 3% consumption on irradiation at 435 nm. The platinum consumption was in accordance with the $^1\text{H-NMR}$ spectra in which on irradiation at 345 and 305 nm, a peak in the olefinic region at 4.3 ppm was seen. Therefore, experiments to investigate the photoreaction of $[\text{PtCl}_6]^{2-}$ with $(\text{}^n\text{Bu}_4\text{N})^+$ cation were conducted under the irradiation of $h\nu > 305$ nm.

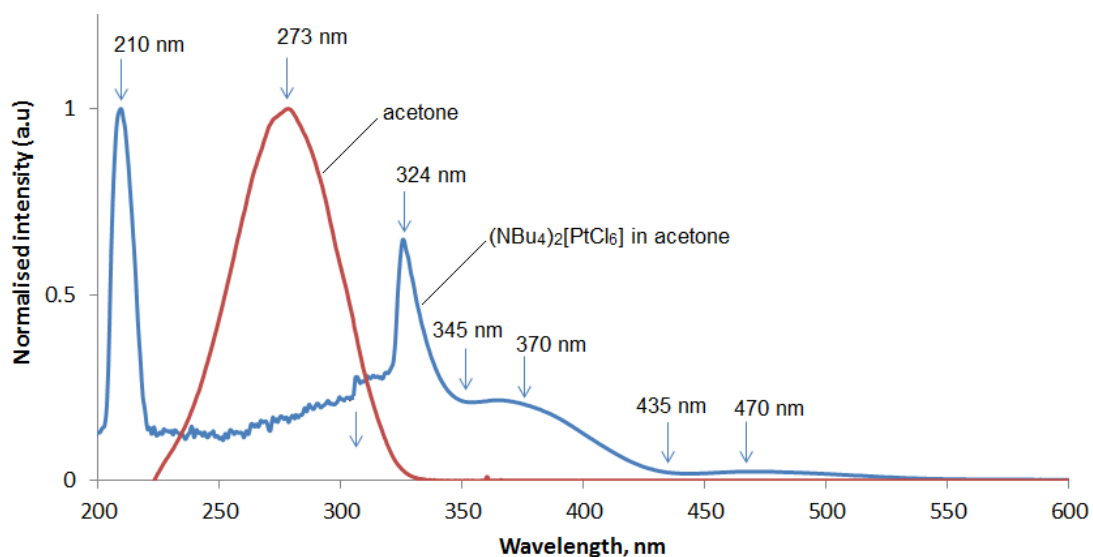


Figure 22: The UV-vis spectra of acetone and $[\text{}^n\text{Bu}_4\text{N}]_2[\text{PtCl}_6]$ in acetone

Light can be considered as an energy source for a homolytic reaction. Red light has an energy of 167 kJ mol^{-1} ($\lambda = 715 \text{ nm}$), blue light ($\lambda = 408 \text{ nm}$) corresponds to energy of 293 kJ mol^{-1} . Ultraviolet radiation ($\lambda = 205 \text{ nm}$) corresponds to an energy of 586 kJ mol^{-1} which theoretically is able to cleave a C–H bond (435 kJ mol^{-1}).⁶ In the activation of the $(\text{}^n\text{Bu}_4\text{N})^+$ cation, the substantial role of light as only a radical initiator through a radical chain reaction was considered. However, irradiation of $\text{}^n\text{Bu}_4\text{NCl}$ compound in acetone did not activate the ammonium ion as confirmed by $^1\text{H-NMR}$ spectroscopy implying an important role of platinum(IV) complex in activation of NBu_4^+ cation.

UV-vis spectra of the starting material, $[\text{}^n\text{Bu}_4\text{N}]_2[\text{PtCl}_6]$ as well as the observed products, $[\text{}^n\text{Bu}_4\text{N}]_2[\text{PtCl}_4]$ and $[\text{}^n\text{Bu}_4\text{N}]_2[\eta^2\text{-Cl}_3\text{Pt}(\text{C}_4\text{H}_6)\text{-}\eta^2\text{-PtCl}_3]$, **I**, in acetone and in

dichloromethane were recorded, and molar absorptivity of those complexes were determined. Data of the molar absorptivity of those complexes are tabulated in Table 5. As mentioned earlier, in acetone $[\text{nBu}_4\text{N}]_2[\text{PtCl}_6]$ absorbs light strongly at 210 nm and 324 nm in which the magnitude of molar extinction coefficient suggests the absorption bands contributed to electronic transitions which are MLCT and LMCT. A weak band observed at 370 nm suggests electronic transitions of spin allowed but Laporte forbidden. The pattern is similar with the spectra of $[\text{nBu}_4\text{N}]_2[\text{PtCl}_4]$ and $[\text{nBu}_4\text{N}]_2[\eta^2\text{-Cl}_3\text{Pt}(\text{C}_4\text{H}_6)\text{-}\eta^2\text{-PtCl}_3]$ as shown in Figure 24. The absorptivity of $[\text{nBu}_4\text{N}]_2[\eta^2\text{-Cl}_3\text{Pt}(\text{C}_4\text{H}_6)\text{-}\eta^2\text{-PtCl}_3]$ at 210 nm was about 10 times higher than that of $[\text{PtCl}_4]^{2-}$ and $[\text{PtCl}_6]^{2-}$, but clearly, at 324 nm the absorptivity of $[\text{nBu}_4\text{N}]_2[\text{PtCl}_6]$ was higher than that of the products. Thus, when the $[\text{nBu}_4\text{N}]_2[\text{PtCl}_6]$ in acetone was irradiated at $\lambda \geq 305$ nm, the products were expected to be fairly stable. This was confirmed when the butadiene-platinum(II) complex was irradiated. Thus isomerisation of the *anti-trans* to the *anti-cis*-conformer was observed during 40-minute illumination, although longer photolysis appeared to lead to decomposition as shown by ^1H NMR spectra (Figure 23).

The absorption spectrum of $[\text{nBu}_4\text{N}]_2[\text{PtCl}_6]$ in dichloromethane (Figure 25) is different where the main peak is at 269 nm, shorter wavelength than the wavelength observed in acetone although the weak signal at 370 nm was also seen. The pattern is also different from the spectra of $[\text{nBu}_4\text{N}]_2[\text{PtCl}_4]$ and $[\text{nBu}_4\text{N}]_2[\eta^2\text{-Cl}_3\text{Pt}(\text{C}_4\text{H}_6)\text{-}\eta^2\text{-PtCl}_3]$ while the molar absorptivity of $[\text{nBu}_4\text{N}]_2[\text{PtCl}_6]$ at the wavelength lower than 305 nm appeared lower than the that of the products. The pattern of the spectrum as well as the absorptivity of $[\text{nBu}_4\text{N}]_2[\text{PtCl}_6]$ perhaps contributes to low rate of $[\text{PtCl}_6]^{2-}$ consumption so the low yield of the photolysis in dichloromethane.

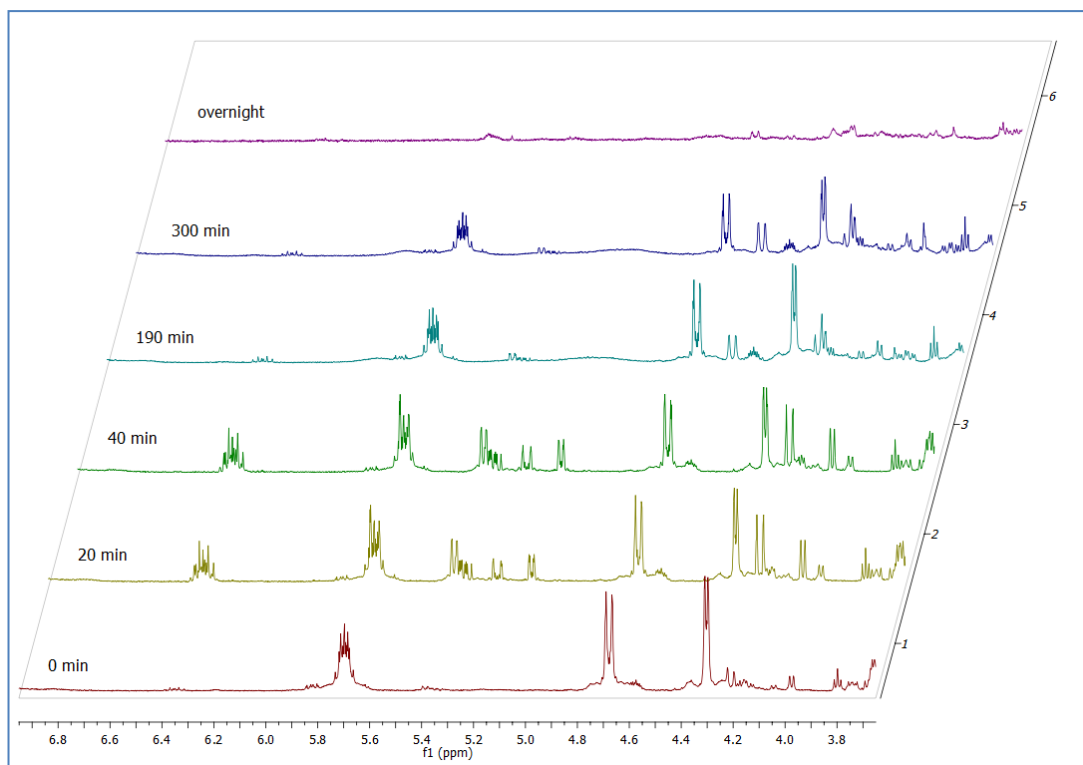


Figure 23: The ^1H NMR spectra of complex I on irradiation in d_6 -acetone.

Table 5: Molar absorptivity of chloroplatinate complexes in different solvents and wavelengths.

Complexes	Solvent	ϵ , $\text{mol}^{-1} \text{dm}^3 \text{cm}^{-1}$
$[\text{nBu}_4\text{N}]_2[\text{PtCl}_6]$	DCM	370 nm: $0.40 \cdot 10^3$
	Acetone	370 nm: $0.45 \cdot 10^3$ 324 nm: $1.29 \cdot 10^3$
$[\text{nBu}_4\text{N}]_2[\text{PtCl}_4]$	DCM	336 nm: $0.07 \cdot 10^3$ 404 nm: $0.06 \cdot 10^3$
	Acetone	336 nm: $0.08 \cdot 10^3$ 404 nm: $0.06 \cdot 10^3$
$[\text{nBu}_4\text{N}]_2[\text{Pt}(\text{C}_6\text{H}_5)_2\text{Cl}_2]$	DCM	310 nm: $0.86 \cdot 10^3$ 227 nm: $7.50 \cdot 10^3$
	Acetone	325 nm: $0.37 \cdot 10^3$ 210 nm: $0.53 \cdot 10^3$

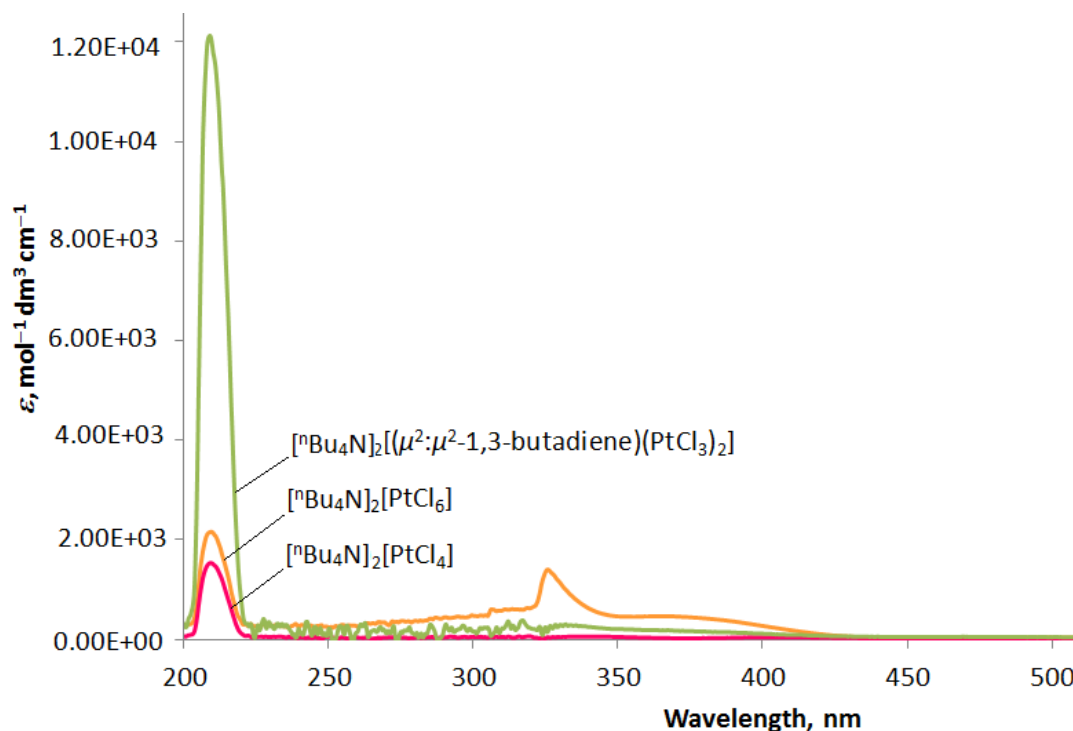


Figure 24: The UV spectra of the chloroplatinate complexes in acetone.

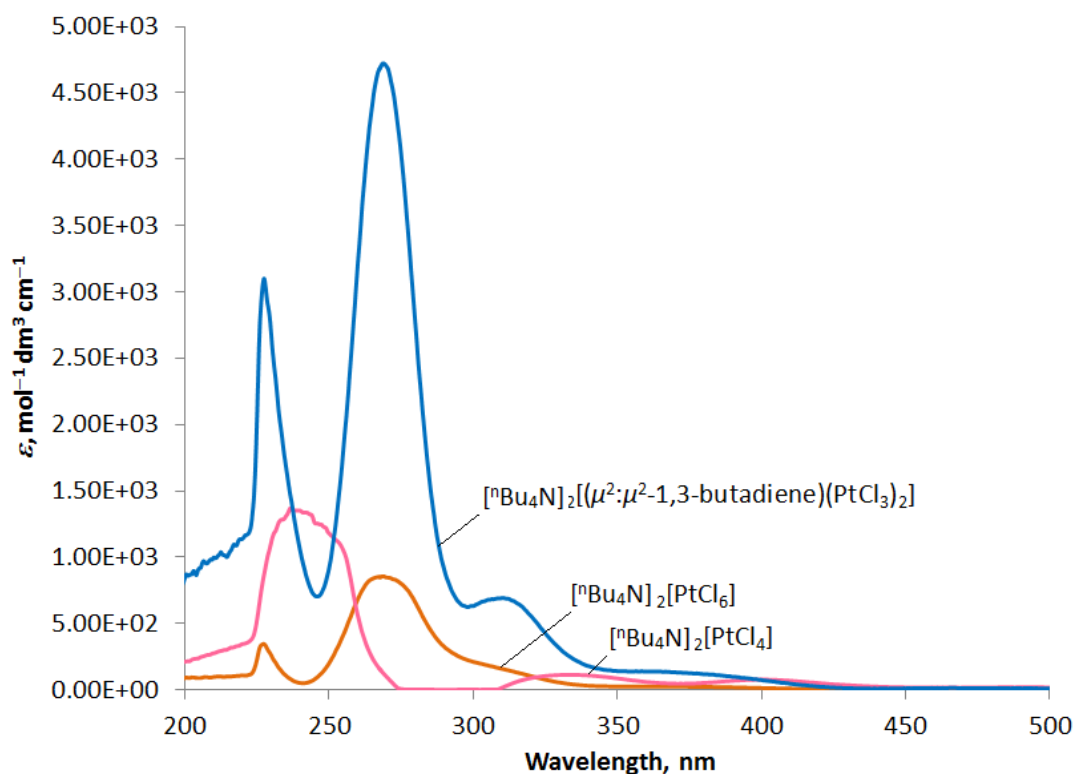


Figure 25: The UV spectra of the chloroplatinate complexes in dichloromethane.

To conclude, the reaction clearly proceeded under ambient light as has shown on the early observation (2.2.1), but the reaction was driven fast under UV light.

Further experiments thus were conducted under UV light completed with the 305 nm filter.

2.2.2.2. Theoretical Calculation on the Excited States of $[\text{PtCl}_6]^{2-}$ Complex

As the reaction proceeded photochemically, it was suggested that an excited state of hexachloroplatinate(IV) plays an important role, therefore, theoretical investigations on the electronic structure of $[\text{PtCl}_6]^{2-}$ excited state were conducted using density functional theory (DFT) approach. Both, ground state geometry optimisation and time dependent (TDDFT) calculations were performed at the B3LYP/TZVP level of theory^{117, 122} utilising ORCA 2.9 code. An effective core potential (ECP) was applied on the platinum atom,¹¹⁷⁻¹¹⁹ and conductor-like screening model (COSMO) was used to accommodate the electrostatic interaction of molecule with solvent by adding the dielectric constant (n_D) and relative permittivity (ϵ) parameters of the solvent into the calculation.¹²³ In this case, the solvent was acetone ($\epsilon = 20.7 \text{ F m}^{-1}$; $n_D = 1.359$).

The calculated absorption spectrum of hexachloroplatinate(IV) in acetone expressed as oscillator strength versus wavelength showed two main bands at 324 nm and 207 nm (Figure 26). The spectrum mirrored the UV spectrum of the complex obtained from the experiment, which implied a reasonable agreement of the calculation method used for the complex. According to the TDDFT calculations, the intense band at $\lambda_{\text{max}} = 207 \text{ nm}$ corresponds to a transition from the ground state (S_0) to an excited singlet state (S_{31}), $S_0 \rightarrow S_{31}$ transition. The visualisation of electron density difference between the ground state (S_0) and the state S_{31} suggests that the state S_{31} has a mixed metal-to-ligand charge transfer (MLCT) and ligand-to-ligand charge transfer (LL'CT) character which together can be denoted as MLL'CT. The absorption band of lower intensity with $\lambda_{\text{max}} = 324 \text{ nm}$ is attributed to a transition to state S_{22} , $S_0 \rightarrow S_{22}$, and the visualisation of electron density difference between S_0 and S_{22} suggests a mixed character of ligand-to-ligand

charge transfer (LL'CT) and ligand-to-metal charge transfer (LMCT). The transition is labelled as LML'CT.

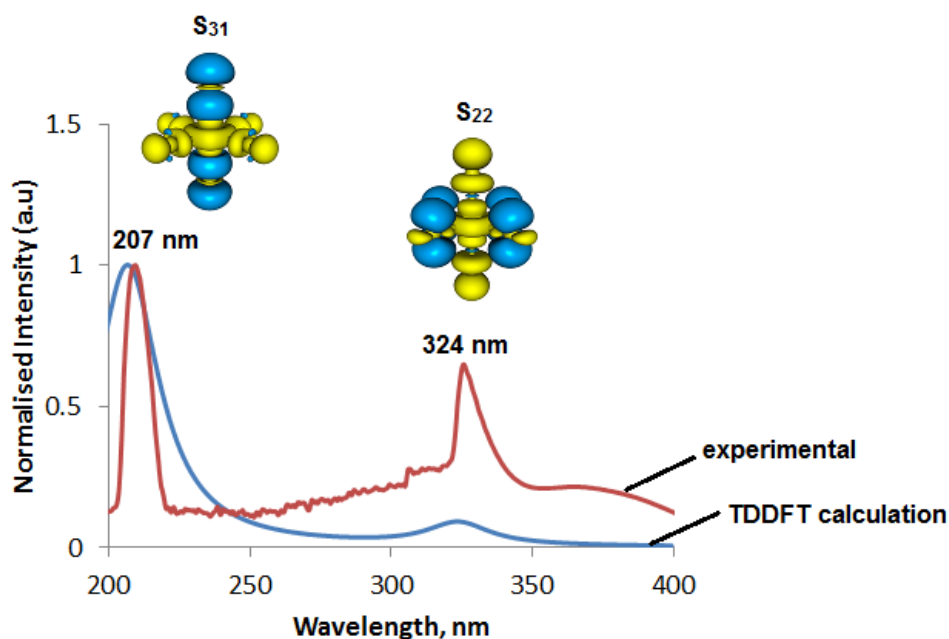


Figure 26: The electronic spectra of $[\text{PtCl}_6]^{2-}$ from the experimental method and the calculation along with the visualisation of electron density difference between the ground state and the excited state associated with the states of S_{31} (207 nm) and S_{22} (324 nm) (note: yellow: increasing of electron density and blue: decreasing of electron density compared to the ground state).

Since the compound contains a heavy Pt atom that provides a strong spin-orbit coupling (SOC) and, consequently, fast inter-system-crossing (ISC) between states of singlet and triplet manifold, it was suggested that the excited state, in which the compound reacts and so the optimised geometry, is the lowest excited triplet state (T_1). The optimised geometry of the state T_1 reveals Pt–Cl bond length changes where the Pt–Cl bond on the z axis was elongated by 0.36 Å from 2.47 Å in the ground state to 2.83 Å in the T_1 state while other four Pt–Cl bonds were shortened by 0.19 Å and became 2.28 Å in the T_1 state. The character of the T_1 state in its own relaxed geometry can be assigned as ligand-to-ligand charge transfer (LL'CT) (Figure 27).

The bond elongation, caused by the electron density from ligand to metal and ligand that populates the anti-bonding molecular orbital, Pt–Cl σ^* , probably leads to the cleavage of the Pt–Cl bonds on the z-axis as shown in the visualisation in Figure 27; those two bonds are the same in bond length. This observation is in accordance with the experimental and theoretical study reported by Kaufman, *et al.*¹²⁴ in which $[\text{PtCl}_6]^{2-}$ undergoes a photodissociation generating $[\text{Pt}^{\text{III}}\text{Cl}_4]^-$, Cl^- , and radical of Cl^\bullet .

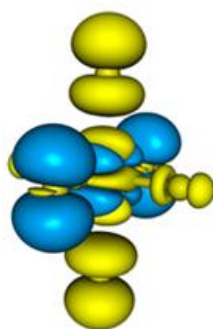


Figure 27: Electron density difference between the ground state (S_0) and the T_1 state calculated for $[\text{PtCl}_6]^{2-}$ in relaxed T_1 state geometry (note: yellow: increasing of electron density and blue: decreasing of electron density compared to the ground state).

2.2.2.3. Identification of paramagnetic species

Having established that the reaction is driven photochemically, it was then important to establish a possible mechanism that would allow for C–H activation. Simple ligand dissociation was ruled out as this can occur thermally and so it seemed that an excited state would be necessary. Shul'pin and Shilov⁷⁵ had reported previously that photochemical reaction of $[\text{PtCl}_6]^{2-}$ with *n*-hexane was possible leading to the formation of a π -hexene-platinum(II) complex although a mechanism was never established. More recently, Kaufman, *et al.*¹²⁴ reported a theoretical study showing that on photodissociation, $[\text{PtCl}_6]^{2-}$ was reduced to $[\text{Pt}^{\text{III}}\text{Cl}_4]^-$ through a reductive fragmentation step in which a dissociation of Cl^- occurred after internal conversion into lower electronic states, along with the formation of a highly vibrationally excited transient $[\text{PtCl}_5]^-$ ion which subsequently loses Cl^\bullet .

The EPR spectra of the *in situ* photoreaction of tetrabutylammonium hexachloroplatinate(IV) in acetone and in dichloromethane were recorded at 120 K. After two-minute irradiation in acetone, the spectrum showed a signal with g value of 2.3998. The peak intensified and more detail was evident when the irradiation was continued for 50 minutes, showing a singlet and a doublet. The signal was assigned to be a Pt(III) radical, in which the electron was coupled to the NMR-active platinum, ^{195}Pt isotope (33.8% abundance, $I = \frac{1}{2}$) to give the doublet with a hyperfine constant (a) of about 42.5 mT, whereas the singlet was the radical corresponding to NMR-inactive isotopes. The same observation with $g = 2.402$ was also made when the spectrum was recorded in dichloromethane given in Figure 28.

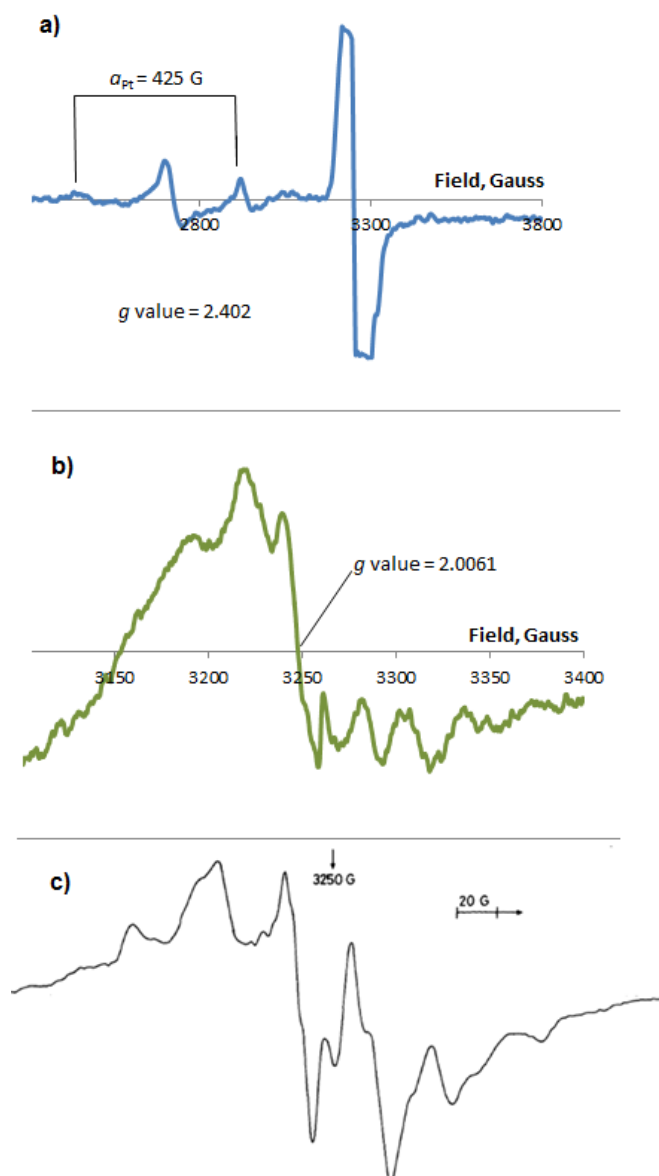


Figure 28: The EPR spectrum of $[\text{Bu}_4\text{N}]_2[\text{PtCl}_6]$ on irradiation for 20 minutes in dichloromethane at 120 K. a) on wide range, b) enlargement in the organic area and c) $\text{Et}_3\text{N}^{\bullet\bullet}$ as reported in ref. ¹²⁵

A signal in the EPR spectrum with a similar g value ($g \cong 2.4$) had been reported previously in irradiation of a frozen acetone solution of $\text{Na}_2[\text{PtCl}_6] \cdot \text{H}_2\text{O}$ and had been attributed to a platinum(III) species.⁷⁸ Moreover, the observation of platinum(III) species using EPR spectroscopy ($g = 2.417$; $a_{195\text{-Pt}} = 45.5 \pm 0.5$ mT) has also been described when a $\text{K}_2[\text{PtCl}_4]$ crystal was irradiated at 77 K.¹²⁶

In addition to the Pt(III) radical, a peak corresponded to an organic radical was observed with $g = 2.0084$ in acetone and $g = 2.0061$ in dichloromethane (Figure 28). A rather similar spectrum for triethylammonium radical cation had been reported by Eastland, *et al.*¹²⁵ The signal recorded at 77 K is a broad quartet at 325.0 mT with a centre split by proton couplings with a $a_H = 3.8$ mT and appeared as a septet with the $a_H = 1.9$ mT when recorded at 140 K due to anisotropy change to isotropy on increase of the temperature. By comparing the signal to the $^{15}\text{N}^+\text{NEt}_3$ spectrum, the organic peak observed in the irradiation of $[\text{nBu}_4\text{N}]_2[\text{PtCl}_6]$ was assigned as an *N*-based radical.

In conclusion, EPR spectroscopy provided evidence of radical generation namely platinum(III) and *N*-based radical on the irradiation of $[\text{nBu}_4\text{N}]_2[\text{PtCl}_6]$.

2.2.2.4. Attempt to quantify platinum species in the mixture during the photolysis of $[\text{nBuN}^+]_2[\text{PtCl}_6]$

$^{195}\text{Pt}\{^1\text{H}\}$ NMR spectroscopy has shown a presence of $[\text{PtCl}_4]^{2-}$ and Pt(II)-olefin in a photoreaction mixture of $[\text{PtCl}_6]^{2-}$ with NBu_4^+ , and attempts to quantify the platinum species by employing ^{195}Pt NMR spectroscopy during the reaction have been made. The first attempt was by direct integration of particular peaks to represent the amount of the related platinum species. To proceed by this method, it was firstly necessary to optimise the relaxation time, T_1 , of the platinum species. The relaxation time represents the time required for NMR-active nuclei to relax from high energy states back to their ground state after application of a pulse. The T_1 of platinum complexes is symmetry dependent in addition to being sensitive to the cation, solvent, field and temperature. In an NMR spectrometer, a pulse delay, D_1 , is generally equal to 1 – 5 times T_1 and can be varied to measure T_1 . Pletcher *et al.* suggested that highly symmetrical Pt complexes, such as $[\text{PtCl}_6]^{2-}$, relax slowly and therefore require a pulse delay, D_1 of about 0.5 seconds, which would be unnecessary for most complexes.¹²⁷ Pregosin reported that T_1 of ^{195}Pt in oxidation states of 0, +2 and +4 is in the range of 0.014 to 8.31 seconds and that the most common value is less than 2 seconds. T_1 also depends on the solvent system used;

for example, for $[\text{}^n\text{Bu}_4\text{N}]_2[\text{PtCl}_6]$ in methanol $T_1 = 1.65$ s, but in dichloromethane $T_1 = 0.89$ s.¹¹²

In this work, experiments to optimise D_1 of $[\text{}^n\text{Bu}_4\text{N}]_2[\text{PtCl}_6]$, $[\text{}^n\text{Bu}_4\text{N}]_2[\text{PtCl}_4]$, and $[\text{}^n\text{Bu}_4\text{N}]_2[\text{Pt}_2\text{Cl}_6(\text{butadiene})]$ were carried out. A solution of each complex was prepared separately and under the same conditions, being at the same concentration. Their spectra were measured for a variety of values of D_1 . Integrations were measured after processing the spectra and all processing parameters were the same for all the spectra. A curve describing the delay time against integration for those three complexes is given in Figure 29. As expected, $[\text{PtCl}_6]^{2-}$ relaxed more slowly than those square-planar complexes. Considering a signal-to-noise ratio (SNR) for each spectrum between 2 and 4, the differences of the integration for $[\text{}^n\text{Bu}_4\text{N}]_2[\text{PtCl}_4]$ and $[\text{}^n\text{Bu}_4\text{N}]_2[\text{Pt}_2(\text{butadiene})\text{Cl}_6]$ were small for all pulse delays used.

To test the consistency of the integration against the known concentrations, an equimolar mixture of $[\text{}^n\text{Bu}_4\text{N}]_2[\text{PtCl}_6]$, $[\text{}^n\text{Bu}_4\text{N}]_2[\text{PtCl}_4]$, and $[\text{}^n\text{Bu}_4\text{N}]_2[\eta^2\text{-Cl}_3\text{Pt}(\text{C}_4\text{H}_6)\text{-}\eta^2\text{-PtCl}_3]$ was prepared. The recording of spectra was carried out in three different areas to cover those three complexes due to the limit of spectral width that can be acquired by the spectrometer. The D_1 for $[\text{}^n\text{Bu}_4\text{N}]_2[\text{PtCl}_6]$, $[\text{}^n\text{Bu}_4\text{N}]_2[\text{PtCl}_4]$, and $[\text{}^n\text{Bu}_4\text{N}]_2[\eta^2\text{-Cl}_3\text{Pt}(\text{C}_4\text{H}_6)\text{-}\eta^2\text{-PtCl}_3]$ was set to be 5 s, 1 s, and 1 s, respectively. The results, however, showed the inconsistency of the peak integration, so that the relative integrations were $[\text{}^n\text{Bu}_4\text{N}]_2[\text{PtCl}_6] : [\text{}^n\text{Bu}_4\text{N}]_2[\text{PtCl}_4] : [\text{}^n\text{Bu}_4\text{N}]_2[\eta^2\text{-Cl}_3\text{Pt}(\text{C}_4\text{H}_6)\text{-}\eta^2\text{-PtCl}_3] = 1 : 6.6 : 10.5$. Thus, employing direct integration to compare the relative amounts of those complexes was unreliable.

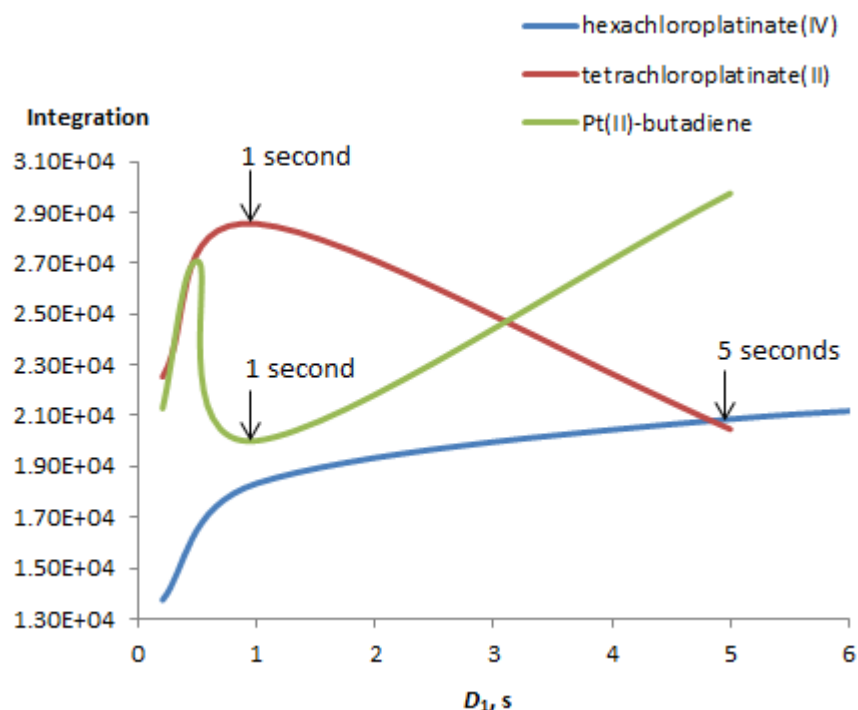
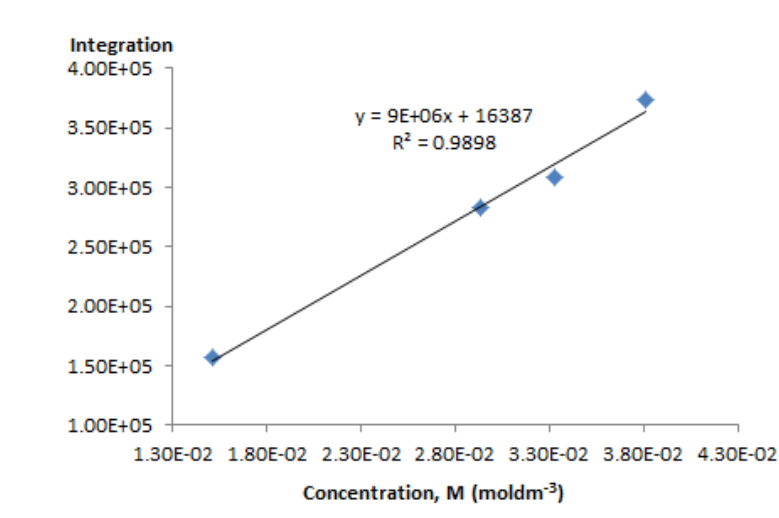


Figure 29: Graph showing integration of peaks in vary of pulse delay, D_1 , for $[\text{nBu}_4\text{N}]_2[\text{PtCl}_6]$, $[\text{nBu}_4\text{N}]_2[\text{PtCl}_4]$, and $[\text{nBu}_4\text{N}]_2[\eta^2\text{-Cl}_3\text{Pt}(\text{C}_4\text{H}_6)\text{-}\eta^2\text{-PtCl}_3]$ in d_6 -acetone solutions.

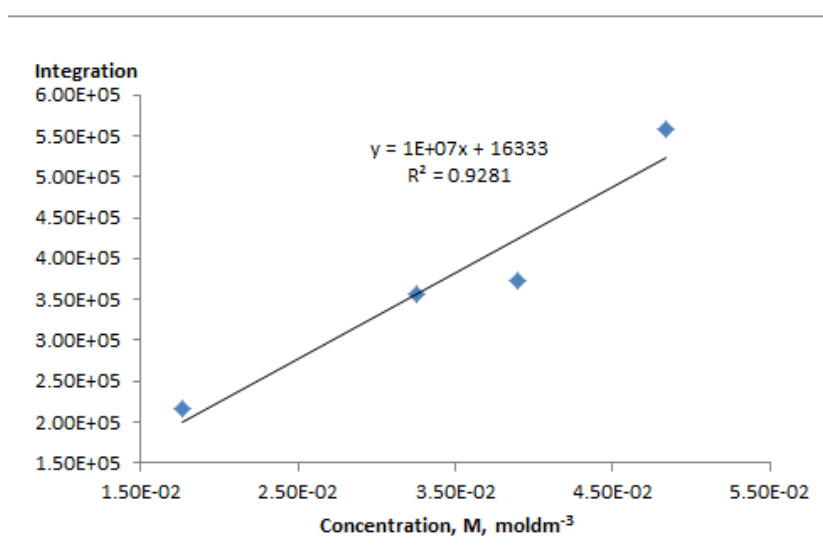
$^{195}\text{Pt}\{^1\text{H}\}$ NMR spectroscopy had been used as a quantitative technique in the photoreduction of $[\text{PtCl}_6]^{2-}$ to generate either $[\text{PtCl}_4]^{2-}$ or Pt^0 depending on conditions. By a calibration method, absolute concentrations of $[\text{PtCl}_6]^{2-}$ and $[\text{PtCl}_4]^{2-}$ in a solution are estimated from integrations of the peaks.^{69, 127}

Knowing that quantifying the platinum changes could not be done by direct integration, a second attempt to measure the amount of platinum was conducted through a calibration method. This method was carried out for $[\text{nBu}_4\text{N}]_2[\text{PtCl}_6]$ and $[\text{nBu}_4\text{N}]_2[\text{PtCl}_4]$, but not for $[\text{nBu}_4\text{N}]_2[\eta^2\text{-Cl}_3\text{Pt}(\text{C}_4\text{H}_6)\text{-}\eta^2\text{-PtCl}_3]$ because the chemical shift of the complex was shifted in the reaction mixture and too weak to be integrated. In a variety of concentrations, spectra were acquired under identical conditions and parameters, the spectra were processed to give good baselines then related peaks were integrated.

Plots of integrated peak area versus concentration for both $[\text{nBu}_4\text{N}]_2[\text{PtCl}_6]$ and $[\text{nBu}_4\text{N}]_2[\text{PtCl}_4]$ are given in Figure 29. In both cases a linear relationship was observed, suggesting this method could be appropriate for determining concentration of platinum species. The equations describing the linear fit are given in Figure 29. To test the validity of this approach a solution of $[\text{nBu}_4\text{N}]_2[\text{PtCl}_6]$ in d_6 -acetone was prepared (5.6 mg in $6.57 \times 10^{-1} \text{ cm}^3$ $M = 9.55 \times 10^{-3}$). Its integration was measured, and by using the equation, the calculation gave a concentration, $M = 9.19 \times 10^{-3}$. A solution of $[\text{nBu}_4\text{N}]_2[\text{PtCl}_4]$ (5.4 mg in $6.68 \times 10^{-1} \text{ cm}^3$ of d_6 -acetone, $M = 9.59 \times 10^{-3}$) was also prepared separately to test the equation and by using the equation, the concentration was $9.09 \times 10^{-3} \text{ M}$. The test demonstrated a good agreement of the equations. However, when the linear fits were used to determine the concentrations of an equimolar mixture of $[\text{nBu}_4\text{N}]_2[\text{PtCl}_4]$ and $[\text{nBu}_4\text{N}]_2[\text{PtCl}_6]$ the concentration values obtained deviated by up to 70% for $[\text{nBu}_4\text{N}]_2[\text{PtCl}_4]$ and 30% for $[\text{nBu}_4\text{N}]_2[\text{PtCl}_6]$. Therefore, in monitoring the photolysis of hexachloroplatinate(IV) complex, integral peaks were utilised to only justify relative concentration changes of $[\text{PtCl}_6]^{2-}$ to the initial amount in percentage.



a



b

Figure 30: Calibration curves of $[\text{}^n\text{Bu}_4\text{N}]_2[\text{PtCl}_6]$ (a) and $[\text{}^n\text{Bu}_4\text{N}]_2[\text{PtCl}_4]$ (b) showing correlations of integral peaks recorded from $^{195}\text{Pt}\{^1\text{H}\}$ NMR experiments with complexes concentration in solutions of in d_6 -acetone.

Recording the $^{195}\text{Pt}\{^1\text{H}\}$ NMR spectra was also tried in an NMR spectrometer with a wider spectral width of 131,579 Hz equals 2000 ppm (spectrometer frequency for ^{195}Pt nuclear: 64.52 MHz) that can span two different platinate complex regions. However, integration of peaks could not be reliable as baseline rolling was observed on the spectra (Figure 31), likely due to acoustic ringing of the probe.

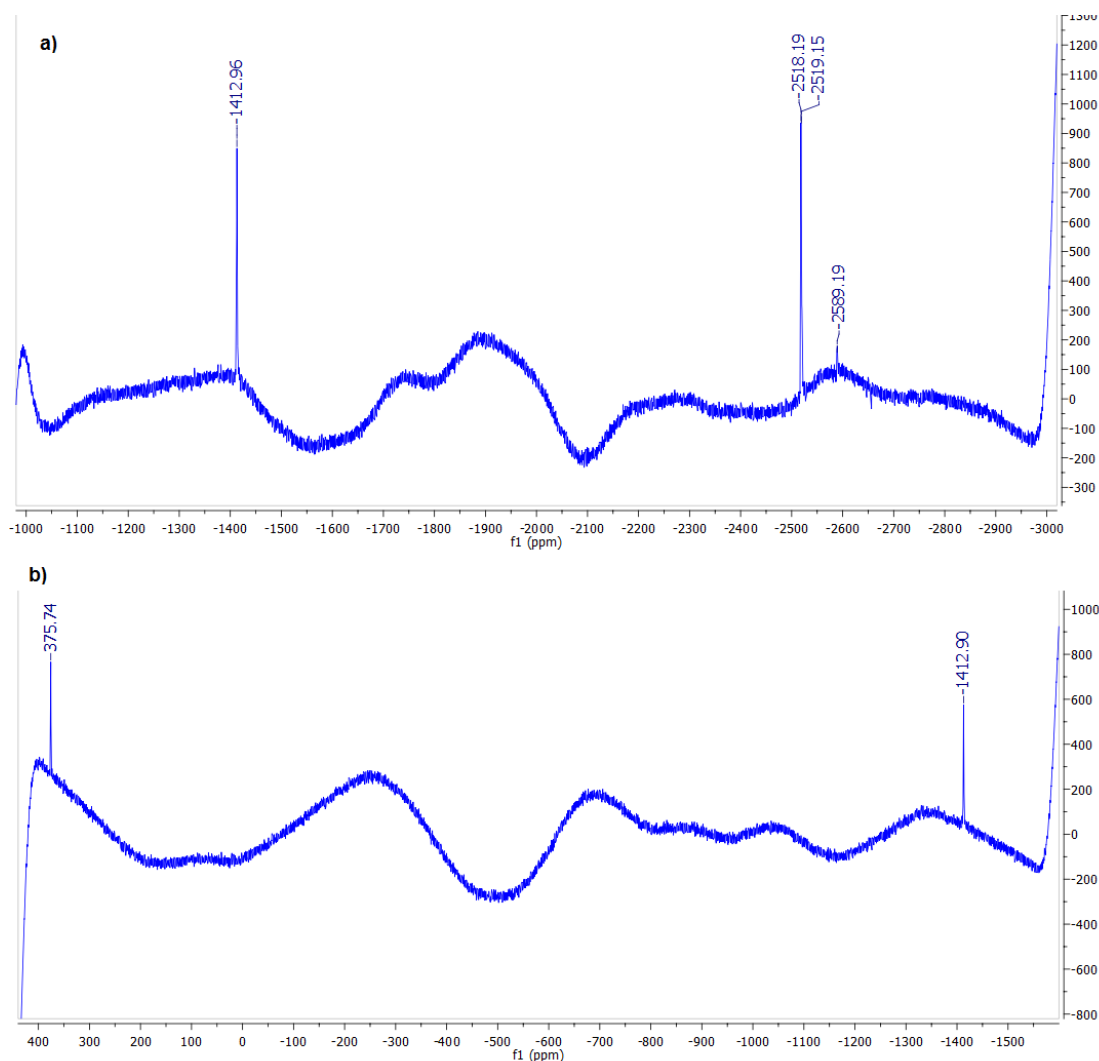


Figure 31: $^{195}\text{Pt}\{^1\text{H}\}$ NMR spectra of a mixture of $[\text{nBu}_4\text{N}]_2[\text{PtCl}_6]$, $[\text{nBu}_4\text{N}]_2[\text{PtCl}_4]$, $[\text{nBu}_4\text{N}]_2[(\text{PtCl}_3)_2(\text{C}_4\text{H}_6)]$ in d_6 -acetone recorded at 64.52 MHz for ^{195}Pt nucleus ($^1\text{H} = 300$ MHz).

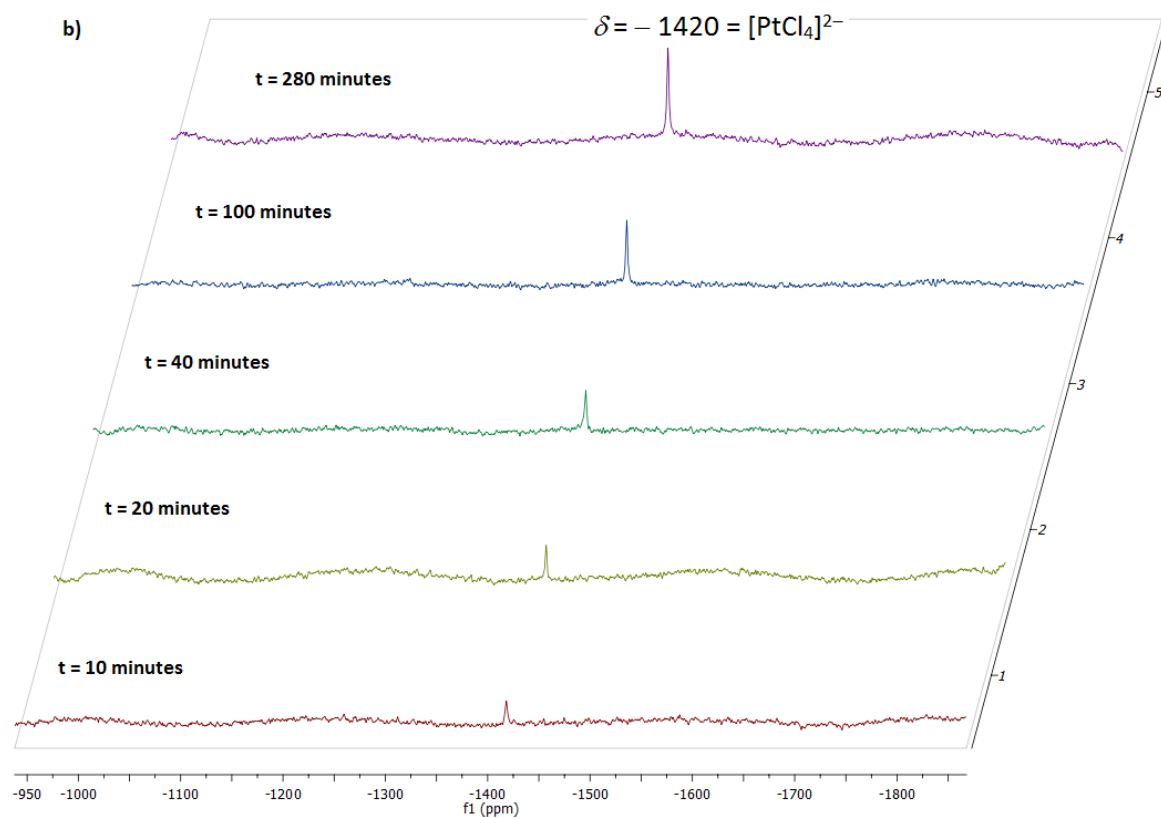
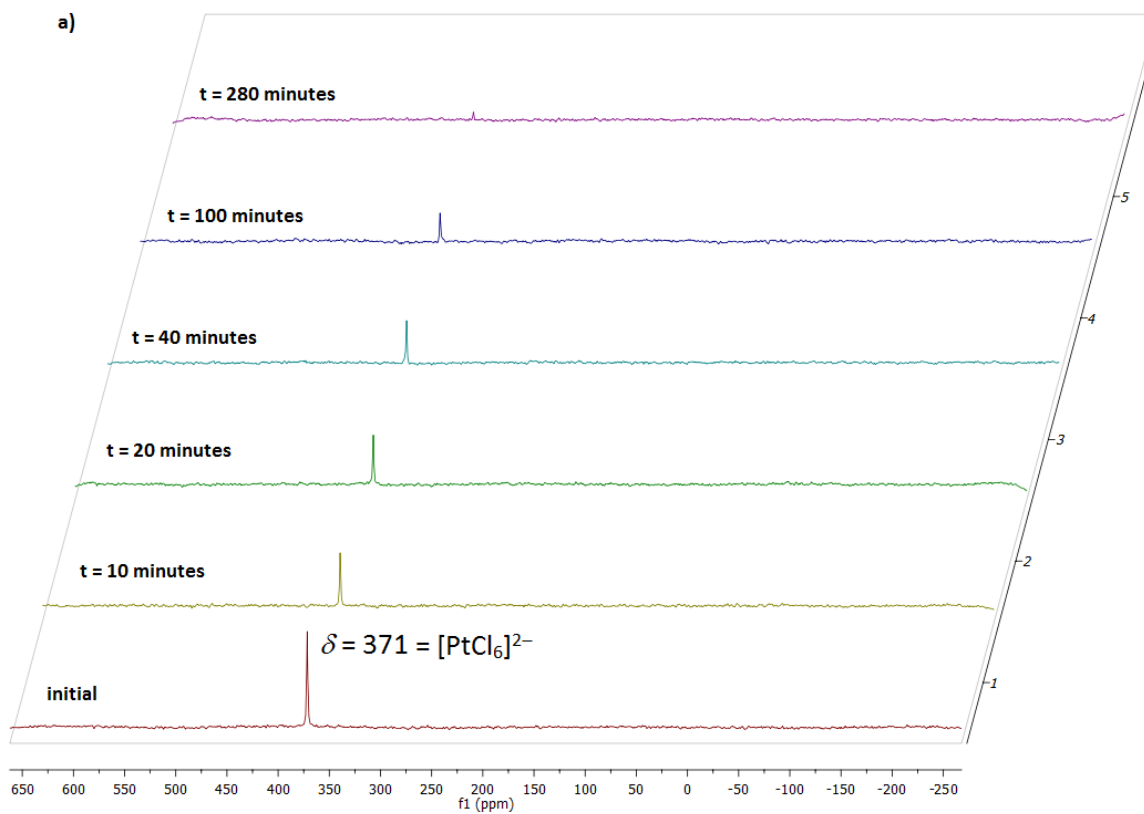
2.2.2.5. Monitoring the photoreaction of $(\text{NBu}_4)_2[\text{PtCl}_6]$ using ^{195}Pt -NMR spectroscopy

Monitoring the platinum speciation was repeated under illumination at room temperature. The $[\text{nBu}_4\text{N}]_2[\text{PtCl}_6]$ was placed in a Young's NMR tube in a solution of d_6 -acetone. The source of light was a 125 W, medium-pressure mercury vapour lamp complete with water flow to maintain room temperature and with a filter to cut out wavelength shorter than 305 nm. An analogous photolysis of $[\text{nBu}_4\text{N}]_2[\text{PtCl}_6]$ in dichloromethane was also carried out.

In acetone, irradiation of $[\text{PtCl}_6]^{2-}$ instantaneously formed $[\text{PtCl}_4]^{2-}$ shown by an appearance of a signal at -1420 ppm after 10 minutes of the illumination. In the longer irradiation, the peak integration of $[\text{PtCl}_6]^{2-}$ species decreased while that of $[\text{PtCl}_4]^{2-}$ went up along with a presence of a signal in the olefin area at -2575 ppm after 100 minutes of photolysis. At the end of photolysis shown by the disappearance of the signal of $[\text{PtCl}_6]^{2-}$, the peaks of the $[\text{PtCl}_4]^{2-}$ and the Pt(II)-olefin remained observed. The evolution of the platinum species is shown in Figure 32.

Similar to the photolysis in d_6 -acetone, in CD_2Cl_2 the $[\text{PtCl}_6]^{2-}$ was consumed to form $[\text{PtCl}_4]^{2-}$ and the olefin-Pt(II) complexes, but the evolution of the platinum species was slower than that in acetone. The $^{195}\text{Pt}\{^1\text{H}\}$ NMR spectra demonstrating the evolution of $[\text{Bu}_4\text{N}]_2[\text{PtCl}_6]$ to $[\text{Bu}_4\text{N}]_2[\text{PtCl}_4]$ and the olefin-platinum(II) complex are given in Figure 33.

The pattern of platinum evolution was also observed when $[\text{Bu}_4\text{N}]_2[\text{PtCl}_6]$ was illuminated under ambient light while heating at 50 °C in d_6 -acetone. As expected, the rate of the Pt(IV) conversion displayed on the graph in the Figure 18 was far slower than the reaction under UV light. The $^{195}\text{Pt}\{^1\text{H}\}$ NMR spectra of the reaction acquired in the olefin-Pt(II) area also gave the peaks which were seen in the photoreaction mixture. Along with the peak of $[\text{PtCl}_4]^{2-}$ at -1420 ppm, which remained until the end of reaction, a signal at -1164 ppm was seen during the reaction, but the signal had disappeared at the end of the reaction. The peak was assigned to be $[\text{Pt}_2\text{Cl}_6]^{2-}$ complex by comparing its chemical shift to the complex prepared separately.



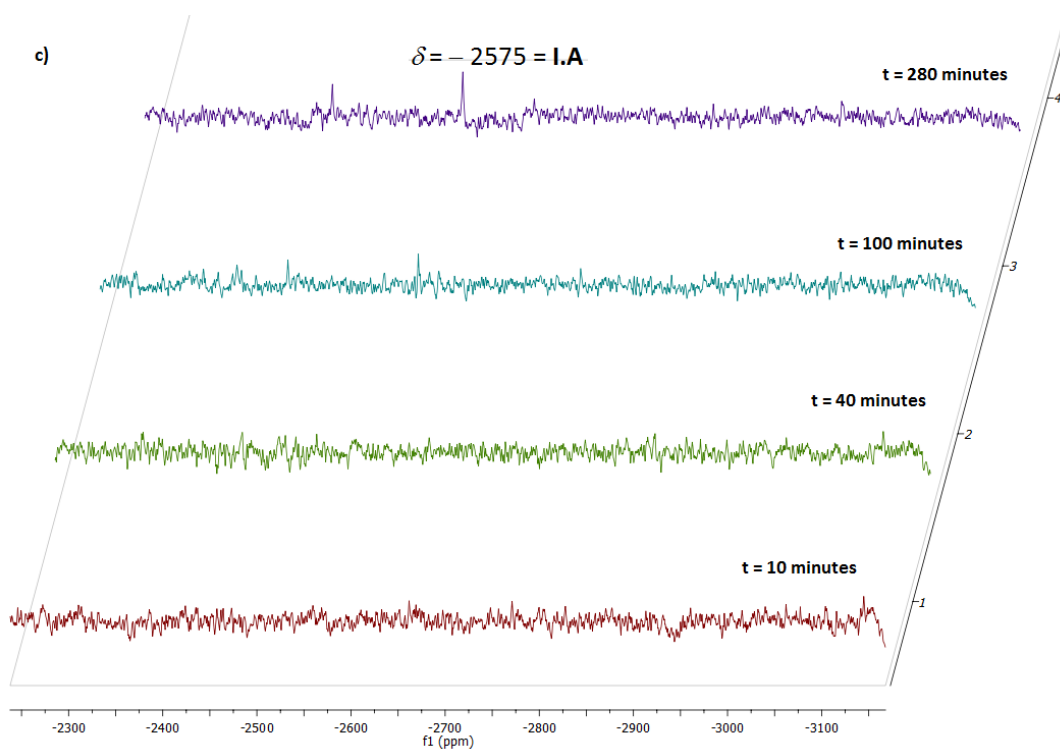
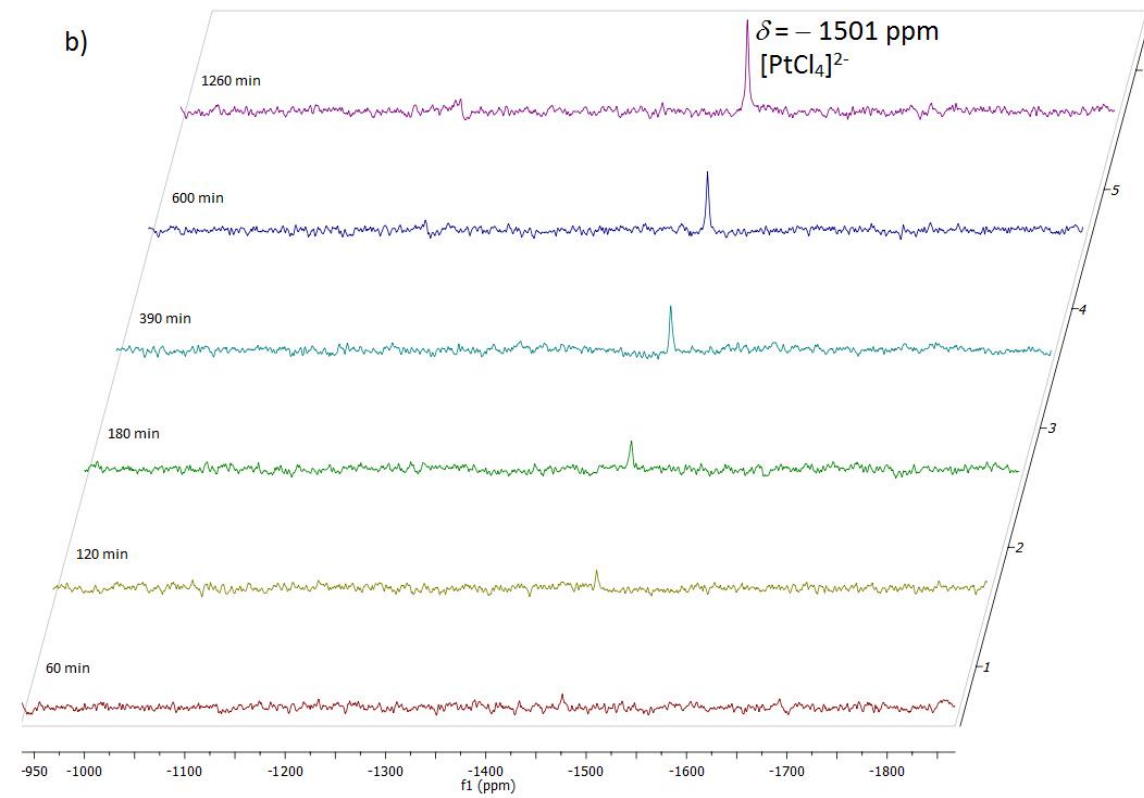
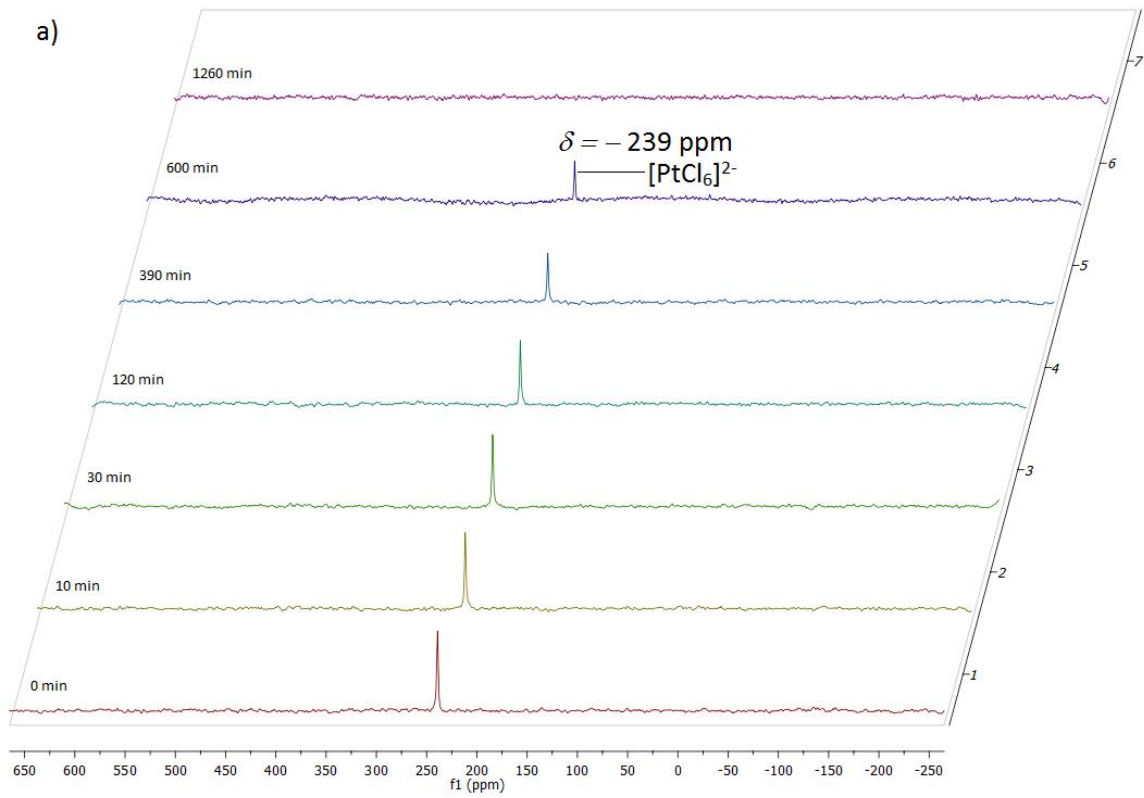


Figure 32: Evolution of platinum species on photolysis of $[\text{Bu}_4\text{N}]_2[\text{PtCl}_6]$ in d_6 -acetone in $^{195}\text{Pt}\{^1\text{H}\}$ NMR spectra (107 MHz) in area spanning a) 650 to -250 ppm b) -950 to -1850 ppm, c) olefin area: -2050 to -2950 ppm.



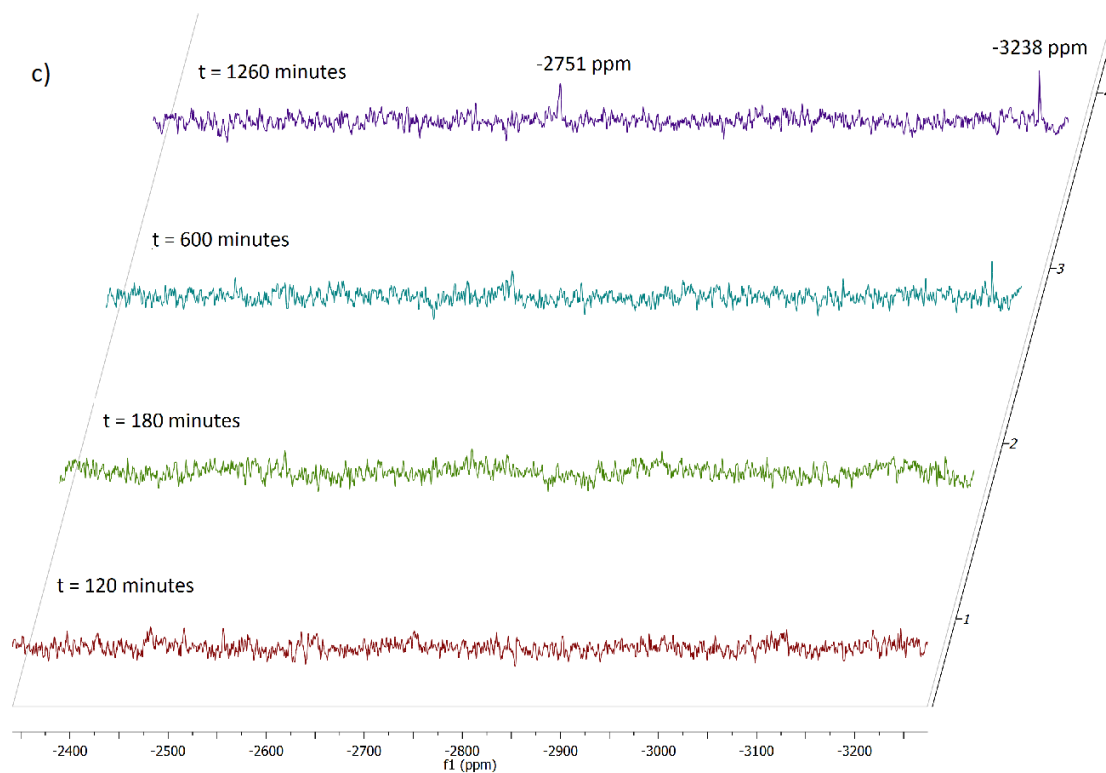


Figure 33: Evolution of platinum species on photolysis of $[\text{nBu}_4\text{N}]_2[\text{PtCl}_6]$ in CD_2Cl_2 in $^{195}\text{Pt}\{^1\text{H}\}$ NMR spectra (107 MHz) in area spanning a) 650 to -250 ppm b) -950 to -1850 ppm, c) olefin area: -2050 to -2950 ppm.

The changes of $[\text{PtCl}_6]^{2-}$ during the reactions relative to its initial amount under different conditions are drawn in Figure 34. The highest rate of hexachloroplatinate(IV) consumption was the photolysis in d_6 -acetone under UV irradiation. In d_6 -acetone, illumination under ambient light had converted 50% of the $[\text{PtCl}_6]^{2-}$ after about six hours and consumed the complex totally after 32 hours. Under UV light 50% conversion took only 10 minutes while almost total consumption was reached after about five hours illumination.

Under the same wavelength of irradiation, the rate of hexachloroplatinate(IV) consumption was found to be higher in d_6 -acetone than in d_2 -dichloromethane by a factor of about six. In CD_2Cl_2 , after 10 hours of illumination, 32% of the $[\text{PtCl}_6]^{2-}$ still remained and the reaction was complete after 21 hours. The different rate of the reaction can be attributed to the absorptivity of the complex in the solvents as explained in Section 2.2.2.1.

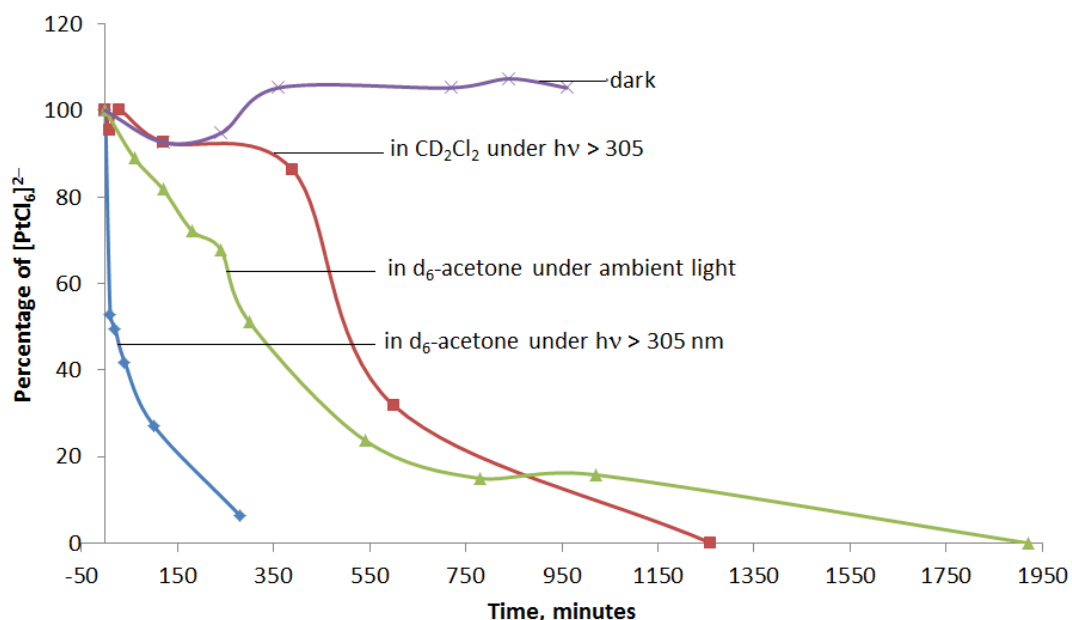


Figure 34: Graphs showing the consumption of $[\text{PtCl}_6]^{2-}$ during the irradiation under different conditions.

In summary, monitoring of the photolysis of the $[\text{PtCl}_6]^{2-}$ showed that early in the photolysis, the amount of $[\text{PtCl}_6]^{2-}$ decreased dramatically with concomitant formation of $[\text{PtCl}_4]^{2-}$. The rate of consumption of $[\text{PtCl}_6]^{2-}$ was fast, but the

formation of the olefin-platinum(II) complexes appeared to be a slow step. Photolysis of $[\text{}^n\text{Bu}_4\text{N}]_2[\text{PtCl}_6]$ was much faster in acetone than in dichloromethane due to the different light absorption properties in solution (Section 2.2.2.1).

2.2.2.6. The analysis of the reaction mixture of $[\text{}^n\text{Bu}_4\text{N}]_2[\text{PtCl}_6]$ after photolysis.

a. Attempts to identify the remainder of tetrabutylammonium cation.

It has been shown that hexachloroplatinate(IV) under illumination activates tetrabutylammonium cations yielding about 68% of the butadiene-platinum(II) complex countered by $(\text{}^n\text{Bu}_4\text{N})^+$ cation, and confirmed by ^1H and $^{195}\text{Pt}\{^1\text{H}\}$ NMR spectroscopy and by single crystal structure by X-ray analysis. The reaction was presumed to be a thermal reaction in accordance with Shilov chemistry, in fact the activation only proceeds when light is applied even under ambient light condition. Investigations confirmed that the source of the C_4 fragment of the butadiene is the $(\text{}^n\text{Bu}_4\text{N})^+$ and if this is true, a question arises about the fate of the remainder of the butylammonium.

Presumption suggested that the compound might be found as ${}^n\text{Bu}_3\text{N}$ as a result of a leaving group elimination, or $\text{H}{}^n\text{Bu}_3\text{NCl}$ formed in the presence of HCl which is likely to be generated during the reaction, or the remainder underwent further reaction and fell apart in the reaction mixture. ^1H -NMR spectroscopy can be utilised to distinguish these compounds in which the spectra of those three compounds (Figure 35) recorded separately showed a difference of chemical shift particularly the proton next to the N -atom ($-\text{N}-\text{CH}_2-$) where appeared at 2.32, 2.97 – 3.02, and 3.43 – 3.53 for ${}^n\text{Bu}_3\text{N}$, $(\text{H}{}^n\text{Bu}_3\text{N})^+$, and $(\text{}^n\text{Bu}_4\text{N})^+$ respectively. However, the ^1H -NMR spectrum of the reaction mixture showed only the chemical shift of ${}^n\text{Bu}_4\text{N}^+$ and it was impossible to observe the signals of $\text{H}{}^n\text{Bu}_3\text{N}^+$ and ${}^n\text{Bu}_3\text{N}$ compounds.

Attempts to identify the fate of the butylammonium residues included ^{14}N -NMR and 2D-HSQC- ^{15}N - ^1H -NMR experiments. The nitrogen species, $(\text{}^n\text{Bu}_4\text{N})^+$, ${}^n\text{Bu}_3\text{N}$, and

($\text{H}^n\text{Bu}_3\text{N}^+$) could be distinguished in the ^{14}N -NMR spectrum by a significant difference in line-width due to their different symmetry. Tetrabutylammonium cation with highly symmetric Td symmetry will give a sharp peak ($^n\text{Bu}_4\text{N}^+$) while the amine with lower symmetry, C_{3v} , promotes fast relaxation giving the very broad peak. The ($\text{H}^n\text{Bu}_3\text{N}^+$) cation is somewhere in-between.^{58, 128, 129} The ^{14}N NMR spectrum of $[\text{Bu}_4\text{N}]_2[\text{PtCl}_6]$ was recorded for comparison to the spectrum recorded from the reaction mixture. The spectrum showed a peak of ($^{14}\text{N}^n\text{Bu}_4$)⁺ at 21 ppm with a line width of about 13 Hz. The ^{14}N NMR spectrum of the reaction mixture however only demonstrated the signal of ($^n\text{Bu}_4\text{N}^+$). Considering that, due to the low symmetry of $\text{H}^n\text{Bu}_3\text{NCl}$, and $^n\text{Bu}_3\text{N}$, the peaks may be so broad so that they are unable to be detected; 2D-HSQC- ^{15}N - ^1H NMR spectroscopy was also employed to identify nitrogen species in the reaction mixture. Optimisation of coupling constant parameter with acquiring spectra of NBu_3 compound was carried out, giving the value of 1.5 Hz. The spectra of tributylammonium chloride, tributylamine and tetrabutylammonium cation were separately recorded as a comparison to the reaction mixture. The spectra of $^n\text{Bu}_3\text{N}$ compound showed a chemical shifts at 42 ppm correlated to protons at 2.4 ($^2J_{\text{NH}}$); 1.4 ($^3J_{\text{NH}}$) and 1.3 ppm ($^4J_{\text{NH}}$); $\text{H}^n\text{Bu}_3\text{NCl}$ was seen at 56 ppm associated with chemical shift of protons at 3.05 ($^2J_{\text{NH}}$) and 1.8 ($^3J_{\text{NH}}$), while a resonance corresponding to NBu_4^+ was observed at 65 ppm correlated to proton peaks at 3.61 ($^2J_{\text{NH}}$); and 1.86 ($^3J_{\text{NH}}$). However, the spectrum recorded from the reaction mixture again showed only NBu_4^+ at 65 ppm (Figure 36).

Among the attempts that have been made, a result was obtained from an analysis of liquid injection field desorption/ionisation- (LIFDI) mass spectrometry, which showed a signal at m/z of 186.29 corresponding to $\text{H}^n\text{Bu}_3\text{N}^+$ ion in addition to signals at m/z of 242.32 and 519.80 corresponding to $[\text{Bu}_4\text{N}]^+$ and $[(\text{Bu}_4\text{N})_2\text{Cl}]^+$, respectively. To ensure this result, UV-mass spectroscopy experiments were carried out by Dessent and co-workers and will be discussed later in the next section.

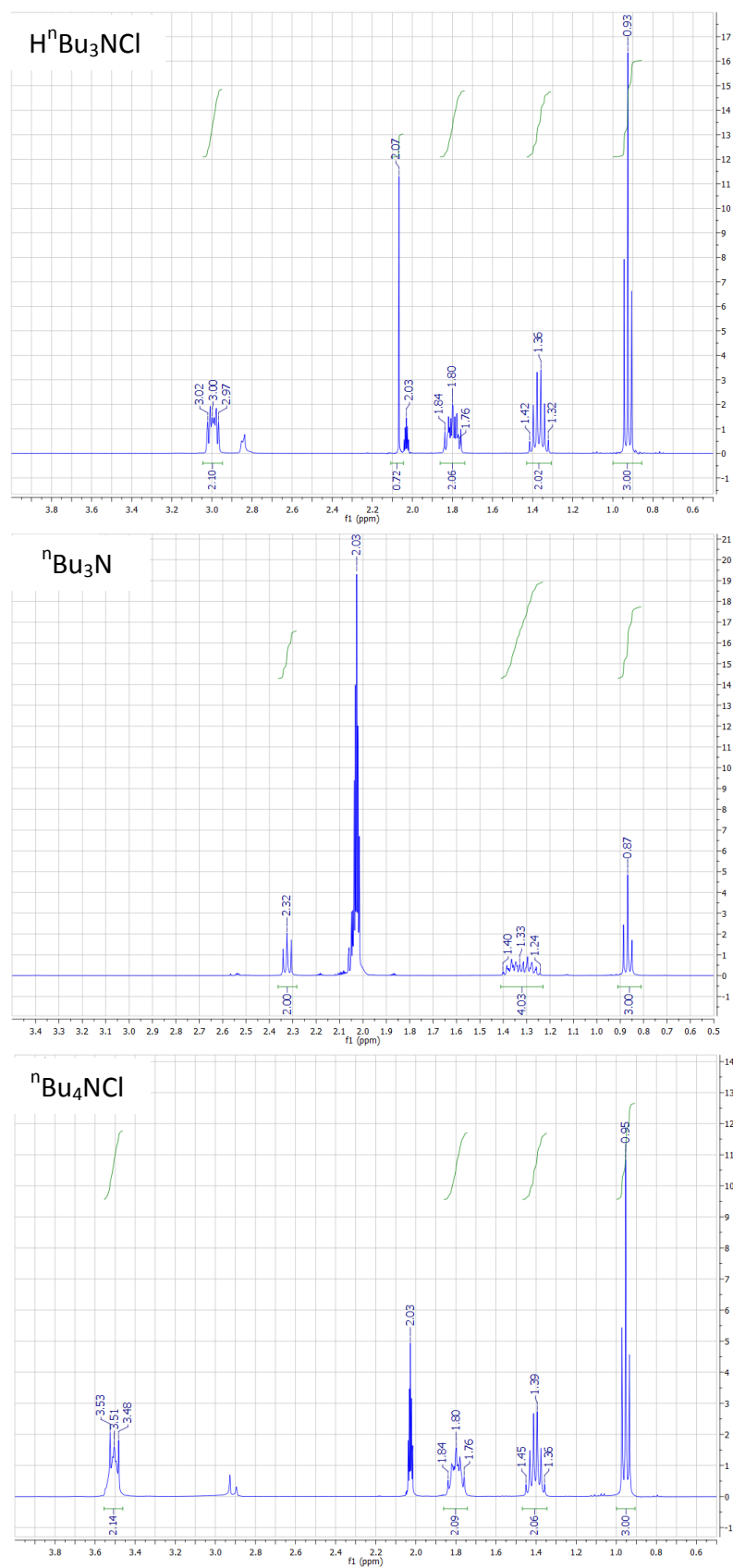


Figure 35: $^1\text{H-NMR}$ spectra (500 MHz) of $\text{H}^n\text{Bu}_3\text{NCl}$, $^n\text{Bu}_3\text{N}$, and $^n\text{Bu}_4\text{NCl}$ in d_6 -acetone.

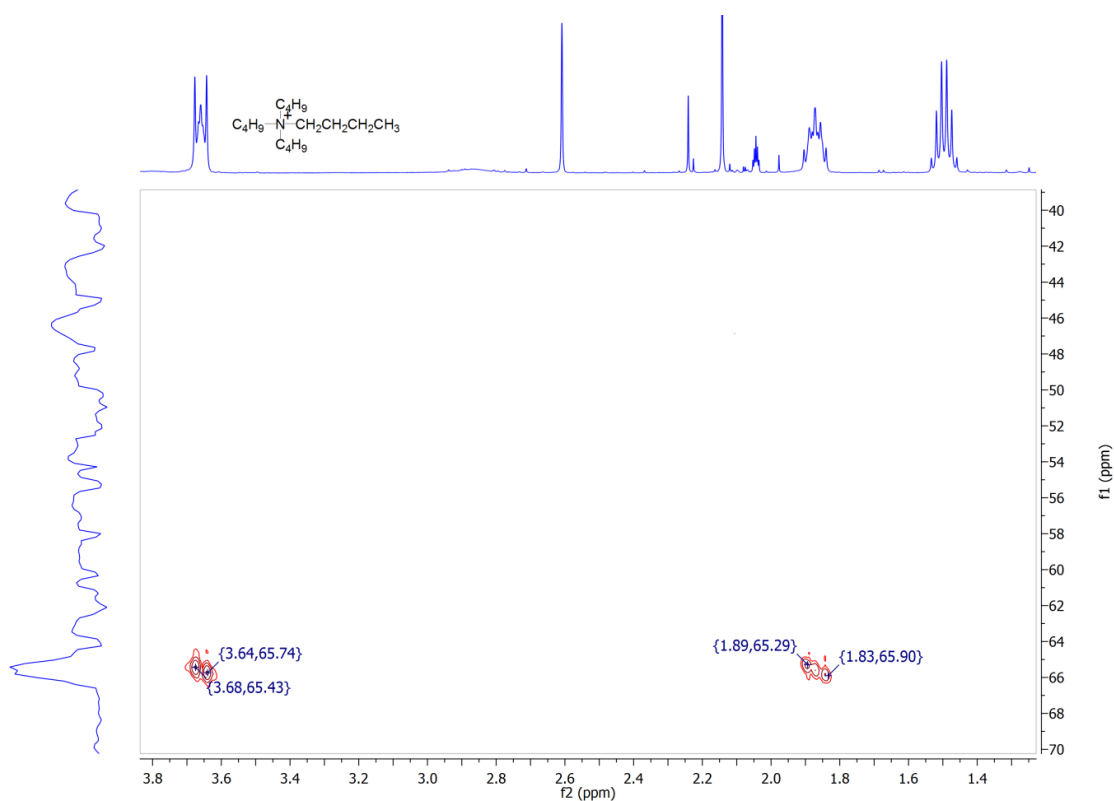


Figure 36: The 2D- ^{15}N - ^1H NMR spectra (500 MHz for ^1H) of the mixture of photolysed $[\text{nBu}_4\text{N}]_2[\text{PtCl}_6]$ under UV light, recorded in d_6 -acetone.

b. Photodissociation Spectroscopy

Photodissociation and photodetachment spectroscopy show the removal of an electron and the subsequent pathway of ionic fragmentation. The method has been employed to investigate the intrinsic photoproperties of platinum(IV) as well platinum(II) dianions including the excited state behaviour of the dianions and redox chemistry of the species.^{59, 124, 130} The observations are based on the response of the complexes to excitation energies in excess of the barriers to both electron detachment and ionic fragmentation. Weber and co-workers reported photodissociation and photodetachment of hexachloroplatinate(IV) anion *in vacuo* studied experimentally by using photodissociation spectroscopy. Photoproduct ions are identified as a function of photon energy from electronic emission.¹²⁴ With the similar method, Dessent and co-workers have also investigated photointeractions of hexachloroplatinate with nucleobases by UV-mass-spectrometry.¹³⁰ Therefore, identification of species resulting from the irradiation

of hexachloroplatinate(IV) by employing photodissociation spectroscopy has been well established.

In this research, UV spectroscopy was utilised to identify photoproduct ions generated from irradiation of $[\text{Bu}_4\text{N}]_2[\text{PtCl}_6]$. The photodissociation was performed in the range of energy from 215 to 320 nm, while the fragment ions were able to detect down to m/z 65 for the positive ion and up to 176 m/z for negative ion; fragments lower than the mass fall outside the mass window of the trap.

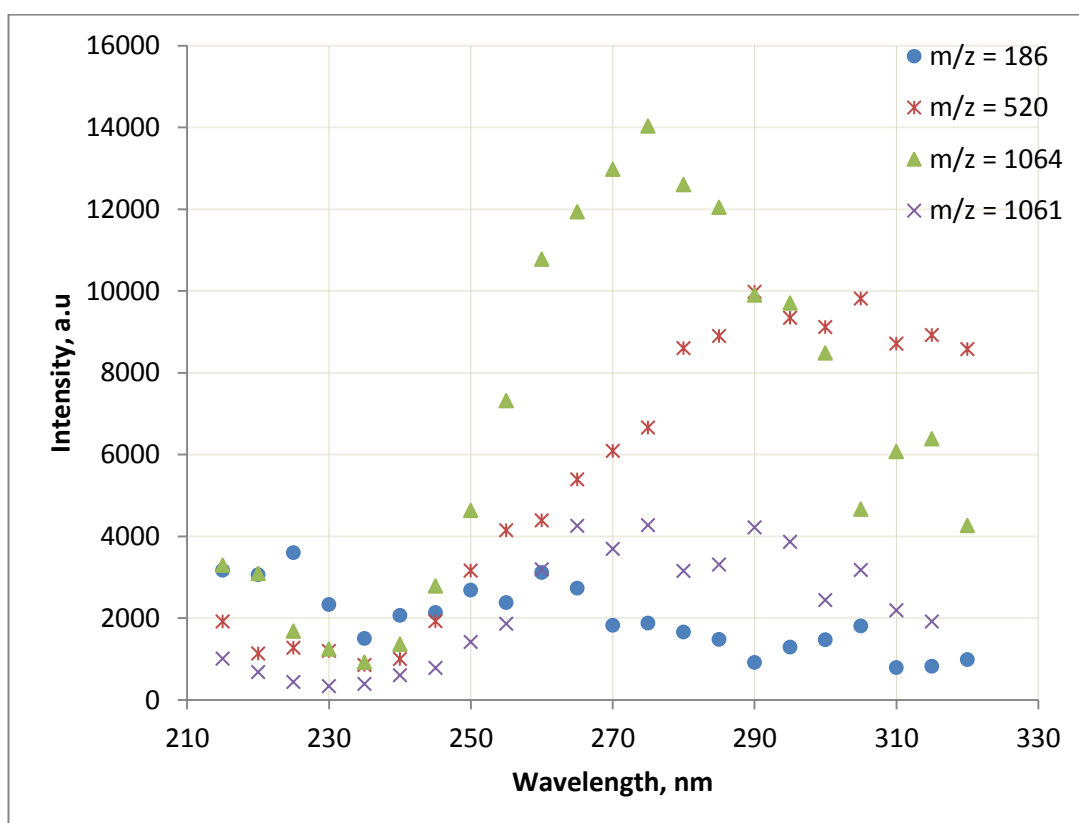


Figure 37: Photofragment spectra of $[\text{HN}^n\text{Bu}_3]^+$ (m/z 186), $[(^n\text{Bu}_4\text{N})_2\text{Cl}]^+$ (m/z 520), $[(^n\text{Bu}_4\text{N})_2\text{Cl}[(^n\text{Bu}_3\text{N}(\text{C}_4\text{H}_7)\text{PtCl}_3)]^+$ (m/z 1061) and $[(^n\text{Bu}_4\text{N})_3[\text{PtCl}_4]]^+$ (m/z 1064)

The positive-ESI-mass spectrum showed the parent ion at m/z 1135 associated with $[\text{Bu}_4\text{N}]_3[\text{PtCl}_6]^+$ ion and a fragment at m/z 242 assigned for $(^n\text{Bu}_4\text{N})^+$ ion. The negative-ESI-mass spectrum demonstrated the parent ion at m/z 926 associated with $[\text{Bu}_4\text{N}]_2[\text{PtCl}_7]^-$ with main fragments at m/z 649 assigned for $[\text{Bu}_4\text{N}] [\text{PtCl}_6]^-$.

Furthermore, the $[\text{}^n\text{Bu}_4\text{N}]_3[\text{PtCl}_6]^+$ and $[\text{}^n\text{Bu}_4\text{N}][\text{PtCl}_6]^-$ ions were isolated and photo-dissociated by applying a laser in the wavelength range of 215 – 315 nm. Photodissociation spectra of $[\text{}^n\text{Bu}_4\text{N}]_3[\text{PtCl}_6]^+$ ion demonstrated fragments at m/z 186 assigned for $[\text{H}^n\text{Bu}_3\text{N}]^+$, m/z 520 corresponding to $(\text{}^n\text{Bu}_4\text{N})^+$ cation, m/z 1061 associated with $[\text{}^n\text{Bu}_3\text{N}(\text{butene})\text{-Pt}^{\text{II}}\text{Cl}_3]^+$, and m/z 1064 assigned for $[(\text{}^n\text{Bu}_4\text{N})_3\text{Pt}^{\text{II}}\text{Cl}_4]^+$ fragment that corresponding with the Pt^{II} complex. The signals were consistently detected over the applied laser energy but the highest intensity was in the range of 260 – 300 nm as shown in Figure 37. Photofragmentation of the negative ion also showed the signals associated with $[\text{Pt}^{\text{II}}\text{Cl}_3]^-$ at m/z 300. These observations are in accordance with LIFDI-MS and negative-ESI analysis of a mixture after irradiation.

c. Identification of platinum species in the reaction mixture.

As a part of acquiring mechanistic insight, attempts to identify platinum species in a mixture after photolysis were done by employing 2D- ^{195}Pt - ^1H NMR spectroscopy. Initially one-dimensional $^{195}\text{Pt}\{^1\text{H}\}$ NMR spectra over the range +2000 until –6000 ppm were recorded but signals were only seen at –1421 ppm, –2567 ppm, and –2570 ppm. The first signal was associated with $[\text{PtCl}_4]^{2-}$ while the last signals allegedly related to olefin-platinum(II) complexes¹¹² but the chemical shifts were slightly different from those of the isolated butadiene-platinum(II) complex (–2521 ppm in d_6 -acetone for *anti-trans*-1,3-butadiene-platinum(II) complex). To identify those chemical shifts, 2D-HMQC ^1H - ^{195}Pt and COSY NMR spectroscopy was utilised to show the correlation between platinum with protons and proton with proton.

Experiments to optimise J_{PtH} on 2D-HMQC- ^{195}Pt - ^1H were conducted by varying the coupling constant (10, 20, 40, 60, 70, 85, and 135 Hz). The value showing the most intense platinum-proton correlations in the reaction mixture was 60 Hz, and was used for further experiments. The 2D-HMQC- ^{195}Pt - ^1H NMR spectrum of a photoreaction mixture carried out in acetone given in Figure 38 showed at least four platinum chemical shifts correlated to protons; two of the signals were also

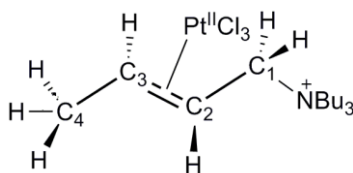
observed in the 1D- $^{195}\text{Pt}\{^1\text{H}\}$ NMR spectrum. The peaks at -2570 and -2567 ppm seen in the one-dimensional ^{195}Pt NMR spectrum were overlapped in the spectrum projection of the two-dimensional spectra due to a bigger line width but they showed splitting and correlations with protons in the 2D spectrum. The two other signals at -2550 and -2536 ppm were only seen on the two dimensional spectrum demonstrating a higher sensitivity of the 2D-HMQC method. Setting the optimum coupling constant parameter may contribute to the better sensitivity of the 2D-HMQC method. The chemical shifts along with related proton chemical shifts are tabulated in Table 6.

Table 6: Chemical shifts of ^{195}Pt with correlated protons observed on 2D-HMQC- ^{195}Pt - ^1H NMR spectrum of photoreaction mixture of $[\text{Bu}_4\text{N}]_2[\text{PtCl}_6]$ in acetone.

Label	$\delta^{195}\text{Pt}$ (ppm)	$\delta^1\text{H}$ (ppm)
I.A	-2570	3.4; 1.56
I.B	-2567	4.39; 4.32
I.C	-2550	4.42; 4.18
I.D	-2536	4.50; 4.38

The signal at -2570 ppm (I.A) was seen in both the 1D as well as the 2D- ^{195}Pt - ^1H spectra correlated to the proton chemical shift at 3.4 and 1.56 ppm. However in the ^1H -NMR spectrum, those signals could not be interpreted due to being weak and poorly resolved. The proton signal at 3.4 ppm likely related to $-\text{NCH}_2$ indicating an olefin compound consisting of alkylammonium bound to a platinum(II) species. Following the suggestion, the peak at 1.56 ppm could be a terminal $-\text{CH}_3$ and the olefin could be a 2-butene. A suggested structure related to the peak at -2570 ppm is drawn in Scheme 55. The signal at 3.45 ppm was assigned to be the proton bound to the carbon atom (C_1) next to NBU_3 , while the peak at 1.56 ppm was corresponded to the methyl proton at the terminal carbon (C_4). Such assignment was not entirely convincing as the compound is not possible to isolate, but there was a little evidence that might support the allegation: mass spectrometry analysis showed the existence of the compound in the mixture. In a LIFDI-mass spectrum, a peak at m/z 783.72 corresponding to

$[(^n\text{Bu}_4\text{N})(\text{NBu}_3)(\text{C}_4\text{H}_7)\text{PtCl}_3]^+$ ion was observed in accordance with a signal seen in a negative-ESI-mass spectrum at m/z 300.87 which was related to $[\text{PtCl}_3]^-$ ion.



Scheme 55: The suggested structure of the intermediate compound (I.A) appeared at -2570 ppm on the $^{195}\text{Pt}\{^1\text{H}\}$ NMR spectra.

A similar palladium(II) alkenyl complex was reported as an intermediate in a reaction of $[\text{Pd}(\text{PPh}_3)_4]$ with moist $(^n\text{Bu}_4\text{N})(\text{CN})$ in which a theoretical study suggests that the intermediate, $[(\text{PPh}_3)_3\text{Pd}---\text{H}---\text{CH}_2=\text{CH}---\text{NBu}_3]$, was generated prior to formation of products of $[\text{Pd}(\text{CN})_3(\text{H})]^{2-}$ anion, 1-butene and NBu_3 . The study assumed the quaternary ammonium as $(\text{EtNMe}_3)^+$ cation to simplify the calculation (Scheme 50).⁹⁰

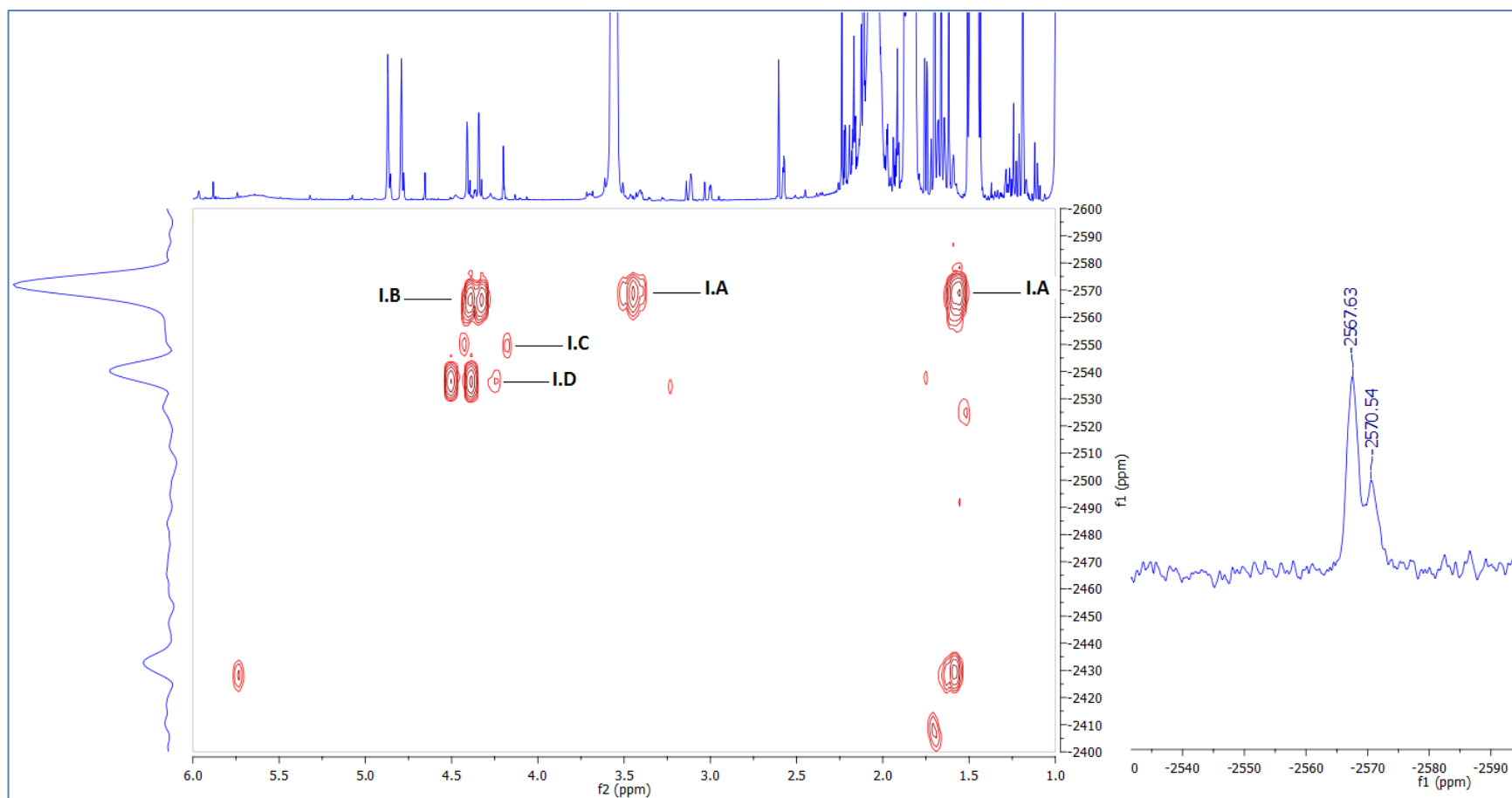


Figure 38: The 2D- $(^1\text{H}-^{195}\text{Pt})$ -NMR spectra (500 MHz for ^1H) of the reaction mixture of $[\text{nBu}_4\text{N}]_2[\text{PtCl}_6]$ in acetone photolysed thermally under ambient light, recorded in d_6 -acetone at 298 K; left: the 1D- $^{195}\text{Pt}\{^1\text{H}\}$ NMR spectrum showing the peaks at -2570 and -2567 ppm.

The peak at -2567 ppm (**I.B**) which was seen in both 1D and 2D ^1H - ^{195}Pt NMR spectra showed correlations with protons at 4.32 and 4.39 ppm. Two other signals at -2550 (**I.C**) and -2536 ppm (**I.D**), appeared only in the 2D ^1H - ^{195}Pt NMR spectra. Those three resonances demonstrated correlations with olefin protons, but were not related to 1-butene or 2-butene-platinum(II) complexes as there was no correlation with, for example, $-\text{CH}_2$ of alkyl or a terminal $-\text{CH}_3$. Therefore, those resonances were suggested to be the butadiene-platinum(II) complexes even though the chemical shifts were shifted from those of the isolated butadiene-platinum(II) complexes signals (-2521 , and -2589 ppm for *anti-trans*, and *syn-trans* conformer, respectively) (Figure 15), and that the proton peaks were poorly resolved.

To see if there was a dynamic process such as an exchange occurring during spectral acquisition, a variable-temperature $^{195}\text{Pt}\{^1\text{H}\}$ NMR experiment was conducted recording the Pt-olefin area between 200 – 298 K (Figure 39). As predicted,^{112, 115} the chemical shifts decreased by 40 ppm when the temperature lowered from 298 K to 200 K. The peaks were broader and less intense on cooling but the pattern remained the same implying an absence of a dynamic process, the broad peaks perhaps being attributed to a decrease in solubility at lower temperature. When the temperature increased back to 298 K, the spectrum reverted to the original intensities and resolution.

To conclude this section, 2D- ^{195}Pt - ^1H NMR spectroscopy was employed to identify the butadiene-platinum(II) complex and an intermediate compound in the reaction mixture. The intermediate likely existed in the solution that ultimately transformed to the stable product on the isolation process.

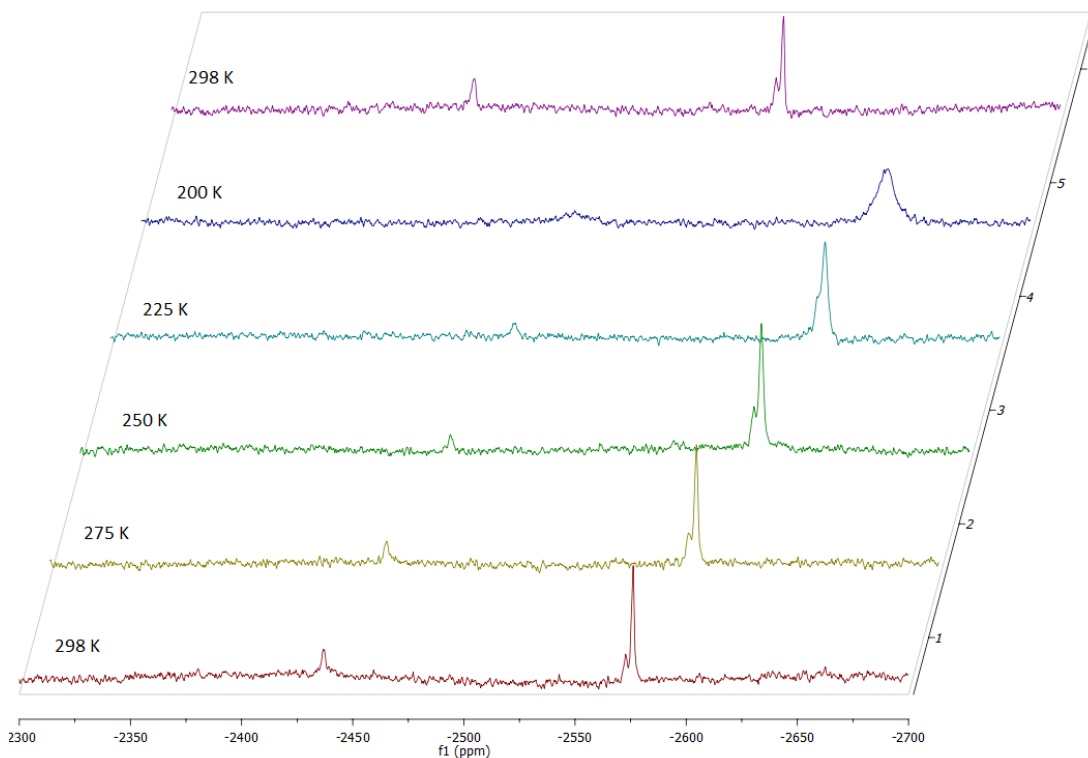


Figure 39: The low-VT $^{195}\text{Pt}\{^1\text{H}\}$ NMR spectra (107 MHz) of the mixture of $[\text{}^n\text{Bu}_4\text{N}]_2[\text{PtCl}_6]$ in d_6 -acetone after photolysis.

2.2.2.7. Analogous Reactions

a. Phosphonium Cation

The tetrabutylammonium cation commonly is employed as a counter ion to engender solubility of the inorganic compound in organic solvents. With $(\text{}^n\text{Bu}_4\text{N})^+$ identified as the source of the butadiene, it was realised that a Hofmann elimination could account for an initial elimination of 1-butene as is found with perfectly dry $\text{}^n\text{Bu}_4\text{NF}$ where the β -hydrogen of a butyl group is abstracted by F^- , which is a strong base under strictly anhydrous conditions, leading to formation of Bu_3NH and 1-butene.⁸⁴

In order to try to evaluate the role of the cation and the proposed involvement of the Hofmann elimination pathway, thus $[\text{}^n\text{Bu}_4\text{P}]_2[\text{PtCl}_6]$ was prepared and photolysed under the condition used with $[\text{}^n\text{Bu}_4\text{N}]_2[\text{PtCl}_6]$. As a control, $\text{}^n\text{Bu}_4\text{P}\text{Cl}$ and

${}^n\text{Bu}_3\text{PHBF}_4$ were also irradiated separately under the same conditions. The ${}^1\text{H}$ and ${}^{31}\text{P}\{{}^1\text{H}\}$ NMR spectra of the post-irradiation solutions demonstrated no change. However, on irradiation of $[{}^n\text{Bu}_4\text{P}]_2[\text{PtCl}_6]$, $[\text{PtCl}_6]^{2-}$ was consumed giving $[\text{PtCl}_4]^{2-}$ complex but no platinum(II)-olefin signals were seen in the ${}^{195}\text{Pt}$ NMR spectra. The ${}^{31}\text{P}\{{}^1\text{H}\}$ NMR spectrum recorded from the photoreaction mixture showed a signal at 46 ppm corresponding to $({}^n\text{Bu}_4\text{P})^+$ (Appendix 7). Attempts to isolate a product from the reaction mixture were made through crystallisation, but no product was able to obtain. This observation indicated the generation of active species from $[\text{PtCl}_6]^{2-}$ under light to form the reduced species $[\text{PtCl}_4]^{2-}$, however the activation of the butyl going in the same manner as for the tetrabutylammonium cation did not occur, demonstrating the importance of the ammonium derivatives properties on the formation of the butadiene.

b. Other Alkylammonium Cation

As discussed in Chapter 1, the tetrachloroplatinate(II) and hexachloroplatinate(IV) system is known for oxidising alkanes to give σ -alkyl complexes of Pt^{IV} , and eventually giving a corresponding π -alkene complex of Pt^{II} if the alkyl group has a β -hydrogen.¹³¹ Assuming this to be correct, one might assume that an analogous reaction would certainly occur for propylammonium species and other longer chains, and possibly Et_4N^+ while this behaviour may be absent for Me_4N^+ .

Thus, the analogous reactions of tetralkylammonium hexachloroplatinate(IV) (alkyl: propyl (Pr) and pentyl (Pe)) were conducted under the same conditions as employed for the $[{}^n\text{Bu}_4\text{N}]_2[\text{PtCl}_6]$ photolysis. Those reactions were monitored by ${}^1\text{H}$ and ${}^{195}\text{Pt}$ NMR spectroscopy. It was intended to conduct the reactions with $[\text{Me}_4\text{N}]_2[\text{PtCl}_6]$ and $[\text{Et}_4\text{N}]_2[\text{PtCl}_6]$ but due to their lack of solubility in acetone, they were not carried out. The reaction of $[{}^n\text{Pe}_4\text{N}]_2[\text{PtCl}_6]$ was expected to be similar to that of $[{}^n\text{Bu}_4\text{N}]_2[\text{PtCl}_6]$ in terms of providing the second C–H activation to give a related diene, whereas the $[{}^n\text{Pr}_4\text{N}]_2[\text{Pt}_2\text{Cl}_6]$ would be expected to undergo just one

activation forming propene and perhaps leading to further reactions. These two reactions are discussed in the next sub-sections.

1. [ⁿPe₄N]₂[PtCl₆]

Under the conditions employed in the photolysis of [ⁿBu₄N]₂[PtCl₆], a solution of [ⁿPe₄N]₂[PtCl₆] in acetone was irradiated under UV light and the reaction was monitored by using ¹H and ¹⁹⁵Pt{¹H} NMR spectroscopy. The reaction of (ⁿPe₄N)⁺ cation with [PtCl₆]²⁻ was also conducted under ambient light and reflux. The ¹H NMR spectra of the photolysed solution of [ⁿPe₄N]₂[PtCl₆] in the various conditions are given in Figure 40 and Figure 41, the ¹⁹⁵Pt NMR spectra are given in Figure 42. The COSY spectrum is depicted in Figure 43 and the 2D-¹⁹⁵Pt-¹H NMR spectra are shown in Figure 44 and Figure 45.

Attempts to isolate a product through crystallisation were carried out but unfortunately no solid was obtained. Therefore, the observation of the analogous reaction can only be made by comparing the proton and platinum NMR spectra to those spectra recorded from the photoreaction mixture of [ⁿBu₄N]₂[PtCl₆]; products from the photolysis of [ⁿPe₄N]₂[PtCl₆] were unable to be determined convincingly.

The ¹⁹⁵Pt{¹H} NMR spectra of the reaction mixture showed a signal corresponding to [ⁿPe₄N]₂[PtCl₄] at -1425 ppm indicating the reduction of [Pt^{IV}Cl₆]²⁻ as found in the photolysis of [ⁿBu₄N]₂[PtCl₆]. Resonances in the platinum(II)-olefin region of the spectrum were also seen in the one-dimensional ¹⁹⁵Pt{¹H} experiment as well as in the two-dimensional ¹⁹⁵Pt-¹H NMR experiments. In addition to the chemical shift of [PtCl₄]²⁻ in 1D-¹⁹⁵Pt{¹H}-NMR spectrum, resonances associated with olefin-platinum(II) complexes were observed at -2573 and -2569 ppm. In the 2D-(¹⁹⁵Pt-¹H) spectra, more olefin-platinum(II) resonances were seen and along with the proton chemical shifts correlated to the signals are tabulated in Table 7.

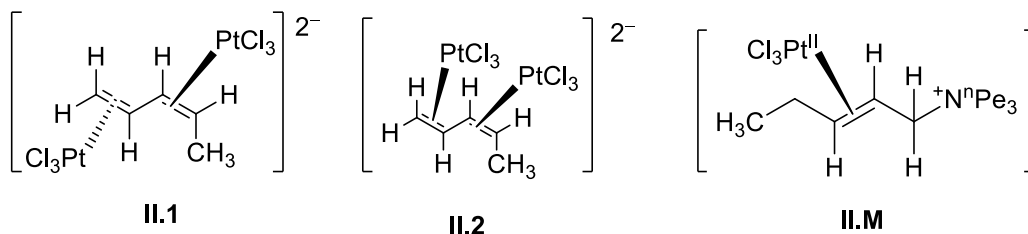
Table 7: Chemical shifts of ^{195}Pt with correlated protons observed on 2D-HMQC- ^{195}Pt - ^1H NMR spectrum the mixture of $[\text{Pe}_4\text{N}]_2[\text{PtCl}_6]$ in acetone after photolysis. *irradiation under $h\nu > 305$ nm at room temperature, ** irradiation under ambient light and heating under reflux.

Label	$\delta^{195}\text{Pt}$ (ppm)	$\delta^1\text{H}$ (ppm)
II.M	-2573* and -2577**	4.4; 4.3; 3.4; 1.6
II.N	-2569* and -2571**	4.4; 4.3; 1.6
II.O	-2559	4.5; 1.5
II.P	-2555	4.4; 4.2; 1.6
II.Q	-2543	4.8; 4.5; 4.2; 1.7
II.1	-2521* and -2525**	4.5; 4.4; 1.6

The ^1H NMR spectrum of the mixture of $[\text{Pe}_4\text{N}]_2[\text{PtCl}_6]$ after photolysis ($h\nu > 305$ nm) given in Figure 41 showed signals of olefin protons, although the resolution was poor, hampering the structural interpretation. The spectra of the mixture irradiated thermally under ambient light are presented in Figure 40 shows better resolution with three series of proton correlated to each other as described in ^1H - ^1H COSY spectra (Figure 43). The first series labelled as **II.1** resonates at 5.7, 4.7, 4.3 ppm. A weak signal at 1.6 ppm is correlated to the peak at 4.7 – 4.9 ppm was observed in association with a methyl although further information about the splitting was unable to see as it is overlapped with the chemical shift of methyl in the pentyl. In 2D- ^{195}Pt - ^1H NMR spectra a platinum peak at -2521 to -2525 ppm which is correlated with those proton resonances was appeared. The series of chemical shifts, the protons as well as the platinum, is similar to the resonances of complex **I.1**, thus the compound was assigned as $[(anti-trans-1,3-pentadiene)(\text{PtCl}_3)_2]^{2-}$ (**II.1**, Scheme 56). The second series labelled as **II.2** appears at 5.8, 4.2, 3.98 ppm that is similar to the resonances of complex **I.2** where the diene is at *s-trans* position and the two platinum coordinate from the same side. In this case, as the source of diene is pentyl, it was expected to see crossing peaks with a methyl chemical shift in the COSY spectra but it was not seen perhaps because of the lack of concentration, perhaps the same reason too for the absence of the ^{195}Pt signal in 2D- ^{195}Pt - ^1H NMR spectra. Nonetheless, the compound **II.2** is proposed as $[(syn-trans-1,3-pentadiene)(\text{PtCl}_3)_2]^{2-}$. The third series was observed at 5.0, 4.2 and 4.1 ppm, but unfortunately the resolution of ^1H NMR spectrum is

not sufficient to provide information in structure determination, thus it was just called an olefin-platinum(II) compound without defining its molecular structure and labelled as **II.R**.

A platinum chemical shift at -2573 correlated to the proton resonance at 3.4 appeared to be similar to the signal at -2570 ppm from the mixture of $[\text{}^n\text{Bu}_4\text{N}]_2[\text{PtCl}_6]$ photolysis thus the signal is proposed to be a pentenyl that is still bound to tripropylammonium, coordinating to Pt^{II} (**II.M**, Scheme 56). Other peaks on the olefin-platinum(II) area were proposed to be pentadiene-platinum(II) complexes in various conformers, but due to insufficient information the certain structures are unable to determine. Nonetheless, these observations indicated the activation of $(\text{}^n\text{Pe}_4\text{N})^+$ cation under the irradiation of $[\text{PtCl}_6]^{2-}$ complex in a similar manner as $(\text{}^n\text{Bu}_4\text{N})^+$ activation.



Scheme 56: Proposed molecular structures of compounds resulted in the photolysis of $[\text{}^n\text{Pe}_4\text{N}]_2[\text{PtCl}_6]$.

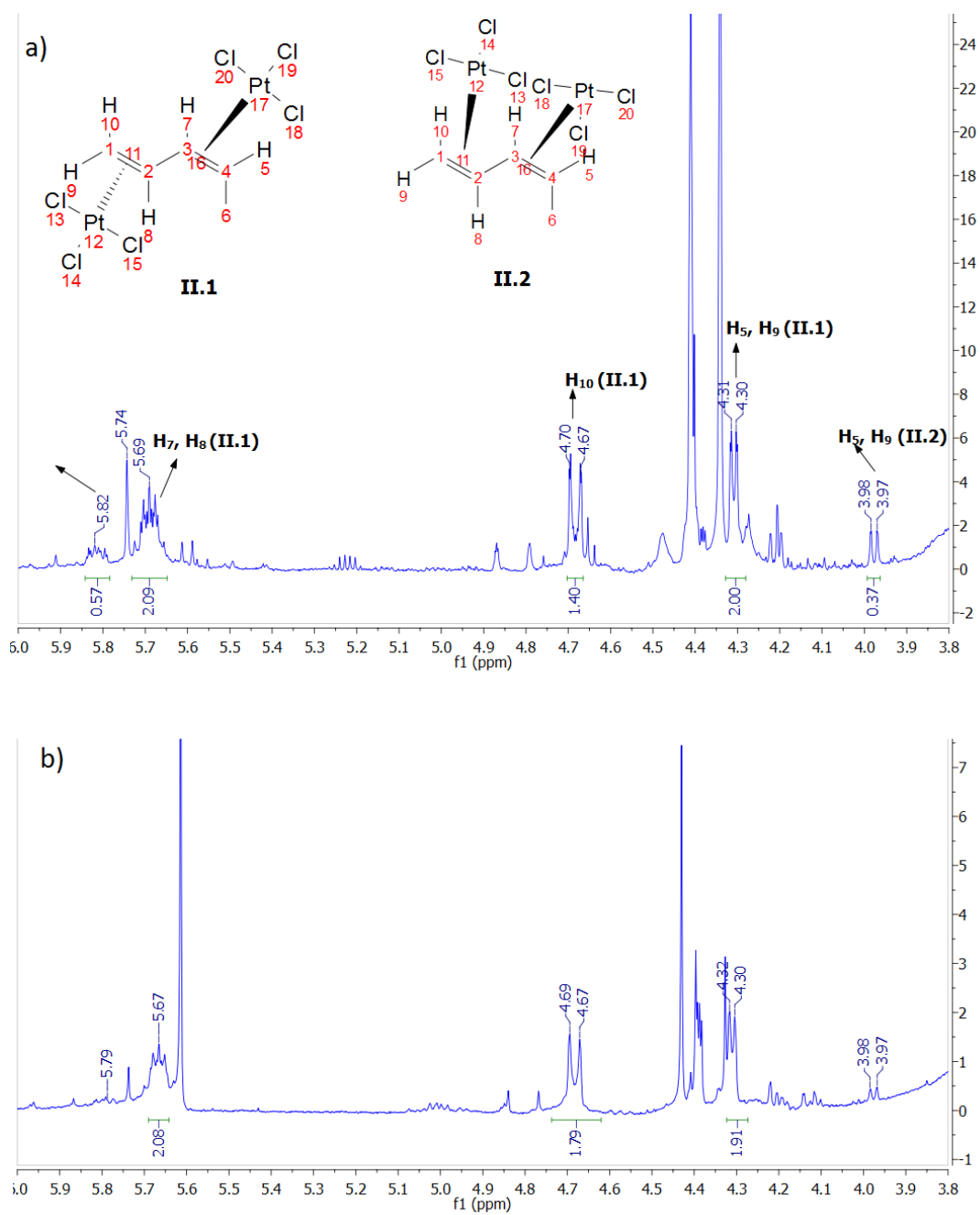


Figure 40: The ^1H NMR spectrum (500 MHz) of the $[\text{nPe}_4\text{N}]_2[\text{PtCl}_6]$ mixture in acetone after 24 hours of heating under reflux and ambient light.

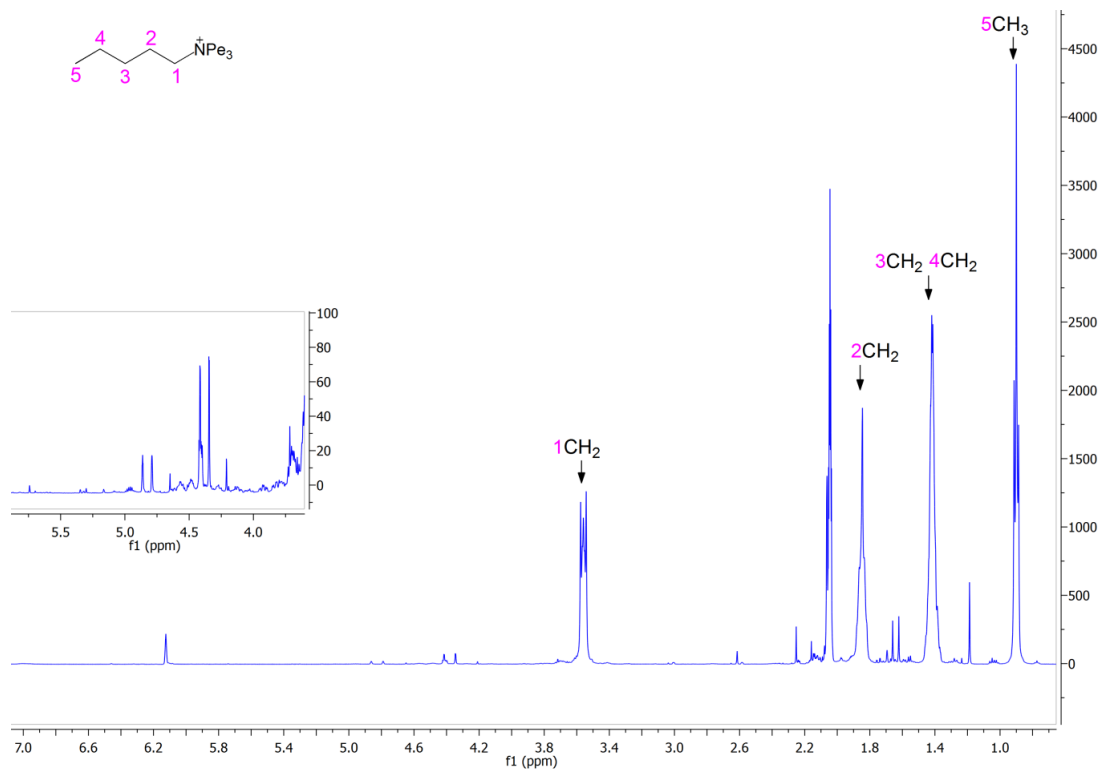


Figure 41: The ^1H NMR spectrum (500 MHz) of the photoreaction mixture of $[\text{Pe}_4\text{N}]_2[\text{PtCl}_6]$ in acetone recorded in d_6 -acetone at 298 K, with expansion of the region containing hydrogen resonances from bound alkene.

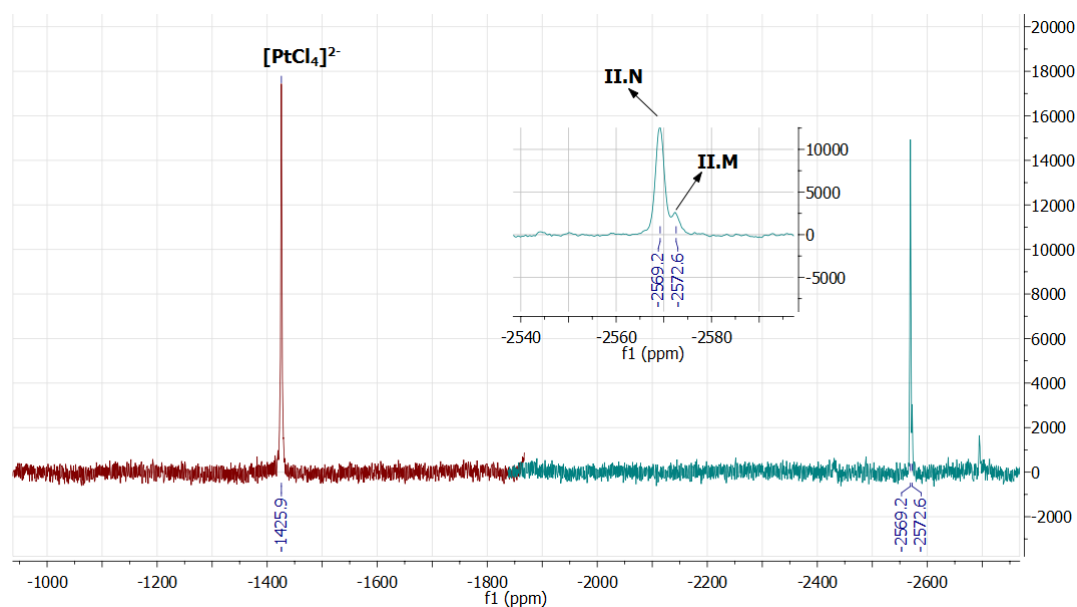


Figure 42: The ^{195}Pt NMR spectra (107 MHz) of the photoreaction mixture of $[\text{Pe}_4\text{N}]_2[\text{PtCl}_6]$ in acetone recorded in d_6 -acetone at 298 K.

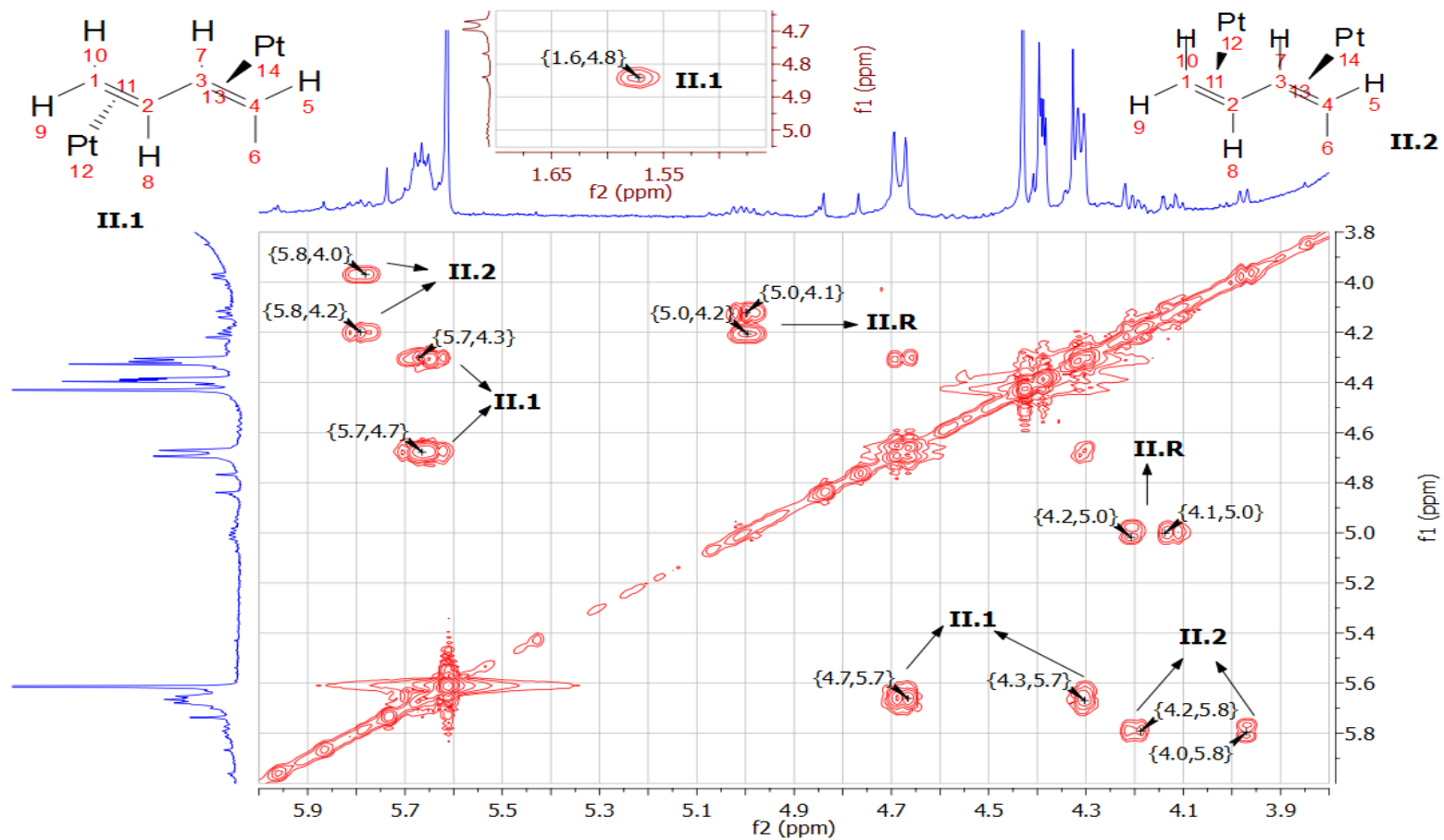


Figure 43: The ^1H - ^1H COSY spectra (500 MHz) of the $[\text{PtCl}_6]^{2-}$ mixture in acetone after 48 hours of heating under reflux and ambient light.

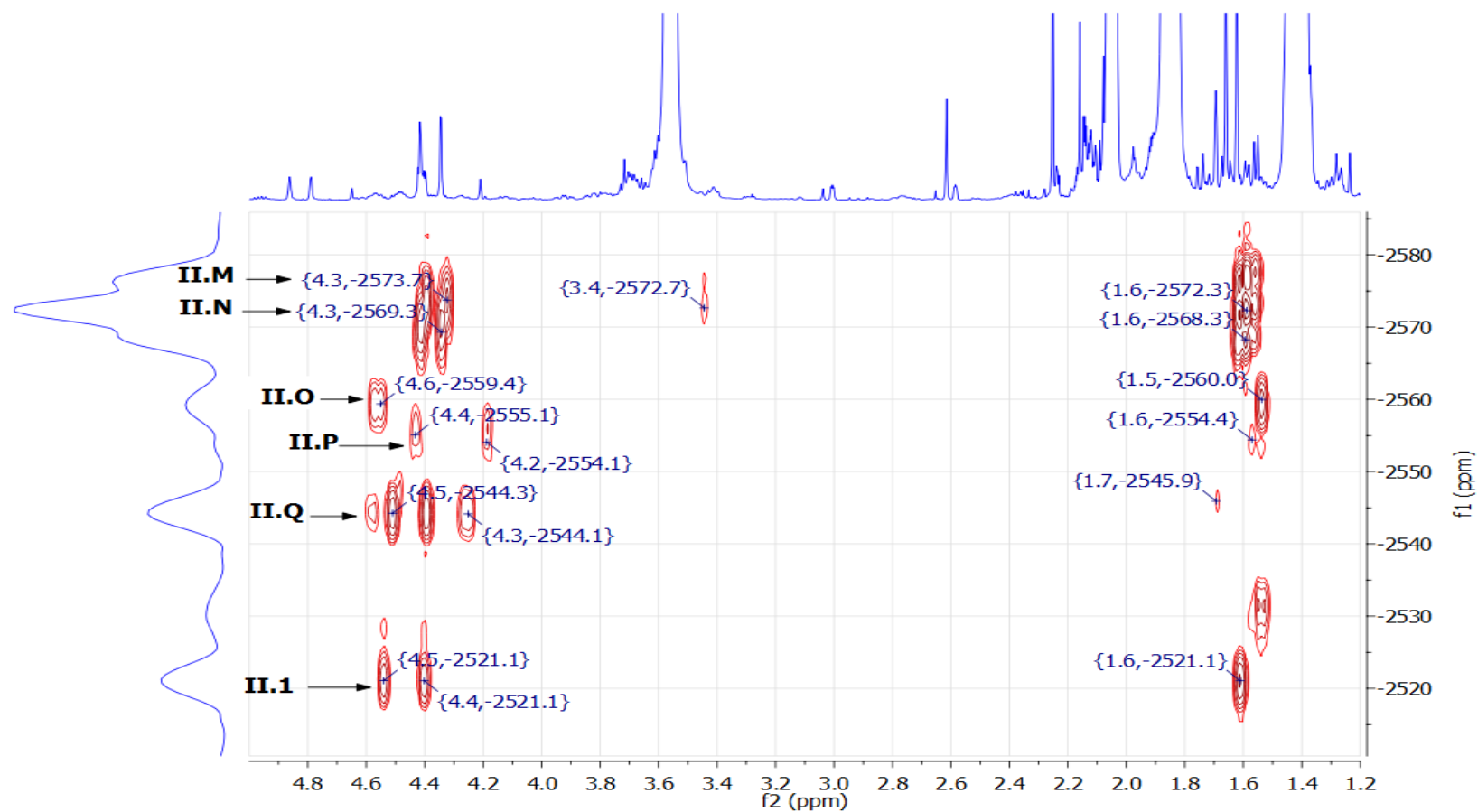


Figure 44: The 2D-(¹⁹⁵Pt-¹H) NMR spectra (500 MHz for ¹H) of the photoreaction mixture of [ⁿPe₄N]₂[PtCl₆] in acetone recorded in d₆-acetone at 298 K.

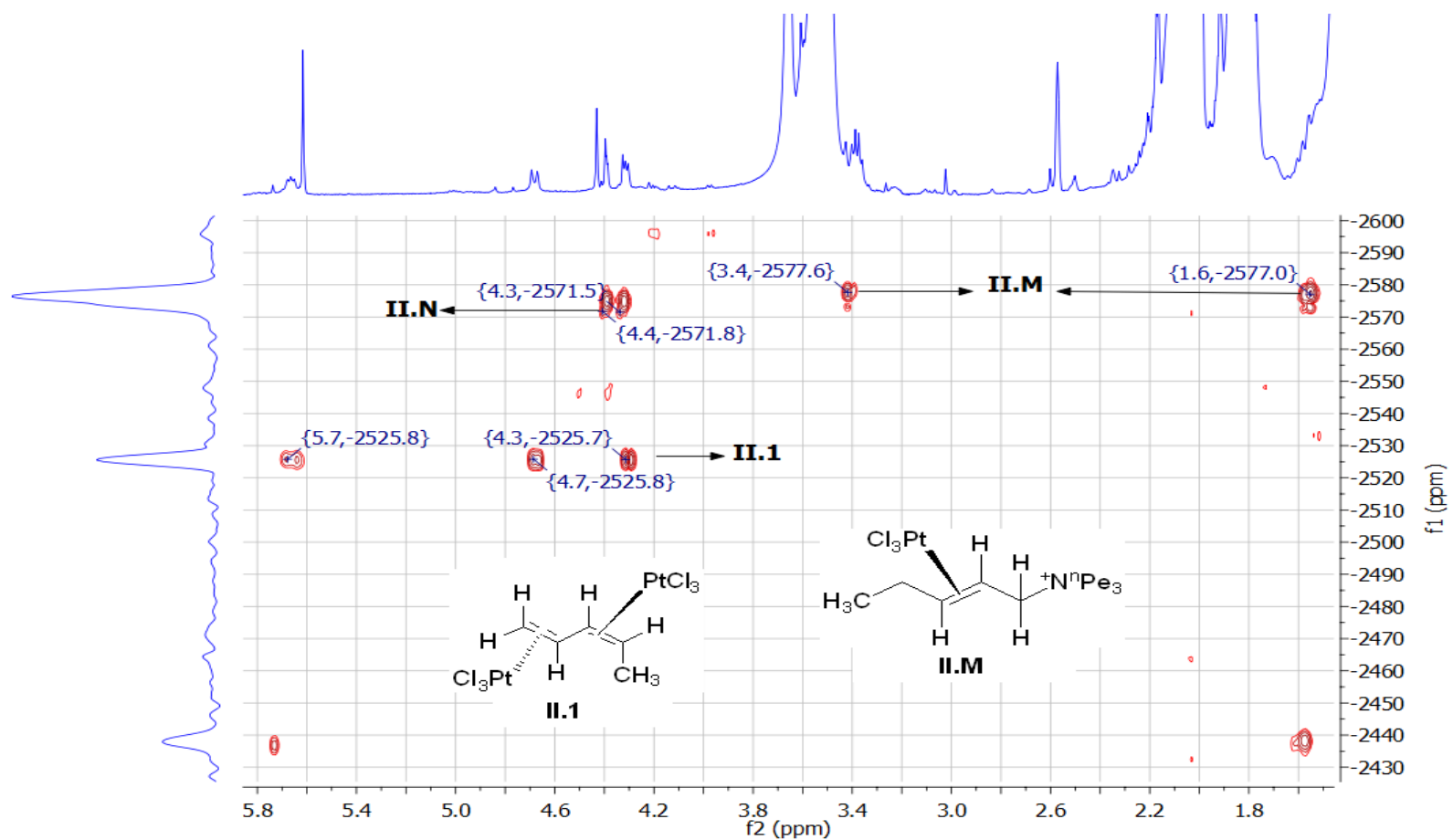


Figure 45: The 2D-¹⁹⁵Pt-¹H NMR spectra (500 MHz for ¹H) of the [ⁿPe₄N]₂[PtCl₆] mixture in acetone after 48 hours of heating under reflux and ambient light.

Experiments of *in-situ*-photo-EPR spectroscopy of $[\text{}^n\text{Pe}_4\text{N}]_2[\text{PtCl}_6]$ imparted a signal of platinum(III) species, with $g = 2.402$ as expected due to a photodissociation of $[\text{PtCl}_6]^{2-}$, and organic radical which suggested an *N*-based radical based on the g value (2.012) and the pattern of hyperfine coupling.¹²⁵ The spectrum compared with EPR spectrum of $[\text{}^n\text{Bu}_4\text{N}]_2[\text{PtCl}_6]$ is given in Figure 46. The observations suggest a similar pathway in the activation of tetrapentylammonium and tetrabutylammonium by hexachloroplatinate(IV) complex.

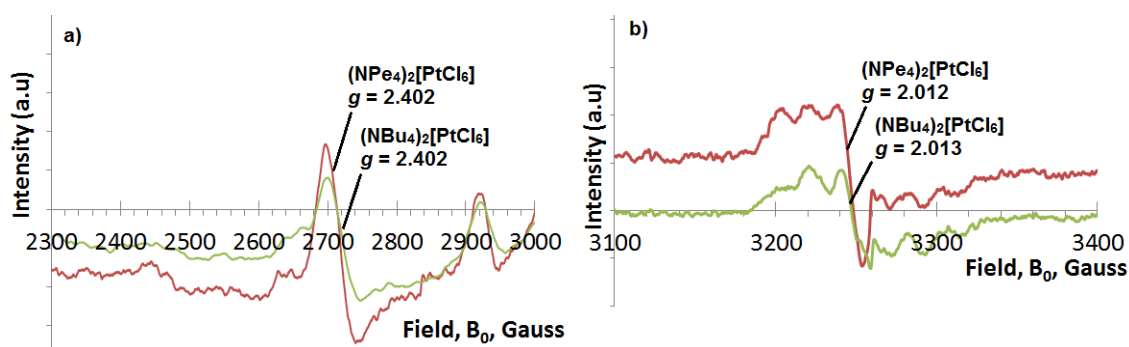


Figure 46: The *in situ*-photo-EPR spectra of $[\text{}^n\text{Pe}_4\text{N}]_2[\text{PtCl}_6]$ compared with $[\text{}^n\text{Bu}_4\text{N}]_2[\text{PtCl}_6]$ recorded in dichloromethane at 120 K showing a) platinum(III) radical and b) organic *N*-based radical.

Considering the products of the photolysis of $[\text{}^n\text{Pe}_4\text{N}]_2[\text{PtCl}_6]$ are postulated as pentadiene-platinum(II) complexes, a calculation was carried out to predict the stability of different conformers. The calculation was conducted by Marsel Shafikov. Theoretically, the platinum(II) complex of pentadiene can possess six conformers in terms of the position of the diene, the conformation of pentadiene and the platinum atom orientation coordinating to the diene. They are drawn and tabulated in Table 8. The conformers **II.1** to **II.4** are conjugated-pentadiene complexes, while the last two conformers are not conjugated.

Table 8: Theoretical conformers of platinum(II)-pentadiene complex; the chloro ligands were removed to simplify the structures.

Label and name	Description	Structure
II.1: [(<i>anti-trans</i> -1,3-pentadiene)(PtCl ₃) ₂] ²⁻	<i>trans</i> -1,3-pentadiene with platinum atoms coordinated from opposite directions	
II.2: [(<i>syn-trans</i> -1,3-pentadiene)(PtCl ₃) ₂] ²⁻	<i>trans</i> -1,3-pentadiene with platinum atoms coordinated from same directions	
II.3: [(<i>anti-cis</i> -1,3-pentadiene)(PtCl ₃) ₂] ²⁻	<i>cis</i> -1,3 pentadiene with platinum atoms coordinated from opposite directions	
II.4: [(<i>syn-cis</i> -1,3-pentadiene)(PtCl ₃) ₂] ²⁻	<i>cis</i> -1,3 pentadiene with platinum atoms coordinated from same directions	
II.5: [(<i>anti</i> -1,4-pentadiene)(PtCl ₃) ₂] ²⁻	1,4-pentadiene with platinum atoms coordinated from opposite directions	
II.6: [(<i>syn</i> -1,4-pentadiene)(PtCl ₃) ₂] ²⁻	1,4-pentadiene with platinum atoms coordinated from same directions	

Geometries of the complexes were optimised at the M06/def2-TZVPP level of theory^{117, 122} with an effective core potential (ECP)^{118, 119} used for platinum. Vibrational frequencies were calculated to ensure that the optimised geometries corresponded to local minima on the respective potential energy surfaces. Additional single point energy and vibrational frequency calculations were carried out at the B3LYP/def2-TZVPP level of theory^{117, 122} to obtain the energies and Gibbs free energies of the isomers.

The geometries of the pentadiene-platinum(II) conformers were optimised successfully at the M06/def2-TZVPP level of theory and are shown in Figure 47. Isomer **II.4** was found as the symmetrical structure of the conformer **II.1** resulted from a rotation of the central C–C bond on the geometry optimisation. The relative energies of the five conformers are in Table 9 demonstrated that the most favourable structure predicted was the conformer **II.1**, followed by the conformers

II.3 and **II.6** although they were insignificantly different from the conformers **II.2** and **II.5**.

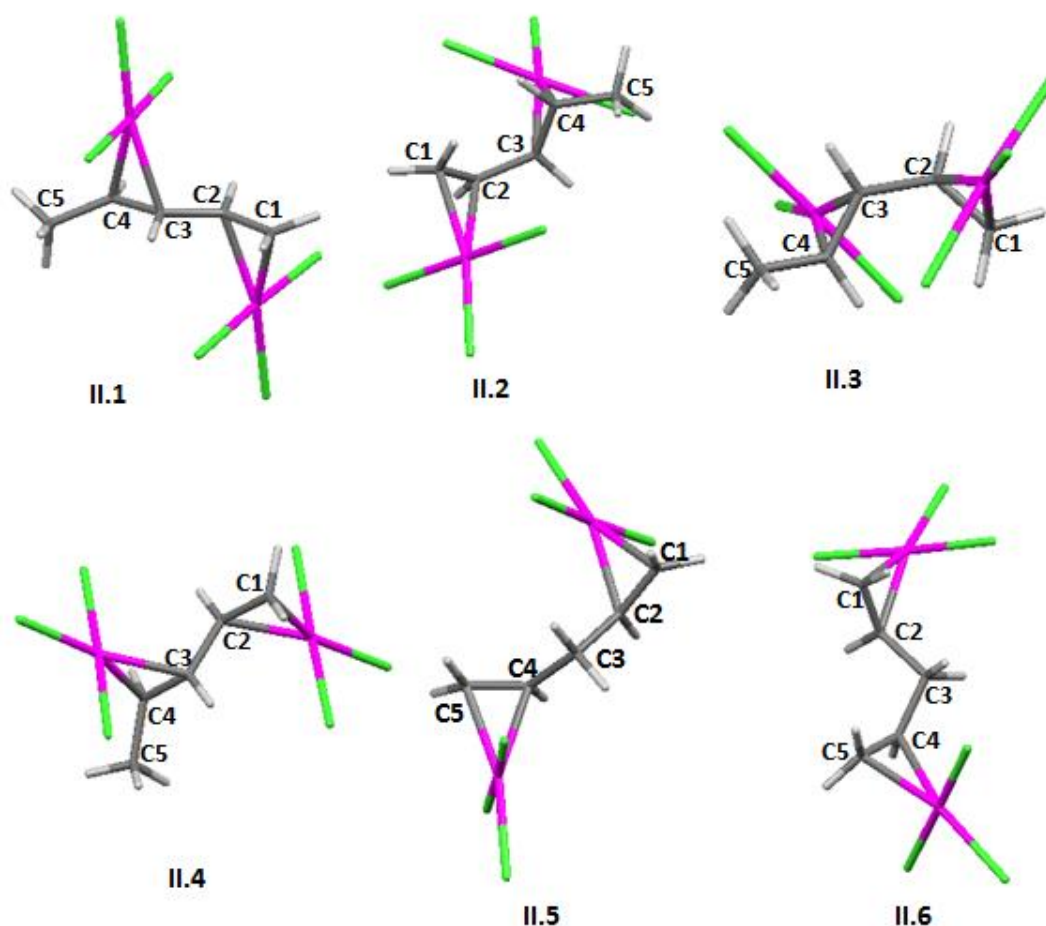


Figure 47: The optimised geometry of pentadiene conformers at M06/def2-TZVPP level of theory.

Table 9: The relative energies of conformers of pentadiene-platinum(II) complexes.

Conformer	$E / \text{kJ mol}^{-1}$	$\Delta E / \text{kJ mol}^{-1}$
II.1	-8394803.608	
II.2	-8394792.313	11
II.3	-8394795.490	8
II.5	-8394792.706	11
II.6	-8394795.467	8

In summary, the product of the photolysis of $[\text{}^n\text{Pe}_4\text{N}]_2[\text{PtCl}_6]$ could not be isolated, but from the reaction mixture analysis it was proposed that the $(\text{}^n\text{Pe}_4\text{N})^+$ cation

was activated under the irradiation of $[\text{PtCl}_6]^{2-}$ to result in the reduced product $[\text{PtCl}_4]^{2-}$ along with the olefin-platinum(II) complexes. NMR spectroscopy experiments showed the formation of **II.1**, $[\mu\text{-anti-trans-}(\eta^2\text{-1,3-pentadiene})(\text{PtCl}_3)_2]^{2-}$ which supported by theoretical calculations suggesting that the conformer is energetically the most favourable. Other conformers of pentadiene-platinum(II) complex are likely existed, but because the product was not able to isolate thus certain structures are unable to determine. The NMR results also suggested the formation of **II.M**, the pentenyl tripropylammonium coordinated to Pt^{II} . These observations are similar to facts obtained in the photolysis of $[\text{nBu}_4\text{N}]_2[\text{PtCl}_6]$ suggesting the activation of tetrapentylammonium cation seems to undergo a similar pathway as the tetrabutylammonium cation experienced.

2. $[\text{nPr}_4\text{N}]_2[\text{PtCl}_6]$

A solution of $[\text{nPr}_4\text{N}]_2[\text{PtCl}_6]$ in acetone was photolysed under the conditions used for the photolysis of $[\text{nBu}_4\text{N}]_2[\text{PtCl}_6]$. The solubility of the complex was poor in acetone, thus when the irradiation was started, not all the complex was soluble, but over the time of photolysis it was totally dissolved, so that the time to totally consume $[\text{PtCl}_6]^{2-}$ becomes averagely two times longer than that for $(\text{nBu}_4\text{N})^+$ and $(\text{nPe}_4\text{N})^+$ cations. Thus, to keep the irradiation time to be the same as the analogous alkylammonium cations, concentration of the solution of $[\text{nPr}_4\text{N}]_2[\text{PtCl}_6]$ was lowered to approximately 10 times lower.

The ^1H -NMR spectrum of the mixture after 18 hours given in Figure 48 demonstrated new broad peaks which were hard to interpret, whereas the $^{195}\text{Pt}\{^1\text{H}\}$ NMR spectra showed signals corresponding to $[\text{PtCl}_4]^{2-}$, olefin-platinum(II) complexes and an unknown peak at -1631 ppm (Figure 49). Single crystals of $[\text{nPr}_4\text{N}]_2[\text{PtCl}_4]$ were isolated but this was not possible for olefin-platinum(II) complexes. Therefore, to confirm an analogy of the $(\text{nBu}_4\text{N})^+$ activation with $(\text{nPr}_4\text{N})^+$ cation, *in situ* photo-EPR spectroscopy and 2D- ^{195}Pt - ^1H NMR

spectroscopy were utilised. The photo-EPR spectrum of $[\text{}^n\text{Pr}_4\text{N}]_2[\text{PtCl}_6]$ given in Figure 50 showed a peak corresponding to paramagnetic platinum(III) with $g = 2.400$. Compared to the resonance of platinum(III) recorded from $[\text{}^n\text{Bu}_4\text{N}]_2[\text{PtCl}_6]$, the related signal from $[\text{}^n\text{Pr}_4\text{N}]_2[\text{PtCl}_6]$ illumination was stronger, but the g value and the hyperfine pattern suggested the resonance of platinum(III). In the organic region, a signal with $g = 2.013$ was seen; again it was more detailed and intense than related signal obtained from $[\text{}^n\text{Bu}_4\text{N}]_2[\text{PtCl}_6]$, but suggested an N -based radical based on the g value and by comparison with the reported spectrum for $\bullet^+\text{NEt}_4$.¹²⁵

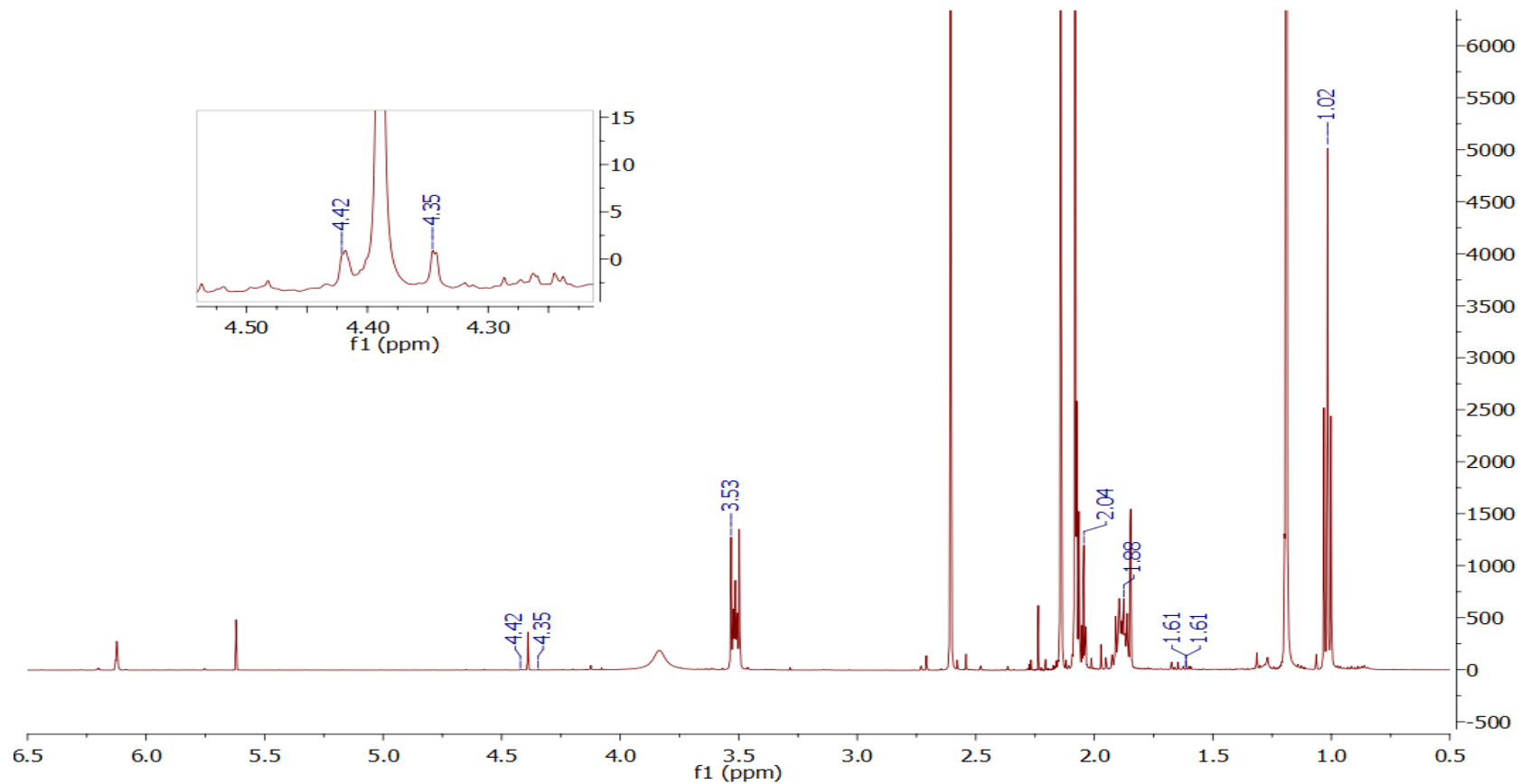


Figure 48: The ^1H NMR spectrum (500 MHz) of the mixture of photolysis of $[\text{Pr}_4\text{N}]_2[\text{PtCl}_6]$ in acetone, recorded in d_6 -acetone. The chemical shifts at 1.02, 1.88 and 3.54 are corresponded with propyl protons; the signals at 4.42 and 4.35 ppm shown in the enlargement spectrum were found to correlate with a ^{195}Pt chemical shift in olefin- Pt^{II} area in 2D- ^{195}Pt - ^1H NMR spectra.

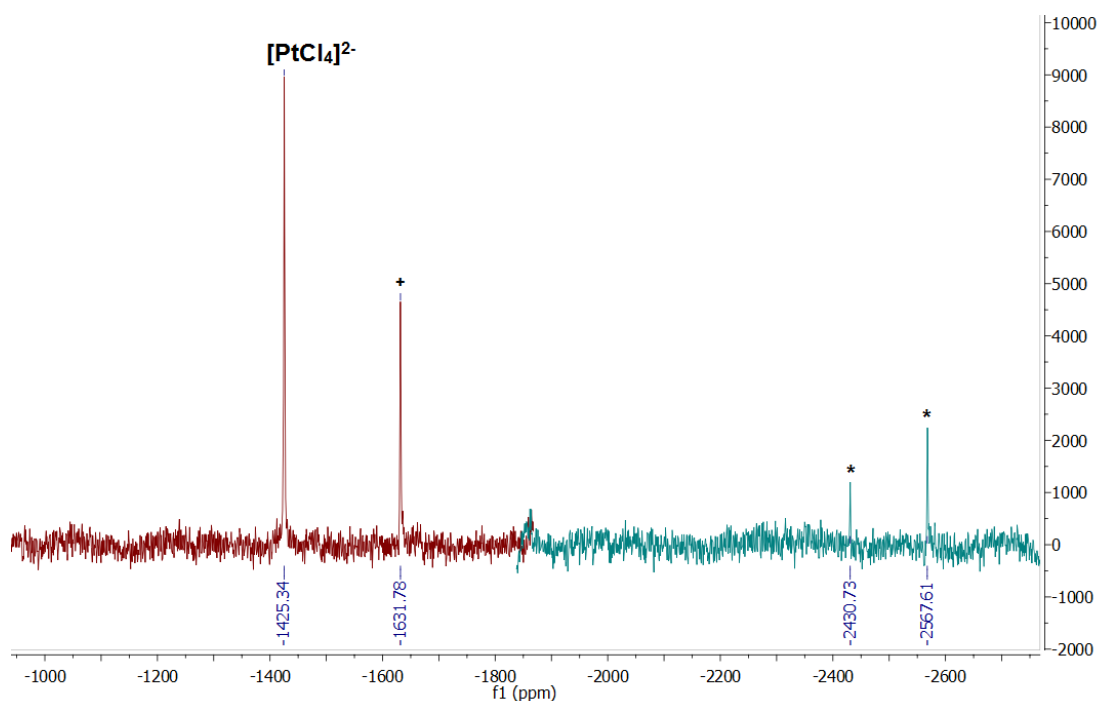


Figure 49: The $^{195}\text{Pt}\{^1\text{H}\}$ NMR spectra (107 MHz) of the mixture of $[\text{}^n\text{Pr}_4\text{N}]_2[\text{PtCl}_6]$ photolysis in acetone recorded in d_6 -acetone at 298 K. (cross: unknown signal; asteriks: olefin-Pt(II) signals).

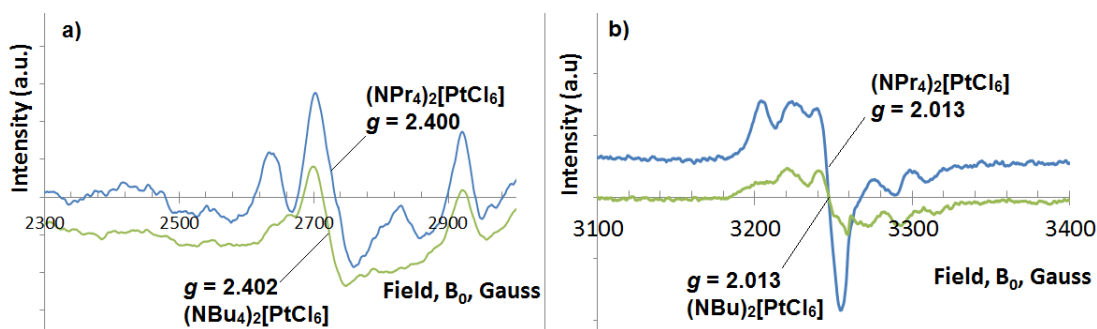


Figure 50: The *in situ*-photo-EPR spectra of $[\text{}^n\text{Pr}_4\text{N}]_2[\text{PtCl}_6]$ compared with $(\text{}^n\text{Bu}_4\text{N})_2[\text{PtCl}_6]$ recorded in dichloromethane at 120 K showing: a) platinum(III) radical and b) organic N-based radical.

The 2D- $^{195}\text{Pt}\text{-}^1\text{H}$ NMR spectra of the mixture of photolysis of $[\text{}^n\text{Pr}_4\text{N}]_2[\text{PtCl}_6]$ is presented in Figure 51. As seen in the 1D- $^{195}\text{Pt}\{^1\text{H}\}$ NMR spectrum, the two-dimensional spectra depicted a signal at -2567 ppm correlated with proton resonances in the olefin area. Similar chemical shift was seen after photolysis of both $[\text{}^n\text{Bu}_4\text{N}]_2[\text{PtCl}_6]$ and $[\text{}^n\text{Pe}_4\text{N}]_2[\text{PtCl}_6]$ and which was proposed to be a platinum complex on an ammonium cation containing a double bond, but as no product could be isolated, a definite structure could not be determined. Nonetheless, the

appearance of the olefin-platinum(II) signals implied activation of tetrapropylammonium cation, most likely *via* a pathway similar to that in the tetrabutylammonium cation.

Tetrapropylammonium hexachloroplatinate(IV) was also heated under reflux in acetone under ambient illumination and after 48 hours of reaction, the resulting mixture was analysed using ^{195}Pt NMR spectroscopy. The spectrum (Figure 52) showed the peak corresponding to $[\text{PtCl}_4]^{2-}$ complex, the binuclear complex $[\text{Pt}_2\text{Cl}_6]^{2-}$ and the unidentified signal at -1676 ppm. The first two complexes were also isolated from the reaction mixture. The appearance of the unknown compound and $[\text{PtCl}_4]^{2-}$ agreed with the observation made under UV photolysis at room temperature, but $[\text{Pt}_2\text{Cl}_6]^{2-}$ appeared only when the mixture was heated. The same observation was made when heating $[\text{nBu}_4\text{N}]_2[\text{PtCl}_6]$ under reflux indicating the need for heating to form the dimer. The peak corresponding to $[\text{PtCl}_6]^{2-}$ was also seen implying that the consumption of $[\text{PtCl}_6]^{2-}$ was far slower when the cation was $(\text{nPr}_4\text{N})^+$ compared to $(\text{nBu}_4\text{N})^+$. But, after 48 h of reaction under reflux in ambient light, the signal from the olefin-platinum(II) complex was still undetectable.

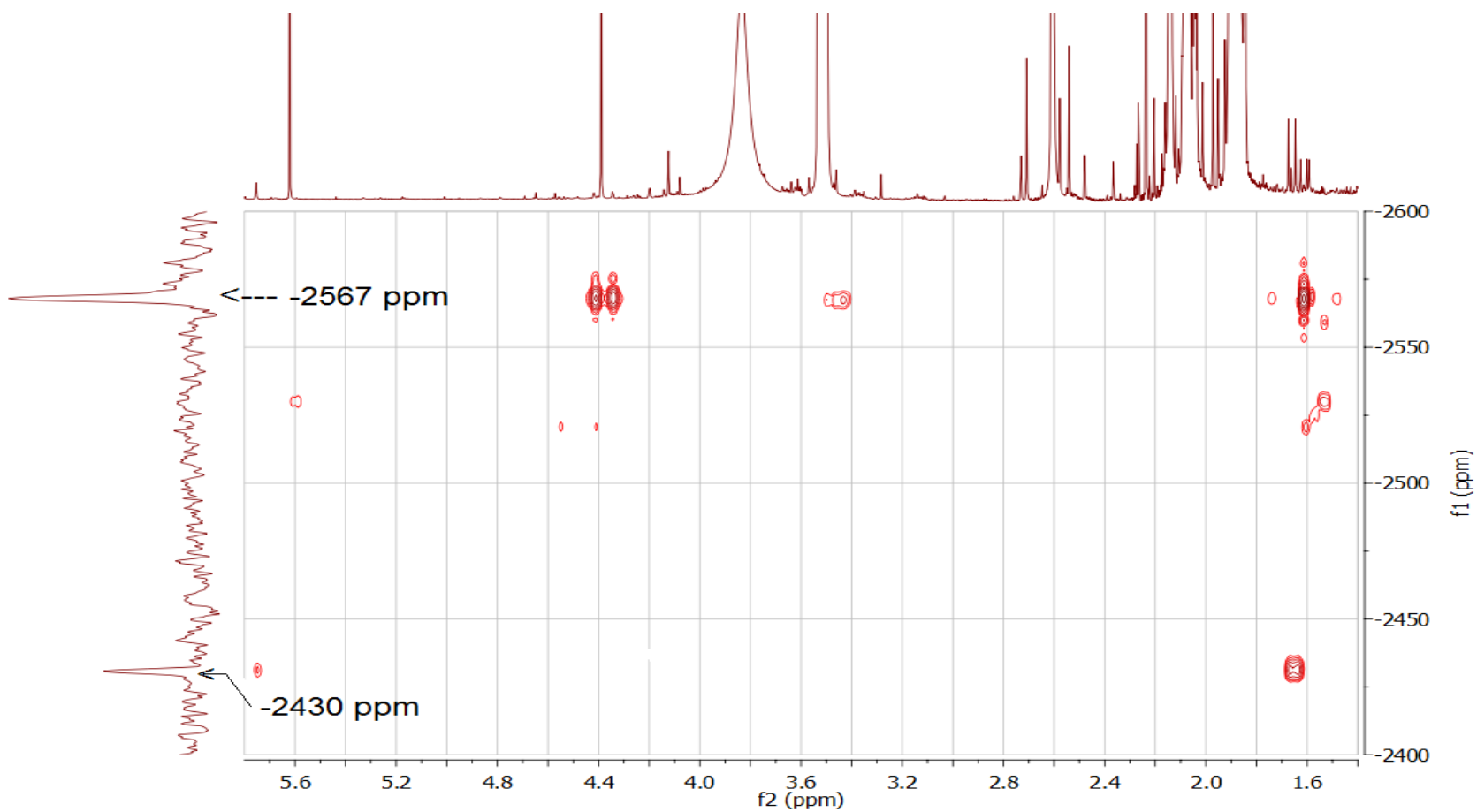


Figure 51: The 2D- ^{195}Pt - ^1H NMR spectra (500 MHz for ^1H) of the mixture of photolysis of $[\text{Pr}_4\text{N}]_2[\text{PtCl}_6]$ in acetone recorded in d_6 -acetone at 298

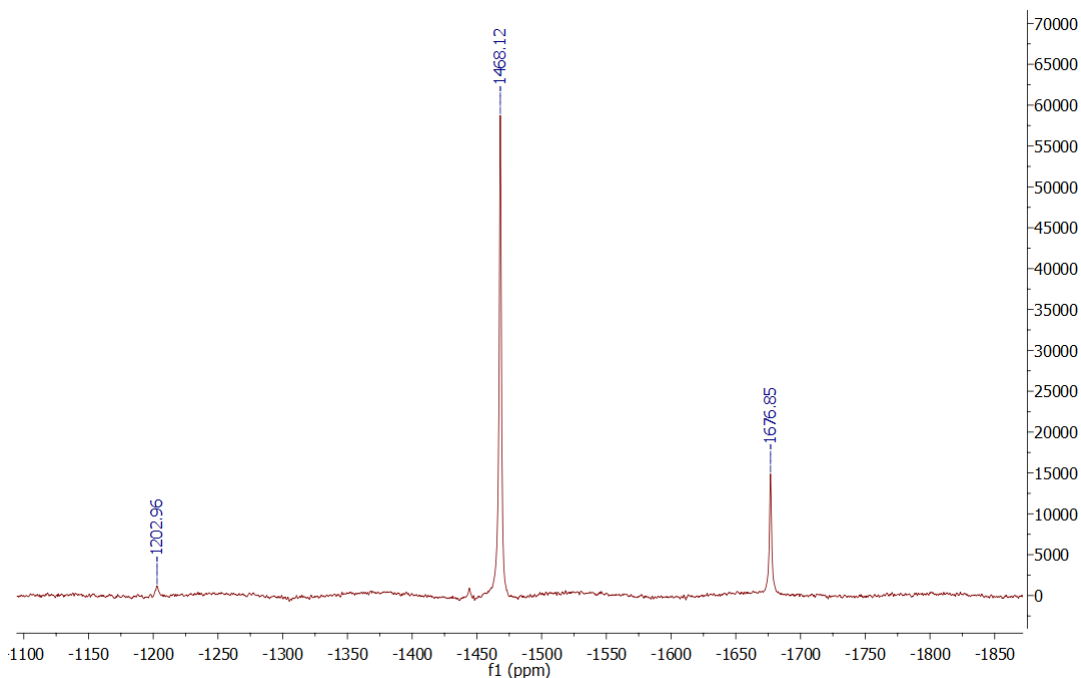
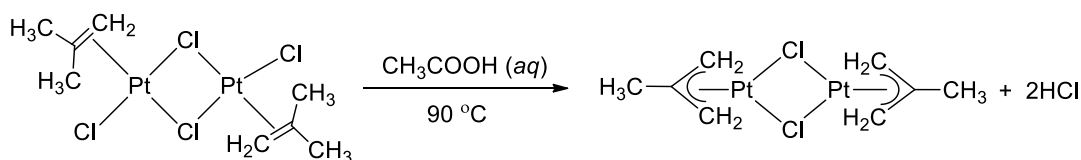


Figure 52: The ^{195}Pt NMR spectra (107 MHz) of the $[\text{}^n\text{Pr}_4\text{N}]_2[\text{PtCl}_6]$ mixture in acetone on heating for 48 hours under reflux and ambient light recorded in CD_2Cl_2 at 295 K.

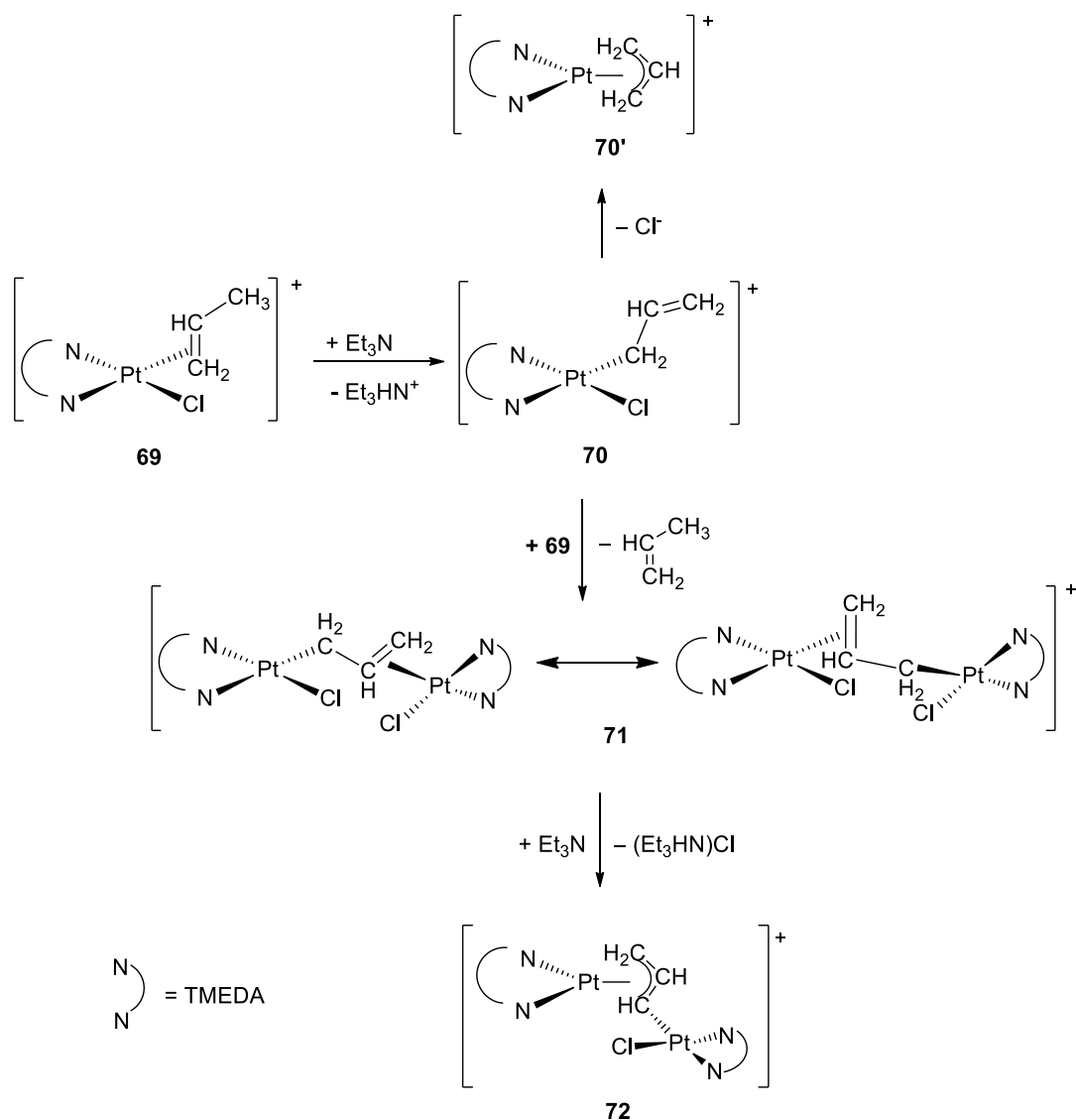
While the experiments with $[\text{}^n\text{Pr}_4\text{N}]_2[\text{PtCl}_6]$ were not conclusive, they perhaps provide some idea for intermediate conclusions. Thus, photolysis of $[\text{}^n\text{Pr}_4\text{N}]_2[\text{PtCl}_6]$ led to the formation of alkene complexes of Pt^{II} , but these were not observed when the reaction was carried out under conditions of reflux. However, under reflux, $[\text{Pt}_2\text{Cl}_6]^{2-}$ was observed. One possible conclusion from this is that the alkene complexes formed could have the formula $[\text{PtCl}_3(\text{alkene})]^-$ (Zeise's salt analogue) and that these complexes were unstable thermally, losing the alkene and forming $[\text{Pt}_2\text{Cl}_6]^{2-}$. In the combined thermal/photochemical reactions of $[\text{}^n\text{Bu}_4\text{N}]_2[\text{PtCl}_6]$, $[\text{Pt}_2\text{Cl}_6]^{2-}$ was also observed, but so was the product, butadiene complex, which is evidently thermally stable under reflux in acetone. One possibility is that alkene- Pt^{II} complexes are the result of a first photochemical C–H activation and the final product (in the case of ${}^n\text{Bu}_4\text{N}^+$ salt) arises from a second activation of these complexes. This point will be developed further later in the chapter (Section 2.2.2.8).

Zeise's salt analogues, $[\text{PtCl}_3(\text{olefin})]^-$ (olefin = propene, pentene, butene) are transformed to dimers, $[\text{Pt}_2(\text{olefin})_2\text{Cl}_4]^{2-}$ in HCl ,^{92, 93} and by heating of the dimers at 90 °C in acetic acid, the related allylic platinum(II) complexes are obtained while losing HCl .¹³² This type of reaction however only proceeds if one olefinic carbon is substituted with two alkyls to accommodate HCl loss (Scheme 57), therefore, in the reaction of $[\text{PtCl}_3(\eta^2\text{-olefin})]^-$ complexes, where olefin = propene, 2-butene, and cyclic olefin, no allylic-platinum products are observed. However, Bandoli reported a transformation of $[\eta^2\text{-(C}_3\text{H}_6\text{)-PtCl(TMEDA)}]$ (TMEDA = tetramethylethylenediamine) complex to $[\eta^1, \eta^3\text{-}\mu\text{-(C}_3\text{H}_4\text{)-Pt}_2\text{Cl(TMEDA)}_2]^+$ through sequential deprotonation of methyl of propene coordinated to Pt^{II} in the presence of trialkylamine as is shown in Scheme 58.¹³³ The deprotonation that follows loss of HCl is accommodated by TMEDA ligand in which the $[\text{PtCl(TMEDA)}]^+$ cation increases the Bronsted acidity of the α -alkyl protons of the alkene, thus deprotonation proceeds under mild conditions. Besides that, the TMEDA ligand stabilises the complex so that the chloride ligand easily dissociates to facilitate the transformation of $\eta^1 \rightarrow \eta^3$ of the allyl moiety.



Scheme 57: The reaction showing a formation of allylic-platinum complex from propene-platinum dimer as reported by Mann *et al.*¹³²

In the case of the photolysis of $[\text{Pr}_4\text{N}]_2[\text{PtCl}_6]$, another possibility is that the propyl undergoes double C–H activations, similar to $(\text{tBu}_4\text{N})^+$ giving a butadiene fragment. The first activation may cause a proton elimination resulting in a propene-coordinated to $[\text{PtCl}_3]^{2-}$, concomitantly the second activation may form an allyl derivative which may decompose. $^{195}\text{Pt}\{^1\text{H}\}$ NMR spectroscopy showed no signal from allyl-Pt in the reaction mixture.



Scheme 58: A proposed mechanism the formation of platinum(II) complex to form $\eta^1, \eta^3\text{-}\mu\text{-allyl}$ -platinum(II) complex via sequential deprotonation of η^2 -propene-platinum(II) complex as reported by Bandoli *et al.*¹³³

2.2.2.8. Investigation of the Second Activation of (ⁿBu₄N)⁺ cation.

As mentioned earlier, if Hofmann elimination is involved in the activation of tetrabutylammonium, so that the first pathway of the reaction forms butene which is likely coordinated to Pt^{II} formed under illumination of Pt^{IV}. Therefore, it was considered that the butadiene-platinum(II) product was a result of the second activation of the butene-Pt^{II} complex. So, the formation of the butadiene complex could involve two step-by-step activations. To test the assumption, experiments were set up, such as preparing [PtCl₃(1-butene)]⁻ (**III**) and [PtCl₃(2-butene)]⁻ (**IV**)

complexes, then following their reactions under a variety of conditions by employing NMR spectroscopy. The results are presented in the following subsections.

a. Irradiation of [ⁿBu₄N][PtCl₃(1-butene)], III.1

Irradiation of tetrabutylammonium (η^2 -1-butene)-trichloroplatinate(II), **III.1**, in d₆-acetone under UV light ($\lambda > 305$ nm) led to a slow decoordination of the complex that was shown by ¹H and ¹⁹⁵Pt{¹H} NMR spectroscopy. In fact, as soon as five minutes of irradiation had passed, the signal of free 1-butene was seen while the proton integration of the coordinated 1-butene (at $\delta = 4.9$ ppm) reduced by about 10%, but over the time of illumination the integration was insignificantly changed (Figure 53). In accordance with the ¹⁹⁵Pt{¹H} NMR spectra, no new signal was found and only the peak of (η^2 -1-butene)-trichloroplatinate(II) which appeared to be similar in integration over the irradiation time (Figure 54). The assignment of the free 1-butene was made by comparing the ¹H NMR signals of 1-butene dissolved in d₆-acetone which was prepared separately. The observation of decomplexation was also made when an ambient light was applied to the solution.

In summary, the insignificant decomplexation occurred upon the irradiation of only tetrabutylammonium (η^2 -1-butene)-trichloroplatinate(II) but no transformation was observed.

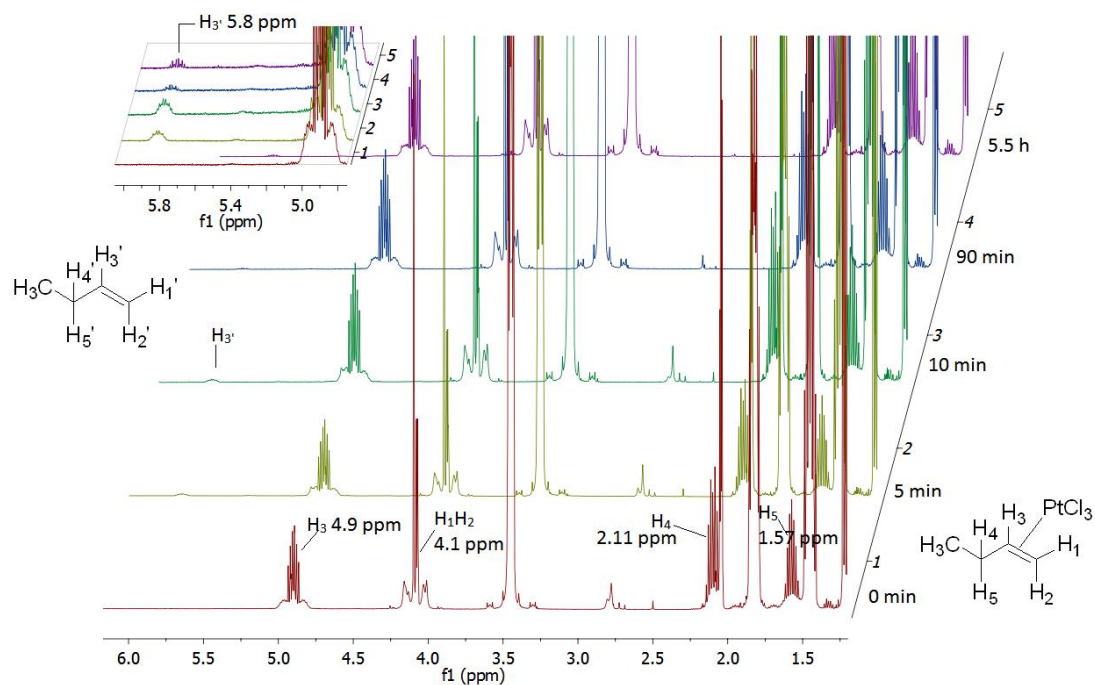


Figure 53: The ^1H NMR spectra (500 MHz) of the $[\text{nBu}_4\text{N}][\text{PtCl}_3(1\text{-butene})]$, **III.1**, in d_6 -acetone on the irradiation under UV light.

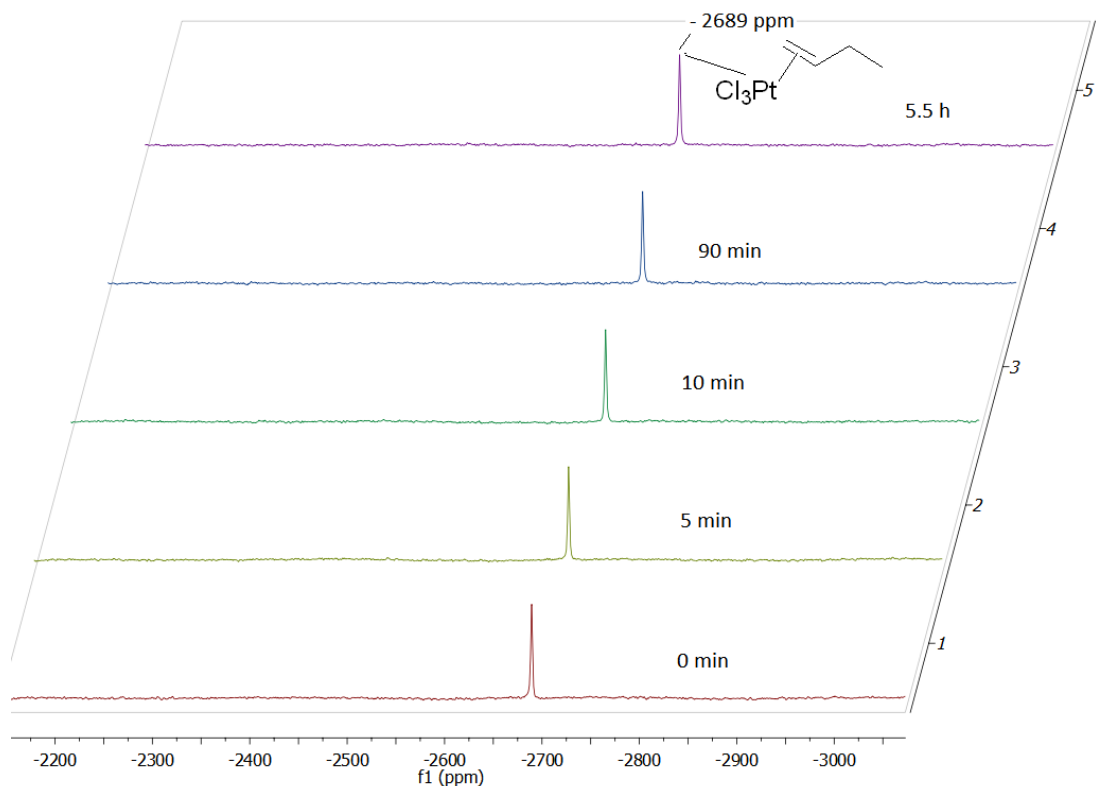


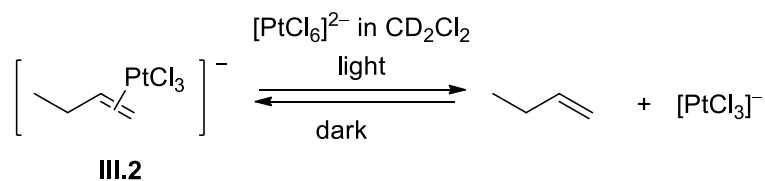
Figure 54: The $^{195}\text{Pt}\{^1\text{H}\}$ NMR spectra (107 MHz) of the $[\text{nBu}_4\text{N}][\text{PtCl}_3(1\text{-butene})]$, **III.1**, in d_6 -acetone on the irradiation under UV light.

b. Irradiation of $[\text{PtCl}_3(1\text{-butene})]^-$ in the presence of $[\text{PtCl}_6]^{2-}$

The irradiation of $[\text{PtCl}_3(1\text{-butene})]^-$ was then carried out in the presence of $[\text{PtCl}_6]^{2-}$. To study the reaction of $[\text{PtCl}_6]^{2-}$ with $[\text{PtCl}_3(1\text{-butene})]^-$ alone and to eliminate the effect of the $(^n\text{Bu}_4\text{N})^+$ cation, the complexes were prepared with bis(triphenylphosphine)iminium (PPN) counter cations, while the reactions were carried out in dichloromethane as the PPN complexes were insoluble in acetone.

When the mixture of $[\text{PtCl}_6]^{2-}$ with $[\text{PtCl}_3(1\text{-butene})]^-$ was irradiated under UV light ($\lambda > 305$ nm), again decomplexation was seen by ^1H NMR spectroscopy (Figure 55) where a series of 1-butene signals was observed but no platinum satellites were seen. Compared to irradiation of $[\text{PtCl}_3(1\text{-butene})]^-$ only, it seemed that the decomplexation process was driven by $[\text{PtCl}_6]^{2-}$ shown by changes of proton signals in integration. After 10 minute irradiation about 25% of the coordinated 1-butene was lowered and only left about 18% after irradiation for 60 minutes. However, when the solution was stored in the dark for two days, the 1-butene re-coordinated to the platinum shown by an increase of the peak integration of the related proton to about 90% implying the reversible coordination of 1-butene in solution. The $^{195}\text{Pt}\{^1\text{H}\}$ (Figure 56) and the 2D- $^{195}\text{Pt}-^1\text{H}$ NMR spectra showed only one peak for the 1-butene-platinum(II) complex in the range of Pt(II)-olefin resonances. On 60-minute irradiation, the proton signals of the 1-butene-Pt(II) had almost totally disappeared and the platinum signal of the 1-butene complex was undetectable by $^{195}\text{Pt}\{^1\text{H}\}$ NMR spectroscopy but when the irradiated solution was stored in the dark for 24 hours, the signals of the complex were re-observed in the ^1H , $^{195}\text{Pt}\{^1\text{H}\}$ and 2D- $^{195}\text{Pt}-^1\text{H}$ NMR spectra. The observation was in line with the appearance of $[\text{PtCl}_4]^{2-}$ and a decrease of integration peak corresponding with Pt^{IV} over the illumination time. These observations suggested the decoordination was reversible and that involves $[\text{PtCl}_6]^{2-}$ (Scheme 59). Further investigation regarding the involvement of $[\text{PtCl}_6]^{2-}$ in the decomplexation is not continued. In the ^1H NMR spectrum, signals in 3.5 – 3.8 ppm were seen, but on the 2D- $^{195}\text{Pt}-^1\text{H}$ NMR spectra, the signals were not

correlated to platinum species. Therefore, the peaks were suggested the result of a decomposition of 1-butene under irradiation.



Scheme 59: The de-coordination of (η^2 -1-butene)-trichloroplatinate(II) anion under light in CD_2Cl_2 solution.

To prove the occurrence of the decomplexation, the mixture of the 1-butene-platinum(II) and hexachloroplatinate(IV) complexes in dichloromethane solution was irradiated in a Young's NMR tube and the reaction was monitored using ^1H NMR spectroscopy. The free 1-butene was removed using the freeze-pump-thaw method $-116\text{ }^\circ\text{C}$, at which temperature, dichloromethane freezes whereas 1-butene is in the liquid phase. The ^1H -NMR spectrum of the solution was then recorded and showed roughly about 50% reduction of the integration corresponding to the proton signals of free 1-butene. The observation demonstrated the removal of 1-butene through freeze-pump-thaw and implied the decomplexation of 1-butene-platinum(II) to free 1-butene. On heating of the mixture of the $[\text{PtCl}_3(\text{1-butene})]^{2-}$ and $[\text{PtCl}_6]^{2-}$ in dichloromethane at $40\text{ }^\circ\text{C}$ for 48 h under the dark conditions, the decomplexation was absent implying the important role of light in the process.

To conclude, under UV light, the decomplexation of $[\text{PtCl}_3(\text{1-butene})]^-$ occurred to free the 1-butene in solution and it was driven by $[\text{PtCl}_6]^{2-}$ complex, but the hexachloroplatinate(IV) complex did not apparently activate 1-butene to form butadiene in the system, ruling out (1-butene)-Pt(II) as an intermediate on the formation of the butadiene-platinum(II) complex.

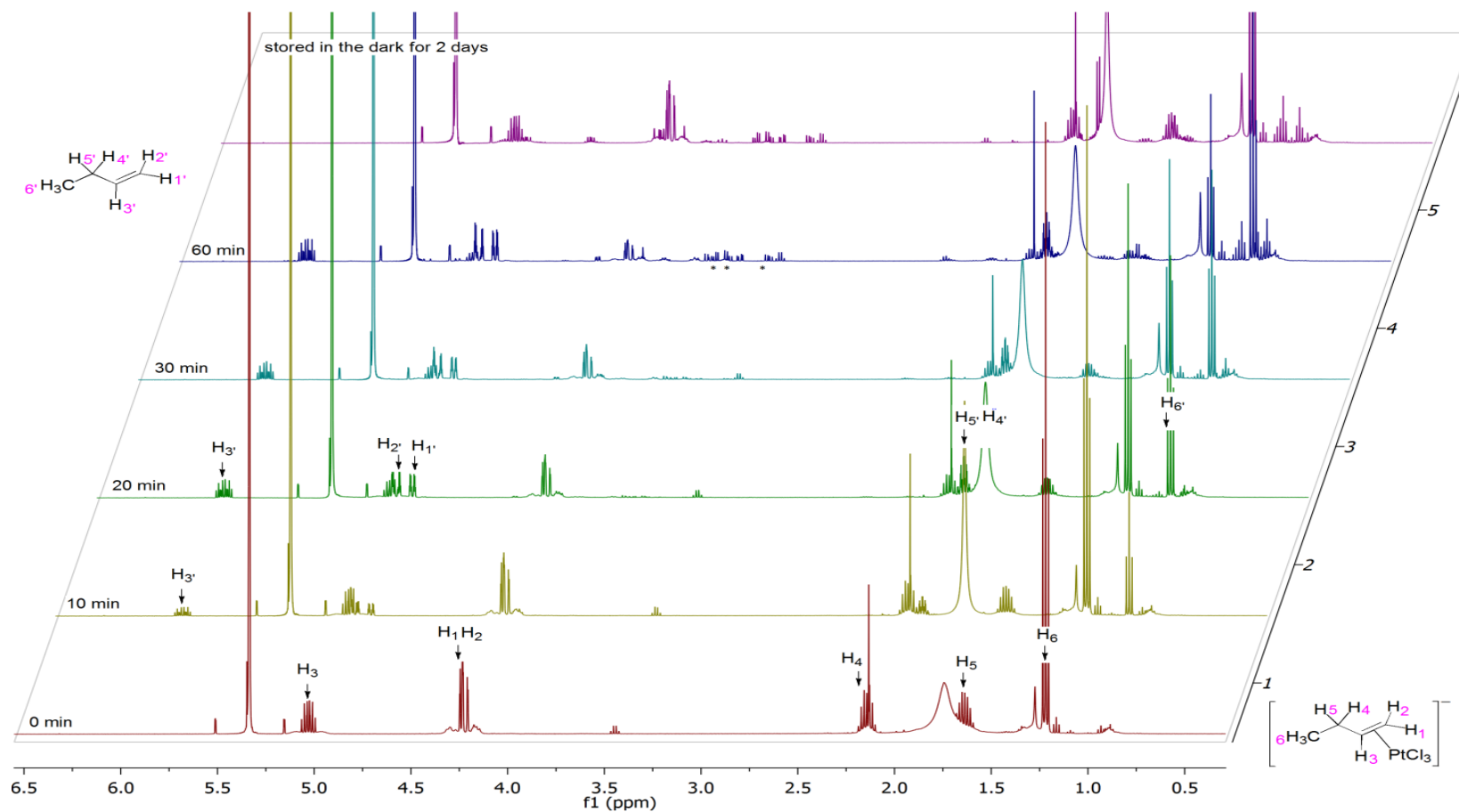


Figure 55: The ^1H NMR spectra (500 MHz) of the mixture of $[\text{PPN}][\text{PtCl}_3(1\text{-butene})]$, **III.2** and $[\text{PPN}]_2[\text{PtCl}_6]$ in CD_2Cl_2 on the irradiation under UV light. (asteriks mark new signals proposed as resulting from decomposition of 1-butene).

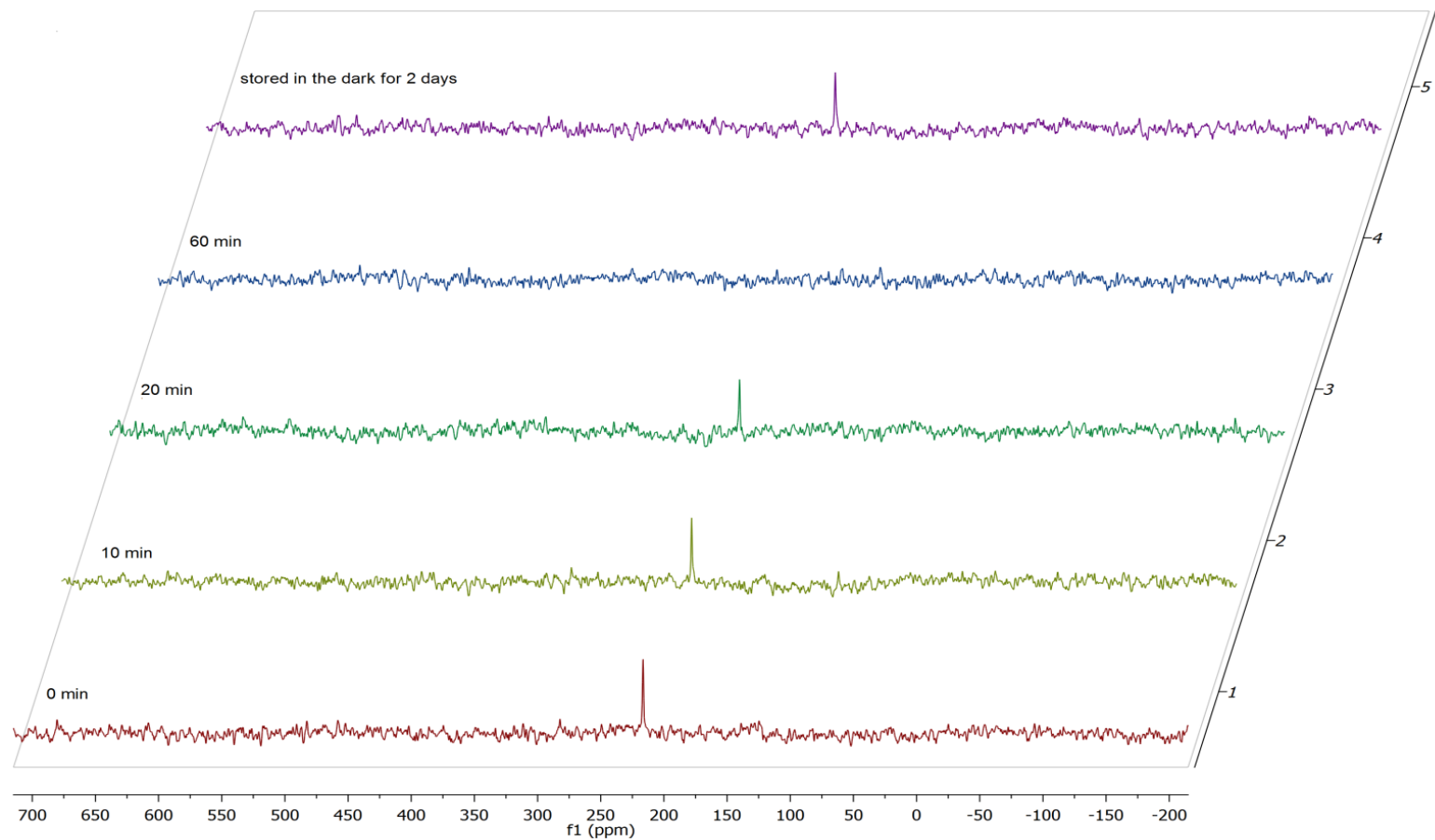


Figure 56: The ^{195}Pt NMR spectra (107 MHz) of the mixture of $[\text{PPN}][\text{PtCl}_3(1\text{-butene})]$, **III.2**, and $[\text{PPN}]_2[\text{PtCl}_6]$ in CD_2Cl_2 on the irradiation under UV light.

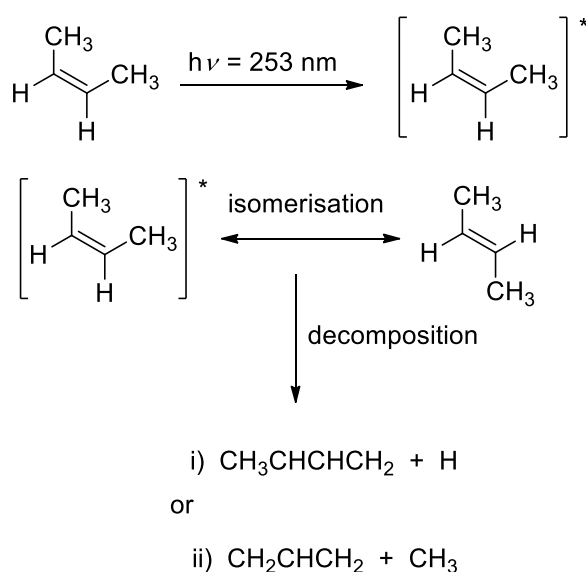
c. The reaction of $[\text{PtCl}_3(2\text{-butene})]^-$, IV, with $[\text{PtCl}_6]^{2-}$.

The complex $[\text{PtCl}_3(2\text{-butene})]^-$, IV, was also considered as an intermediate in the formation of the butadiene-platinum(II) complex, thus the reaction of the complex with $[\text{PtCl}_6]^{2-}$ was conducted. The mixture was again freed from $(\text{}^n\text{Bu}_4\text{N})^+$ cation to simplify observations so that the complexes were prepared with $(\text{PPN})^+$ as the counter cation. The mixture was dissolved in dichloromethane as the complexes were insoluble in acetone, was irradiated with UV light ($\lambda > 305 \text{ nm}$) and monitored using proton and platinum NMR spectroscopy.

Based on ^1H NMR spectra, the $(\text{PPN})^+$ protons remained unchanged under irradiation. As soon as the light was applied to the mixture, new proton signals were seen at 5.44 and 1.63 ppm (Figure 57) which were assigned to free 2-butene, indicating the decomplexation like the observation made with the 1-butene-platinum(II) complex (Section 2.2.2.8.b). The assignment was done by comparing the signals to the proton signal of 2-butene from a solution that was prepared separately. Along with the increase in integration of these signals, the integration of signals corresponding to the 2-butene-Pt(II) complex decreased. After irradiation for 120 minutes, the proton peaks of the complex were hardly present (only about 10% with respect to the initial integration), but in addition to the peaks of the free 2-butene, signals in the range of 3.8 to 4.8 ppm were found. The peaks however had no correlation with platinum as shown in 2D $^{195}\text{Pt}\text{-}^1\text{H}$ NMR spectra (Figure 58) so these new signals were proposed to be the result of 2-butene decomposition. No additional olefin-Pt(II) peaks were seen in 2D- $^1\text{H}\text{-}^{195}\text{Pt}$ NMR spectra of the mixture after irradiation for 120 minutes. The $^{195}\text{Pt}\{^1\text{H}\}$ NMR spectra showed a slow decrease in integration of $[\text{PtCl}_6]^{2-}$ (Figure 59), and a weak signal from $[\text{PtCl}_4]^{2-}$ was seen during the photolysis.

Experimental observations of illumination of *cis*-2-butene at 253 nm were reported, and the compounds produced from the photolysis were analysed directly by using gas chromatography,¹³⁴ or identified by further reactions with

methane.¹³⁵ It was proposed that on the irradiation there was isomerisation from *cis* to *trans* alkene and that when an equilibrium of those two isomers was achieved, a slow decomposition was observed that proceeded through two main reactions: the first reaction resulting in C₄H₇ and H fragments while the second one gave C₃H₅ and CH₃ (Scheme 60). In the gas phase those fragments suggest allyl, hydrogen atom and methyl radicals.^{134, 135} In the case of the illumination of 2-butene discussed in this research, the decomposition likely occurred, but as the irradiation took place in solution, the decomposition product, may interact with solvent giving rise to more complicated compounds; this was not investigated further.



Scheme 60: Photolysis reaction of *cis*-2-butene in the gas phase as reported by Cundall *et al.* and Chesick *et al.*^{134, 135}

To conclude, similar to the reaction of the 1-butene-Pt(II) complex with [PtCl₆]²⁻, irradiation of the 2-butene-Pt(II) complex in the presence of [PtCl₆]²⁻ only caused the decomplexation, and further reaction leading to the formation of the butadiene-Pt(II) complex did not occur.

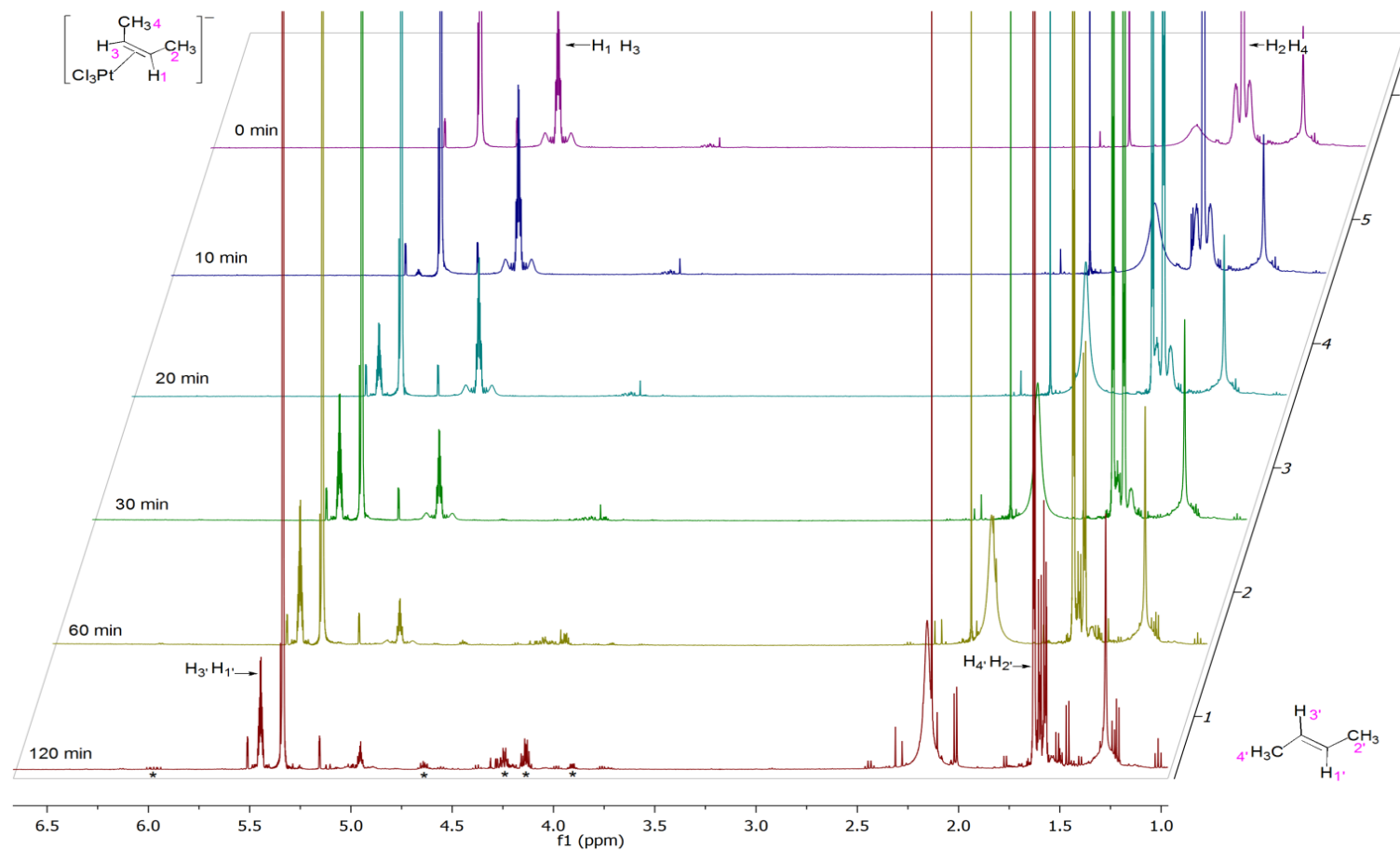


Figure 57: The ^1H NMR spectra (500 MHz) of the mixture of $[\text{PPN}][\text{PtCl}_3(2\text{-butene})]$, **IV**, and $[\text{PPN}]_2[\text{PtCl}_6]$ in CD_2Cl_2 during the irradiation. (asteriks mark new signals proposed as resulting from decomposition of 2-butene).

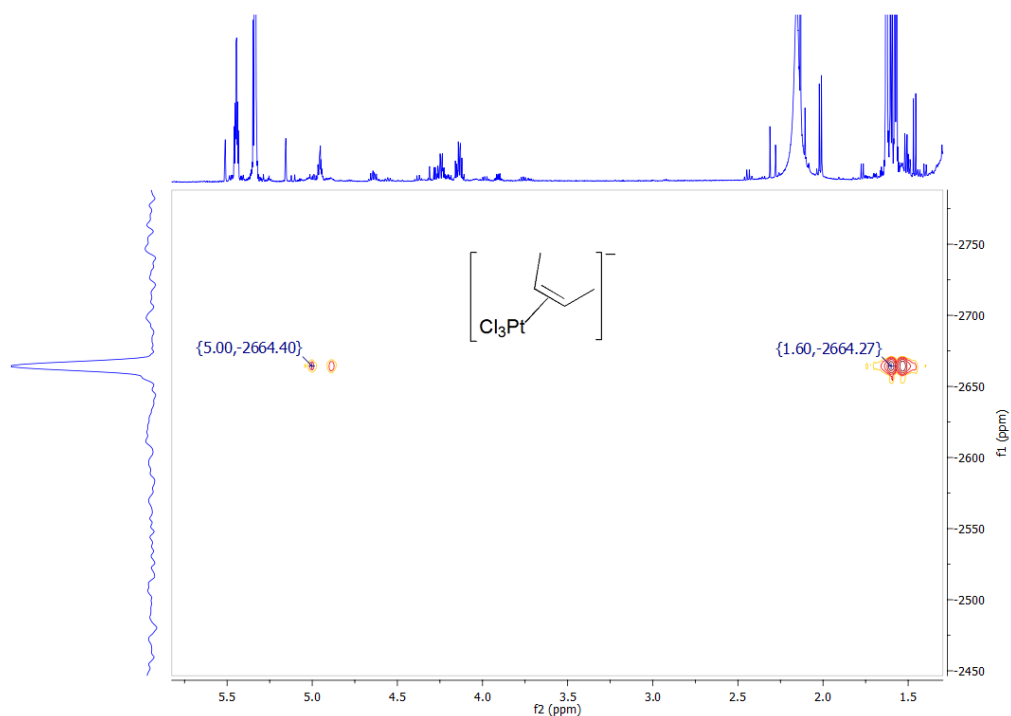


Figure 58: The 2D- ^{195}Pt - ^1H NMR spectra (500 MHz for ^1H) of the mixture of $[\text{PPN}][\text{PtCl}_3(\text{2-butene})]$, IV, and $[\text{PPN}]_2[\text{PtCl}_6]$ in CD_2Cl_2 after the irradiation for 120 minutes.

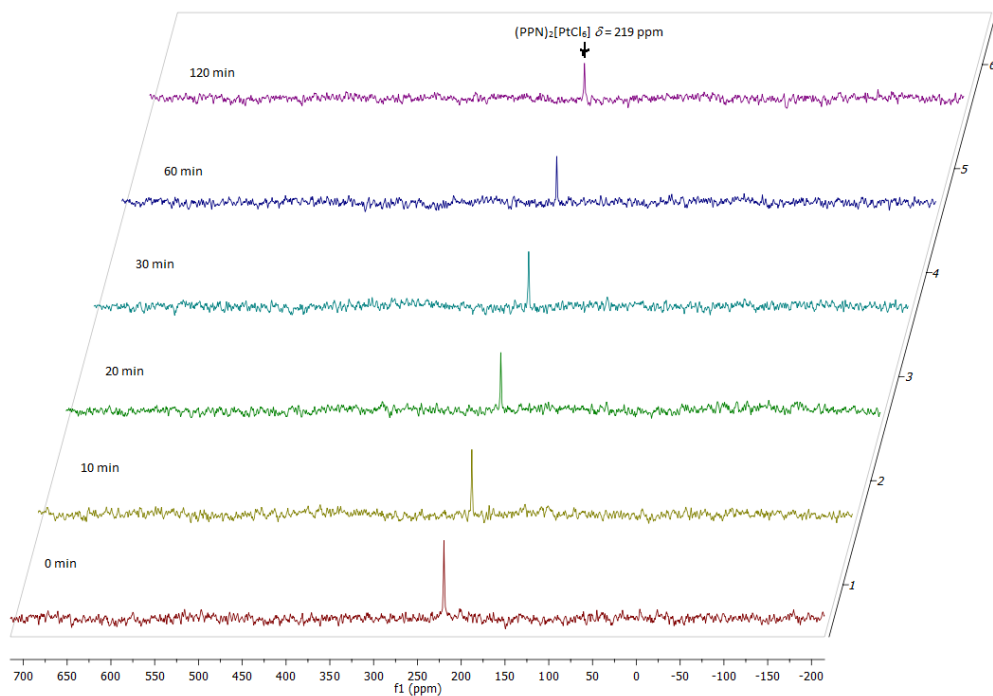


Figure 59: The $[\text{PPN}]_2[\text{PtCl}_6]$ signal on the $^{195}\text{Pt}\{^1\text{H}\}$ NMR spectra (107 MHz) during the irradiation of the mixture of $[\text{PPN}][\text{PtCl}_3(\text{2-butene})]$ and $[\text{PPN}]_2[\text{PtCl}_6]$ in CD_2Cl_2 .

d. Identification of radicals in the mixture of $(\text{PPN})_2[\text{PtCl}_6]$ with $(\text{PPN})[\text{PtCl}_3(1\text{-butene})]$, III.2

On irradiation of III.2 in the presence of $(\text{PPN})_2[\text{PtCl}_6]$, the possibility of generating a carbon-based radical was considered. An *in situ* irradiation-EPR experiment was carried out upon the mixture in dichloromethane at 120 K. Two weak signals with g values of 2.408 and 2.008 were seen after two minutes of irradiation, while the intensities strengthened over the illumination time (Figure 60). The signal at $g = 2.408$ came from a platinum(III) radical generated from $[\text{PtCl}_6]^{2-}$ under irradiation, the same observation that had been made on irradiation of $[\text{nBu}_4\text{N}]_2[\text{PtCl}_6]$. While the second signal was observed in the organic radical area at $g = 2.008$ appearing like a doublet indicating a radical coupled to one environment of EPR-active nuclear. Therefore, the signal suggests a radical corresponding with an N -based radical of PPN^+ cation coupled to ^{31}P which is EPR-active possessing $I = \frac{1}{2}$ to give a doublet hyperfine coupling.

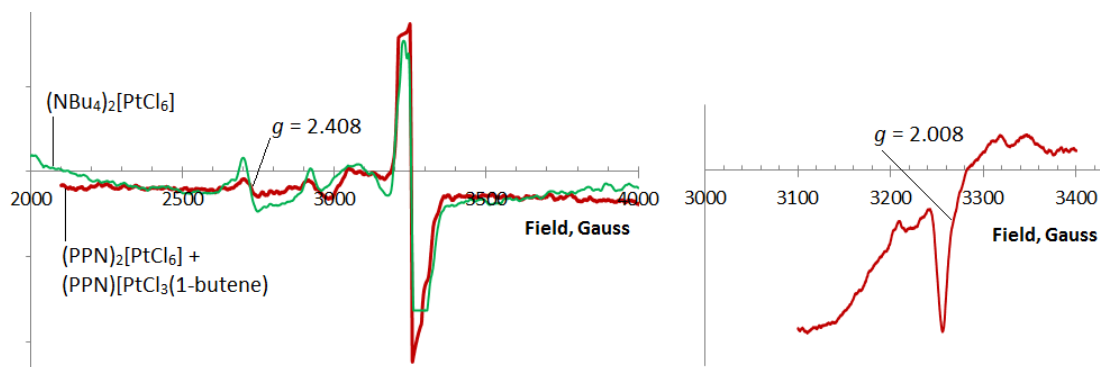


Figure 60: The EPR spectrum of the mixture of III.2 and $(\text{PPN})_2[\text{PtCl}_6]$ in dichloromethane at 120 K under the UV irradiation for 25 minutes, compared with the spectrum of $[\text{nBu}_4\text{N}]_2[\text{PtCl}_6]$ (left); expansion on the organic region (right).

2.2.2.9. Investigation of the role of $[\text{PtCl}_4]^{2-}$ in the activation of the $(\text{nBu}_4\text{N})^+$ cation

As shown in section 2.2.2.5, the $[\text{PtCl}_4]^{2-}$ signal in the ^{195}Pt -NMR spectra was immediately seen in the photolysis of $[\text{nBu}_4\text{N}]_2[\text{PtCl}_6]$. In acetone, the peak

appeared after the first 10 minute irradiation followed by the first appearance of olefin-platinum(II) chemical shift after 100 minutes of irradiation.

In the Shilov system, the role of $[\text{PtCl}_4]^{2-}$ as the catalyst in an alkane oxidation in the system of $\text{CH}_3\text{COOH}/\text{H}_2\text{O}$ is known along with $[\text{PtCl}_6]^{2-}$ as the oxidation agent to oxidize the Pt(II)-alkyl moiety to give a Pt(IV)-alkyl complex. The insertion of C–H into $[\text{PtCl}_4]^{2-}$ was proposed to proceed by the electrophilic C–H activation mechanism, although it is not entirely clear yet.²⁷ There is no report about photochemical C–H activation involving $[\text{PtCl}_4]^{2-}$. Therefore, experiments to investigate the role of $[\text{PtCl}_4]^{2-}$ were set, namely i) heating $[\text{nBu}_4\text{N}]_2[\text{PtCl}_4]$ only in acetone under the dark conditions; ii) heating $[\text{nBu}_4\text{N}]_2[\text{PtCl}_4]$ in acetone under ambient light; iii) irradiating $[\text{nBu}_4\text{N}]_2[\text{PtCl}_4]$ in acetone under UV ($\lambda > 305$ nm). The photolysis of $[\text{nBu}_4\text{N}]_2[\text{PtCl}_6]$ was repeated in the presence of $[\text{nBu}_4\text{N}]_2[\text{PtCl}_4]$ in various molar ratios to see the effect of initial Pt^{II} present in the reaction. The reactions were monitored using ^1H and $^{195}\text{Pt}\{^1\text{H}\}$ NMR spectroscopy. EPR spectra of the *in-situ* irradiation of $[\text{nBu}_4\text{N}]_2[\text{PtCl}_4]$ were also recorded.

Here are some observations that have been made; firstly, the product, **I** (2 mg, 1.5%) complex was isolated when $[\text{nBu}_4\text{N}]_2[\text{PtCl}_4]$ (188.7 mg) was heated under reflux in dry acetone (40 cm^3) for 48 h under ambient light. The yield was far lower than the product isolated from the reaction of $[\text{nBu}_4\text{N}]_2[\text{PtCl}_6]$ under the same conditions.

Secondly, when $[\text{nBu}_4\text{N}]_2[\text{PtCl}_4]$ in d_6 -acetone was irradiated ($\lambda > 305$ nm) and the reaction was followed by ^{195}Pt -NMR spectroscopy, the formation of resonances characteristic of olefin-platinum(II) complexes was observed after 17 h of irradiation. Signals in this area were seen at -2365 , -2437 and -2480 ppm. After 21 h irradiation, along with those three previous signals, a peak at -2575 ppm was also observed. The peaks at -2437 , -2480 and -2575 ppm were seen in the photoreaction mixture of $[\text{nBu}_4\text{N}]_2[\text{PtCl}_6]$. The signal for $[\text{PtCl}_6]^{2-}$ was not detected during the photolysis. Compared to photolysis of $[\text{nBu}_4\text{N}]_2[\text{PtCl}_6]$, the rate of the

formation of the olefin-platinum(II) complex shown by ^{195}Pt NMR spectra from the irradiation of $[\text{nBu}_4\text{N}]_2[\text{PtCl}_4]$ was much lower.

Thirdly, in the absence of light, using an amber-coated NMR Young's tube, $(\text{NBu}_4)_2[\text{PtCl}_4]$ was heated in d_6 -acetone but no change was observed in the amount of $[\text{PtCl}_4]^{2-}$ and signals corresponding to olefin-platinum(II) were also not seen. This observation was the same as that observed from $[\text{nBu}_4\text{N}]_2[\text{PtCl}_6]$ under the same thermal conditions.

The presence of $[\text{nBu}_4\text{N}]_2[\text{PtCl}_4]$ in the photoreactions of $[\text{nBu}_4\text{N}]_2[\text{PtCl}_6]$ in d_6 -acetone had no significant effect on the rate of $[\text{PtCl}_6]^{2-}$ depletion and the appearance time of the olefin-platinum(II) signal. Similar to the reaction of $[\text{nBu}_4\text{N}]_2[\text{PtCl}_6]$ only, about 56% of $[\text{PtCl}_6]^{2-}$ was converted after 40 minute irradiation and the olefin-Pt(II) chemical shift at -2487 ppm was seen after 100 to 120 minute irradiation. The graph showing the $[\text{nBu}_4\text{N}]_2[\text{PtCl}_6]$ decrease in the presence of $[\text{nBu}_4\text{N}]_2[\text{PtCl}_4]$ is given in Figure 61. When the reactions were repeated under heating for 48 h in the dark, the ^1H and $^{195}\text{Pt}\{^1\text{H}\}$ NMR spectra showed no formation of olefin-Pt(II) complexes while the amount of the Pt^{II} and Pt^{IV} complexes remained unchanged.

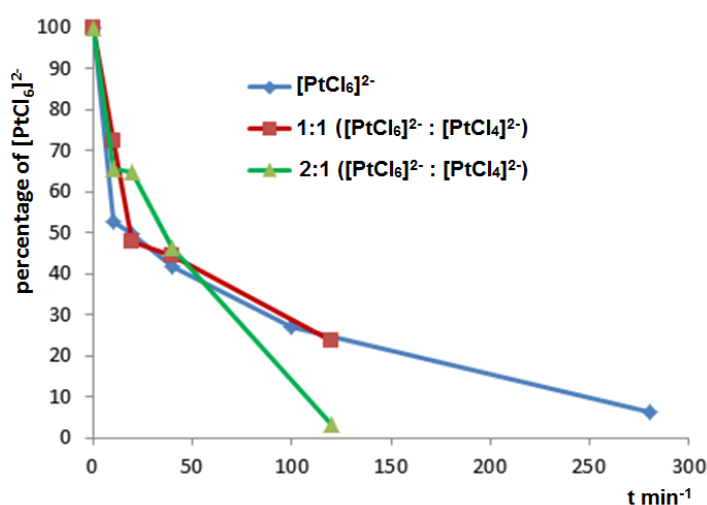


Figure 61: The percentage of $[\text{PtCl}_6]^{2-}$ recorded during photoreactions in variable moles of $[\text{PtCl}_4]^{2-}$.

The observation of even a small amount of Pt(II)-butadiene complex on irradiation of $[\text{Bu}_4\text{N}]_2[\text{PtCl}_4]$ was surprising given previous results that showed that the reaction required photochemical initiation in the presence of $[\text{PtCl}_6]^{2-}$. It was therefore decided to irradiate a frozen matrix of $[\text{Bu}_4\text{N}]_2[\text{PtCl}_4]$ in CH_2Cl_2 at 120 K in the cavity of an EPR spectrometer. The same conditions were used for the study of $[\text{Bu}_4\text{N}]_2[\text{PtCl}_6]$.

The spectrum obtained (Figure 62) shows a very small amount of an organic radical ($g = 2.013$) with no sign of a Pt-based signal. However, the presence of a small amount of a Pt-based radical is not ruled out entirely as, when compared with the spectrum obtained from irradiation of $[\text{Bu}_4\text{N}]_2[\text{PtCl}_6]$, the intensity of the platinum signal is much lower compared to the organic radical. Additionally, far-infrared spectroscopy revealed that there was a weak absorption at 326 cm^{-1} corresponding to $[\text{PtCl}_6]^{2-}$ in addition to a strong signal at 307 cm^{-1} contributed to a vibration band of E_u symmetry, $\nu_{\text{Pt-Cl}}$, corresponding with $[\text{PtCl}_4]^{2-}$.¹³⁶ It was, therefore, concluded that the small amount of Pt(II)-butadiene complex formed was due to a small contamination of $[\text{PtCl}_6]^{2-}$ in $[\text{PtCl}_4]^{2-}$.

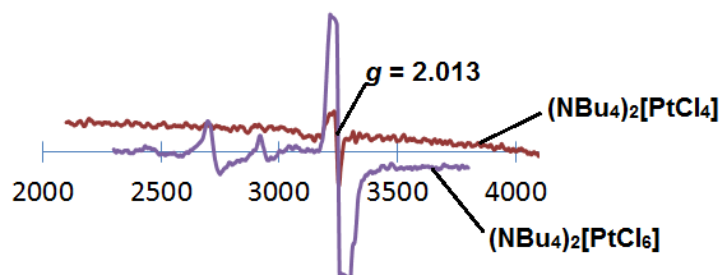


Figure 62: The photochemical *in-situ* EPR spectra of $[\text{Bu}_4\text{N}]_2[\text{PtCl}_4]$ in CH_2Cl_2 at 120 K compared to that of $[\text{Bu}_4\text{N}]_2[\text{PtCl}_6]$

2.3. Discussion

This project has its origin in the observation that reaction of $[\text{}^n\text{Bu}_4\text{N}]_2[\text{PtCl}_4]$ with $[\text{}^n\text{Bu}_4\text{N}][\text{AuCl}_4]$ led to the formation of $[\text{}^n\text{Bu}_4\text{N}]_2[\text{Cl}_3\text{Pt}(\eta^2:\eta'^2\text{-CH}_2=\text{CH}-\text{CH}=\text{CH}_2)\text{PtCl}_3]$, **I**. Further investigation showed that the role of the $[\text{AuCl}_4]^-$ was an oxidant to give $[\text{PtCl}_6]^{2-}$ and then that the product arose from the reaction of $[\text{PtCl}_6]^{2-}$ with $(\text{}^n\text{Bu}_4\text{N})^+$.

Thus, reaction of $[\text{}^n\text{Bu}_4\text{N}]_2[\text{PtCl}_6]$ in acetone and dichloromethane under reflux led to conversion to **I**, with slightly greater yields being obtained in acetone. $^{195}\text{Pt}\{^1\text{H}\}$ NMR spectroscopy identified Pt^{II} -alkene complexes in the reaction solution as well as formation of $[\text{PtCl}_4]^{2-}$. That the reaction proceeded in dichloromethane ruled out acetone as the source of carbon for the butadiene ligand showing unequivocally that it arose from a decomposition of the tetrabutylammonium cation. That the reaction proceeded driven by Pt^{IV} suggested consideration of so-called Shilov chemistry, since C–H bond activation had been reported in a series of papers by Shul'pin and Shilov mediated by Pt^{IV} , sometimes in conjunction with Pt^{II} .^{1, 75} However, in attempting to follow the process on one occasion by NMR spectroscopy, no reaction was observed, which was eventually explained by the fact that there is no ambient light in the probe of the spectrometer; this implied a photochemical mechanism. This suggestion was confirmed both by carrying out the reaction under direct UV illumination where isolated yields in excess of 65% could be obtained after 18 hours of irradiation, and by carrying out the reaction strictly in the absence of light, where no reaction took place.

Being a photochemically driven process, it is necessary first to understand the nature of the excited state and possible subsequent reactions. Calculations by Shafikov¹³⁷ showed two excited states based on absorptions at 324 nm and 207 nm. In the case of the higher-energy state, calculations showed a LMLCT excited state, where electron density from two *trans* chlorides to the four remaining chloride ligands *via* the metal, whereas the lower-energy state also showed a

LMLCT but from four co-planar chlorides to the two remaining chloride ligands. TDDFT calculations also demonstrated an elongation of Pt–Cl bonds along the z-axis in the relaxed excited state of $[\text{PtCl}_6]^{2-}$ along with an increase in electron density compared to its ground state that may contribute to an increase of the basicity of the complex. Calculations of the reactivity of the excited states by Kaufman *et al.*,¹²⁴ then proposed that from the lower-energy state, a chloride anion was ejected to give $[\text{Pt}^{\text{IV}}\text{Cl}_5]^-$, which was still energetically excited and so reacted further to give $[\text{Pt}^{\text{III}}\text{Cl}_4]^-$ and Cl^\bullet . All of these latter calculations were performed in the gas phase.

The postulation by theory of the formation of Pt^{III} was supported experimentally by EPR experiments conducted in a frozen matrix of $(\text{NBu}_4)_2[\text{PtCl}_6]$, whereupon irradiation led to the formation of a Pt-based radical ($g = 2.402$)^{78, 126} and an N-based radical ($g = 2.001$).¹²⁵

Carrying out the reaction using a $(^n\text{Bu}_4\text{P})^+$ cation showed no reaction and only (from ^{195}Pt NMR spectroscopy) the formation of $[\text{PtCl}_4]^{2-}$. Similarly, using a $(\text{PPN})^+$ cation, the reaction caused the formation of $[\text{PtCl}_4]^{2-}$ shown by ^{195}Pt NMR spectroscopy and also the generation of Pt^{III} detected by EPR spectroscopy. However, reaction did occur using the $(^n\text{Pr}_4\text{N})^+$ and $(^n\text{Pe}_4\text{N})^+$ counter cations. In the former case, with no possibility for a second activation, no alkene- Pt^{II} complexes were identified as products and indeed it was possible to find $[\text{Pt}_2\text{Cl}_6]^{2-}$ was a product showing total loss of alkene coordination. However, with $(^n\text{Pe}_4\text{N})^+$, alkene- Pt^{II} complexes were again formed, although they proved resistant to isolation and it was not readily possible to identify the complexes formed by ^1H NMR spectroscopy, given the variety of different isomers possible.

Changing cation from $(\text{R}_4\text{N})^+$ ($\text{R} = ^n\text{Pr}, ^n\text{Bu}, ^n\text{Pe}$) to $(^n\text{Bu}_4\text{P})^+$ seemed to affect reactivity of the alkyls. The alkyls in particular the carbon directly bound to the nitrogen experience an effect of the electronwithdrawing influence of the cationic nitrogen, whereas in alkylphosphonium cations, the alkyl feels less strong effect of

the electronwithdrawing as phosphor atom is larger than nitrogen thus having lower charge density and so less electronwithdrawing effect.¹³⁷ The effect perhaps contributes to less reactive of tetrabutylphosphonium cation than tetraalkylammonium cations upon the photolysis implying the important role and so the requirement of ammonium cation for the activation.

A need for ammonium cation led the Hofmann elimination to be taken into account and as discussed previously in Results section, if the pathway is involved, a step to eliminate an alkene should be taken place prior to a further step to form a diene. The resulted alkene could coordinate to reduced Pt^{II} and to test the involvement of the pathway, [PtCl₃(alkene)]⁻ (alkene = 1-butene or 2-butene) that assumed as the product of the first step was irradiated under various conditions. In both conditions, the absence and the presence of [PtCl₆]²⁻, [PtCl₃(alkenes)]⁻ were not the source of complex I. However, in a reaction mixture of [ⁿBu₄N]₂[PtCl₆] photolysis, a compound, butenyltributylammonium where the butene coordinating Pt^{II} (**I.A**) was identified by employing NMR spectroscopy, mass spectrometry and photodissociation spectroscopy. The compound is proposed to be an intermediate that is apperent still containing the ammonium cation in which Hofmann elimination perhaps can evacuate to eliminate butadiene then give the product, **I.1**.

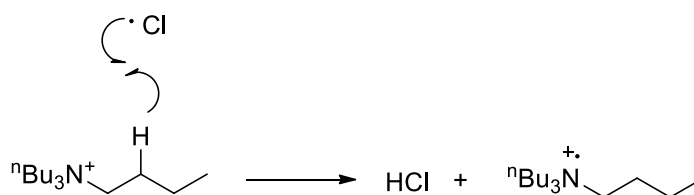
An instaneous formation of [PtCl₄]²⁻ in irradiation of [ⁿBu₄N]₂[PtCl₆] was considered to participate in an activation of tetraalkylammonium cations, however experimental investigations demonstrate [PtCl₄]²⁻ to be photochemically inert and thermally unreactive with tetrabutylammonium cation. This observation rules out the possible role in the activation of tetraalkylammonium cations and so does the Shilov pathway.²³

Bringing these observations together, the following mechanistic pathway is proposed (Scheme 62), based both on this evidence, the various pieces of

experimental observation, plus the precedent from Hofmann elimination reactions and Shilov chemistry.

It is therefore assumed that photoexcitation results in the formation of $[\text{PtCl}_5]^-$ that still retains excited state energy and is predisposed to formation of Pt^{III} . This would involve a homolytic fission of a Pt–Cl bond and, as the fission progresses and Pt^{III} forms, then Jahn-Teller distortion would be expected from the low-spin d^7 complex, lengthening the Pt–Cl bond further. This fragment is believed to play the key role in the activation of alkylammonium.

There are two ways of thinking of how excited-state species may be involved in the activation. Firstly, considering the high electron density of the *trans* Pt–Cl bonds along the z-axis,¹³⁷ it could be that the Cl^- generated is quite basic so that H^+ can be removed from C–H bond of the alkylammonium cation (Scheme 62, step **1i**). Secondly, having evidence of formation of Pt^{III} and *N*-based radicals, supported by the theoretical work of Kaufman *et al.*,¹²⁴ a radical-induced activation of the C–H bond may be proposed (Scheme 62, step **1ii**). Those two possibilities are open to further investigation. The *N*-based radical perhaps is a resulted fragment from Cl^\bullet radical which abstracting a proton in tetrabutylammonium cation (Scheme 61).



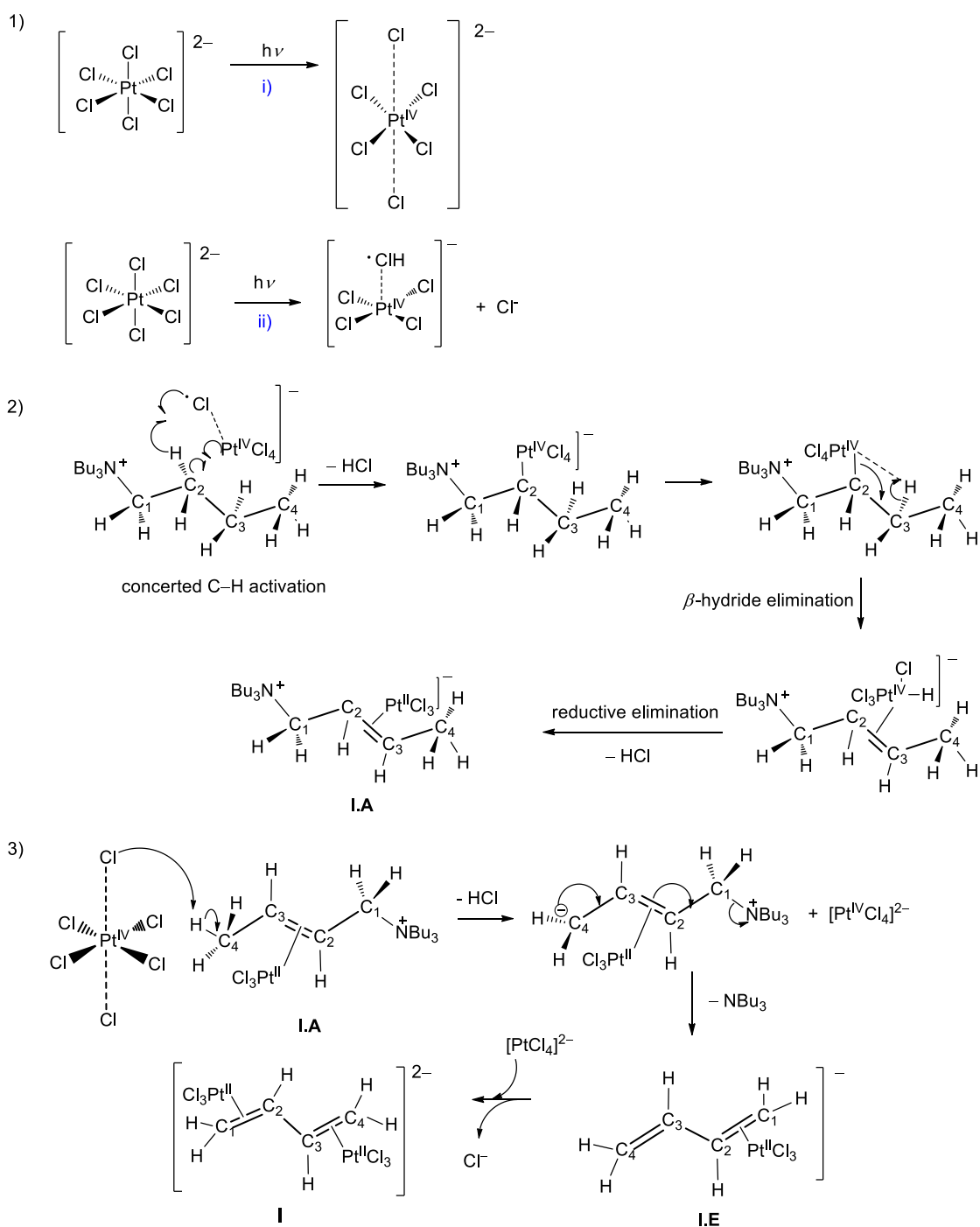
Scheme 61: The proposed reaction to form the *N*-based radical in irradiation of $[\text{nBu}_4\text{N}]_2[\text{PtCl}_6]$

The reaction is then proposed to occur *via* two parts. In the first activation (Scheme 62, step **2**) a concerted movement of single electrons is proposed as the excited state interacts with the $(\text{nBu}_4\text{N})^+$ cation that has the effect of eliminating HCl and forming a Pt–carbon bond, leaving a complex that is formally Pt^{IV} . Although written as a concerted mechanism, it could equally be envisaged as Cl^\bullet abstracting H^\bullet from the butyl group and the carbon-based radical that forms then

reacting with the Pt^{III} centre to give the σ -bonded complex. From this σ -complex, β -hydride elimination followed by reductive elimination of HCl leads smoothly to a η^2 -alkene complex. It is postulated that the alkene remains bound to the quaternary nitrogen centre (**I.A**), both because there is evidence for such complexes in photodissociation spectroscopy and also because [PtCl₃(alkene)]⁻ (alkene = 1-butene or 2-butene) prepared separately did not react with further [PtCl₆]²⁻ under illumination.

It is, therefore, then tempting to propose an analogous reaction to give a second C–H activation, but the problem with this is that once the σ -bonded Pt^{IV} species is formed, there is no way to move the electrons to eliminate the NBU₃ group.

Therefore, the second C–H activation is proposed to follow the pathway where the active species demonstrates its basicity deprotonating C₄ to give a carbanion and followed by elimination of HCl (Scheme 62, step **3**). Movement of electrons then allows NBU₃ to become a leaving group to give the second alkene at C₄ (**I.E**). This is all consistent with the accepted base-induced Hofmann elimination mechanism.⁶ Furthermore, as it has been presented earlier that the photoactivation of [PtCl₆]²⁻ results in [PtCl₄]²⁻ as shown in the photodissociation spectroscopy experiments, and to complete the reaction the formed [PtCl₄]²⁻ easily coordinates to the resulting alkene to give the butadiene-platinum(II) product (**I**).



Scheme 62: A proposed mechanism of photochemical activation of tetrabutylammonium cation by hexachloroplatinate(IV) complex.

Evidently, it is perhaps less elegant to propose two steps operating by a different mechanism, but this appears necessary as radical initiation can lead to double bond formation without loss of NBU_3 , while the base-induced reaction can generate the free alkenes as observed in the product. This mechanism may not be

correct in every detail, but it does have the advantage of accounting for the formation of the product and as such is at least worthy of some consideration.

2.4. Conclusion

It is then clear that irradiation of hexachloroplatinate(IV) complex in the presence of the tetrabutylammonium cation leads to the formation of $\eta^2:\eta^2$ -1,3-butadiene-bis(trichloroplatinate(II)) demonstrating generation of an active platinum species that facilitates activation of the tetrabutylammonium cation. Investigations suggest that the excited state of hexachloroplatinate(IV) likely drives the activation *via* a concerted mechanism in which chlorine radical and platinum(III) are inserted concertedly into the C–H bond. It is proposed that this happens in the first step of activation. However, this approach is unlikely occur in the last step where the final product is formed so that it is proposed that the basic property of the excited state may play the role, thus allowing the elimination of tributylamine by Hofmann elimination. Indeed, further investigations are expected to gain more mechanistic insight.

Chapter Three: Synthesis, the Liquid-crystalline and the Luminescence Properties of Polycatenar-diphenylpyridine Complexes of Palladium(II)

3.1. Introduction to Emissive Metallomesogens

Metallomesogens are metal complexes that possess liquid-crystalline properties.¹³⁸ Liquid crystals represent the fourth state of matter in addition to the three better known states of matter, which are gases, liquids and solids. The liquid crystal state lies between the solid and the liquid in accordance to position and orientation of molecules in the state, so that while molecules in the solid state are in positional and/or orientational order and in the liquid state, molecules are fluid and isotropic. Liquid crystals combine the fluidity of liquids and the positional order in solids which means that liquid crystals are fluid while the molecules are ordered giving anisotropic properties.^{139, 140}

Metal insertion into liquid crystals can be expected to provide new or enhanced properties of the materials such as luminescence, polarisability, dielectric response, paramagnetism, colour, viscosity and phase type that lead to new effects and applications.¹³⁸ Emissive, liquid-crystalline materials may have application in polarised organic light-emitting diode (OLED) devices.^{141, 142}

This section contains a short introduction of liquid crystals followed by a discussion of examples of emissive and mesomorphic complexes, in particular platinum(II) and palladium(II) complexes.

3.1.1 Liquid Crystals

Reinitzer first recognised the liquid crystal state in 1888 when measuring the melting point of cholesteryl benzoate. He observed that the compound melted at 150 °C forming a turbid fluid that stayed until 178 °C when the turbidity disappeared and the liquid turned clear. The behaviour was also observed on

cooling showing the reversibility. In fact, the turbid state is a liquid crystal state which later was identified as a cholesteric or chiral nematic phase.

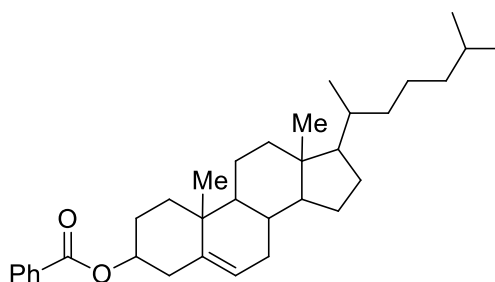


Figure 63: The structure of cholesteryl benzoate.¹³⁸

Initial identification of mesophases used polarised optical microscopy in which as a function of temperature, characteristic textures representing phases are observed as a result of birefringence. The mesophases temperature and types then are confirmed and assigned by utilisation of differential scanning calorimetry (DSC) and low-angle X-ray scattering in the mesophase.¹⁴³

Liquid crystals can be classified into two types based on the way phases form, namely lyotropic and thermotropic. Transitions in lyotropic liquid crystals are driven by solvent, while phase transitions in thermotropic liquid crystals are driven by temperature in the absence of solvent. In this section, only thermotropic liquid crystals will be discussed.

3.1.1.1 Thermotropic Liquid Crystals

Liquid-crystalline molecules can be of different shapes leading to different types of phases. Based on the molecular shapes, thermotropic mesogens may be classified within three types, namely calamitic, discotic and bent-core liquid crystals.

a. Calamitic Mesogens

Calamitic liquid crystals refer to compounds with a molecular shape of a rod where one molecular axis is much longer than the other two. A general molecular structure of the calamitic mesogens is drawn in Figure 64. The molecule is

structurally built with normally at least three rings connected either directly or by linking group(s) (**B**) with terminal groups (**A** and **C**) which can be identical or different; sometimes attached with a lateral group (**D**). The ring structures are a core that will maintain rigidity and the rod-like shape of the molecule and can be phenyl, alicyclic, heterocyclic or polycyclic. The linking groups conserve the overall anisotropy of the system, for example $-\text{CH}=\text{CH}-$, $-\text{C}\equiv\text{C}-$, $-\text{CH}=\text{N}-$, $-\text{N}=\text{N}-$, $-\text{CO}_2-$, but not necessary the conjugation. The terminal groups are usually alkyl or alkyloxy chains which generally increase anisotropy and decrease melting point of materials. It is important that the molecule is structurally anisotropic which will contribute to anisotropic intermolecular dispersion forces stabilising the mesophases.¹³⁹

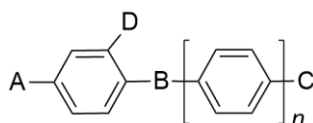


Figure 64: A general molecular structure of calamitic mesogens.¹³⁸

Calamitic mesogens exhibit phases in accordance with how molecules arrange themselves. A nematic phase, abbreviated N, is the simplest phase and is very fluid thus it is the most disordered as described in Figure 65. On average, molecules point in one direction but without positional orientation thus it is said there is a one-dimensional order which is only the orientation. An enantiomer or a racemic mixture or a mixture of enantiomers with one in excess or non-chiral compound but doped with a chiral material can exhibit a chiral nematic phase which is labeled with N* (Figure 66). The example of the phase is cholesteryl benzoate.

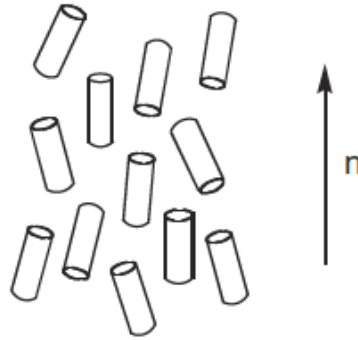


Figure 65: A picture of molecular arrangement in nematic phase.⁵⁹

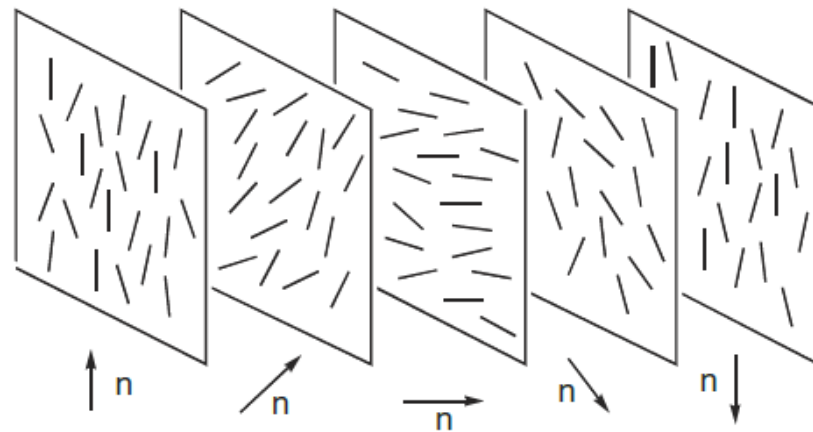


Figure 66: A diagram of the chiral nematic phase.⁵⁹

A smectic phase has some orientational and positional order exhibiting some arrangement of molecules into layers (partial translational order). The common smectic phases are smectic A (SmA), smectic B (SmB), smectic C (SmC), smectic F (SmF), and smectic I (SmI) (Figure 67). The smectic A phase is the least ordered among the smectic phases; orientational order exists along with partial translational order; the molecules point in a direction perpendicular to the layer planes. A modification of the molecules so that the orientation of the molecules is tilted creates the smectic C phase. Similar to the SmA, the order of the layers is also weak and both phases are very fluid so the molecules can move by up to 20° from the normal direction. If a smectic A phase is modified so there is in-layer hexagonal symmetry, then a smectic B phase is formed, the degree of positional order is higher compare to SmA and SmC. The smectic F is related to SmB with the

molecules tilted towards the 'vertex' of the hexagon whereas in the SmI phase, the molecules are tilted towards the 'edge' of the hexagon.¹³⁹

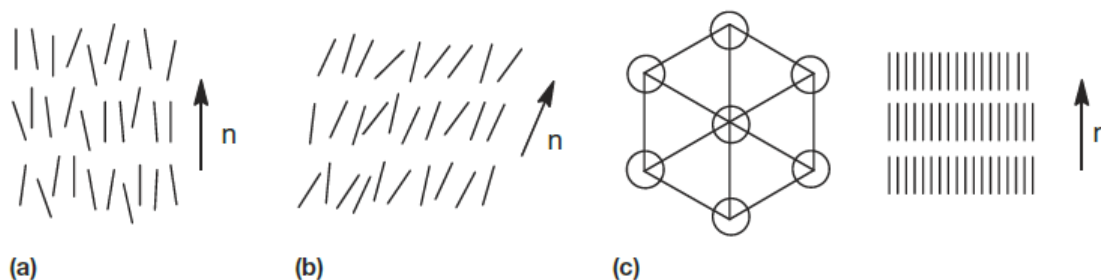


Figure 67: Diagrams of a) Smectic A, b) Smectic C, and c) Smectic B (viewed from above and from the side) phases.⁵⁹

b. Discotic Mesogens

In contrast to the rod-like shape, discotic liquid crystals consist of molecules with disc-like shape where one molecular axis is much shorter than the other two. The first experimental observation establishing the discotic mesogens, which is considered as the birth of discotic liquid crystals, is credited to Sadashiva and Chandrasekhar in 1977.¹⁴⁴ The study involved observations of benzene-hexa-*n*-alkanoates, which showed columnar phases.¹⁴⁵ The general structure of molecules that form the discotic mesogens consists of a flat core, which is often aromatic, with five or more alkyl chains on the periphery (Figure 68).

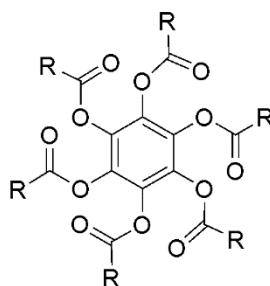


Figure 68: A general structure of *disc*-like mesogens.⁵⁹

The most common phases shown by disc-like molecules are the columnar phases in which the molecules stack into columns arranged relative to one another as shown in Figure 69.¹³⁹

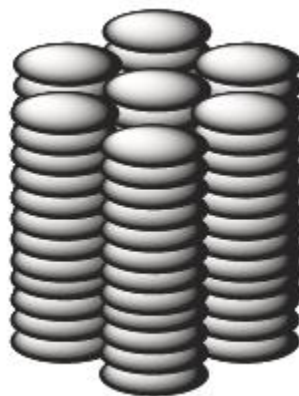


Figure 69: A diagram of the columnar phase.⁵⁹

3.1.1.2 Polycatenar Mesogens

Polycatenar mesogens consist of an elongated molecular core (normally at least four rings) with three or more terminal chains which may be disposed symmetrically or unsymmetrically. Tricatenar compounds tend to show nematic and SmC phases, while penta- and hexa-catenar compounds show columnar phases. Tetracatenar compounds are often of particular interest as shorter-chain homologues normally show N and/or SmC phases while longer-chain homologues show columnar phases.¹⁴⁶⁻¹⁴⁸

As positions of chains can vary, polycatenar mesogens can possess isomers. For example, tetracatenar mesogens can be made where alkyl or alkyloxy chains are symmetrically bound at the 3,4-positions of the terminal rings or at 3,5- positions, or unsymmetrically 3,4- at one end and 3,5- at the other (Figure 70). Likewise, the hexacatenar, pentacatenar and tricatenar can be found in a variety of isomers.

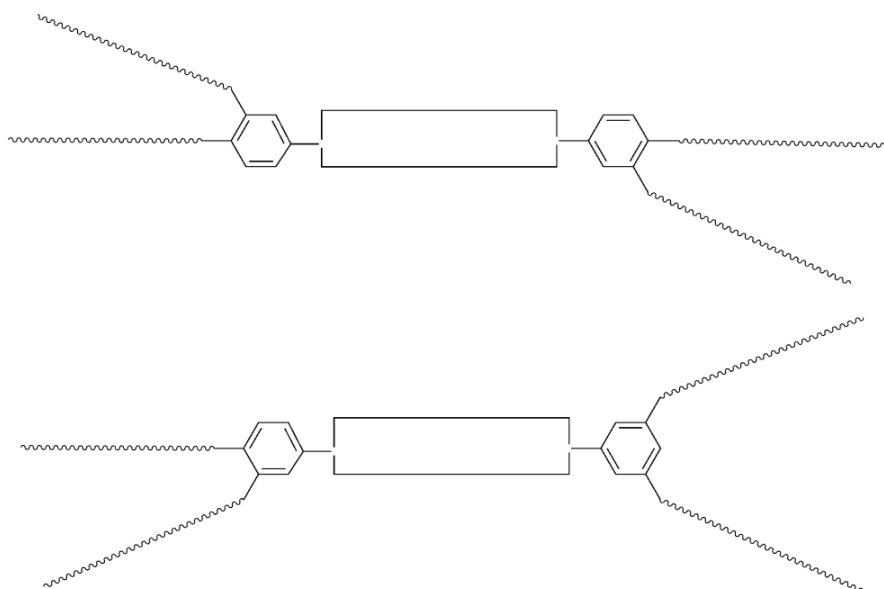
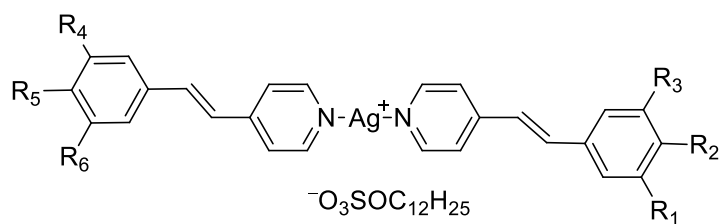


Figure 70: The description of tetracatenar mesogen in (A) symmetrical system and (B) unsymmetrical system.

Insertion of metals into mesogens contributes to an enrichment of the mesomorphism and a development of advantages and applications of liquid crystals. Bruce *et al.* have studied the mesomorphism of polycatenar stilbazole ligands which complexed with metals such as silver(I), palladium(II), platinum(II) and iridium(III).¹³⁹ Some of the metallomesogens were reported to demonstrate luminescence properties in addition to liquid-crystalline properties.¹⁴⁹⁻¹⁵³

Introduction of silver(I) led to symmetrical polycatenar mesogens with dialkoxystilbazoles ligands (**73**) giving an ionic liquid-crystalline material with a counter anion. The anion was counted as a lateral group, affecting the mesomorphism of the compound. The length and the number of the terminal chains affect the exhibited mesophases. The two-chain mesogens bearing short terminal chains exhibit nematic and smectic C phases, while an extension of the length contributes to an alteration of the phases to be columnar. For intermediate length chains, a cubic phase was formed between the SmC and columnar phases. The tetracatenar silver mesogens with short to intermediate terminal chains ($n = 6 - 10$) displayed cubic and columnar mesophases while the mesogens possessing longer chains ($n = 12$) showed the columnar phase only; no smectic phase was

detected. The hexacatenar-silver mesogens exhibit the columnar phase over the whole length range of the terminal chains.¹⁴⁶



73 (1): $R_2, R_5 = \text{OC}_n\text{H}_{2n+1}$; $R_1, R_3, R_4, R_6 = \text{H}$

73 (2): $R_1, R_2, R_4, R_5 = \text{OC}_n\text{H}_{2n+1}$; $R_3, R_6 = \text{H}$

73 (3): $R_1, R_2, R_3, R_4, R_5, R_6 = \text{OC}_n\text{H}_{2n+1}$

Figure 71: Molecular structure of silver(I) complex of the symmetrical polycatenar-alkoxystilbazole.¹⁴⁶

Analogues tetracatenar palladium mesogens (**74**) however exhibited SmC phase at shorter chain lengths, while at longer terminal chains, a columnar phase was displayed. The cubic phase was not observed and all the complexes showed only a single mesophase as shown in Figure 72.¹⁴⁶

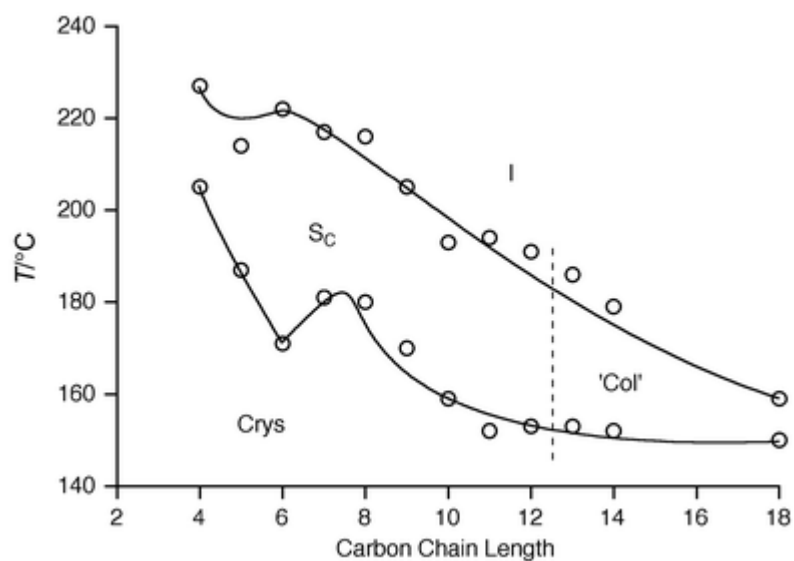
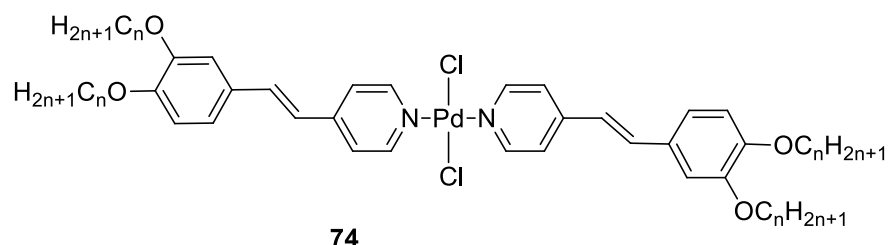


Figure 72: The molecular structure of the symmetrical polycatenar-palladium(II) mesogens (74).¹⁴⁶

The formation of the lamellar phase (SmC) in the tetracatenar mesogens is rationalised with two explanations. Firstly, nanophase separation drives formation of the lamellar phase where the aromatic cores tend to associate with each other and similarly the alkyl chains prefer to sit near one other. Secondly, there is a difference at interface between the area of the aromatic cores and of the alkyl chains, which can be accommodated by the cores tilting to form the smectic C phase as described in Figure 73.

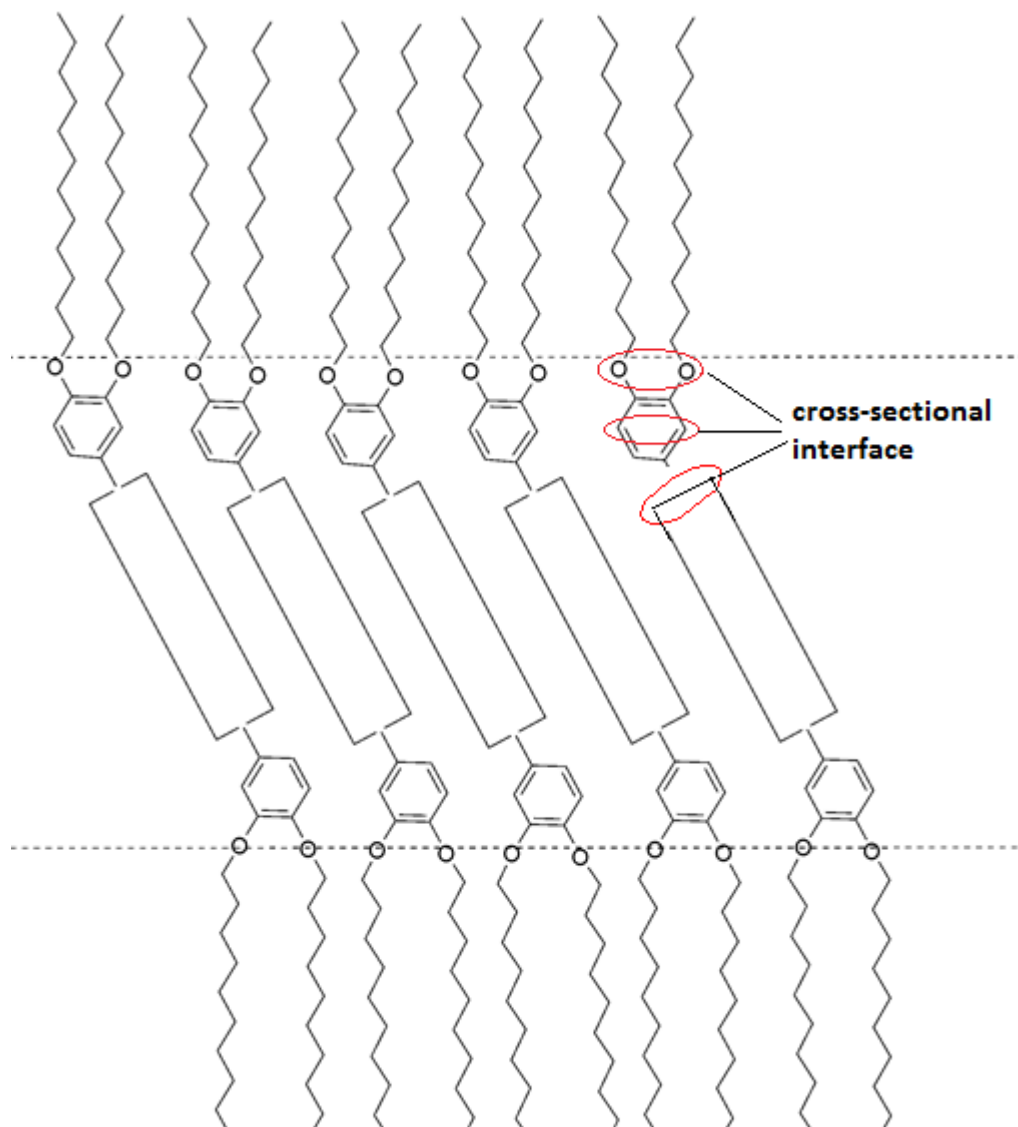


Figure 73: An illustration of the formation of SmC phase on the tetracatenar mesogens.¹⁴⁶

3.1.2. Emissive Metallomesogens of the Group 10 Elements (M = Pd^{II}, Pt^{II})

The group 10 elements are the most commonly found in metallomesogens^{138, 154} and among the metals, the square planar platinum(II) metal is the most attractive for reasons including an ability to tune the luminescence and a capability to form aggregations that originated from its natural ability to form metal-metal and metal-ligand bonds.¹⁵⁴ Cycloplatinated complexes are found to show high luminescence quantum yield in solution and have become one of the most attractive derivatives in OLED technology although in many cases, the

luminescence properties are exhibited in the absence of the liquid crystal properties and *vice versa*.^{154, 155}

Hegmann, *et al.*¹⁵⁶ reported mesomorphic and emissive cycloplatinated complexes of 2-phenylpyrimidines (**75**) and 2-phenylpyridines (**76**) with 1,3-diketonate co-ligands. Terminal chain lengths as well as their distribution affect the mesomorphism and the emission properties of the complexes. For instance, the complexes with short chains show smectic phases (SmA/SmC) or a nematic phase, while an extension of the chain led to formation of a Col_h phase with an enhancement of the phase stability. All the complexes demonstrate luminescence properties in solution as well as in the solid state as a result of d^8-d^8 interactions of the square-planar coordinated Pt(II) atoms. The analogous palladium complexes are mesomorphic but not emissive.¹⁵⁶

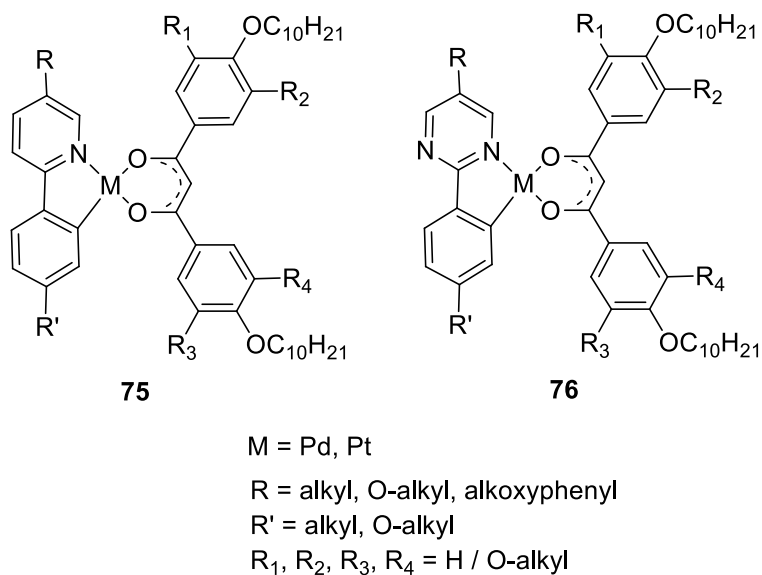


Figure 74: Molecular structure of the metallomesogens based on platinum and palladium metals synthesised by Hegmann *et al.*¹⁵⁶

Santoro, *et al.*¹⁵⁰ reported liquid-crystalline and emissive cycloplatinated complexes of diphenylpyridine ligands with ancillary acetylacetonate (acac) (**77**). While the ligands exhibit polymorphism, with many types of smectic phases, the complexes display a SmA mesophase. The complexes of diphenylpyridine ligands bearing a fused cyclopentene ring (**78**) showed the SmA mesophase only when $n =$

12. However, the complexes with shorter chains showed nematic phase ($n = 6$ and 8) or nematic and SmA phases for $n = 10$. The fused cyclopentene can be considered as a lateral substituent which commonly enhances the packing distance of molecules, thus minimising the possibility of forming lamellar mesophases, and in the system, it requires longer alkyl chains ($n \geq 12$) to induce smectic phases. All the complexes are luminescent in solution at room temperature as well as in thin films. In dichloromethane solutions, the complex of diphenylpyridine emits light at λ_{\max} 541 nm while the complex with the fused ring exhibits emission at λ_{\max} 523 nm, at the slightly higher energy caused by a steric effect of the *ortho*-CH₂ groups of the cyclopentene ring towards the planar structure contributing to the reduction of the conjugation between the rings. It was observed also that the introduction of an alkoxy chain lowers the emission energy with a shift of wavelength of about 36 nm due to the HOMO destabilisation resulting from an effect of the electron donating group, alkoxy, on the metal and/or cyclometallated ring system. The complexes are very brightly luminescent with emission lifetimes at room temperature of 27 μ s and the quantum yields are around 0.5 which is higher than that of [Pt(ppy)(acac)]. In films, intermolecular interactions such as face-to-face interactions, for square-planar platinum(II) complexes are introduced. These contribute to emission at higher wavelength. The complexes of diphenylpyridine exhibited a new emission peak at 600 nm at room temperature when at least 90% concentration of the complex was added in a film. The complexes containing the fused ring showed intermolecular interactions when the materials were heated to their clearing point.¹⁵⁰

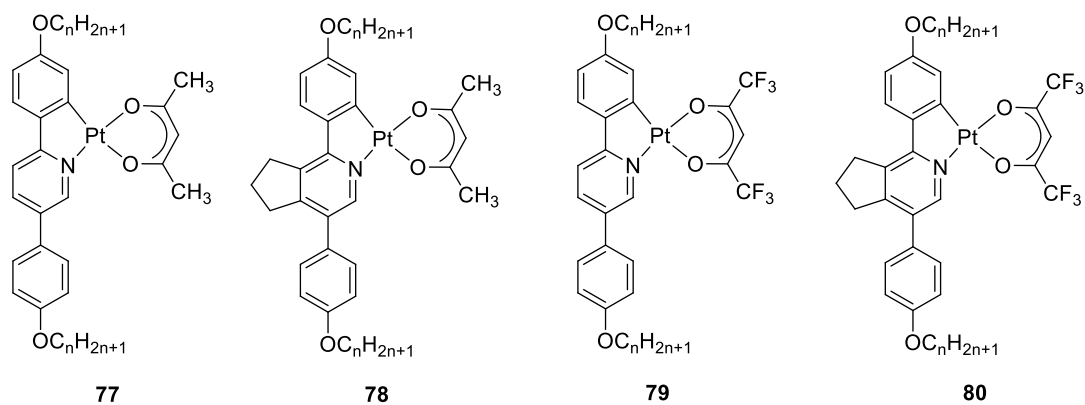


Figure 75: Molecular structures of the emissive metallomesogens of platinum(II) complexed with biphenylpyridine ligand derivatives.^{150, 157}

When the cycloplatinated complexes of diphenylpyridines contain hexafluorinated acac co-ligand (**79** and **80**), no mesomorphism and emission properties were exhibited. A theoretical study suggests that having two electron withdrawing substituent groups, CF_3 , alters the frontier orbitals in which LUMO is on the β -ketonate co-ligand instead of the phenylpyridine ligand. This lowers orbital overlap so emissions are absent.¹⁵⁷

Cycloplatinated complexes based on the 2-phenylpyridine and 2-(3-fluorophenyl)pyridine ligands (**81**) were reported to demonstrate polarised emission.¹⁵⁸ Similar to other cycloplatinated phenylpyridine derivatives, with $n = 12$, the metallomesogen exhibits a lamellar mesophase while substitution of H with F increases the phase stability. The complexes showed polarised emission at room temperature at 532 nm in their aligned polyimide films which open an opportunity for exploiting the compounds in display technology.¹⁵⁸

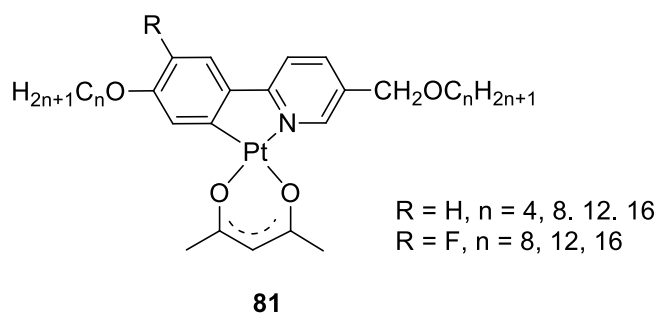


Figure 76: The molecular structure of polarised emissive platinum(II) mesogens on the basis of phenylpyridine ligand derivatives.¹⁵⁸

Metallomesogens based on 1,3-dipyridylbenzene, N[^]C[^]N-coordinated to platinum(II) (**82**), were prepared successfully by reacting K₂[PtCl₄] with the related ligands in acetic acid. The hexacatenar ligands are non-liquid crystalline but coordination to the platinum(II) induced mesomorphism giving a columnar phase. The phase (Col_r) was seen when the alkyl chain number (*n*) is six whereas the complexes bearing a fused cyclopentene ring displayed the mesophase when the alkyl chain is longer with *n* = 10 and 12. The complexes with the fused cyclopentene rings (**83**) require longer alkyl chains to exhibit the hexagonal columnar phase and the mesophase is more stable due to a steric contribution from the fused ring.¹⁴⁹

Both types of complex are luminescent at room temperature in dichloromethane solution demonstrating, the reproducing properties of the parent complex (**84**).¹⁵⁹ In thin films, prepared by spin coating at various concentration within a polycarbonate (PC) host, after heating the samples to the isotropic state then cooling slowly to the liquid crystal state, the mesophase emitted light at λ_{\max} 575 and 624 nm (orange). While in a glassy state, obtained by fast cooling of the isotropic phase, emission at λ_{\max} 660 nm (red) was found which arose from structured excimer-like through face-to-face Pt...Pt interactions attributed to MMLCT transitions. In dichloromethane solution, the complexes emitted light at λ_{\max} 556 nm (green).¹⁴⁹

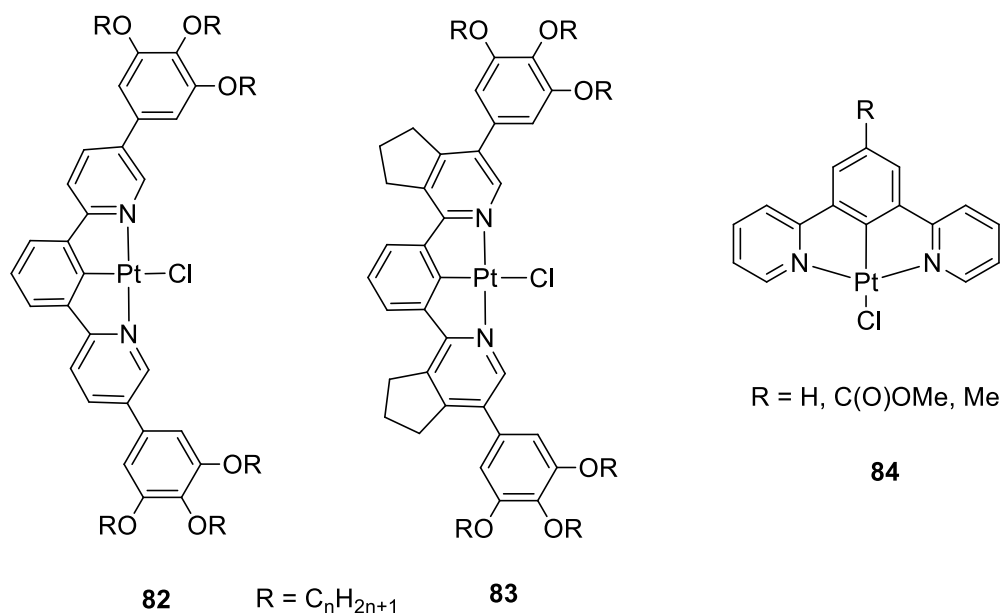


Figure 77: The molecular structure of emissive platinum(II) mesogens based on 1,3-dipyridylbenzene ligand derivatives (82, 83)¹⁴⁹ and the parent complex (84).¹⁵⁹

Platinum(II) complexes of pyridyl pyrazolate ligands substituted with tris-alkoxyphenyl terminal groups (**85**) were reported.¹⁶⁰ All the complexes demonstrated a columnar mesophase ($n = 4$ Col_r and Col_h; $n = 6, 8$ and 12 only Col_h) over a very wide range of temperatures. For example the complex with $n = 12$ exhibited a columnar phase from 68 to 320 °C. In dichloromethane solution, all the complexes showed green light emission at about 520 nm attributed to a phosphorescent emission originating from an MLCT transition in the band range of 380 – 500 nm. In thin films, the complexes displayed a lower energy emission in the red region (630 – 660 nm) arising from intermetallic interactions and metal/metal-to-ligand charge-transfer (MMLCT). In the film, the complex molecules are structurally allowed to undergo intermolecular interactions. This property is accommodated by the presence of the tris(alkoxy)phenyl groups.¹⁶⁰

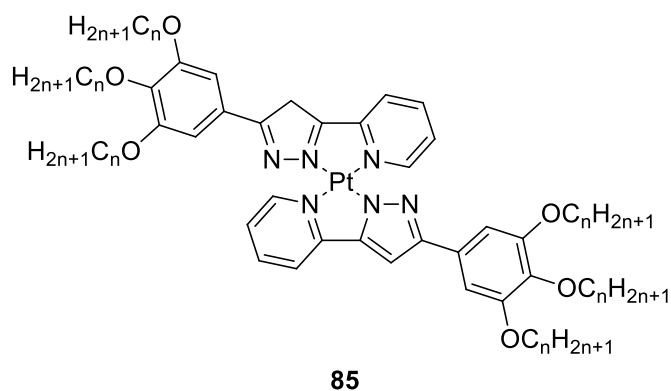
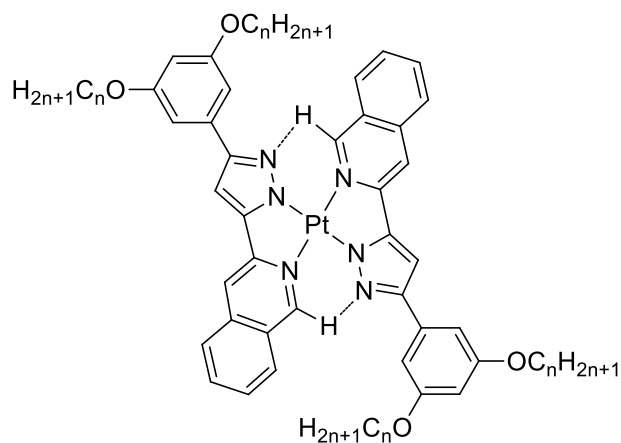


Figure 78: The molecular structure of emissive metallomesogens of the platinum(II) complexes of pyridyl pyrazolate ligands.¹⁶⁰

Similar platinum(II) complexes in which the pyrazole ligands functionalised with two-terminal-chain isoquinolines (**86**) were reported.¹⁶¹ In accordance with the properties of platinum(II) complexes of pyridyl pyrazolate derivatives,¹⁶⁰ the complexes exhibited columnar mesophases over a wide range of temperature as well as demonstrating phosphorescent emission in dichloromethane solution and in the solid state, with the emission originate from MMLCT transitions in the film. In addition, the luminescence is responsive to a variety of external stimuli, for example temperature, mechanical grinding, pressure, solvents and vapours.¹⁶¹ The luminescence can also be tuned by wetting the complex using various solvents. Different polarity of solvents changes the Pt...Pt stacking interactions, therefore they exhibit emission at different wavelength. For example in a polar solvent such as acetone, the emission is red-shifted by about 34 nm, from 622 nm in xylenes to 656 nm in acetone.¹⁶²

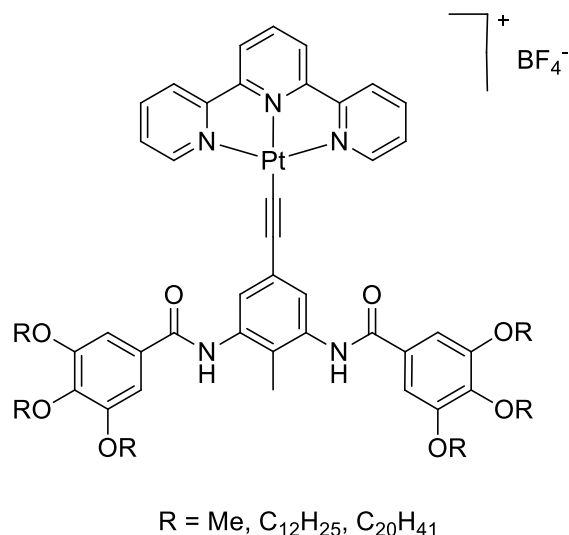


$$n = 4, 6, 8, 10, 12, 16, 18$$

86

Figure 79: The molecular structure of emissive metallomesogens of the platinum(II) complexes of isoquinoline pyrazolate ligands.¹⁶¹

Camerei¹⁶³ reported luminescent σ -alkynyl platinum(II) terpyridine complexes (**87**) exhibiting a Col_h mesophase at room temperature. The complexes are solvatochromic and potentially undergo gel formation. In polar solvents such as dichloromethane/methanol, the complexes showed a bathochromic shift of 16 nm, whereas in non-polar solvents such as dodecane in which the complexes formed a gel state, they exhibited a hypsochromic shift of 11 nm, attributed to the MMLCT transitions.¹⁶³



87

Figure 80: The molecular structure of the luminescent σ -alkynyl platinum(II) terpyridine complexes.¹⁶³

Complexes of palladium(II) also have the potential to be phosphorescent materials as the d^8 metal square-planar geometry. The heavy metal character enables the complex to exhibit spin-orbit coupling through intersystem crossing, populating the triplet excited state from the singlet excited state. The radiative decay from the triplet state to the ground state is slower than the decay from the excited singlet state to the ground state, characteristic of phosphorescence. The square-planar geometry may also facilitate the metal-metal interactions (MMLCT) that can contribute to the luminescence properties. However, in palladium(II) the lowest lying excited states of the Pd^{II} that are responsible for metal-to-ligand charge-transfer (MLCT) transitions can be deactivated by the higher-lying metal-centred states that favour a rapid, radiationless process.¹⁶⁴ This can limit the use of the palladium(II) complexes as phosphorescence emitters.

Although not as many as platinum(II) complexes, there are a few examples of palladium(II) complexes which possess liquid-crystalline and luminescence properties. The selection of ligands and design of molecular structures become important strategies to employ palladium(II). The strategy of ligand complexation *via* cyclometallation is also applied for palladium complexes.

Cyclopalladated complexes with Nile Red (9-diethylamino-5H-benzo[a]phenoxazine-5-one) with acac-like co-ligand, (4-hydroxy-3-methoxyphenyl)-1,6-heptadiene-3,5-dione (**89**) were reported.¹⁶⁵ The complexes exhibited a columnar mesophase over a broad range of temperature and showed emission at λ_{max} 640–660 nm in solution as well as in the solid state at room temperature. The emission properties are similar to simpler palladium(II) complexes of Nile Red (**88**) reported earlier by the same group¹⁶⁴ in which MLCT transitions were observed in addition to LC transitions. Although the complex **89** emits light over the longer wavelength, observations suggest the contribution originally from the chromophore Nile Red demonstrating that the ligands are unperturbed on coordination to palladium(II).¹⁶⁵

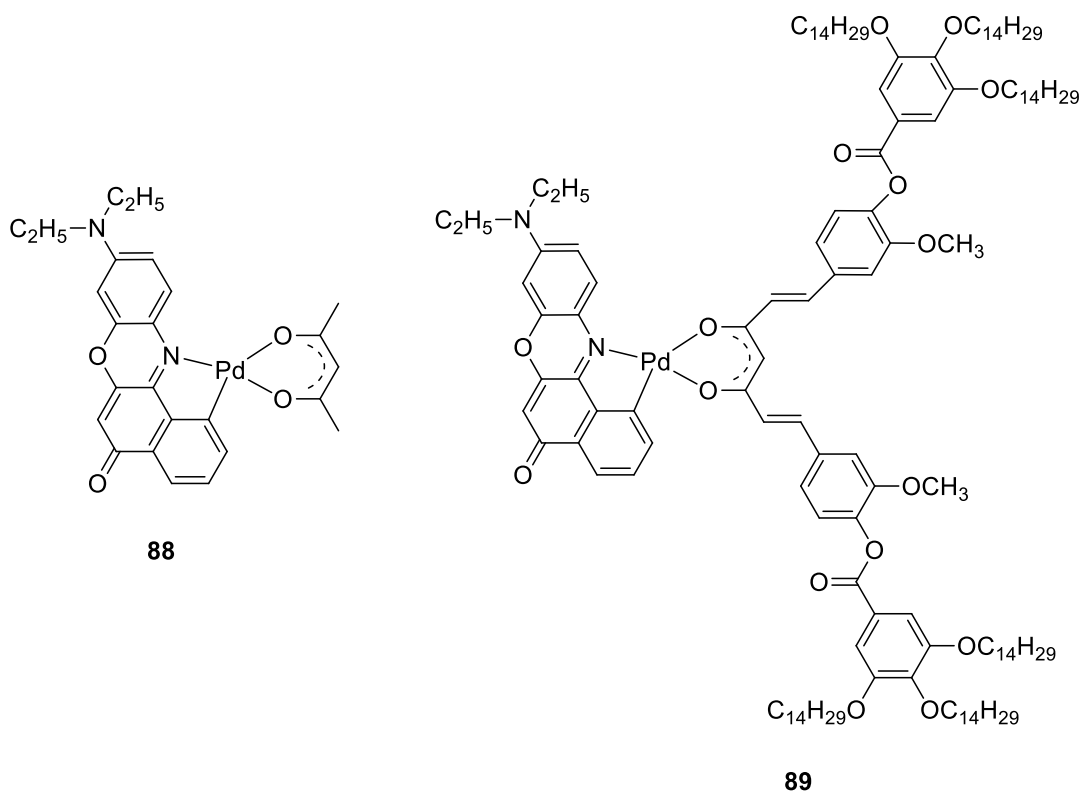


Figure 81: The molecular structure of the emissive metallomesogens of Nile-Red-palladium(II) derivatives.^{164, 165}

Allyl palladium(II) complexes with 1-pyridyl-3-pyridiniumyl-1,3-diketonate co-ligand (**90**) were reported.¹⁶⁶ Strategies to accommodate mesomorphism and luminescence properties were the introduction of long lateral chains, alkoxy, onto

the phenyl ring and insertion of a polar group such as pyridine in the co-ligand which was expected to increase the electron density of the diketonate core. Complex **90** exhibited an enantiotropic SmC mesophase between 158 – 170 °C and showed luminescence properties in dichloromethane solution at λ_{max} 492 nm which was slightly red-shifted in the solid state at λ_{max} 513 nm. However, similar to known palladium(II) complexes, the emission originates from LC transitions, both in the solution and in the solid state. The property remains preserved as a function of temperature so that in its mesophase, the complex still emitted light.¹⁶⁶

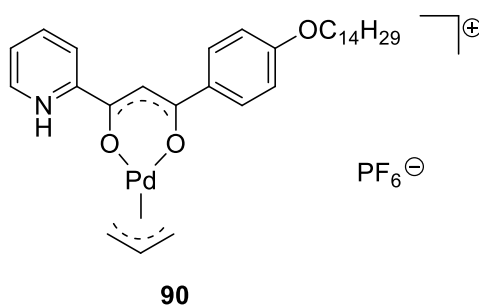
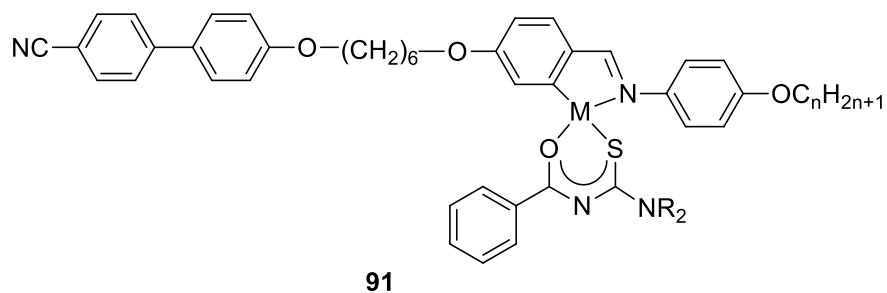


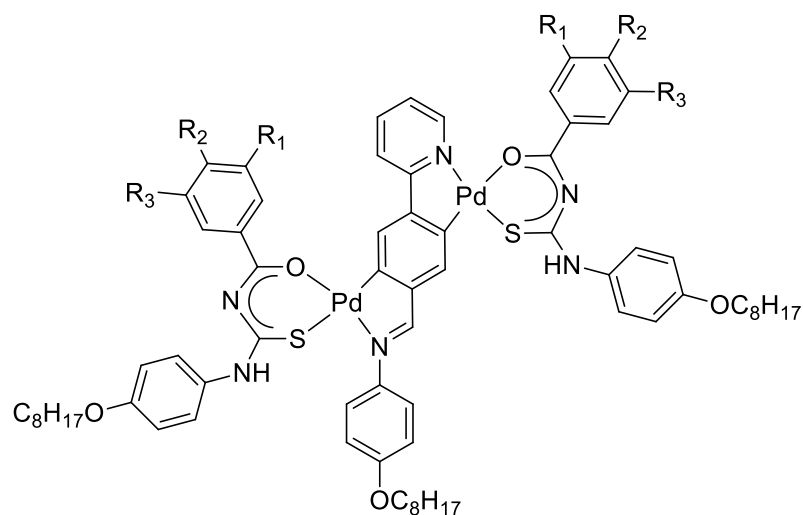
Figure 82: The molecular structure of emissive mesomorphic allyl-palladium(II) complexes with 1-pyridyl-3-pyridiniumyl-1,3-diketone co-ligand.¹⁶⁶

Cyclopalladated complexes of Schiff base ligands with the co-ligand, *N*-benzoyl thiourea (**91**), were reported to show mesomorphic behaviour but unlike the analogous cycloplatinated complexes, the palladium complexes are not luminescent.¹⁶⁷ However, a modification of the palladium(II) complex by double cyclopalladation (**92**) promotes emission properties. Similar to other current palladium(II) metallomesogens, absorption bands were seen at wavelengths less than 450 nm attributed to MLCT and LC transitions, while emission bands were observed at λ_{max} 410 and 470 nm attributed to intraligand transitions. In the solid state, however, the complex emitted light in the red region (660 – 685 nm and 725 – 745 nm) suggesting a contribution of excimeric $\pi\pi^*$ intraligand excited state; MMLCT is ruled out considering Pd...Pd interactions are unlikely as the shortest distance in the crystal lattice of the complex is 7.5 Å. The emission was still seen in a columnar mesophase although slightly red-shifted due to the columnar organisation in the phase.¹⁶⁸



M = Pd, Pt
 $n = 2-4, 6, 8$
 R = $-\text{CH}_3, \text{C}_{10}\text{H}_{21}$

Figure 83: The molecular structure of metallomesogens palladium(II) complexes of Schiff base ligands with co-ligand of *N*-benzoyl thiourea.¹⁶⁷



92 (1): $\text{R}_1 = \text{R}_3 = \text{H}; \text{R}_2 = 2\text{-ethylhexyloxy}$
92 (2): $\text{R}_1 = \text{R}_2 = -\text{OC}_{12}\text{H}_{25}; \text{R}_3 = \text{H}$
92 (3): $\text{R}_1 = \text{R}_2 = \text{R}_3 = -\text{OC}_{12}\text{H}_{25}$

Figure 84: The molecular structure of emissive and mesomorphic palladium(II) complexes of Schiff base ligands with co-ligand of *N*-benzoyl thiourea.¹⁶⁸

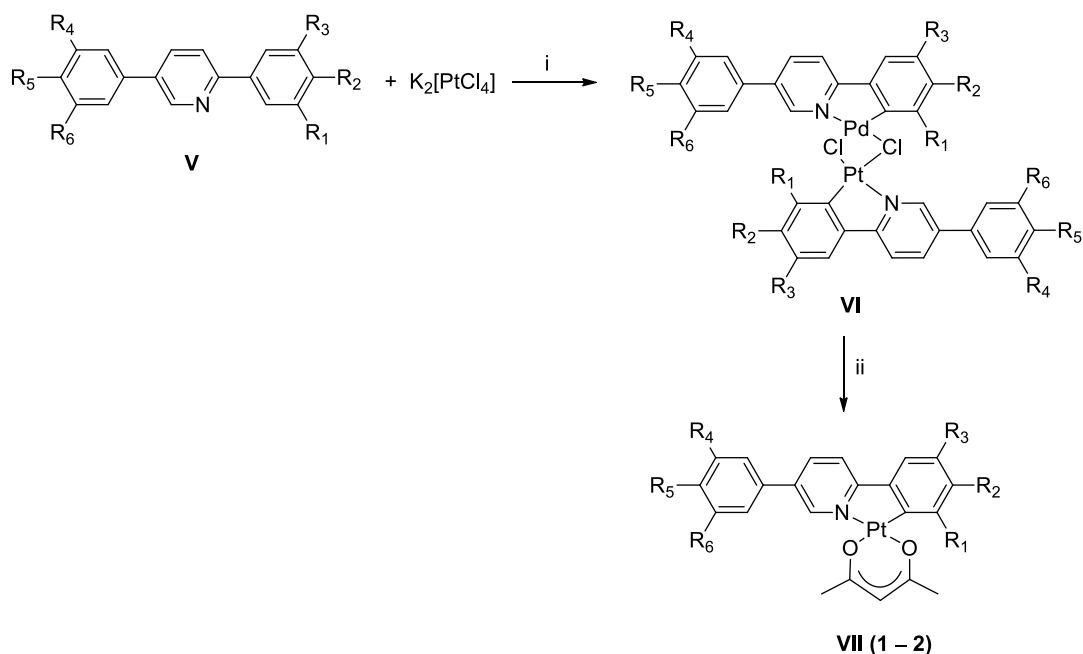
3.2. Results and Discussion

3.2.1. Introduction

The Bruce group at the University of York previously prepared emissive metallomesogens based mainly on platinum and iridium as discussed in

Section 3.1.2. The complexes were made *via* a cyclometallation strategy utilising N[^]C- and N[^]C[^]N-coordinating ligands and an acetylacetonato (acac) co-ligand. The approach accommodates the process of spin-orbit coupling which allows population of the triplet excited state (T₁) through intersystem crossing (ISC) from the excited single state (S₁), followed by the decay of the excited state to the ground state on the microsecond timescale with high quantum yield. Mesomorphism can be induced by employing terminal alkoxy chains attached to the ligand and/or co-ligand. Molecular shape and metal-core geometry are modified through ligand and co-ligand functionalisation, which also contribute to the mesomorphism and luminescence of materials.

In an attempt to vary the mesomorphism of the platinum(II) mesogens on the basis of complex **77**, a number of analogous polycatenar diphenylpyridine complexes of platinum(II) (Scheme 63) were prepared by Prokhorov.¹⁶⁹ The platinum(II) complexes of the symmetric tetracatenar ligand (**V (1)**) and a pentacatenar ligand (**V (2)**) were made successfully but when the synthesis was attempted using ligands with R₁, R₃ = OC₁₂H₂₅ (*i.e.* hexacatenar: R₁ to R₆ = –OC₁₂H₂₅O; pentacatenar: R₁ to R₃ and R₄ and R₅ = –OC₁₂H₂₅; tetracatenar: R₁ to R₃ and R₅ = –OC₁₂H₂₅), cleavage of the O – C bond of the alkoxy chain at the *ortho* and *para* positions with respect to the carbon atom coordinated to platinum(II) was observed. Ether cleavage is known to be catalysed by strong acid such as halogenated acid and sulfuric acid, but the cleavage process during the platinum complexation of the diphenylpyridines ligands was regioselective, suggesting an involvement of the platinum(II) centre.



VII (1): $R_2, R_3, R_4, R_5 = OC_{12}H_{25}; R_1, R_6 = H$

VII (2): $R_2, R_3, R_4, R_5, R_6 = OC_{12}H_{25}; R_1 = H$

Scheme 63: Preparation of the platinum(II)-acac complexes of the diphenylpyridine ligands by Prokhorov. Conditions: (vii) CH_3COOH , reflux, overnight; (viii) $K(acac) \cdot H_2O$, under reflux in: a. ethoxyethanol; b. $CHCl_3 / EtOH$.

It was decided to investigate the same chemistry using palladium(II) for several reasons. The properties of Pd(II) and Pt(II) are similar with both possessing a d^8 outer shell, thus their reactivity can be comparable although platinum(II) complexes are known to be kinetically more inert than their palladium(II) analogues.¹⁷⁰ Further, palladium(II) complexes have been reported to have liquid-crystalline and luminescence properties,^{164, 165, 168} therefore there is some interest in comparing the properties of complexes of the two metals. Generally, the strategies to drive the luminescence of the palladium(II) complexes are choices of ligands in which the ligands are sufficiently strong to raise the metal-centered state,¹⁷¹ for instance dipyridine derivatives;¹⁶⁸ or by incorporating chromophoric ligands like nile red derivatives (9-diethylamino-5H-benzophenoxazine-5-one).¹⁶⁵

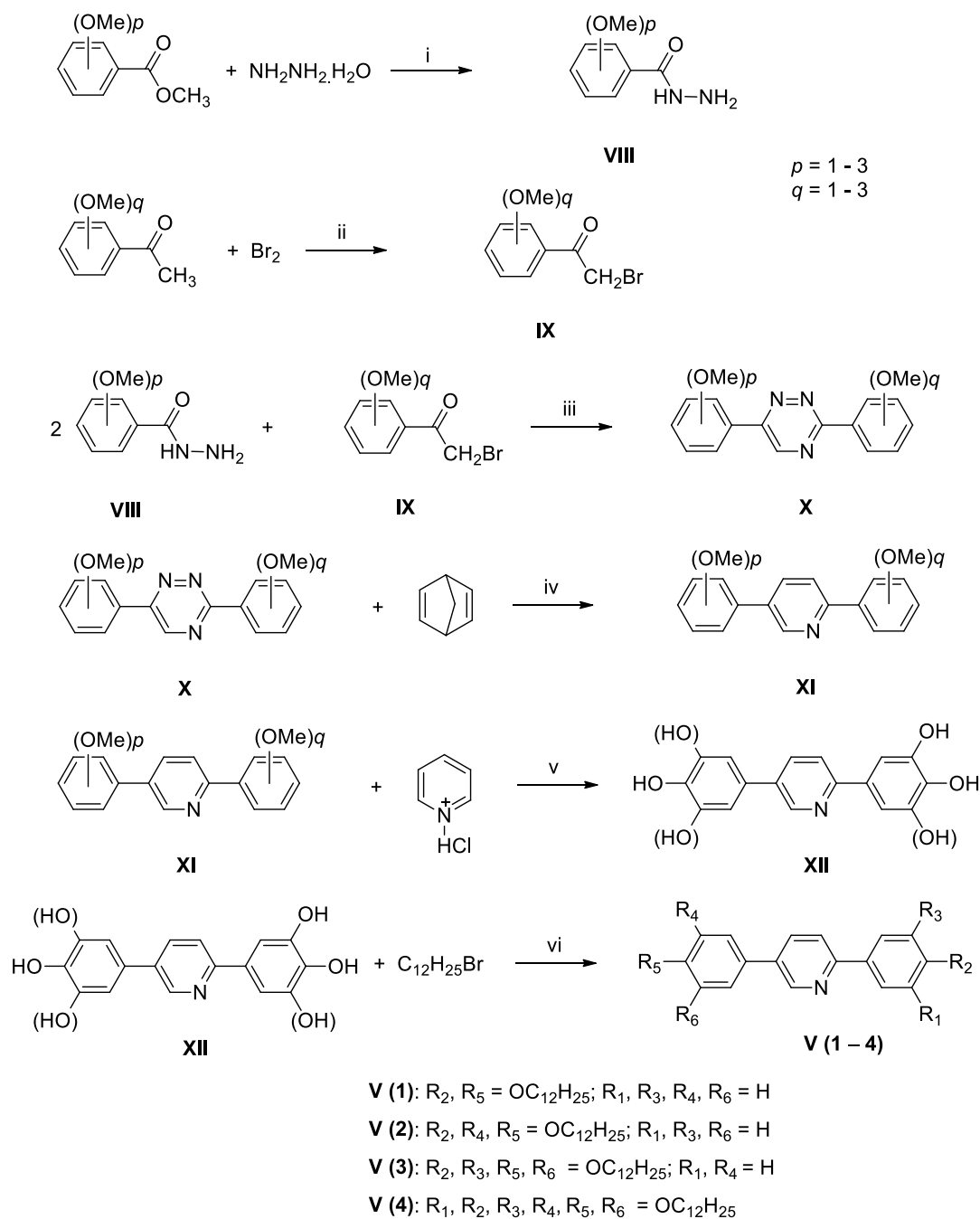
The objectives of this research are to synthesise and to study the liquid-crystalline properties as well as the possible photophysical response of polycatenar-diphenylpyridine-palladium(II) complexes.

3.2.2. Synthesis

3.2.2.1. Synthesis of Ligands

The ligands were prepared based on methods reported by Santoro *et al.*^{150, 172} The important step in the diphenylpyridine preparation is the synthesis of intermediate 1,2,4-triazine (**X**), the formation of a heterocyclic aromatic system. The aromatisation proceeds through a condensation reaction in the presence of a base. The triazine then is transformed into the related pyridine (**XI**) by a reverse Diels-Alder reaction. Three polycatenar-diphenylpyridine ligands (**V (2 -4)**) were made as shown in Scheme 64.

The 3,6-disubstituted triazines (**X**) were made by the condensation of bromo-acetophenones (**IX**) with two equivalents of acid benzohydrazide (**VIII**) in the presence of sodium acetate. The yield varied from 46% for 3-(3,4-dimethoxyphenyl)-6-(3,4-dimethoxyphenyl)-1,2,4-triazine to 61% for 3-(3,4-dimethoxyphenyl)-6-(3,4,5-trimethoxyphenyl)-1,2,4-triazine.¹⁷³ The pyridines (**XI**) were made from the reaction of the related triazines with norbornadiene with various yields from 44% for the hexacatenar pyridine to 82% (the highest) for the tricatener pyridine, and then were demethylated to hydroxyphenylpyridines (**28**). The ligands (**V**) were then obtained after alkylation of the hydroxyphenylpyridine with 1-bromododecane. The yield of the tricatener ligand (**V (2)**) was good at 73%, but on adding more chains, the yield decreased to only 59% for the hexacatenar ligand (**V (4)**). The ligands then were reacted with $(\text{NH}_4)_2[\text{PdCl}_4]$ and $\text{Na}(\text{acac})\cdot\text{H}_2\text{O}$ to produce the target complexes.

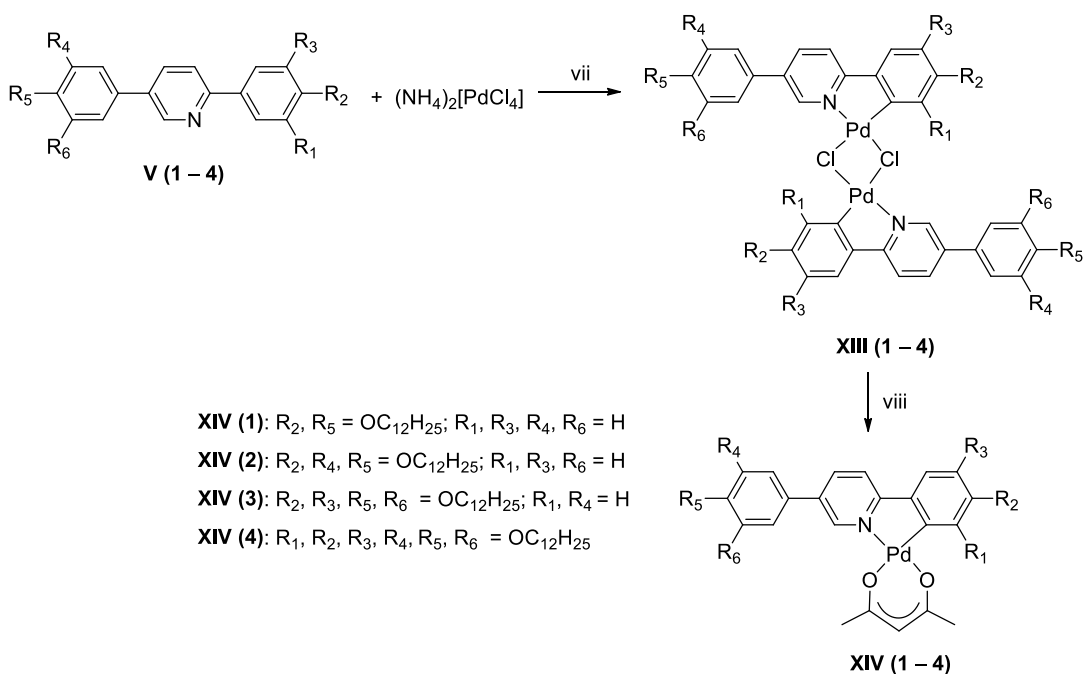


Scheme 64: Preparation of the polycatenar-diphenylpyridine ligands. Conditions: (i) MeOH, reflux, 17 h; (ii) Et₂O; (iii) NaHCO₃, EtOH/CH₃COOH, 120 °C, 7 h; (iv) *o*-xylene, 200 °C, overnight; (v) 200 °C, 5 h; (vi) DMF, K₂CO₃, 100 °C, 12 h.

3.2.2.2. Synthesis of the Polycatenar Palladium(II) Complexes.

The preparation of cyclopalladated complexes using a variety of conditions such as varying reagent, base, solvent, temperature and reaction time, has been reported

and reviewed.¹⁷⁴ In this research, the palladium(II) complexes with polycatenar-diphenylpyridine ligand and an acac co-ligand were prepared based on the general method employed in the Bruce group for the synthesis of analogous complexes of platinum(II). The synthesis consists of two steps: the formation of the metal dimer, **XIII**, followed by the reaction with acetylacetonate as described in Scheme 65.¹⁵⁰, 152, 153



Scheme 65: Preparation of the palladium-acac complexes of the diphenylpyridine ligands. Conditions: (vii) CH_3COOH , reflux, overnight; (viii) reagent: $\text{Na}(\text{acac}) \cdot \text{H}_2\text{O}$ in a. acetone, reflux; b. $\text{CHCl}_3 / \text{EtOH}$, reflux.

The ligands, **V**, were reacted with the metal precursor, $(\text{NH}_4)_2[\text{PdCl}_4]$ in AcOH to give the chloro-bridged dimers (**XIII**), which were soluble in chloroform and dichloromethane although the analogous platinum dimer was reported to have a poor solubility in organic solvents.¹⁵⁰ The ^1H NMR spectrum confirmed the cyclopalladation of the ligand at N atom and the C atom next to the nitrogen shown by the disappearance of the related proton signal at 7.51 ppm (Figure 86). The dimer can exist as a *trans* isomer where the N-C ligands coordinating to palladium(II) centre from the opposite side, and a *cis* isomer in which the ligands coordinate from the same side as shown in Figure 85. It is impossible to distinguish

those two conformers based on the ^1H NMR spectrum only; other NMR methods can be employed such as Nuclear Overhauser Effect (NOE) experiments in which spin-spin couplings can be observed through space rather than chemical bonds, but further separation as well as characterisation are not carried out as no matter which the isomer is, both will give the same target complexes.

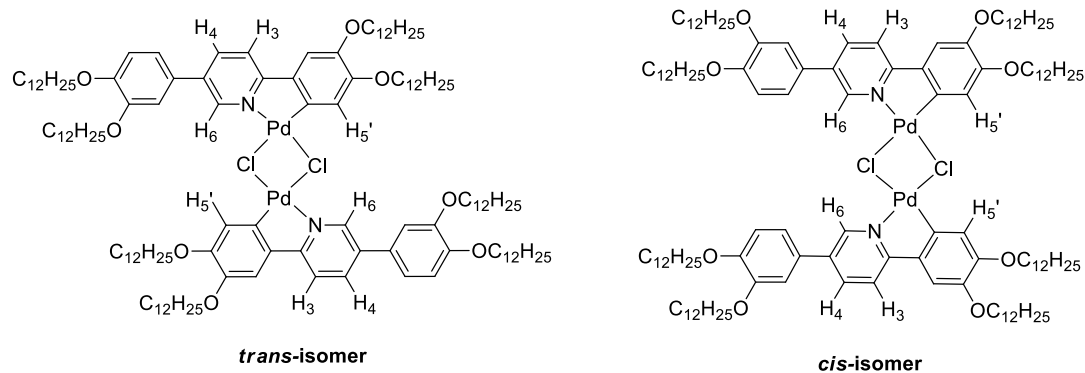


Figure 85: Possible molecular structure of dichloro-bridged-tetracatenar-palladium(II) complex.

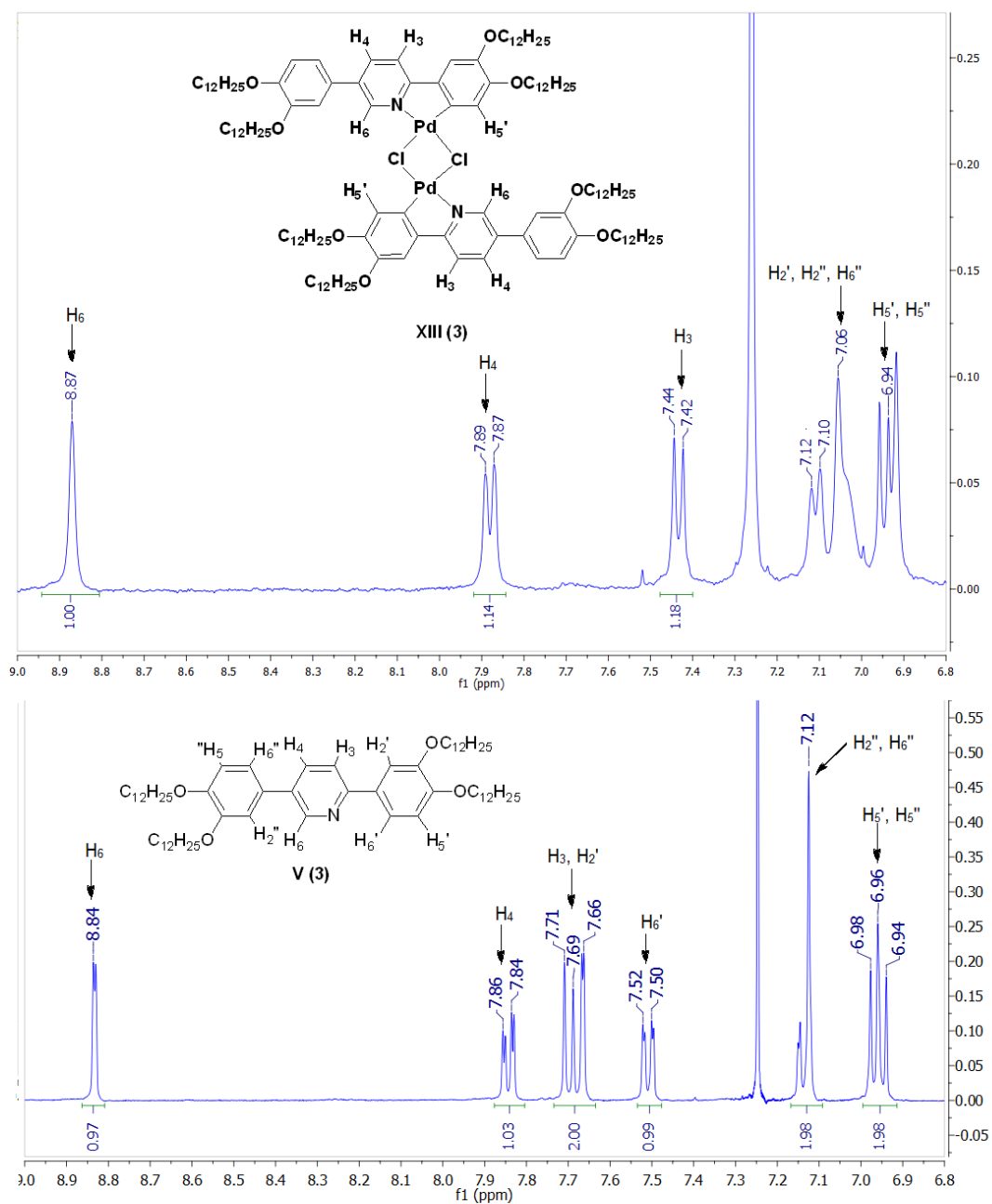


Figure 86: The ¹H-NMR (400 MHz) spectra of the tetracatenar-palladium(II) dimer complex (top) and the ligand (bottom) in the aromatic area.

The next step was the cleavage of the dimer and reaction with Na(acac).H₂O to give the target complex **XIV**. The complexes can be formed in the presence of Na(acac).H₂O,¹⁷⁵ but the conditions need to be adjusted depending on the electronic and steric properties of the ligands. The target complex containing the two-chained diphenylpyridine ligand (**XIV (1)**) was prepared by stirring the

corresponding dimer with sodium acac in chloroform/ethanol under reflux for five hours giving a yield of 55%, but the hexacatenar complex (**XIV (4)**) and the tricaténar complex (**XIV (2)**) required a slightly lower temperature so that the reaction proceeded on heating under reflux in acetone, albeit with a longer reaction time, although the yields were still not good at, 19% and 56% for the tricaténar and hexacatenar complexes, respectively. The tetracatenar-palladium(II) complex (**XIV (3)**) could be made using either set of conditions but the reaction at higher temperature (chloroform/ethanol) was more favourable giving higher yield (83%).

The complexes were characterised by using ^1H NMR spectroscopy and their purity confirmed by elemental analysis. The ^1H NMR spectrum of the tetracatenar palladium(II)-acac complex along with the spectrum of the ligand are shown in Figure 87. The resonances associated with the aromatic protons are similar to the related chemical shifts in the dimer, for which the main sign of complexation is the loss of the proton signal at the metallated carbon. The coordination of the acac co-ligand into palladium(II) was demonstrated by three new chemical environments belonging to the two terminal methyl groups and a CH proton. Two peaks at 2.03 and 2.09 ppm are assigned to two methyl resonances that are in different chemical environment due to the N[^]C coordination to the palladium. A signal at 5.39 ppm that integrates for one hydrogen is associated with the CH proton.

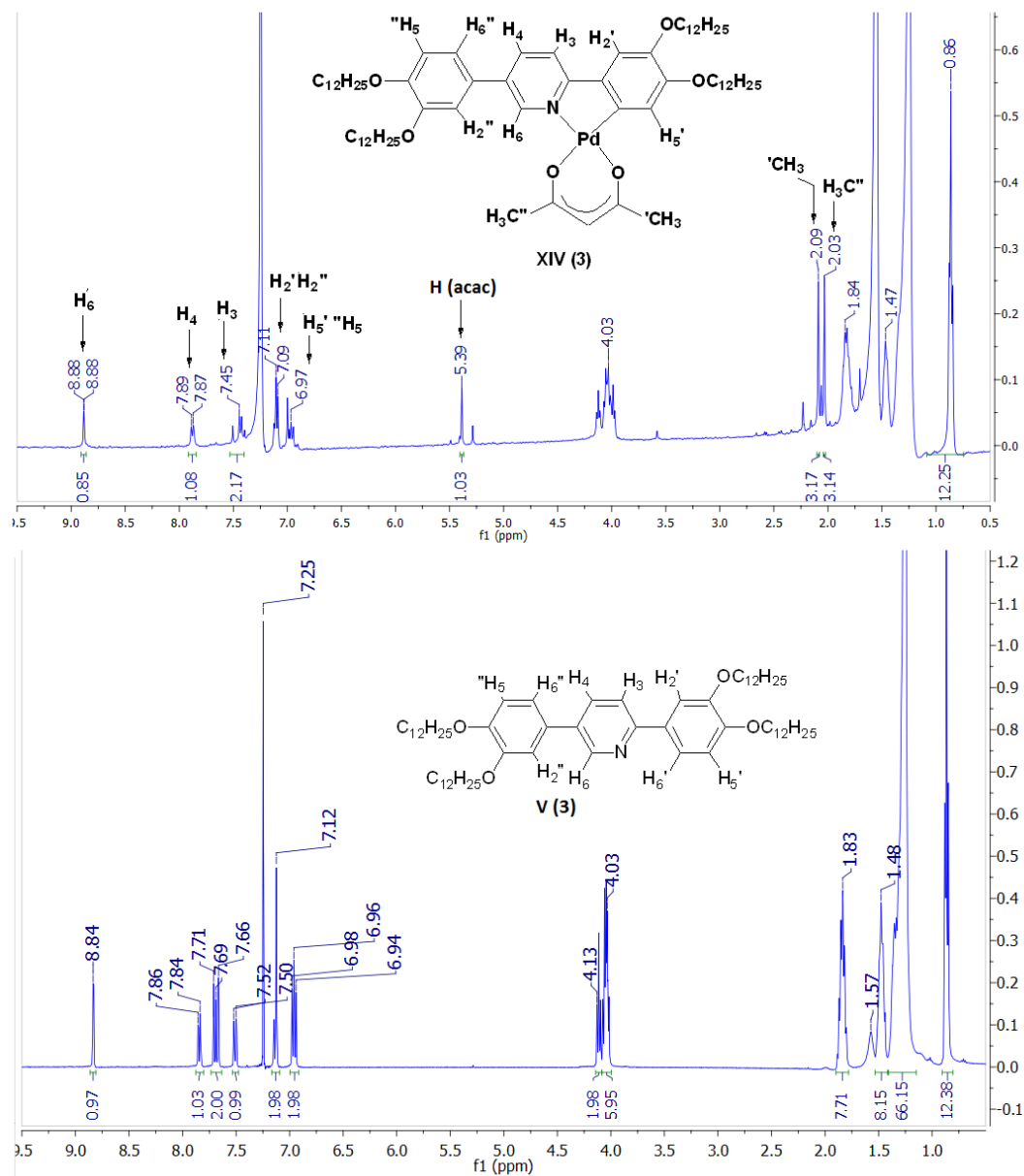


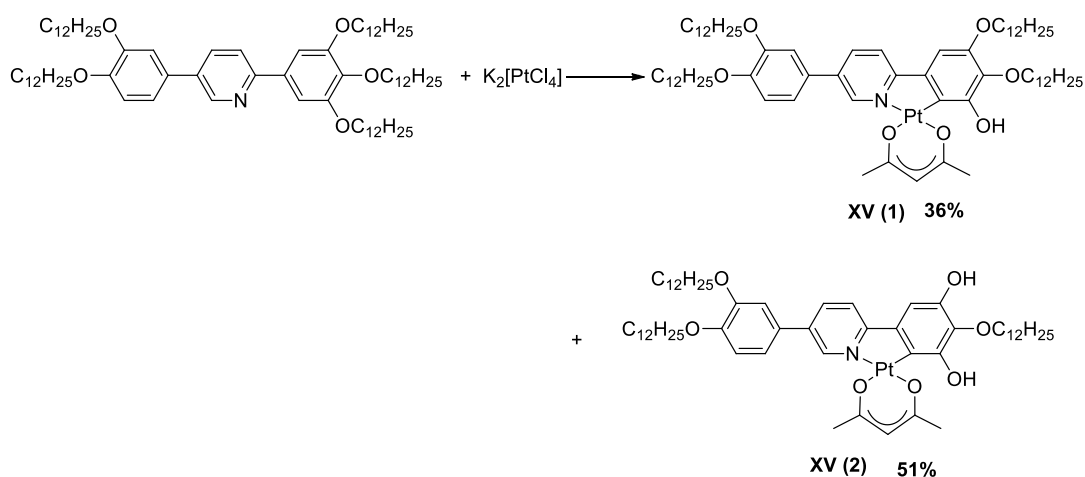
Figure 87: ¹H-NMR spectra (400 MHz) of tetracatenar-phenylpyridine-palladium(II) complex (top) and the ligand (bottom) in CDCl₃.

3.2.2.3. The Observation of Regioselective C–O Cleavage in the Platinum(II) Complexes of the Polycatenar-diphenylpyridine Ligand.

It is well-known that ethers undergo a C–O cleavage with strong acid and a nucleophile present to give alcohols and alkyl derivatives. The strong acid protonates the ether oxygen and the resulting OH⁺ becomes a better leaving group while the nucleophile attacks the carbon which activates the link making it

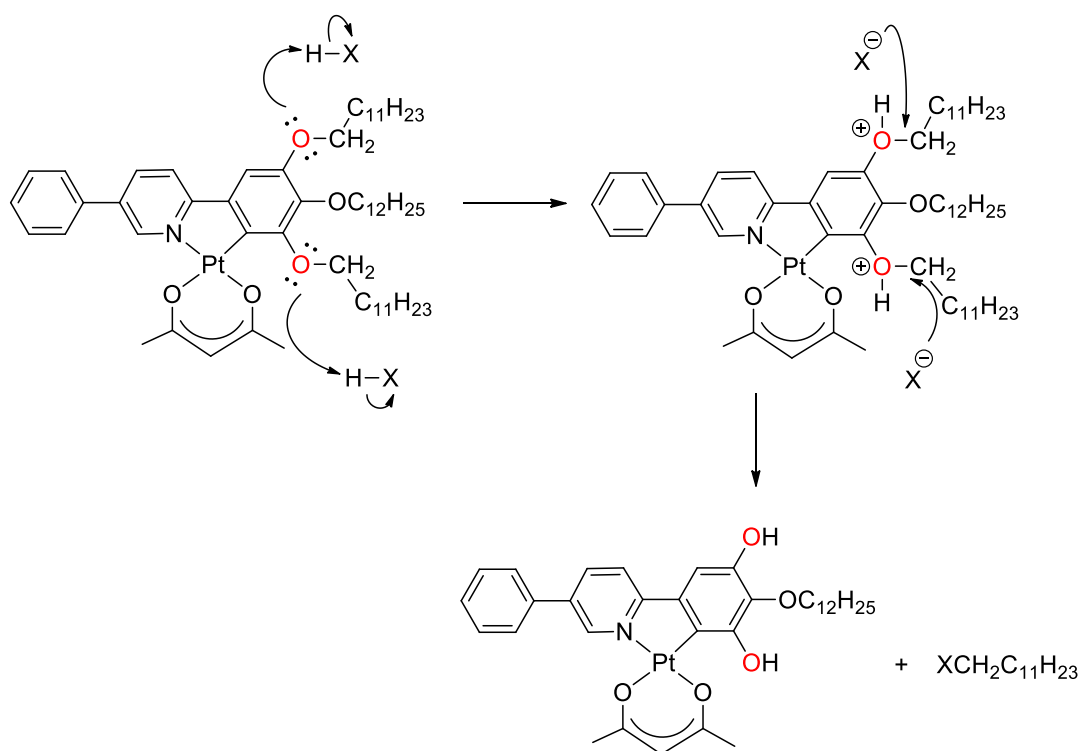
susceptible to cleavage.⁶ The successful reaction depends on the nucleophile, the acid and the nature of the ether (basicity of the ether). The reaction usually requires a strong nucleophile and an acid such as sulfuric acid or hydrohalic acid (HI, HCl, and HBr). Weak acids such as acetic acid, are usually not acidic enough to protonate ethers.¹⁷⁶

As mentioned earlier (Section 3.2.1), it had been shown previously that when the 2-(3,4,5-tridodecyloxyphenyl)-5(4-dodecyloxyphenyl)pyridine was reacted with potassium tetrachloroplatinate(IV) and potassium acac in acetic acid, dealkylation was observed in the orthoplatinated ring at the positions *ortho* and *para* to the metallated carbon (Scheme 66).



Scheme 66: The reaction of the phenyl pyridine ligands with $K_2[PtCl_4]$ leading to $-O-C$ bond cleavage observed by Prokhorov. Reaction conditions: reagent: $K(acac).H_2O$ in $CHCl_3$ / EtOH, under reflux.

The C–O cleavage proceeded selectively upon treatment with a mild acid (acetic acid) suggesting the important role of the platinum(II). Platinum atom is proposed to give an electronic effect through the phenyl ring which increases the basicity of the alkoxy groups at the *ortho* and *para* positions allowing protonation by the weak acid. The conjugated base then attacks the alkyl group resulting in the dealkylated complex. The proposed pathway of the C–O cleavage is shown in Scheme 67.



Scheme 67: The proposed pathway of ether cleavage occurred in the cycloplatination of the diphenylpyridines ligand in acetic acid.

The observation for the platinum(II) complexes was not found in the analogous palladium(II) complexes as in fact that the hexacatenar-palladium(II)-acac was obtained from a reaction of $[\text{PdCl}_4]^{2-}$ with the ligand implying the electronic stability of the alkoxy group in a presence of palladium metal.

3.2.3. Liquid Crystal Properties of the Ligands and Complexes

The thermal behaviour of the polycatenar diphenylpyridine ligands and the palladium(II) complexes was investigated by differential scanning calorimetry (DSC) thermal analysis and polarising optical microscopy (POM). The mesophases were identified under the microscope while the transition temperatures as well as the enthalpy changes were determined by using DSC. The thermal data are given in Table 10 for the ligands and in Table 11 for the complexes.

The two-chain ligand was reported previously to have SmI and SmC phases on cooling with a relatively high isotropic temperature at 200 °C.¹⁵⁰ The addition of

further chains seemed to suppress the mesomorphism as well as lower the melting temperature so that the tricatener ligand only showed a SmC phase identified by a Schlieren texture between 92 and 98 °C (Figure 88 a). Neither the tetracatenar ligand nor the hexacatenar ligand was mesomorphic, which is consistent with a 'rule of thumb' that the number of rings should be at least four and often equal to the number of terminal chains in order to observe mesomorphism.^{146, 148}

The palladation of **V (1)** and **V (2)** reduced the anisotropy altering the mesomorphism to a SmA phase identified by a focal conic fan texture and homeotropic regions (Figure 88 b). Complex **XIV (1)** exhibited a very wide range SmA phase that persisted for about 147 °C, while complex **XIV (2)** displayed the mesophase for only about 39 °C between 80 and 119 °C. Complexation of the ligands raised the isotropic temperature by about 11 °C, which is attributed to the introduction of the metal. The analogous platinum(II) complex with two-chains showed a larger increase in the isotropic temperature of 31 °C.¹⁵⁰

The symmetric tetracatenar ligand (**V (3)**) exhibited two crystal phases observed on cooling. The first crystal phase showed an onset at 106.6 °C from the isotropic state and lasted for about 39 °C, then transformed into the second crystal phase that remained until room temperature. The two crystal states can be distinguished under the microscope and by DSC. The isotropic temperature of **V (3)** was lower than that of **V (1)** due to the additional chains but it was slightly higher than that of the tricatener ligand (**V (2)**), most likely as it is more symmetrical. The palladium(II) complex of this ligand, **XIV (3)**, displayed no mesomorphism and simply melted to the isotropic state at 94.8 °C. The melting point of the complex was lower than that of the ligand, which was unusual.

The palladium(II) complex **XIV (4)** also showed no mesomorphism and melted at 44.4 °C. The six dodecyloxy tails in the ligand contributed to the low melting point and the introduction of the palladium(II)-acac evidently did not affect the thermal behaviour.

Table 10: Thermal behaviour of the ligands observed by POM and DSC.

Ligands	Transition	T ($^{\circ}\text{C}$)	ΔH (kJ mol^{-1})
V (1)	Cr-Sml	121.7	63.0
	Sml-SmC	171.6	2.4
	SmC-Iso	200.0	18.5
V (2)	Cr-SmC	92.19	35.0
	SmC-Iso	98.45	4.5
V (3)	Cr – Cr'	67.48	10.9
	Cr' – Iso	106.61	121.5
V (4)	Cr-Iso	43.30	66.4

Table 11: Thermal behaviour of the complexes observed by POM and DSC.

Compound	Transition	T ($^{\circ}\text{C}$)	ΔH (kJ mol^{-1})
XIV (1)	Cr-SmA	64.19	1.9
	SmA-Iso	211.32	7.4
XIV (2)	Cr-SmA	80.46	4.6
	SmA-Iso	118.87	0.5
XIV (3)	Cr-Iso	94.77	47.9
XIV (4)	Cr-Iso	44.42	70.3

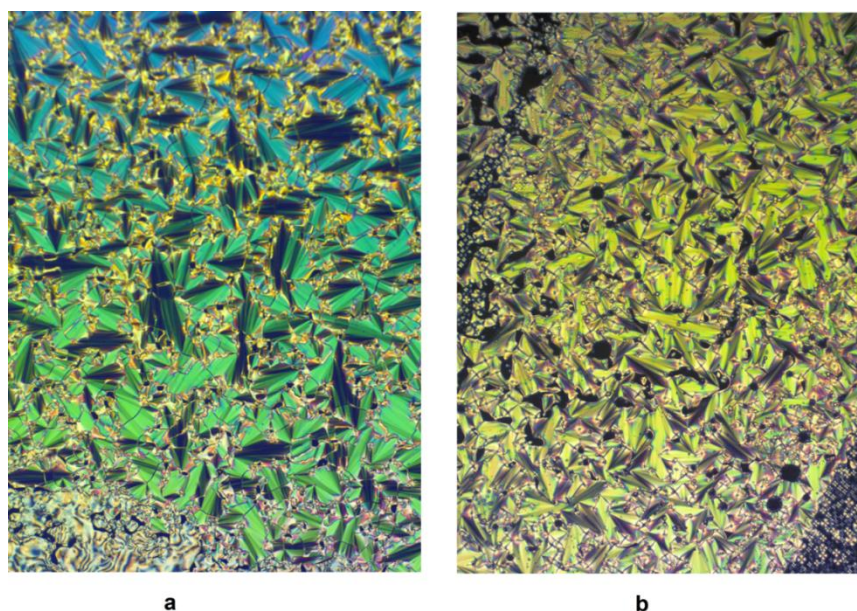


Figure 88: Optical micrographs (on cooling) of the (a) SmC phase of the tricatener ligand (V (2)) and (b) SmA phase of the tricatener-palladium(II) complex (XIV (2)).

3.2.4. Small Angle X-ray Scattering of Complexes XIV (1) and XIV (2)

The scattering patterns for complexes **XIV (1)** and **XIV (2)** as a function of temperature were recorded by small angle X-ray scattering (SAXS). The two-dimensional patterns for the complexes, are shown in Figure 89 and 90, respectively, confirmed the existence of smectic mesophases, shown by a sharp and bright ring corresponding to the layer spacing, which would normally equate to the molecular length.

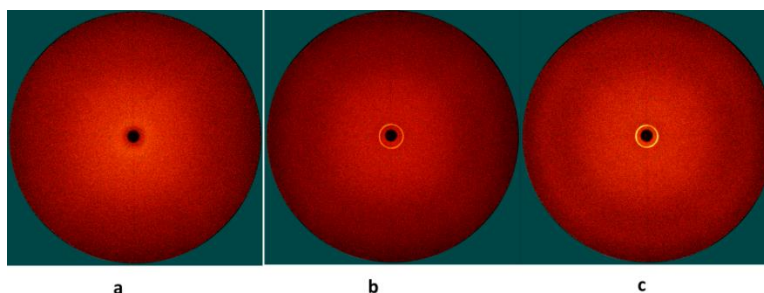


Figure 89: Two-dimensional small angle X-ray scattering patterns obtained for complex XIV (1): (a) in isotropic phase ($T = 255\text{ }^{\circ}\text{C}$); (b) in the Smectic A phase ($T = 222\text{ }^{\circ}\text{C}$) and (c) in crystal phase ($T = 127\text{ }^{\circ}\text{C}$).

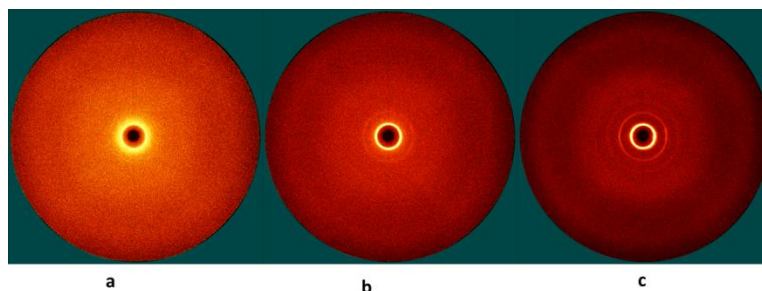


Figure 90: Two dimensional-small angle X-ray scattering patterns obtained for the complex XIV (2): (a) in isotropic phase at ($T = 149\text{ }^{\circ}\text{C}$); (b) in the Smectic A phase ($T = 116\text{ }^{\circ}\text{C}$) and (c) in crystal phase ($T = 55\text{ }^{\circ}\text{C}$).

The scattering is described in a graph of 2θ vs intensity at different temperature for **XIV (1)** given in Figure 91, which shows a d -spacing of about 36 \AA in the SmA phase at a variety of temperatures. The d -spacing is in accordance with the predicted molecule length which is about 42 \AA when calculated using Chem3D software, the difference likely being accounted for by a combination of chain folding and/or some inter-digitation.

Similarly for complex **XIV (2)**, the scattering pattern as a function of 2θ is given in Figure 92 and shows a single reflection at $2\theta = 2.55^\circ$ corresponding to a spacing of 34.6 \AA .

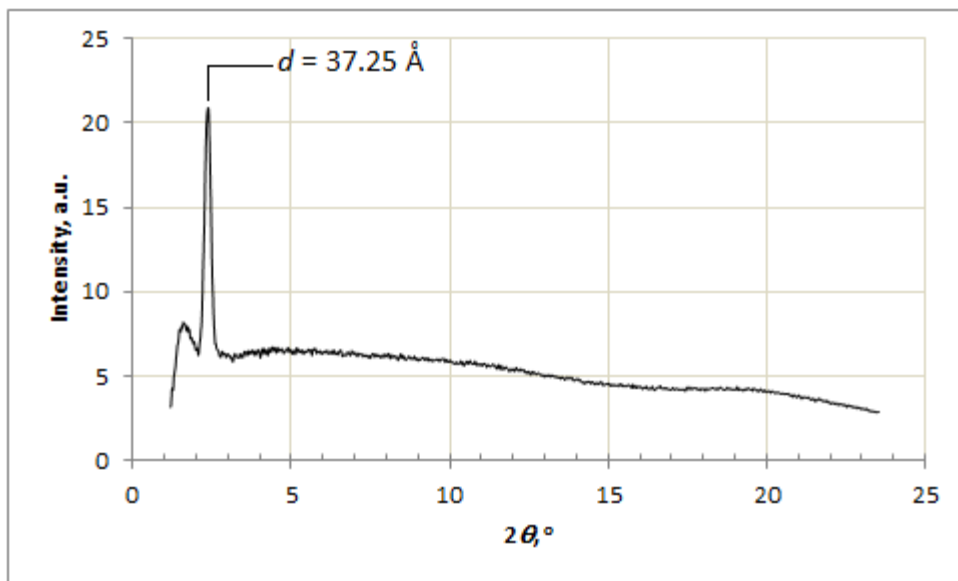


Figure 91: The small-angle X-ray scattering pattern of complex XIV (1) in the SmA state ($T = 205^\circ\text{C}$)

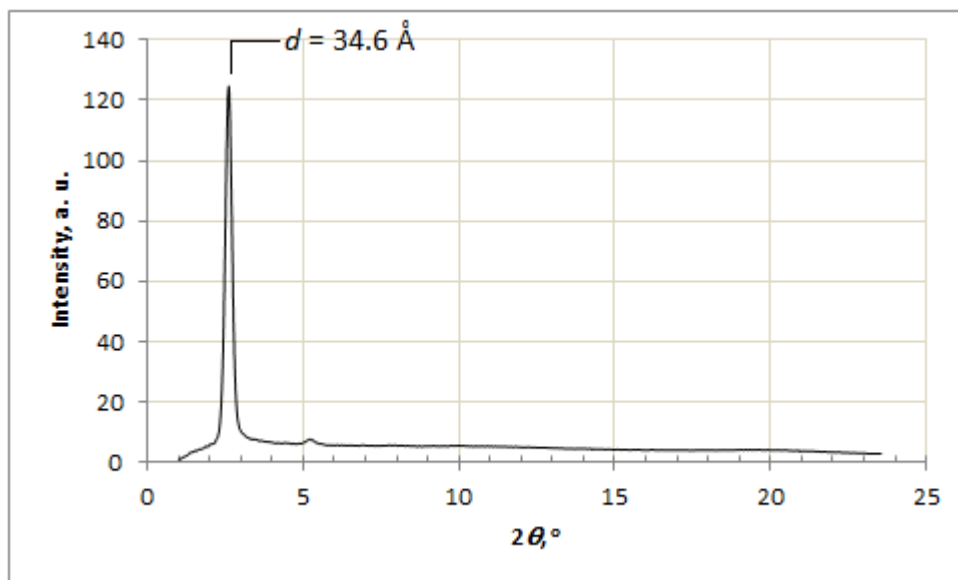


Figure 92: The small-angle X-ray scattering pattern of complex XIV (2) in the SmA state ($T = 105^\circ\text{C}$)

3.2.5. Photophysical Properties of the Complexes

The photophysical characterisation of the complexes and ligands was carried out in dichloromethane solution at room temperature. The absorption spectra of ligands and complexes are shown in Figure 93 and Figure 94, whereas the spectra overlaying each complex with its ligand are given in Figure 95. In the spectra of ligands, two bands were observed with intense absorptivity shown in

Table 13 suggesting ligand-centered charge-transfer attributed to $n-\pi^*$ and $\pi-\pi^*$ transitions. In the spectra of complexes **XIV (1 – 3)**, an additional band was observed at 378 nm for **XIV (1)** and **XIV (2)** and at 400 nm for **XIV (3)**, which was not seen in the ligand spectra. The absorptivity as given in Table 12, is between 15,000 and 80,000 $\text{M}^{-1} \text{cm}^{-1}$ suggesting CT transitions. Additional shorter wavelength bands were also observed in the spectra of **XIV (2)** and **XIV (3)**. Signals at λ_{max} 284 nm for **XIV (2)** and 294 nm for **XIV (3)** which appear to overlap with the absorption band of the ligands; a shoulder peak also appeared in the spectrum of **XIV (3)** at 267 nm. Those bands were also intense with absorptivity of 80,213 to 164,550 $\text{M}^{-1} \text{cm}^{-1}$ suggesting charge transfer transitions. It appears that the complexes demonstrated electronic interactions between the ligand and palladium metal but the electronic properties of the ligands in the palladium complexes still remained.

The absorption spectrum of hexacatenar-palladium(II)-acac complex (**XIV (4)**) showed two similar bands with the ligand with higher absorptivity from $16.7 \cdot 10^3 \text{M}^{-1} \text{cm}^{-1}$ for the ligand to $478.8 \cdot 10^3 \text{M}^{-1} \text{cm}^{-1}$ for the complex. The observation indicates that the incorporating of the hexacatenar ligand into palladium(II) metal did not significantly contribute to the character of the electronic transitions.

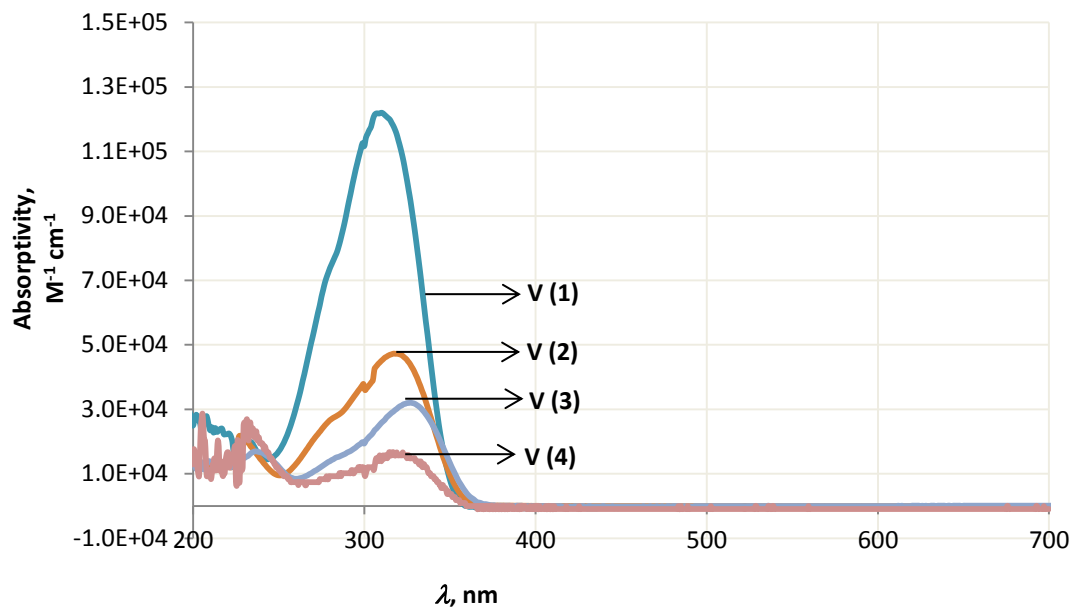


Figure 93: The absorption spectra of polycatenar ligands in dichloromethane solution at room temperature.

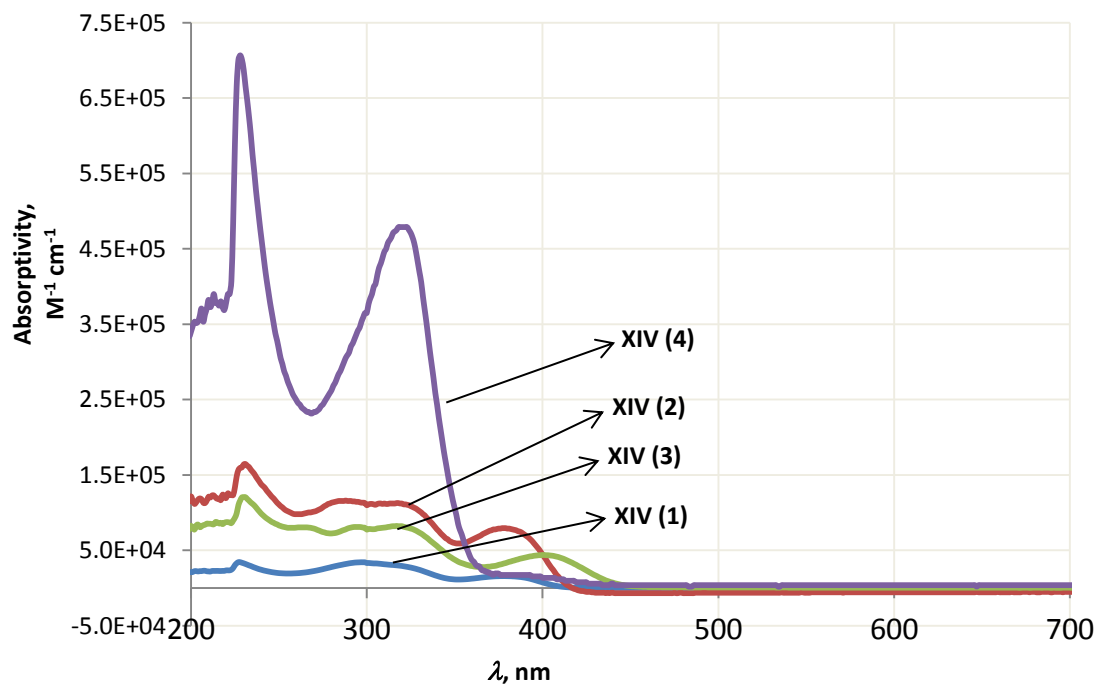


Figure 94: The absorption spectra of polycatenar palladium(II) complexes in dichloromethane solution at room temperature.

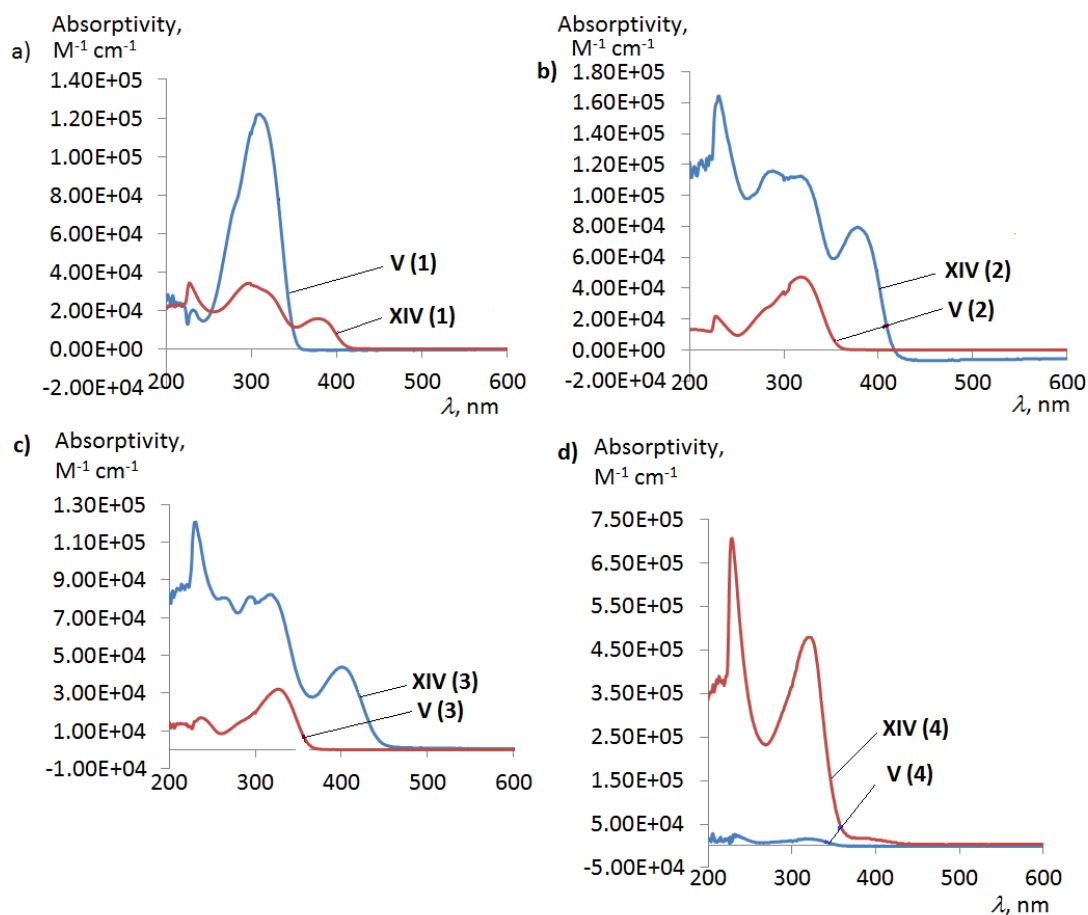


Figure 95: The absorption spectra of polycatenar ligands and palladium(II) complexes in dichloromethane solution at room temperature.

Table 12: Photophysical Properties of Palladium Complexes in CH₂Cl₂ Solution at 298 K.

Palladium Complexes				
	XIV (1)	XIV (2)	XIV (3)	XIV (4)
Absorption, λ_{\max}/nm ($\epsilon/\times 10^3$, $\text{M}^{-1}\text{cm}^{-1}$)	297 (34.2), 227 (34.4), 378 (15.9)	231 (164.55), 288 (116.08), 318 (112.70), 378 (79.45)	229 (120.32), 267 (80.21), 294 (81.02), 317 (82.3), 400 (43.8)	228 (706.7), 321 (478.8)
Emission, λ_{\max}/nm	380, 430	391, 437	391, 472	410
Lifetime, τ degassed	0.49 ns (380 nm) 0.15 ns (430 nm)	0.38 ns (437 nm)	1.15 ns (391 nm)	1.5 ns (410 nm)

Table 13: Photophysical Properties of Ligands in CH₂Cl₂ Solution at 298 K.

	Ligands			
	V (1)	V (2)	V (3)	V (4)
Absorption, λ_{\max}/nm ($\epsilon/x 10^3 \text{ M}^{-1} \text{ cm}^{-1}$)	310 (122.9), 231 (20.3)	227 (21.7), 317 (47.2)	237 (16.9), 327 (32.1)	231 (26.8), 319 (16.7)
Emission, λ_{\max}/nm	380	390	390	410
Lifetime, τ degassed	0.5 ns (380 nm)	0.78 ns (390 nm)	1.13 ns (390 nm)	1.5 ns (390 nm)

Ghedini and co-workers reported a palladium(II) complex of fluorophore Nile Red (**88**) that demonstrating an MLCT transition at λ_{\max} 452 nm along with metal-perturbed LC transitions,¹⁶⁴ while when the acac co-ligand was modified by introducing polycatenar-methoxyphenyl derivatives (**89**), the electronic properties remained unperturbed.¹⁶⁵ Similar observations were also reported by Micutz, *et al.* where the electronic character of the ligands (LC) was maintained in the palladium(II) complexes (**90**) while bands at λ_{\max} 450 nm suggested MLCT transitions.¹⁶⁸ The emission lifetime of all complexes were on the range of 0.5 – 1.5 ns indicating an absence of phosphorescence. Although bands proposed to arise from MLCT transitions were observed, it seems that phosphorescent emission was absent.

3.3. Conclusion

The synthesis and characterisation of metallomesogens of palladium(II) complexes based on polycatenar-diphenylpyridine ligands and acac co-ligand were carried out. In this system where the core mesogens possess three rings, three terminal chains are required to display mesomorphisms. For tetracatenar- and hexacatenar-systems, ligands as well as the complexes showed no liquid-crystallinity. Complexation of the ligands slightly increased the isotropic temperatures although it reduced the anisotropy. The chains play an important role on the thermal behavior. All ligands and complexes exhibited luminescence properties; the complexes emitted light in the range of 430 – 472 nm in addition to the emission

that also demonstrated by ligands alone, in the range of 380 – 410 nm with emission lifetimes of 0.38 – 1.50 ns suggesting the absence of phosphorescence.

Chapter Four: Experimental Methods

4.1. Instrumentation

NMR Spectroscopy

^1H and NMR spectra were recorded using Jeol ECS400 and Jeol ECX400 spectrometers operating at 400 MHz (^1H) and ^1H at 500 MHz, ^2D and $^{15}\text{N}\{^1\text{H}\}$ NMR spectra were recorded on Bruker Avance 500 spectrometer using Topspin software. The resonance frequencies applied for $^{195}\text{Pt}\{^1\text{H}\}$, $^2\text{D}\{^1\text{H}\}$ and $^{15}\text{N}\{^1\text{H}\}$ nuclei were 107 MHz and 76.8 MHz and 50.7 MHz, respectively. Two dimensional $^{195}\text{Pt}\text{-}^1\text{H}$ and $^{15}\text{N}\text{-}^1\text{H}$ NMR spectra were acquired using hmqcgpqf pulse program *via* heteronuclear zero and double quantum coherence with decoupling during acquisition using gradient pulses for selection. The processing of all spectra was carried out using MestreNova software. For ^1H -NMR, the residual protic solvent was used as the internal standard (CDCl_3 : 7.26 ppm, CD_2Cl_2 : 5.32 ppm, CD_3COCD_3 : 2.04 ppm), for the ^{195}Pt -NMR spectra were referenced to $\text{K}_2[\text{PtCl}_6]$ in D_2O .

Far-Infrared

Far infrared spectra (600 to 150 cm^{-1}) were recorded on a Bruker-Tensor 37 spectrometer using a Bruker platinum ATR stage.

UV-Visible and Luminescence Spectroscopy

UV-visible spectra were recorded in solution on a Shimadzu UV-2401PC Spectrophotometer using quartz cuvettes of 1 cm path length and a spectral window between 190 nm and 800 nm. Steady-state emission-excitation spectra were recorded on Hitachi F-4500 Fluorimeter. The determination of the emission lifetime was performed by kinetic scans on Edinburgh Instruments FLS980 with its own operating software, using LED source of 375.60 nm (pulse width: 0.9 ns and bandwidth: 9.8 nm). The detector count rate was set to be < 5% of the source

count rate. Emission lifetime was measured when the absorbance of the interest wavelength was < 0.5 . The lifetime value was obtained through a fitted decay from a reconvolution fit with applying Instrument Response Function (IRF), using a scattering sample, Ludox (colloidal silica in H_2O with 40% of concentration). Degasing of samples was performed through three freeze-pump-thaw cycles on the vacuum Schlenk line.

Mass Spectrometry (MS)

Electrospray ionisation mass spectrometry (ESI-MS) and liquid injection field desorption/ionisation mass spectrometry (LIFDI-MS) analysis was carried out using a Bruker Daltronics microTOF-Agilent series 1200LC spectrometer.

Elemental Analysis

CHN percentages were measured using an Exeter Analytical Inc., CE-440 Elemental Analyser and Sartorius S2 analytical balance. Calibration was performed against acetanilide standards and verified by the use of *S*-benzyl thiuronium chloride as internal standard (analytical grade, supplied by Exeter Analytical). The carrier gas was CP-grade helium and the combustion gas was N5.5 grade oxygen, both from BOC.

Gas Chromatography-Mass Spectroscopy (GC-MS)

Samples of the reaction headspace were passed through a HP-AL/S column (30 m, 0.25 mm id, 5 μm film thickness, Agilent Technologies) using a Agilent 7890 GC system. The carrier gas was helium (flow rate: 1.5 mL min^{-1}) and the injection was split with a ratio, 10:1. The initial oven temperature of $100 \text{ }^\circ\text{C}$ was held for 1 min, then ramped at $5 \text{ }^\circ\text{C min}^{-1}$ to $195 \text{ }^\circ\text{C}$ and held for 5 minutes; giving a total run time of 25 minutes. Analytes were eluted from the GC column into a Waters GCT Premier time-of-flight instrument (scan time = 0.19 s, interscan = 0.01 s, internal standard = perfluorotributylamine also known as heptacosyl) equipped with an electron-impact ionisation source.

Electron Paramagnetic Resonance Spectroscopy

EPR spectroscopy was performed using a JEOL JES-RE1X-ESR spectrometer equipped with a 100 W Mercury lamps without a filter ($\lambda > 250$ nm). A sample of a solution of the analyte was loaded into a flat, quartz cell. A background spectrum was recorded at room temperature followed by the spectrum of sample at 120 K. The spectra were processed using SpecView software.

UV-Mass Spectrometry

Experiments were performed using a modified Bruker Esquire 6000 quadrupole ion trap mass spectrometer. The mass spectrometer was modified for the laser experiments by drilling holes (1 mm) in the ion trap ring electrode to allow laser access.¹²⁹ The source of UV photons for the laser spectroscopy experiments was from an Nd:YAG (Powerlite) pumped OPO (Panther Ex), producing ~ 2 mJ across the range 220 – 280 nm. $(\text{NBu}_4)_2[\text{PtCl}_6]$ dissolved in water was prepared for the electrospraying.

Small-Angle X-ray Scattering (SAXS)

Small angle X-ray diffraction was performed using a Bruker D8 Discover equipped with a temperature-controlled, bored graphite rod furnace, custom built at the University of York. The radiation used was copper $K\alpha$ ($\lambda = 0.154056$ nm) from a 1 μS microfocus source. Diffraction patterns were recorded on a 2048 x 2048 pixel Bruker VANTEC 500 area detector. Samples were filled into a 1 mm capillary tubes and aligned with a pair of 1 T magnets. Diffraction patterns were collected as a function of temperature and the data processed using Excel.

Differential Scanning Calorimetry (DSC) and Polarised Optical Microscopy (POM)

Differential scanning calorimetry was performed on a Mettler DSC822 equipped with a sample robot TS 0801RO operating with Mettler Staressoftware and calibrated before use against an indium standard ($T_{\text{onset}} = 156.55 \pm 0.2$ °C, $\Delta H =$

$28.45 \pm 0.40 \text{ J g}^{-1}$) under an atmosphere of dry nitrogen. Polarised optical microscopy was performed on an Olympus BX50 polarising microscope equipped with a Linkam TP93 heating stage, Linkam LNP cooling pump. Photomicrographs were captured *via* Pixelink camera mounted atop the microscope.

4.2. Materials

$\text{K}_2[\text{PtCl}_6]$, $\text{K}_2[\text{PtCl}_4]$ and $(\text{NH}_4)_2[\text{PdCl}_4]$ were obtained from Johnson Matthey. Tetrapropylammonium chloride and tetrapentylammonium chloride were obtained from Alfa Aesar and other materials including deuterated solvents used for NMR spectroscopy, were obtained commercially from Sigma Aldrich or Alfa Aesar.

Purification of Solvents and Reagents

Deuterated chloroform was neutralised using sodium carbonate and stored over 3 Å molecular sieves. Acetone and butanone were dried over CaSO_4 and were then distilled and stored over 3 Å molecular sieves. For dichloromethane, acetonitrile, THF, hexane, and DMF were purchased from Fisher Scientific UK, dried by percolation over activated alumina prior to use and then stored under nitrogen.

4.3. Methods for Investigation of Photochemical Activation of Tetraalkylammonium by Hexachloroplatinate(IV) Complex.

1. Preparation of Tetrabutylammonium Hexachloroplatinate(IV)

In a round-bottom flask, potassium hexachloroplatinate (1.15 g; 2.37 mmol) was stirred with acetone (15 cm^3). While stirring, tetrabutylammonium chloride (1.31 g; 4.73 mmol) was added into the flask. The mixture was stirred overnight to afford an orange solution and a colourless precipitate. The solution was filtered *in vacuo* to remove the precipitate and then the solvent was removed resulting in an orange precipitate. The solid was allowed to dry *in vacuo* in for two of hours to

give a crystalline orange solid. Yield: 97% (2.04 g; 2.28 mmol). Anal. calc. for $C_{32}H_{72}N_2Cl_6Pt$: Calc.: C = 43.05, H = 8.13, N = 3.14%. Found: C = 43.11, H = 8.08, N = 3.03%. 1H NMR, δ_H (400 MHz, d_6 -acetone): 0.98 (24 H, t, $-CH_3$), 1.45 (16 H, m, $-CH_2-$), 1.80 (16 H, m, $-CH_2-$), 3.46 (16 H, m, $-NCH_2-$). ^{195}Pt NMR, δ_{Pt} (107.5 MHz, d_6 -acetone, 298 K): 377. Far-IR ($\bar{\nu}_{Pt-Cl}$): 324 cm^{-1} .

2. Preparation of Tetrabutylammonium Tetrachloroplatinate(II)

To a solution of potassium tetrachloroplatinate (0.40 g; 0.96 mmol) in water (10 cm^3), a solution tetrabutylammonium chloride (0.54; 2.08 mmol) in water was added while stirring. The solution was stirred at room temperature for 3 hours. The mixture was placed in a separating funnel, then into the mixture, dichloromethane (30 cm^3) was added, forming two layers. The lower halogenated layer was collected in a conical flask. The solution was dried over anhydrous $MgSO_4$ then dichloromethane was removed using a rotary evaporator to give a pink solid. Yield: 0.69 g, 0.86 mmol = 90%. Anal. calc. for $C_{32}H_{72}N_2Cl_4Pt$: Calc.: C = 46.77, H = 8.83, N = 3.41%. Found: C = 46.42, H = 8.86, N 3.29%. 1H NMR δ_H (400 MHz, d_6 -acetone): 0.96 (24 H, t, $-CH_3$), 1.48 (16 H, m, $-CH_2-$), 1.87 (16 H, m, $-CH_2-$), 3.69 (16 H, m, $-NCH_2-$). ^{195}Pt NMR, δ_{Pt} (107.5 MHz, d_6 -acetone, 298 K): -1418 . Far-IR ($\bar{\nu}_{Pt-Cl}$): 307 cm^{-1} .

3. Preparation of Tetraethylammonium Hexachloroplatinate(IV)

Tetraethylammonium hexachloroplatinate(IV) was prepared as for the $(NBu_4)_2[PtCl_6]$ salt. Yield: 53.7 mg, 0.080 mmol, 35%. Anal. calc. for $C_{16}H_{40}N_2Cl_6Pt$: Calc.: C = 28.76, H = 6.03, N = 4.19%. Found: C = 28.72, H = 5.83, N 4.10%. The NMR analysis was not performed due to the poor solubility of the compound.

4. Preparation of Tetrapropylammonium Hexachloroplatinate(IV)

Tetrapropylammonium hexachloroplatinate(IV) was prepared as for the $(\text{NBu}_4)_2[\text{PtCl}_6]$ salt. Yield: 0.81 g, 1.04 mmol, 98%. Anal. calc. for $\text{C}_{24}\text{H}_{56}\text{N}_2\text{Cl}_6\text{Pt}$: Calc.: C = 36.93, H = 7.23, N = 3.59%. Found: C = 36.75, H = 7.20, N = 3.47%. ^1H NMR, δ_{H} (400 MHz, d_6 -acetone): 1.02 (24 H, t, $-\text{CH}_3$), 1.89 (16 H, m, $-\text{CH}_2-$), 3.48 (16 H, m, $-\text{NCH}_2-$). IR ($\bar{\nu}_{\text{Pt-Cl}}$): 316 cm^{-1} . ^{195}Pt NMR, δ_{Pt} (107.5 MHz, CD_2Cl_2 , 295 K): 236.

5. Preparation of Tetrapropylammonium Tetrachloroplatinate(II)

Tetrapropylammonium tetrachloroplatinate(II) was prepared as for the $(\text{NBu}_4)_2[\text{PtCl}_4]$ salt. Yield: 143.8 mg, 0.2020 mmol, 84%. Anal. calc. for $\text{C}_{24}\text{H}_{56}\text{N}_2\text{Cl}_4\text{Pt}$: Calc.: C = 40.62, H = 7.95, N = 3.95%. Found: C = 40.25, H = 7.86, N = 3.89%. ^1H NMR, δ_{H} (500 MHz, CD_2Cl_2): 1.06 (24 H, t, $-\text{CH}_3$), 1.72 (16 H, m, $-\text{CH}_2-$), 3.23 (16 H, m, $-\text{NCH}_2-$). ^{195}Pt NMR, δ_{Pt} (107.5 MHz, CD_2Cl_2 , 295 K): -1482 .

6. Preparation of Tetrapentylammonium Hexachloroplatinate(IV)

Tetrapentylammonium hexachloroplatinate(IV) was prepared as for the $(\text{NBu}_4)_2[\text{PtCl}_6]$ salt. Yield: 452.8 mg, 0.4501 mmol, 98%. Anal. calc. for $\text{C}_{40}\text{H}_{88}\text{N}_2\text{Cl}_6\text{Pt}$: Calc.: C = 47.81, H = 8.83, N = 2.79%. Found: C = 47.57, H = 8.75, N = 2.71%. ^1H NMR, δ_{H} (500 MHz, d_6 -acetone): 0.90 (24 H, t, $-\text{CH}_3$), 1.39 (32 H, m, $-\text{CH}_2-\text{CH}_2$), 1.84 (16 H, m, $-\text{CH}_2$), 3.49 (16 H, m, $-\text{NCH}_2-$). ^{195}Pt NMR, δ_{Pt} (107.5 MHz, d_6 -acetone, 298 K): 375.

7. Preparation of Tetrapentylammonium Tetrachloroplatinate(II)

Tetrapentylammonium tetrachloroplatinate(II) was prepared as for the $(\text{NBu}_4)_2[\text{PtCl}_4]$ salt. Yield: quantitative. ^1H NMR, δ_{H} (500 MHz, d_6 -acetone): 0.90 (24 H, t, $-\text{CH}_3$), 1.43 (32 H, m, $-\text{CH}_2-\text{CH}_2$), 1.91 (16 H, m, $-\text{CH}_2$), 3.71 (16 H, m, $-\text{NCH}_2-$). ^{195}Pt NMR, δ_{Pt} (107.5 MHz, d_6 -acetone, 298 K): -1419 ppm.

8. Preparation of Tributylammonium Salts

8.1. Tributylammonium Chloride

A solution of tributylamine (10 cm³; 40 mmol) dissolved in diethylether (20 cm³) was stirred with concentrated hydrochloric acid (3 cm³; 40 mmol) for 2 h to form two liquid layers. The aqueous layer was separated, and then washed twice with diethylether. Water was removed from the solution *in vacuo* to give a hygroscopic, yellowish white solid. Due to the hygroscopic properties, the elemental analysis for carbon exceeded the theoretical percentage so that the result is not included in this thesis, but ¹H NMR spectrum demonstrated the purity based on the integration. Yield: quantitative. Anal. calc. for C₁₂H₂₈ClN: Calc.: C = 64.98; H = 12.72; Cl = 15.98; N = 6.31%. Found: C = 64.37; H = 12.80; N = 6.22%. ¹H NMR, δ_{H} (400 MHz, d₆-acetone): 0.95 (9 H, t, -CH₃), 1.40 (6 H, m, -CH₂-), 1.83 (6 H, m, -CH₂-), 3.01 (6 H, m, -NCH₂-).

8.2. Tributylammonium Hexachloroplatinate(IV)

Solution of potassium hexachloroplatinate (112.8 mg; 0.2321 mmol) in water (10 cm³) was stirred with tributylammonium chloride (103.6 mg, 0.4670 mmol) for 2 h at room temperature to give a yellow solid and an orange solution. Dichloromethane (20 cm³) was added in order to extract the product. The halogenated layer was separated and then the solvent was removed using a rotary evaporator to give an orange solid which was dried *in vacuo*. Yield: 158.6 mg, 0.2032 mmol, 88%. Anal. calc. for C₂₄H₅₆N₂Cl₆Pt: Calc.: C = 36.93, H = 7.23, N = 3.59%. Found: C = 37.06; H = 7.34; N = 3.52%. δ_{H} (400 MHz, d₆-acetone): 0.94 (9 H t, -CH₃), 1.35 – 1.44 (6 H, m, -CH₂), 1.81 – 1.89 (6 H, m, -CH₂-) 3.21 – 3.27 (6 H, m, -NCH₂-). ¹⁹⁵Pt NMR, δ_{Pt} (107.5 MHz, d₆-acetone, 298 K): 264.

8.3. Tributylammonium Hexafluorophosphate(VI)

A solution of tributylammonium chloride, (135.6 mg; 0.6115 mmol) in water (3 cm³) was added into a solution of ammonium hexafluorophosphate (104.2 mg; 0.6394 mmol) in water (5 cm³). The mixture was stirred for 0.5 h to obtain a colourless precipitate. The precipitate was filtered, washed with water and dried *in vacuo* for 5 h to afford the title compound as a colourless solid. Yield: 96.3 mg, 0.290 mmol, 47%. Anal. calc. for C₁₂H₂₈NF₆P: Calc.: C = 43.50, H = 8.52, N = 4.23%. Found: C = 43.62, H = 8.41, N = 4.10%. ¹H NMR, δ_H (400 MHz, CDCl₃): 0.98 (9 H t, -CH₃), 1.41 (6 H, m, -CH₂), 1.71 (6 H, m, -CH₂-) 3.09 (6 H, m, -NCH₂-) 6.71 (1 H, s, broad, H-N-).

9. Preparation of Bis(triphenylphosphine)iminium Hexachloroplatinate(IV)

A solution of potassium hexachloroplatinate(IV) (110 mg; 0.20 mmol) and bis(triphenylphosphine)iminium chloride (285 mg; 0.490 mmol) in acetone (10 cm³) was stirred for 3 h at room temperature to give an orange solution. The solution was concentrated and washed with water to afford the title compound as a crystalline orange solid. Yield: quantitative. Anal. calc. for C₇₂H₆₀N₂P₄Cl₆Pt: Calc.: C = 58.24, H = 4.07, N = 1.89%. Found: C = 58.14, H = 4.13, N = 1.83%. NMR, ¹H NMR, δ_H (400 MHz, CD₂Cl₂): 7.46 (12 H, m, H-Ar), 7.64 (3 H, m, H-Ar). ¹⁹⁵Pt{¹H} NMR: δ_{Pt} (107.5 MHz, CD₂Cl₂, 295 K): 219.

10. Preparation of Tetrabutylphosphonium Hexachloroplatinate(IV)

To a solution of potassium hexachloroplatinate(IV) (313 mg; 0.644 mmol) in acetone (10 cm³), tetrabutylphosphonium chloride (416 mg; 1.41 mmol) was added while stirring. The mixture was stirred for 3 h at room temperature to give a mixture an orange solution and white precipitate. The solution was collected, concentrated, washed with water, and allowed to dry to afford the title compound as a crystalline solid. Yield: quantitative. Anal. calc. for C₃₂H₇₂P₂Cl₆Pt: Calc.: C = 41.48, H = 7.83%. Found: C = 41.92, H = 7.75%. ¹H NMR, δ_H (500 MHz, d₆-acetone):

0.95 (24 H, t, -CH₃), 1.54 (16 H, m, -CH₂), 1.66 (16 H, m, -CH₂), 2.51 (16 H, m, -PCH₂-). NMR, ¹⁹⁵Pt{¹H} NMR, δ_{Pt} (107.5 MHz, d₆-acetone, 298 K): 373. ³¹P{¹H} NMR δ_{P} (202.4 MHz, d₆-acetone, 298 K): 33.6 ppm.

11. Preparation of Tetrabutylammonium Hexachlorodiplatinate(II), (NBu₄)₂[Pt₂Cl₆]

To a solution of tetrabutylammonium tetrachloroplatinate(II) (208.3 mg; 0.2535 mmol) in water (3 cm³), potassium chloride (43.5 mg; 0.575 mmol) was added while stirring. The mixture was heated for 6 hours to give a mixture of a brown precipitate and an aqueous solution. The precipitate was isolated *via* filtration and washed with water. The precipitate was crystallised from acetone and diethylether to give a brown crystalline solid. Yield: 50.45 mg, 0.0464 mmol, 37%. Anal. calc. for C₃₂H₇₂N₂Cl₆Pt₂: Calc.: C = 35.33, H = 6.67, N = 2.58%. Found: C = 35.35, H = 6.63, N = 2.47%. ¹H NMR, δ_{H} (500 MHz, CD₂Cl₂, 295 K): 1.07 (24 H, t, -CH₃), 1.58 (16 H, m, -CH₂-), 1.83 (16 H, m, -CH₂), 3.51 (16 H, m, -NCH₂-). ¹⁹⁵Pt NMR, δ_{Pt} (107.5 MHz, CD₂Cl₂, 295 K): - 1218.

12. Thermal Reaction of Tetraalkylammonium Hexachloroplatinate(IV) under Ambient Illumination

A general procedure to carry out the reaction of tetraalkylammonium with hexachloroplatinate(IV) was as follows: tetraalkylammonium hexachloroplatinate(IV) dissolved in the solvent of choice was heated under reflux under an atmosphere of N₂. When all of the [PtCl₆]²⁻ was consumed (followed by ¹⁹⁵Pt{¹H} NMR spectroscopy), the product was isolated *via* precipitation in which the concentrated reaction mixture was dissolved in a small amount of acetone, layered with diethyl ether and allowed to precipitate slowly at room temperature. Solid products can only be isolated from the reaction of tetrabutylammonium cation with hexachloroplatinate(IV). When NPr₄⁺ and NPe₄⁺ salts were used, no solids were isolated from solution and the reaction products were studied by solution ¹H, ¹⁹⁵Pt{¹H} NMR spectroscopy.

12.1. Reaction of tetrabutylammonium hexachloroplatinate(IV) in dry acetone

Tetrabutylammonium hexachloroplatinate(IV) (202.9 mg; 0.2273 mmol) in dry acetone (40 cm³) was heated under reflux under an atmosphere of nitrogen and ambient light for 48 h. The mixture was concentrated using a rotary evaporator to afford a brown paste which was dissolved in a small amount of acetone and crystallised by addition of diethyl ether to give a pale yellow precipitate and a supernatant. The precipitate was isolated by decanting of the solution, and it was then dried in air to afford (NBu₄)₂[η²-Cl₃Pt(C₄H₆)-η²-PtCl₃], **I**, as a yellow, crystalline solid. The precipitation was then repeated a few times to obtain a greater yields. Yield: 88.21 mg, 0.077 mmol, 68%. Anal. calc. for C₃₆H₇₈N₂Cl₆Pt₂: Calc.: C = 37.87, H = 6.88, N = 2.45%. The CHN analysis was conducted for compounds randomly taken from three batches of precipitation. Found: 1: C = 37.51, H = 6.75, N = 2.28%. 2: C = 38.16, H = 6.93, N = 2.38%. 3: C = 37.98, H = 6.51, N = 2.18%. δ_H (500 MHz, CD₂Cl₂, 295 K): *anti-trans*-butadiene-conformer: 5.56 (2H, m, H_X, H_{X'}), 4.80 (2H, *dd*, ³J_{HH} = 12.8 Hz, ²J_{HH} = 1.2 Hz, ²J_{PtH} = 60 Hz, H_A, H_{A'}), 4.44 (2H, *dd*, ³J_{HH} = 7.1 Hz, ²J_{HH} = 1.2 Hz, ²J_{PtH} = 60 Hz, H_M, H_{M'}), *syn-trans*-butadiene-conformer: 5.80 (2H, m, H_X, H_{X'}), 4.32 (2H, *d*, ³J_{HH} = 13.2 Hz, H_A, H_{A'}), 4.12 (2H, *d*, ³J_{HH} = 7.6 Hz, H_M, H_{M'}), *anti-cis*-butadiene-conformer: 6.33 (2H, *d of t*, ³J_{HH} = 17.2 Hz, ³J_{HH} = 10.4, ³J_{HH} = 10.4 Hz, H_X, H_{X'}), 5.80 (2H, *d*, ³J_{HH} = 17.2 Hz, H_A, H_{A'}), 5.52 (2H, *d*, ³J_{HH} = 10.4 Hz, H_M, H_{M'}). ¹⁹⁵Pt NMR, δ_{Pt} (107.5 MHz, CD₂Cl₂, 295 K): - 2521 (*anti-trans*-butadiene-conformer), - 2591 (*syn-trans*-butadiene-conformer).

12.2. Reaction of tetrabutylammonium hexachloroplatinate(IV) in dichloromethane

Tetrabutylammonium hexachloroplatinate(IV) (196.5 mg; 0.2201 mmol) in dry dichloromethane (40 cm³) was heated to reflux under an atmosphere of nitrogen and ambient light for 48 h. The mixture was concentrated using a rotary evaporator to afford a brown paste which was dissolved in a small amount of acetone and crystallised by addition of diethyl ether to give a pale yellow

precipitate. The precipitate was isolated by a decantation and dried in air to afford $(\text{NBu}_4)_2[\eta^2\text{-Cl}_3\text{Pt}(\text{C}_4\text{H}_6)\text{-}\eta^2\text{-PtCl}_3]$, **I**, as a yellow, crystalline solid. Yield: 17.33 mg, 0.015 mmol, 14%. δ_{H} (500 MHz, CD_2Cl_2 , 295 K): *anti-trans*-butadiene-conformer: 5.56 (2H, m, H_X , $\text{H}_{X'}$), 4.80 (2H, *dd*, $^3J_{\text{HH}} = 12.8$ Hz, $^2J_{\text{HH}} = 1.2$ Hz, $^2J_{\text{PtH}} = 60$ Hz, H_A , $\text{H}_{A'}$), 4.44 (2H, *dd*, $^3J_{\text{HH}} = 7.1$ Hz, $^2J_{\text{HH}} = 1.2$ Hz, $^2J_{\text{PtH}} = 60$ Hz, H_M , $\text{H}_{M'}$), *syn-trans*-butadiene-conformer: 5.80 (2H, m, H_X , $\text{H}_{X'}$), 4.32 (2H, *d*, $^3J_{\text{HH}} = 13.2$ Hz, H_A , $\text{H}_{A'}$), 4.12 (2H, *d*, $^3J_{\text{HH}} = 7.6$ Hz, H_M , $\text{H}_{M'}$), *anti-cis*-butadiene-conformer: 6.33 (2H, *d* of *t*, $^3J_{\text{HH}} = 17.2$ Hz, $^3J_{\text{HH}} = 10.4$, $^3J_{\text{HH}} = 10.4$ Hz, H_X , $\text{H}_{X'}$), 5.80 (2H, *d*, $^3J_{\text{HH}} = 17.2$ Hz, H_A , $\text{H}_{A'}$), 5.52 (2H, *d*, $^3J_{\text{HH}} = 10.4$ Hz, H_M , $\text{H}_{M'}$). ^{195}Pt NMR, δ_{Pt} (107.5 MHz, CD_2Cl_2 , 295 K): - 2521 (*anti-trans*-butadiene-conformer), - 2591 (*syn-trans*-butadiene-conformer).

12.3. Reaction of tetrabutylammonium hexachloroplatinate(IV) in dry butanone

Reaction of tetrabutylammonium hexachloroplatinate(IV) (189.0 mg; 0.2117 mmol) in dry butanone (40 cm^3) was carried out under the same conditions as for the salt in dry acetone and the isolation of products were also similar to afford the $(\text{NBu}_4)_2[\eta^2\text{-Cl}_3\text{Pt}(\text{C}_4\text{H}_6)\text{-}\eta^2\text{-PtCl}_3]$, **I**, as a yellow, crystalline solid. Yield: 68 mg, 0.06 mmol, 57%. δ_{H} (500 MHz, CD_2Cl_2 , 295 K): *anti-trans*-butadiene-conformer: 5.56 (2H, m, H_X , $\text{H}_{X'}$), 4.80 (2H, *dd*, $^3J_{\text{HH}} = 12.8$ Hz, $^2J_{\text{HH}} = 1.2$ Hz, $^2J_{\text{PtH}} = 60$ Hz, H_A , $\text{H}_{A'}$), 4.44 (2H, *dd*, $^3J_{\text{HH}} = 7.1$ Hz, $^2J_{\text{HH}} = 1.2$ Hz, $^2J_{\text{PtH}} = 60$ Hz, H_M , $\text{H}_{M'}$), *syn-trans*-butadiene-conformer: 5.80 (2H, m, H_X , $\text{H}_{X'}$), 4.32 (2H, *d*, $^3J_{\text{HH}} = 13.2$ Hz, H_A , $\text{H}_{A'}$), 4.12 (2H, *d*, $^3J_{\text{HH}} = 7.6$ Hz, H_M , $\text{H}_{M'}$), *anti-cis*-butadiene-conformer: 6.33 (2H, *d* of *t*, $^3J_{\text{HH}} = 17.2$ Hz, $^3J_{\text{HH}} = 10.4$, $^3J_{\text{HH}} = 10.4$ Hz, H_X , $\text{H}_{X'}$), 5.80 (2H, *d*, $^3J_{\text{HH}} = 17.2$ Hz, H_A , $\text{H}_{A'}$), 5.52 (2H, *d*, $^3J_{\text{HH}} = 10.4$ Hz, H_M , $\text{H}_{M'}$). ^{195}Pt NMR, δ_{Pt} (107.5 MHz, CD_2Cl_2 , 295 K): - 2521 (*anti-trans*-butadiene-conformer), - 2591 (*syn-trans*-butadiene-conformer).

13. Photoreactions of Tetrabutylammonium Hexachloroplatinate(IV)

Tetrabutylammonium hexachloroplatinate(IV) (10.18 mg, 0.01140 mmol) in dry acetone (2.0 cm^3) was irradiated with UV light with $\lambda > 305$ nm for 18 h, parallel reaction in three Young's NMR tubes. The mixture was concentrated *in vacuo* to

give a yellowish paste which was crystallised by addition of diethyl ether to give a pale yellow precipitate. The precipitate was isolated by decantation, and dried in air to afford $(\text{NBu}_4)_2[\eta^2\text{-Cl}_3\text{Pt}(\text{C}_4\text{H}_6)\text{-}\eta^2\text{-PtCl}_3]$, **I**, as a yellow, crystalline solid. Yield: 4.52 mg, 0.004 mmol, 69%. δ_{H} (500 MHz, CD_2Cl_2 , 295 K): *anti-trans*-butadiene-conformer: 5.56 (2H, m, $\text{H}_X, \text{H}_{X'}$), 4.80 (2H, *dd*, $^3J_{\text{HH}} = 12.8$ Hz, $^2J_{\text{HH}} = 1.2$ Hz, $^2J_{\text{PtH}} = 60$ Hz, $\text{H}_A, \text{H}_{A'}$), 4.44 (2H, *dd*, $^3J_{\text{HH}} = 7.1$ Hz, $^2J_{\text{HH}} = 1.2$ Hz, $^2J_{\text{PtH}} = 60$ Hz, $\text{H}_M, \text{H}_{M'}$), *syn-trans*-butadiene-conformer: 5.80 (2H, m, $\text{H}_X, \text{H}_{X'}$), 4.32 (2H, *d*, $^3J_{\text{HH}} = 13.2$ Hz, $\text{H}_A, \text{H}_{A'}$), 4.12 (2H, *d*, $^3J_{\text{HH}} = 7.6$ Hz, $\text{H}_M, \text{H}_{M'}$), *anti-cis*-butadiene-conformer: 6.33 (2H, *d* of *t*, $^3J_{\text{HH}} = 17.2$ Hz, $^3J_{\text{HH}} = 10.4$, $^3J_{\text{HH}} = 10.4$ Hz, $\text{H}_X, \text{H}_{X'}$), 5.80 (2H, *d*, $^3J_{\text{HH}} = 17.2$ Hz, $\text{H}_A, \text{H}_{A'}$), 5.52 (2H, *d*, $^3J_{\text{HH}} = 10.4$ Hz, $\text{H}_M, \text{H}_{M'}$). ^{195}Pt NMR, δ_{Pt} (107.5 MHz, CD_2Cl_2 , 295 K): - 2521 (*anti-trans*-butadiene-conformer), - 2591 (*syn-trans*-butadiene-conformer).

14. Photolysis of Analogous Hexachloroplatinate(IV) Complexes

The method and equipment used for the irradiation of the analogous complexes was identical to the one employed to irradiate $(\text{NBu}_4)_2[\text{PtCl}_6]$ complex described previously. The photolysis experiments were carried out in Young's NMR tubes for followed by ^1H and $^{195}\text{Pt}\{^1\text{H}\}$ NMR spectroscopy. Quantities of the starting materials used are tabulated below (Table 14).

Table 14: Amount of starting materials for the photolysis of analogous hexachloroplatinate(IV) complexes

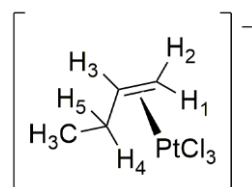
Substrates	Quantities
$(\text{NPe}_4)_2[\text{PtCl}_6]$	21.30 mg (0.02 mmol in dry acetone (1 cm^3))
$(\text{NPr}_4)_2[\text{PtCl}_6]$	14.67 mg (0.02 mmol) in dry acetone (12.5 cm^3)
$(\text{NPr}_4)_2[\text{PtCl}_6]$	3.57 mg (0.0045 mmol) in CD_2DCl_2 (0.5 cm^3)
$(\text{PBu}_4)_2[\text{PtCl}_6]$	8.24 mg (0.008 mmol) in d_6 -acetone (2 cm^3)

15. Synthesis of Trichloro(η^2 -butene)platinate(II) Complexes, III

A general procedure to prepare complexes of $[\text{Pt}(\eta^2\text{-butene})\text{Cl}_3]^-$ with different counter cations is as follows. In a Fisher-Porter vessel, $\text{K}_2[\text{PtCl}_4]$ was dissolved in concentrated HCl and water in a ratio of 1 : 5. The mixture was out-gassed by using the freeze-pump-thaw method. The last cycle was to out-gas the line attached to

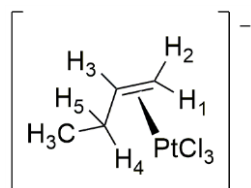
butene cylinder followed by flushing the butene gas into the vessel while stirring at room temperature. After a while, the gas was condensed in a vessel submerged in a bath of liquid nitrogen in order to allow the butene to react with the tetrachloroplatinate(II). The mixture was allowed to stir vigorously at room temperature for few days to gradually give a yellow solution while consuming the butene liquid. To obtain $K[Pt(\eta^2\text{-butene})Cl_3]$ complex, the acidic water was removed through rotary evaporation and the product was extracted using acetone. To prepare the complex with other cations such as NBu_4^+ and PPN^+ , the yellow solution was treated with a saturated solution of the cation of interest by stirring at room temperature to give the products as a precipitation.

15.1. $(NBu_4)[PtCl_3(1\text{-butene})]$, III (1)



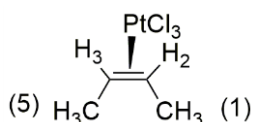
$K_2[PtCl_4]$ (250 mg, 0.590 mmol) in concentrated HCl (0.2 cm^3) and water (5 cm^3) was stirred with 1-butene liquid to give a yellow solution of $[PtCl_3(1\text{-butene})]$. Then, an aqueous, saturated NBu_4Cl (332 mg, 1.19 mmol) was added to afford a yellow precipitation of tetrabutylammonium trichloro(1-butene)platinate(II). The precipitate was washed with water followed by diethyl ether at room temperature and dried *at vacuo*. Yield: 321 mg, 0.535 mmol, 91%. Anal. calc. for $C_{20}H_{44}Cl_3NPt$: Calc.: C = 40.04, H = 7.39, N = 2.33%. Found: C = 39.74, H = 7.22, N = 2.11%. 1H -NMR, δ_H (500 MHz, d_6 -acetone): 1-butene: 5.13 (1H, m, $^3J_{HH} = 7\text{ Hz}$, $^3J_{PtH} = 70\text{ Hz}$, H₃), 4.30 (1H, d of d, $^2J_{HH} = 2\text{ Hz}$, $^3J_{HH} = 8.5\text{ Hz}$, $^3J_{PtH} = 63\text{ Hz}$, H₂), 4.32 (1H, d, $^2J_{HH} = 1.5\text{ Hz}$, $^3J_{PtH} = 63\text{ Hz}$, H₁), 2.18 (1H, quintet, $^3J_{HH} = 7.5\text{ Hz}$, $^3J_{PtH} = 43\text{ Hz}$, H₅), 1.71 (1H, quintet, $^3J_{HH} = 7.5\text{ Hz}$, $^3J_{PtH} = 44\text{ Hz}$, H₄), 1.24 (3H, triplet, $^3J_{HH} = 7\text{ Hz}$); butyl: 3.22 (8H, m, -N-CH₂-), 1.67 (8H, sextet, $^3J_{HH} = 7.5\text{ Hz}$, -CH₂-), 1.48 (8H, sextet, $^3J_{HH} = 7.5\text{ Hz}$, -CH₂-), 1.04 (12H, t, $^3J_{HH} = 7.5\text{ Hz}$, -CH₃). ^{195}Pt NMR, δ_{Pt} (107 MHz, d_6 -acetone, 298 K): - 2683 ppm; ($CDCl_3$, 298 K): - 2707 ppm; (CD_2Cl_2 , 295 K): - 2705 ppm.

15.2. (PPN)[Pt(1-butene)Cl₃], III (2)



The complex was prepared as for (NBu₄)[PtCl₃(1-butene)]. Yield: 135.2 mg, 0.1451 mmol, 94%. ¹H-NMR: δ_H (500 MHz, CD₂Cl₂): 1-butene: 5.03 (1H, m, *J*_{PtH} = 68 Hz, H₃), 4.24 (2H, m, *J*_{PtH} = 68 Hz, H₁, H₂), 2.14 (1H, heptet, ³*J*_{HH} = 7.0 Hz, H₅), 1.64 (1H, heptet, ³*J*_{HH} = 7.0 Hz, H₄), 1.22 (3H, t, ³*J*_{HH} = 7.0 Hz, -CH₃). PPN⁺: 7.69 (3H, m, H-Ar); 7.50 (12H, m, H-Ar); ¹⁹⁵Pt NMR, δ_{Pt} (107 MHz, CD₂Cl₂, 295 K): – 2708.

15.3. (PPN)[Pt(2-butene)Cl₃], IV



The complex was prepared as for (NBu₄)[PtCl₃(1-butene)]. Yield: 83.5 mg, 0.0896 mmol, 67%. ¹H-NMR, δ_H (500 MHz, CD₂Cl₂): 2-butene: 4.95 (2H, m, *J*_{PtH} = 60.5 Hz, H₂, H₃); 1.57 (6H, d, ³*J*_{HH} = 5.5 Hz, *J*_{PtH} = 34 Hz, -CH₃(1), -CH₃(5)); PPN⁺: 7.69 (3H, m, H-Ar); 7.50 (12H, m, H-Ar); ¹⁹⁵Pt NMR, δ_{Pt} (107 MHz, d₆-acetone, 298 K): – 2639 ppm, (CD₂Cl₂, 295 K): – 2663 ppm.

16. EPR experiments

Recording of spectra was performed at *T* = 120 K with sweep time of 120 seconds and time constant of 0.3 s. At 176 K or above, no signals were able to observe. Before sample analysis, a background was recorded at an identical temperature over a wide range where the sweep width was 75 mT and centre of the field was 325.4 mT. The internal standard was di(phenyl)-(2,4,6-trinitrophenyl)iminoazanium (DPPH) with a *g* value of 2.0036. Parameters of the analysis and observed *g* value of samples are showed in Table 15.

Table 15: Parameters of EPR experiments and observed g value in vary of samples.

Sample description	Frequency (GHz)	Power (mWatt)	Sweep width (mT)	Centre field (mT)	Modulation width (mT)	Receiver gain	g value
(NBu ₄) ₂ [PtCl ₆] (40.80 mg) in acetone (1 cm ³) solution was irradiated for 50 minutes	9.1270	10	25	275.0	0.4	630	2.3998
	9.1270	10	10	325.4	0.4	50	2.0084
(NBu ₄) ₂ [PtCl ₆] (40.10 mg) in dichloromethane (1 cm ³) solution was irradiated for 25 minutes	9.1270	10	200	300	0.4	790	2.4020
	9.1270	1	30	325	0.05	790	2.0130
(NPr ₄) ₂ [PtCl ₆] (18.3 mg) in dichloromethane (0.5 cm ³) solution was irradiated for 20 minutes	9.1269	10	150	305	0.4	1600	2.3930
	9.1269	1	30	325	0.05	1600	2.0120
(NPe ₄) ₂ [PtCl ₆] (18.7 mg) in dichloromethane (0.5 cm ³) solution was irradiated for 20 minutes	9.1270	10	150	300	0.4	790	2.4020
	9.1270	1	30	325	0.05	2000	2.0120
(NBu ₄) ₂ [PtCl ₄] (22.20 mg) in dichloromethane (0.5 cm ³) solution was irradiated for 40 minutes	9.1260	10	200	310	0.4	3200	-
	9.1260	1	30	320	0.4	3200	2.0120
(PPN) ₂ [PtCl ₆] (18.5 mg, 0.02 mmol) and PPN[Pt(1-butene)Cl ₃] (9.0 mg, 0.015 mmol) in dichloromethane (0.5 cm ³) mixture was irradiated for 25 minutes	9.1270	10	200	310	0.4	630	2.4020
	9.1270	1	30	325	0.05	1250	2.0000

17. Irradiation of [PtCl₃(butene)]⁻ complexes under varied conditions.

The method and equipment used for the irradiation of the [PtCl₃(butene)]⁻ complexes were identical to those employed to irradiate (NBu₄)₂[PtCl₆] described previously. The photolysis experiments were carried out in Young's NMR tubes and followed by ¹H and ¹⁹⁵Pt{¹H} NMR spectroscopy. Quantities of the starting materials used are tabulated below (Table 16). Control reactions in the dark were also carried out.

Table 16: Descriptions quantities of starting materials used and conditions of reactions.

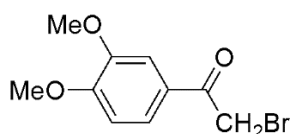
Substrates	Quantities
PPN[Pt(2-butene)Cl ₃]	9.14 mg (0.01 mmol) + (PPN) ₂ [PtCl ₆] (14.50 mg, 0.01 mmol) in CD ₂ Cl ₂ illuminated under hν > 305 nm
PPN[Pt(1-butene)Cl ₃]	9.01 mg (0.01 mmol) + (PPN) ₂ [PtCl ₆] (13.53 mg, 0.01 mmol) in CD ₂ Cl ₂ illuminated under hν > 305 nm
PPN[Pt(1-butene)Cl ₃]	8.19 mg (0.013 mmol) + (PPN) ₂ [PtCl ₆] (15.34 mg, 0.016 mmol) in CD ₂ Cl ₂ heated under reflux and dark.
(NBu ₄)[Pt(1-butene)Cl ₃]	18.56 mg (0.03 mmol) in d ₆ -acetone was irradiated under hν > 305 nm.

4.4. Method for Synthesis, the Liquid-crystalline and the Luminescence Properties of Polycatenar-diphenylpyridine Complexes of Palladium(II)

4.4.1. Synthesis of Ligands

4.4.1.1. Tricatenar diphenylpyridine derivatives

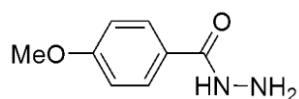
Bromo-3,4-dimethoxyacetophenone



In a conical flask complete with a suba seal, 3,4-dimethoxyacetophenone (10.0 g, 55.5 mmol) was dissolved in diethyl ether (150 cm³). Bromine (2.9 cm³, 55.5 mmol)

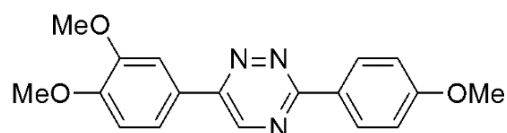
was added dropwise into the solution while stirring. The mixture was stirred at room temperature for 2 hours. Saturated aqueous sodium bicarbonate (130 cm³) was added to quench the bromination affording a colorless, two layers mixture. The organic layer was collected and the solvent was removed through rotary evaporation to give an oily, colourless residue. The residue was washed with hot ethanol (50 cm³) to afford the title compound as a colourless crystalline solid. Yield: 10.8 g (42.0 mmol, 75%). ¹H-NMR δ_H (400 MHz, CDCl₃): 7.60 (1H, dd, ⁴J_{HH} = 2.0 Hz, ³J_{HH} = 8.4 Hz, H⁶), 7.53 (1H, d, ⁴J_{HH} = 2.0 Hz, H²), 6.90 (1H, d, ³J_{HH} = 8.8 Hz, H⁵), 4.40 (2H, s, CH₂Br), 3.95 (3H, s, OCH₃), 3.93 (3H, s, OCH₃).

4-Methoxybenzohydrazide



In a round-bottom flask, methyl anisate (10.05 g, 0.060 mol) was dissolved in methanol (40 cm³). Hydrazine monohydrate (24 cm³, 0.498 mol) was added and the mixture was heated under reflux and stirred for 17 hours. Methanol was removed through rotary evaporation to give a colourless solid. The solid was washed with water (200 cm³) and dried in air to afford the title compound as a white solid. Yield: 9.0 g (0.05 mol, 90%). ¹H-NMR δ_H (400 MHz, d₆-DMSO): 9.61 (1H, s, NH), 7.79 (2H, d, ³J_{HH} = 8.8 Hz, H², H⁶), 6.97 (2H, d, ³J_{HH} = 8.8 Hz, H³, H⁵), 4.40 (2H, s, NH₂), 3.79 (3H, s, OCH₃).

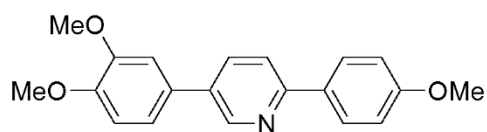
6-(3,4-Dimethoxyphenyl)-3-(4-methoxyphenyl)-1,2,4-triazine



In a 250 mL round-bottom flask, sodium acetate (1.28 g, 15.6 mmol) was dissolved in a mixture of acetic acid (25 cm³, glacial) and ethanol (45 cm³). Bromo-3,4-dimethoxyacetophenone (3.03 g, 12.0 mmol) and 4-methoxybenzohydrazide (4.02

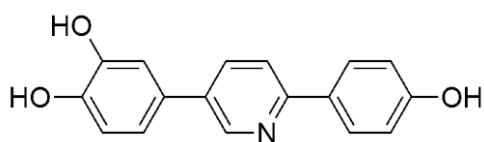
g, 24.0 mmol) were added to the solution then the mixture was stirred and heated under reflux for 24 hours to afford a yellow precipitate. After cooling, the precipitate formed was filtered, washed with ethanol (50 cm³), and dried in air. Yield: 1.81 g (5.60 mmol, 47%). ¹H-NMR δ_H (400 MHz, CDCl₃): 8.98 (1H, s, H⁵), 8.51 (2H, dd ⁴J_{HH} = 2.0 Hz, ³J_{HH} = 6.8 Hz H^{2'} H^{6'}), 7.90 (1H, d, ⁴J_{HH} = 2.0 Hz, H^{2''}), 7.58 (1H, dd, ³J_{HH} = 8.4 Hz, ⁴J_{HH} = 2.0 Hz, H^{6''}), 7.05 (2H, dd, ³J_{HH} = 6.8 Hz, ⁴J_{HH} = 2.0 Hz H^{3'} H^{5'}), 7.01 (1H, d, ³J_{HH} = 8.4 Hz, H^{5''}), 4.00 (3H, s, OCH₃), 3.97 (3H, s, OCH₃), 3.90 (3H, s, OCH₃).

2-(4-Methoxyphenyl)-5(3,4-dimethoxyphenyl)pyridine



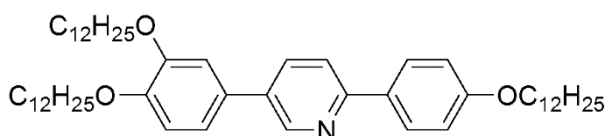
In an autoclave complete with a stirring bar, 6-(3,4-dimethoxyphenyl)-3-(4-methoxyphenyl)-1,2,4-triazine (2.20 g, 6.8 mmol) and bicyclo[2.2.1]hepta-2,5-diene (4 cm³, 40 mmol) were dissolved in *o*-xylene (24 cm³). The mixture was stirred and heated at 200 °C overnight. After the mixture was cooled, the solvent was removed on the rotary evaporator to give a yellowish residue. Methanol (50 cm³) was added to the residue to afford a yellow precipitate which was collected and dried in the air to obtain the title compound as a yellow solid. Yield: 1.81 g (5.60 mmol, 82%). ¹H-NMR δ_H (400 MHz, CDCl₃): 8.86 (1H, d, ⁴J_{HH} = 1.6 Hz, H⁶), 8.00 (2H, dd, ³J_{HH} = 6.8 Hz, ⁴J_{HH} = 2.0 Hz, Ar H^{2'} H^{6'}), 7.88 (1H, dd, ³J_{HH} = 6.8 Hz, ⁴J_{HH} = 2.4 Hz, H⁴), 7.73 (1H, d, ³J_{HH} = 8.4 Hz, H³), 7.19 (1H, dd, ³J_{HH} = 8.4 Hz, ⁴J_{HH} = 2.4 Hz, Ar H^{6''}), 7.13 (1H, d, ⁴J_{HH} = 2.0 Hz, Ar H^{2''}), 7.02 (2H, dd, ³J_{HH} = 6.8 Hz, ⁴J_{HH} = 2.0 Hz, Ar H^{3'} H^{5'}), 6.97 (1H, Ar H^{5''}), 3.96 (3H, s, OCH₃), 3.94 (3H, s, OCH₃), 3.88 (3H, s, OCH₃).

2-(4-Hydroxyphenyl)-5(3,4-dihydroxyphenyl)pyridine



In a two-neck round-bottom flask equipped with a magnetic stirring bar, 2-(4-methoxyphenyl)-5-(3,4-dimethoxyphenyl)pyridine (1.80 g, 5.00 mmol) was added to molten pyridinium chloride (19.2 g, 160 mmol) at 200 °C and the mixture was stirred for 5 h. When the mixture was cooled to about 120 °C, water (50 cm³) was poured into the flask to give a grey precipitate. The precipitate was filtered off and dried in the air to afford the title compound as a greyish-white solid. Yield: 1.10 g (3.93 mmol, 79%). ¹H-NMR δ_{H} (400 MHz, d₆-DMSO): 10.48 (not integrable, broad s, OH), 8.78 (1H, s, H⁶), 8.57 (1H, d, ³J_{HH} = 8.4 Hz, H⁴), 8.25 (1H, d, ³J_{HH} = 8.8 Hz, H³), 8.00 (2H, d, ³J_{HH} = 8.8 Hz, Ar H^{2'}, H^{6'}), 7.25 (1H, s, Ar H^{2''}), 7.18 (1H, dd, ³J_{HH} = 8.0 Hz, ⁴J_{HH} = 1.2 Hz, Ar H^{6''}), 7.01 (2H, d, ³J_{HH} = 8.4 Hz, Ar H^{3'}, H^{5'}), 6.93 (1H, d, ³J_{HH} = 8.0 Hz, Ar H^{5''}).

2-(4-Dodecyloxyphenyl)-5(3,4-didodecyloxyphenyl)pyridine, V (2)

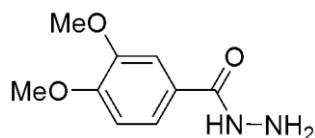


2-(4-Hydroxyphenyl)-5(3,4-dihydroxyphenyl)pyridine (1.00 g, 3.60 mmol), 1-bromododecane (3.50 cm³, 14.3 mmol) and potassium carbonate (3.96 g, 28.6 mmol) were dissolved in DMF (90 cm³). The solution was stirred and heated at 100 °C for 18 h to afford a mixture of a colourless precipitate and a yellow solution. The solid was filtered off and the DMF filtrate was concentrated using a rotary evaporator to give brown oil. An amount of methanol (30 cm³) was added to the oil to precipitate the product as a colourless solid. Meanwhile, the solid was dissolved in dichloromethane to extract the product. The solution was collected

and evaporated to give a solid which was washed with methanol and dried in air giving the colourless solid. Those solids were collected and characterised as the product. Yield 2.06 g (2.60 mmol, 73%). $^1\text{H-NMR}$ δ_{H} (400 MHz, CDCl_3): 8.83 (1H, d, $^4J_{\text{HH}} = 2.4$ Hz, H^6), 7.96 (2H, dd, $^3J_{\text{HH}} = 8.4$ Hz, $^4J_{\text{HH}} = 2.4$ Hz, Ar $\text{H}^{2'}\text{H}^{6'}$), 7.85 (1H, dd, $^3J_{\text{HH}} = 8.4$ Hz, $^4J_{\text{HH}} = 2.4$ Hz, H^4), 7.69 (1H, d, $^3J_{\text{HH}} = 8.4$ Hz, H^3), 7.15 (1H, d, $^3J_{\text{HH}} = 8.0$ Hz, Ar $\text{H}^{6''}$), 7.13 (1H, s, Ar $\text{H}^{2''}$), 6.98 (3H, Ar $\text{H}^{3'}$, $\text{H}^{5'}$, $\text{H}^{5''}$), 4.03 (6H, m, OCH_2), 1.82 (6H, m, $-\text{CH}_2$), 1.46 (6H, m, $-\text{CH}_2$), 1.25 (48H, m, $-\text{CH}_2$), 0.87 (9H, t, CH_3). Anal. calc. for $\text{C}_{53}\text{H}_{85}\text{NO}_3$: C = 81.17%, H = 10.92%, N = 1.79%. Found: C = 80.97%, H = 10.85%, N = 1.65%.

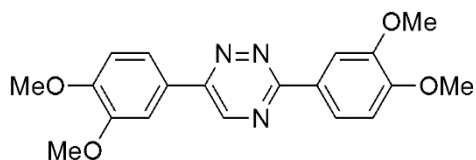
4.4.1.2. Tetracatenar diphenylpyridine derivatives

3,4-Dimethoxybenzohydrazide



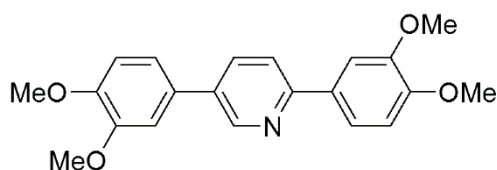
In a round-bottom flask, methyl 3,4-dimethoxybenzoate (10.0 g, 0.050 mol) was dissolved in methanol (70 cm^3). Hydrazine monohydrate (24.0 cm^3 , 0.489 mol) was added and the mixture was heated under reflux while stirring for 17 hours. Methanol was removed through evaporator to give a white precipitate. The precipitate was washed with water (200 cm^3) and dried in the air to afford the title compound as a white solid. Yield: quantitative. $^1\text{H-NMR}$ δ_{H} (400 MHz, CDCl_3): 7.35 (1H, s, NH), 7.37 (1H, d, $^4J_{\text{HH}} = 1.6$ Hz, H^3), 7.26 (1H, not integrable as overlapped with deuterated solvent peak at 7.25 H^5), 6.87 (1H, d, $^3J_{\text{HH}} = 8.4$ Hz, H^6), 4.08 (2H, s, broad NH_2), 3.93 (6H, s, OCH_3).

3,6-Bis(3,4-dimethoxyphenyl)-1,2,4-triazine



In a 250 mL round-bottom flask, sodium acetate (1.23 g, 15.0 mmol) was dissolved in a mixture of acetic acid (30 cm³, glacial) and ethanol (50 cm³). Bromo-3,4-dimethoxyacetophenone (3.00 g, 11.6 mmol) and 3,4-dimethoxybenzohydrazide (6.50 g, 33.0 mmol) were added to the solution and the mixture was stirred and heated under reflux for 24 hours to afford a yellow precipitate. The precipitate was collected, washed with ethanol (50 cm³) and dried in the air to give the title compound as a yellow crystalline solid. Yield: 1.99 g (5.40 mmol, 46%). ¹H-NMR δ_H (400 MHz, CDCl₃): 8.99 (1H, s, H⁵), 8.18 (1H, dd, ³J_{HH} = 8.4 Hz, ⁴J_{HH} = 2.0 Hz, H^{6'}), 8.15 (1H, d, ⁴J_{HH} = 2.0 Hz, H^{2'}), 7.93 (1H, d, ⁴J_{HH} = 2.0 Hz, H^{2''}), 7.59 (1H, dd, ³J_{HH} = 8.4 Hz, ⁴J_{HH} = 2.0 Hz, H^{6''}), 7.02 (2H, d, ³J_{HH} = 8.4 Hz, H^{5''}H^{5'}), 4.02 (3H, s, OCH₃), 4.01 (3H, s, OCH₃), 3.98 (3H, s, OCH₃), 3.97 (3H, s, OCH₃).

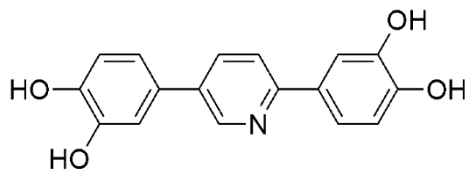
2,5-Bis(3,4-dimethoxyphenyl)pyridine



In an autoclave complete with a stirring bar, 3,6-bis(3,4-dimethoxyphenyl)-1,2,4-triazine (1.95 g, 5.00 mmol) and bicyclo[2.2.1]hepta-2,5-diene (3.0 cm³, 30.0 mmol) were dissolved in *o*-xylene (25 cm³). The mixture was stirred and heated at 200 °C overnight, after which it was concentrated and methanol (50 cm³) was added to the residue, afforded a yellow precipitate. The precipitate was filtered and allowed to dry in the air. Yield: 1.30 g (4.0 mmol, 74%). ¹H-NMR δ_H (400 MHz, CDCl₃): 8.85 (1H, s, H⁶), 7.86 (1H, dd, ³J_{HH} = 8.4 Hz, ⁴J_{HH} = 2.4 Hz, H⁴), 7.72 (1H, d, ³J_{HH} = 8.4 Hz, H³), 7.70 (1H, d, ⁴J_{HH} = 2.0 Hz, Ar H^{2'}), 7.53 (1H, dd, ³J_{HH} = 8.4 Hz, ⁴J_{HH} =

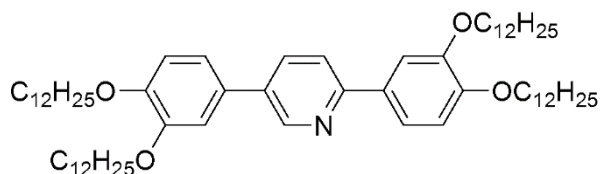
2.0 Hz, Ar H^{6'}), 7.17 (1H, dd, ³J_{HH} = 8.4 Hz, ⁴J_{HH} = 2.4 Hz, Ar H^{6''}), 7.11 (1H, d, ⁴J_{HH} = 2.0 Hz, Ar H^{2''}), 6.96 (2H, d, ³J_{HH} = 8.0 Hz, Ar H^{5'} H^{5''}), 4.00 (3H, s, OCH₃), 3.95 (3H, s, OCH₃), 3.93 (6H, s, OCH₃), 3.92 (3H, s, OCH₃).

2,5-Bis(3,4-dihydroxyphenyl)pyridine



In a two-neck round-bottom flask equipped with a magnetic stirring bar, 2,5-bis(3,4-dimethoxyphenyl)pyridine (1.30 g, 4.0 mmol) was added to molten pyridinium chloride (18.5 g, 160 mmol) at 200 °C and the mixture was stirred for 5 h. Water (50 cm³) was poured into the mixture when the temperature was about 120 °C to afford a grey precipitate, which was collected and dried in the air. Yield: 1.33 g (4.0 mmol, quantitative). ¹H-NMR δ_H (400 MHz, d⁶-DMSO): 9.37 (not integrable, broad s, OH), 8.73 (1H, d, ⁴J_{HH} = 2.0 Hz, H⁶), 8.42 (1H, d, ³J_{HH} = 8.8 Hz, H³), 8.07 (1H, d, ³J_{HH} = 8.4 Hz, H⁴), 7.46 (1H, d, ⁴J_{HH} = 2.0 Hz, Ar H²), 7.39 (1H, dd, ³J_{HH} = 8.4 Hz, ⁴J_{HH} = 2.4 Hz, Ar H^{6'}), 7.18 (1H, d, ⁴J_{HH} = 2.4 Hz, Ar H^{2''}), 7.11 (1H, dd, ³J_{HH} = 8.4 Hz, ⁴J_{HH} = 2.4 Hz, Ar H^{6''}), 6.90 (1H, d, ³J_{HH} = 8.0 Hz, Ar H^{5'}), 6.86 (1H, d, ³J_{HH} = 8.0 Hz, Ar H^{5''}).

2,5-Bis(3,4-bis(dodecyloxy)phenyl)pyridine, V (3)

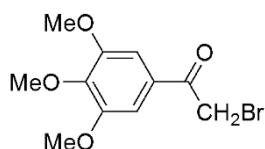


2,5-Bis(3,4-bis(dihydroxyphenyl)pyridine (1.12 g, 3.79 mmol), 1-bromododecane (4.0 cm³, 4.152 g, 16.65 mmol) and potassium carbonate (7.05 g, 51.0 mmol) were dissolved in DMF (100 cm³). The solution was stirred and heated at 100 °C for 18 h to afford a mixture of a colourless precipitate and a yellow solution. The solid was

filtered off and the DMF filtrate was concentrated using a rotary evaporator to give brown oil. An amount of methanol (30 cm³) was added to the oil to precipitate the product as a colourless solid. Meanwhile, the solid was dissolved in dichloromethane to extract the product. The solution was collected and evaporated to give a solid which was washed with methanol and dried in air giving the colourless solid. Those solids were collected and characterised as the product. Yield 2.31 g (2.38 mmol, 60%). ¹H-NMR δ_H (400 MHz, CDCl₃): 8.84 (1H, d, ⁴J_{HH} = 2.4 Hz, H⁶), 7.85 (1H, dd, ³J_{HH} = 8.4 Hz, ⁴J_{HH} = 2.4 Hz, H⁴), 7.70 (1H, d, ³J_{HH} = 8.4 Hz, H³), 7.67 (1H, d, ⁴J_{HH} = 2.4 Hz, Ar H^{2'}), 7.51 (1H, dd, ³J_{HH} = 8.4 Hz, ⁴J_{HH} = 1.6 Hz, Ar H^{6'}), 7.15 (1H, d, ⁴J_{HH} = 2.0 Hz, Ar H^{2''}), 7.13 (1H, d, Ar H^{6''}), 6.96 (2H, d, ³J_{HH} = 6.4 Hz, Ar H^{5'}, H^{5''}), 4.12 (2H, t, OCH₂), 4.05 (6H, m, CH₂), 1.84 (8H, m, -CH₂), 1.48 (8H, m, -CH₂), 1.37 (8H, m, -CH₂), 1.26 (56H, m, -CH₂), 0.87 (12H, t, CH₃). Anal. calc. for C₆₅H₁₀₉NO₄: C = 80.60; H = 11.34; N = 1.45%. The elemental analysis result for carbon was not in a good agreement with the analytical calculation, but the ¹H NMR spectrum showed the accordant integrations with the number of protons.

4.4.1.3. Hexacatenar diphenylpyridine derivatives

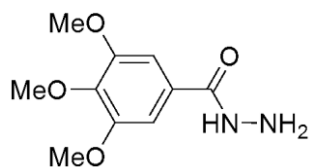
Bromo-3,4,5-trimethoxyacetophenone



In a conical flask complete with a suba seal, 3,4,5-trimethoxyacetophenone (10.0 g, 55.5 mmol) was dissolved in diethyl ether (250 cm³). Bromine (2.44 cm³, 55.5 mmol) was added dropwise into the solution with stirring. Once addition was complete, the mixture was stirred at room temperature for 2 hours. Saturated sodium bicarbonate (130 cm³) was added to quench the bromination reaction affording a colourless, two-layer mixture. The organic layer was collected and concentrated to give a colourless, oily residue, which was washed with hot ethanol (50 cm³) to afford the title compound as a colourless crystalline solid. Yield: 7.0 g

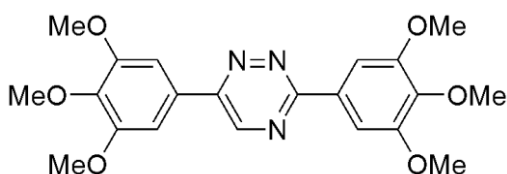
(24.2 mmol, 48%). $^1\text{H-NMR}$ δ_{H} (400 MHz, CDCl_3): 7.23 (2H, s, H^2, H^6), 4.40 (2H, s, $-\text{CH}_2\text{Br}$), 3.93 (3H, s, OCH_3), 3.91 (6H, s, OCH_3).

3,4,5-Trimethoxybenzohydrazide



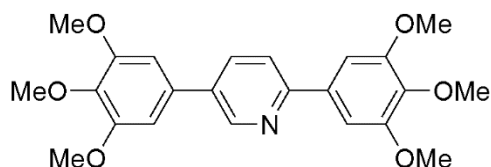
To a solution of methyl 3,4,5-trimethoxybenzoate (10.02 g, 0.044 mol) in methanol (70 cm^3) hydrazine monohydrate (20.31 cm^3 , 0.414 mol) was added. The mixture was stirred and heated under reflux for 17 hours. The mixture was concentrated using a rotary evaporator to give a white precipitate, which was washed with water (200 cm^3) and dried in the air. Yield: quantitative. $^1\text{H-NMR}$ δ_{H} (400 MHz, CDCl_3): 7.49 (1H, s, NH), 6.97 (2H, s, H^2, H^6), 4.11 (2H, s, broad NH_2), 3.89 (6H, s, OCH_3), 3.88 (3H, s, OCH_3).

3,6-Bis(3,4,5-trimethoxyphenyl)-1,2,4-triazine



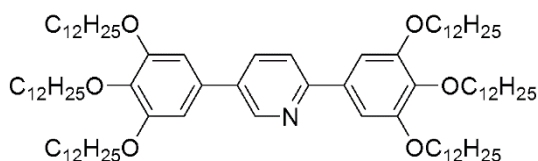
In a 250 mL round-bottom flask, sodium acetate (1.23 g, 15.0 mmol) was dissolved in a mixture of acetic acid (30 cm^3 , glacial) and ethanol (50 cm^3). Bromo-3,4,5-trimethoxyacetophenone (3.43 g, 9.80 mmol) and 3,4,5-trimethoxybenzohydrazide (6.65 g, 29.4 mmol) were added to the solution, which was stirred and heated under reflux for 24 hours to afford a yellow precipitate. The precipitate was collected, washed with ethanol (50 cm^3) and dried in the air to give the title compound as a yellow crystalline solid. Yield: 2.34 g (6.0 mmol, 58%). $^1\text{H-NMR}$ δ_{H} (400 MHz, CDCl_3): 9.00 (1H, s, H^5), 7.89 (2H, s, $\text{H}^{2'} \text{H}^{6'}$), 7.41 (2H, s, $\text{H}^{2''} \text{H}^{6''}$), 3.99 (6H, s, OCH_3), 3.98 (6H, s, OCH_3), 3.95 (3H, s, OCH_3), 3.94 (3H, s, OCH_3).

2,5-Bis(3,4,5-trimethoxyphenyl)pyridine



In an autoclave complete with a stirring bar, 3,6-bis(3,4,5-trimethoxyphenyl)-1,2,4-triazine (2.00 g, 5.00 mmol) and bicyclo[2.2.1]hepta-2,5-diene (3.20 cm³, 33.3 mmol) were dissolved in *o*-xylene (25 cm³). The mixture was stirred and heated at 200 °C overnight, after which it was concentrated on a rotary evaporator and methanol (50 cm³) added to afford a yellow precipitate. The precipitate was collected and dried in the air to give the title compound as a yellow solid. Yield: 0.91 g (2.21 mmol, 44%). ¹H-NMR δ_H (400 MHz, CDCl₃): 8.87 (1H, d, ⁴J_{HH} = 2.4 Hz, H⁶), 7.90 (1H, dd, ³J_{HH} = 8.0 Hz, ⁴J_{HH} = 2.4 Hz, H³), 7.75 (1H, dd, ³J_{HH} = 7.6 Hz, ⁴J_{HH} = 0.4 Hz, H⁴), 7.29 (2H, 2, Ar H^{2'} H^{6'}), 6.80 (2H, s, Ar H^{2''} H^{6''}), 3.98 (6H, s, OCH₃), 3.94 (6H, s, OCH₃), 3.91 (3H, s, OCH₃), 3.90 (3H, s, OCH₃).

2,5-Bis(3,4,5-tris(dodecyloxy)phenyl)pyridine, V (4)



2,5-Bis(3,4,5-trihydroxyphenyl)pyridine (0.48 g, 1.50 mmol), 1-bromododecane (2.32 cm³, 9.70 mmol) and potassium carbonate (3.73 g, 27.0 mmol) were dissolved in DMF (60 cm³). The solution was stirred and heated at 100 °C for 18 h to afford a mixture of a colourless precipitate and a yellow solution. The solid was filtered off and the DMF filtrate was concentrated using a rotary evaporator to give brown oil. An amount of methanol (30 cm³) was added to the oil to precipitate the product as a colourless solid. Meanwhile, the solid was dissolved in dichloromethane to extract the product. The solution was collected and evaporated to give a solid which was washed with methanol and dried in air giving the colourless solid. Those solids were collected and characterised as the product.

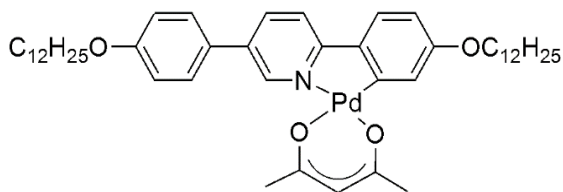
Yield 1.18 g (0.88 mmol, 59%). $^1\text{H-NMR}$ δ_{H} (400 MHz, CDCl_3): 8.83 (1H, d, $^4J_{\text{HH}} = 2.4$ Hz, H^6), 7.85 (1H, dd, $^3J_{\text{HH}} = 8.4$ Hz, $^4J_{\text{HH}} = 2.0$ Hz, H^4), 7.69 (1H, d, $^3J_{\text{HH}} = 8.0$ Hz, H^3), 7.23 (2H, s, Ar $\text{H}^{2'}$ $\text{H}^{6'}$), 6.76 (2H, s, Ar $\text{H}^{2''}$ $\text{H}^{6''}$), 3.99 – 4.08 (12H, t, OCH_2), 1.76 – 1.83 (12H, m, alkyl- CH_2 -), 1.48 (12H, m, alkyl- CH_2 -), 1.25 (96H, m, alkyl- CH_2 -), 0.87 (18H, m, alkyl CH_3). Anal. calc. for $\text{C}_{89}\text{H}_{157}\text{NO}_6$: Calc.: C = 79.9, H = 11.8, N = 1.1%, Found: C = 79.1, H = 11.4, N = 1.2%. The elemental analysis result for carbon was not in a good agreement with the analytical calculation, but the ^1H NMR spectrum showed the accordant integrations with the number of protons.

4.4.2. Palladium Complexes

Na(acac).H₂O

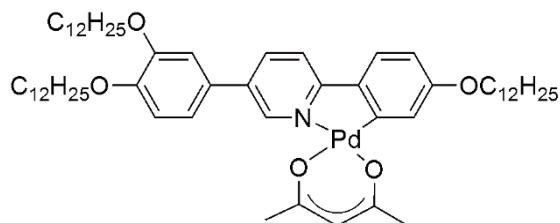
Sodium metal was taken carefully and cut into smaller pieces and weighed. Fresh ethanol (200 cm^3) purged with N_2 was placed in a round-bottom flask completed with a condenser then the equipment was placed in an ice bath. The sodium metal (12.68 g, 0.55 mol) was dissolved slowly in the ethanol. To the resulting solution, acetylacetonone (60 cm^3 , 0.60 mol) was poured portion by portion from the top of the condenser to spontaneously afford a colourless precipitate, which was collected, washed with cold ethanol, and dried *in vacuo* to give the title compound as a colourless solid. Yield: 46.98 g (0.335 mol, 61%). Anal. calc. for: $\text{C}_5\text{H}_9\text{NaO}_3$: C = 42.86%, H = 6.47%. Found: C = 42.57%, H = 6.42%. $^1\text{H-NMR}$ δ_{H} (400 MHz, $\text{d}_6\text{-DMSO}$): 4.85 (1H, s, H-acac), 1.61 (6H, s, acac- CH_3).

[Pd(acac)(2,5-bis(4-(dodecyloxy)phenyl)pyridine), XIV (1)]



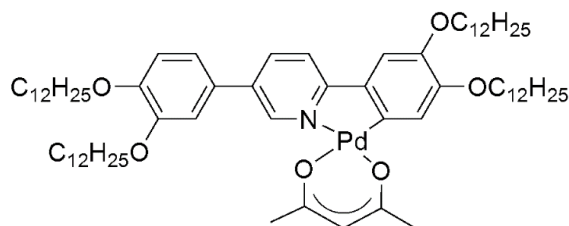
To a solution of 2,5-bis(4-(dodecyloxy)phenyl)pyridine (0.20 g, 0.33 mmol) in acetic acid (glacial, 20 cm³), ammonium tetrachloropalladate(II) (95.10 mg, 0.33 mmol) dissolved in a small amount of water (1 cm³) was added. The mixture was stirred and heated at 70 °C for 6 hours to afford a yellow precipitate, which was collected, washed with water (30 cm³) and methanol (10 cm³), and then dried in the air to give a yellow solid. The solid (0.19 g, 0.10 mmol) and sodium acetylacetonate (0.03 g, 0.21 mmol) in chloroform / ethanol (12 : 20 cm³) were stirred and heated under reflux for 5 hours. The mixture was then concentrated using a rotary evaporator to give a residue which was then extracted with dichloromethane. The halogenated layer was collected, washed with water (3 x 10 cm³), and dried with anhydrous MgSO₄. The dichloromethane was removed to give a yellow precipitate which was dried at *vacuo* to afford the title compound as a yellow solid. Yield: 0.18 g (0.18 mmol, 55%). ¹H-NMR δ_H (400 MHz, CD₂Cl₂): 8.87 (1H, d, ⁴J_{HH} = 2.0 Hz, H⁶), 7.92 (1H, dd, ³J_{HH} = 8.4 Hz, ⁴J_{HH} = 2.4 Hz, H⁴), 7.52 (3H, d, ³J_{HH} = 8.4 Hz, Ar H^{2''} H^{6''} H^{2'}), 7.34 (1H, d, ³J_{HH} = 8.4 Hz, H³), 6.98 (2H, d, ³J_{HH} = 8.4 Hz, Ar H^{3''} H^{5''}), 6.62 (1H, dd, ³J_{HH} = 8.0 Hz, ⁴J_{HH} = 2.0 Hz H^{3'}), 7.02 (1H, d, ⁴J_{HH} = 2.4 Hz, H⁴), 5.41 (1H, s, H-acac), 3.99 (4H, m, OCH₂), 2.07 (3H, s, acac -CH₃), 2.04 (3H, s, acac -CH₃), 1.77 (4H, m, alkyl-CH₂-), 1.44 (4H, m, alkyl-CH₂-), 1.25 (42H, m, alkyl-CH₂-), 0.85 (6H, m, alkyl CH₃). Anal. calc. for C₄₆H₆₇NO₄Pd: Calc.: C = 68.7, H = 8.4, N = 1.7%, Found: C = 69.3, H = 8.6, N = 1.8%. The elemental analysis showed more carbon than expected due to perhaps an impurity of solvent, even though the ¹H NMR spectrum showed the reasonable integration of proton resonances corresponding with the compound.

[Pd(acac)(2-(4-dodecyloxyphenyl)-5(3,4-didodecyloxyphenyl)pyridine)], XIV (2)



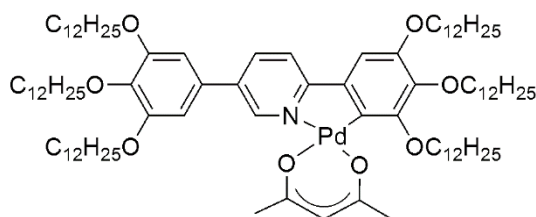
To a solution of 2-(4-dodecyloxyphenyl)-5(3,4-didodecyloxyphenyl)pyridine (0.53 g, 0.68 mmol) in acetic acid (glacial, 20 cm³), ammonium tetrachloropalladate(II) (192.43 mg, 0.677 mmol) dissolved in a small amount of water (1 cm³) was added. The mixture was stirred and heated at 100 °C for 6 hours to afford a yellow precipitate. The precipitate was collected, washed with water (3 x 10 cm³) and ethanol (10 cm³), and then dried in the air to give a dimer, [Pd(μ -Cl)(2-(4-dodecyloxyphenyl)-5(3,4-didodecyloxyphenyl)pyridine)]₂ as a yellow solid. Yield: 836.6 mg (0.56 mmol, 41%). A mixture of the dimer (268 mg, 0.14 mmol) and sodium acetylacetonate (54 mg, 0.28 mmol) in acetone was then stirred and heated under reflux for three days to afford a yellow precipitate, which was collected and purified on a silica column with high-purity grade silica gel (pore size: 60 Å, particle size: 35 – 75 μ m), using dichloromethane/methanol (5:1) as the eluent. The title compound was obtained as a yellow solid. Yield: 52.2 mg (0.053 mmol, 19%). ¹H-NMR δ_{H} (400 MHz, CDCl₃): 8.90 (1H, d, ⁴J_{HH} = 1.6 Hz, H⁶), 7.87 (1H, dd, ³J_{HH} = 8.4 Hz, ⁴J_{HH} = 2.0 Hz, H⁴), 7.47 (1H, d, ³J_{HH} = 8.4 Hz, H³), 7.31 (1H, d, ³J_{HH} = 8.8 Hz, Ar H^{2'}), 7.10 (3H, Ar H³, H⁵, H^{2''}), 6.97 (1H, d, ³J_{HH} = 8.8 Hz, Ar H^{5''}), 6.63 (1H, dd, ³J_{HH} = 8.4 Hz, ⁴J_{HH} = 2.4 Hz, Ar H^{6''}), 5.39 (1H, s, H-acac), 4.05 (6H, m, OCH₂), 2.10 (3H, s, acac -CH₃), 2.04 (3H, s, acac -CH₃), 1.83 (6H, m, alkyl-CH₂-), 1.46 (6H, m, alkyl-CH₂-), 1.25 (45H, m, alkyl-CH₂-), 0.87 (9H, m, alkyl CH₃). Anal. calc. for C₅₈H₉₁NO₅Pd: Calc.: C = 70.4, H = 9.3, N = 1.4%, Found: C = 69.7, H = 9.0, N = 1.3%. The elemental analysis showed more carbon than expected due to suggested an impurity of solvent, even though the ¹H NMR spectrum showed the reasonable integration of proton resonances corresponding with the compound.

[Pd(acac)(2,5-Bis(3,4-bis(dodecyloxy)phenyl)pyridine)], XIV (3)



To a solution of 2,5-bis(3,4-bis(dodecyloxy)phenyl)pyridine (0.59 g, 0.61 mmol) in acetic acid (glacial, 40 cm³), ammonium tetrachloropalladate(II) (178 mg, 0.60 mmol) dissolved in a small amount of water (1 cm³), was added. The mixture was stirred and heated at 70 °C for 6 hours to afford a yellow precipitate. The precipitate was separated from the mixture, washed with water (3 x 10 cm³) and methanol (10 cm³), and dried through *vacuum* line to afford a dimer, [Pd(μ -Cl)(2-(3,4-didodecyloxyphenyl)-5(3,4-didodecyloxyphenyl)pyridine)]₂ as a yellow solid. Yield: 0.57 g (0.25 mmol, quantitative). A mixture of the dimer (0.10 g, 0.045 mmol) and sodium acetylacetonate (0.06 g, 0.45 mmol) in chloroform / ethanol (10 : 5 cm³) was stirred and heated under reflux for 5 hours to afford a yellow precipitate. The mixture was concentrated using a rotary evaporator to give a residue which was then extracted with dichloromethane. The halogenated layer was collected, washed with water (3 x 10 cm³), and dried with anhydrous MgSO₄. The dichloromethane was removed to give a yellow precipitate, which was dried on a *vacuum* line to afford the title compound as a yellow solid. Yield: 88.3 mg (0.075 mmol, 83.6%). ¹H-NMR δ_{H} (400 MHz, CD₂Cl₃): 8.89 (1H, d, ⁴J_{HH} = 2.0 Hz, H⁶), 7.88 (1H, dd, ³J_{HH} = 8.4 Hz, ⁴J_{HH} = 2.0 Hz, H⁴), 7.44 (1H, d, ³J_{HH} = 8.4 Hz, H³), 7.11 (3H, Ar H^{2'} H^{6''} H^{2'}), 7.00 (1H, s, H^{5'}), 6.96 (1H, d, ³J_{HH} = 8.0 Hz, Ar H^{5''}), 5.39 (1H, s, H-acac), 3.99 – 4.13 (8H, m, OCH₂), 2.09 (3H, s, acac -CH₃), 2.04 (3H, s, acac -CH₃), 1.83 (8H, m, alkyl-CH₂-), 1.48 (8H, m, alkyl-CH₂-), 1.25 (64H, m, alkyl-CH₂-), 0.87 (12H, m, alkyl CH₃). Anal. calc. for C₇₀H₁₁₅NO₆Pd: Calc.: C = 71.67, H = 9.88, N = 1.19%, Found: C = 71.41, H = 9.77, N = 1.10%.

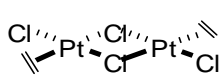
[Pd(acac)(2,5-Bis(3,4,5-tris(dodecyloxy)phenyl)pyridine), XIV (4)]



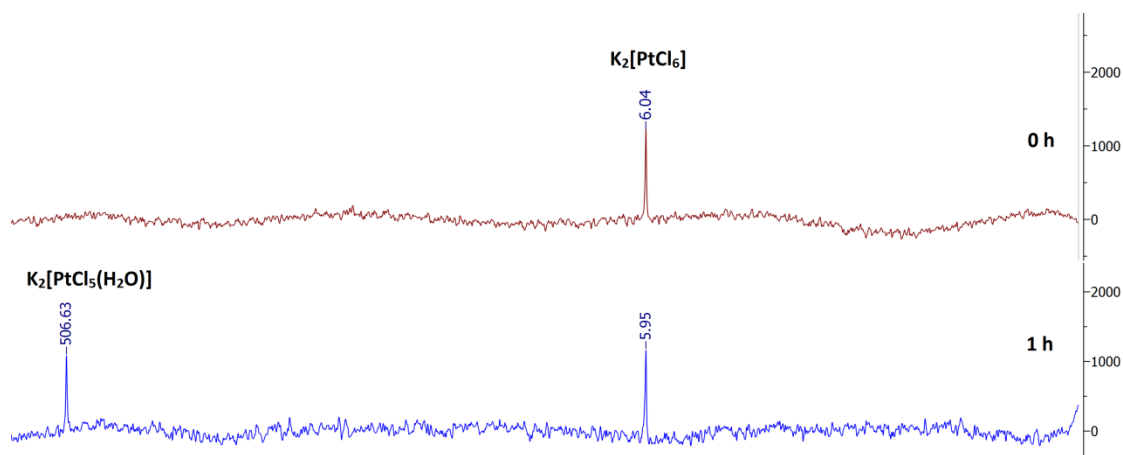
2,5-Bis(3,4,5-tris(dodecyloxy)phenyl)pyridine (0.22 g, 0.16 mmol) was dissolved in acetic acid (glacial, 12 cm³) by heating at 70 °C. Ammonium tetrachloropalladate(II) (50 mg, 0.176 mmol) dissolved in a small amount of water (1 cm³) was added into the ligand solution. The mixture was stirred and heated at 70 °C for 6 hours to afford a yellow precipitate, which was separated from the mixture, washed with water (3 x 10 cm³) and methanol (10 cm³), and then dried in air to give a yellow solid. A mixture of the solid and sodium acetylacetonate (95.5 mg, 0.67 mmol) in acetone was stirred and heated under reflux overnight. The mixture was concentrated to afford a yellow residue. The residue was purified on a silica column with high-purity grade silica gel (pore size: 60 Å, particle size: 35 – 75 μm), using dichloromethane/methanol (5:1) as the eluent. The title compound was obtained as a yellow solid. Yield: 117 mg (0.076 mmol, 56%). ¹H-NMR δ_H (400 MHz, CDCl₃): 8.83 (1H, d, ⁴J_{HH} = 2.0 Hz, H⁶), 7.85 (1H, dd, ³J_{HH} = 8.4 Hz, ⁴J_{HH} = 2.4 Hz, H⁴), 7.69 (1H, d, ³J_{HH} = 8.0 Hz, H³), 7.23 (1H, s, Ar H^{2'}), 6.76 (2H, s, Ar H^{2''} H^{6''}), 5.41 (1H, s, H-acac), 4.00 – 4.08 (12H, t, OCH₂), 2.06 (6H, s, acac -CH₃), 1.76 – 1.82 (12H, m, alkyl-CH₂-), 1.48 (12H, m, alkyl-CH₂), 1.25 (96H, m, alkyl-CH₂-), 0.86 (18H, m, alkyl CH₃). Anal. calc. for C₉₄H₁₆₃NO₈Pd: Calc.: C = 73.23, H = 10.66, N = 0.91%, Found: C = 73.38, H = 10.22, N = 0.934%.

Appendices

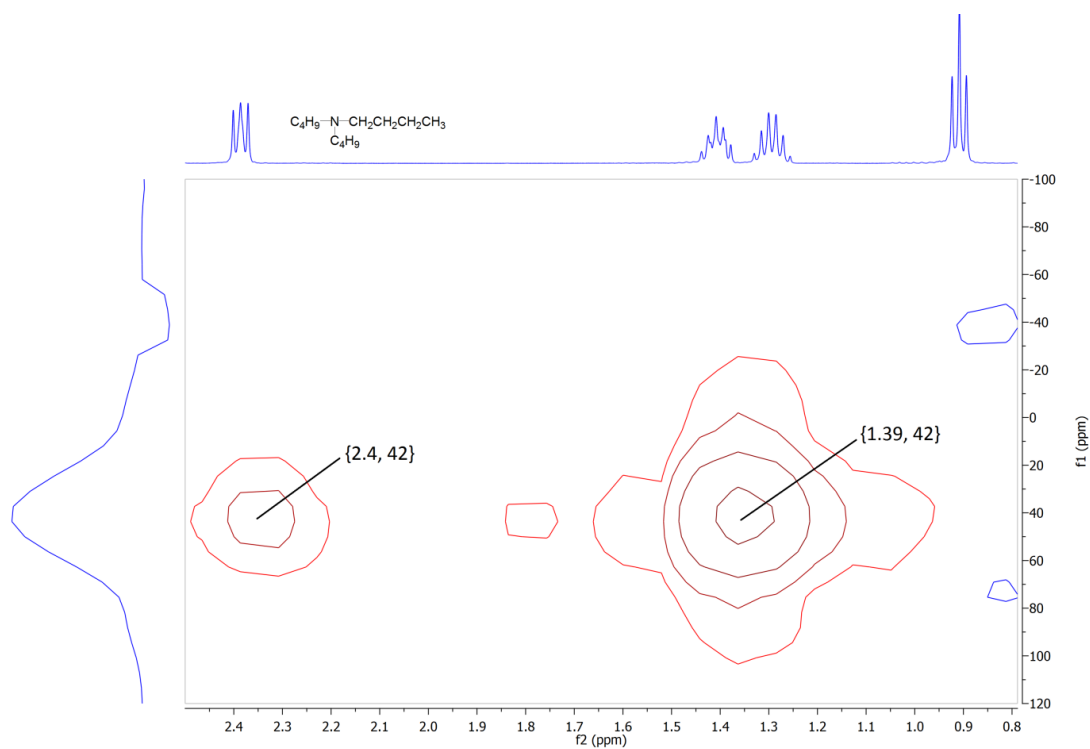
Appendix 1: The ^{195}Pt NMR data for platinum complexes

Complex	^{195}Pt NMR chemical shift (δ)	Solvent (T , K)
$(\text{NBu}_4)_2[\text{PtCl}_6]$	377	d_6 -acetone (298 K)
	239	CD_2Cl_2 (295 K)
$(\text{NBu}_4)_2[\text{PtCl}_4]$	- 1418	d_6 -acetone (298 K)
	- 1501	CD_2Cl_2 (295 K)
$(\text{NBu}_3\text{H})_2[\text{PtCl}_6]$	264	d_6 -acetone (298 K)
$(\text{NPr}_4)_2[\text{PtCl}_6]$	236	CD_2Cl_2 (295 K)
$(\text{NPr}_4)_2[\text{PtCl}_4]$	- 1482	CD_2Cl_2 (295 K)
$(\text{NBu}_4)_2[\text{Pt}_2\text{Cl}_6]$	- 1218	CD_2Cl_2 (295 K)
	- 1169	d_6 -acetone (298 K)
$(\text{NPe}_4)_2[\text{PtCl}_6]$	376	d_6 -acetone (298 K)
$(\text{NPe}_4)_2[\text{PtCl}_4]$	- 1419	d_6 -acetone (298 K)
$(\text{NBu}_4)_2[\mu\text{-C}_4\text{H}_6\text{Pt}_2\text{Cl}_6]$	- 2521 (<i>anti-trans</i> -conformer, major)	d_6 -acetone (298 K)
	- 2591 (<i>anti-cis</i> -conformer)	
	- 2515 (<i>syn-trans</i> -conformer)	
	- 2547 (<i>anti-trans</i> -conformer, major)	CD_2Cl_2 (295 K)
	- 2543 (<i>anti-cis</i> -conformer)	
	- 2490 - 2495	CDCl_3 (300 K) ¹⁰⁶
$\text{NPr}_4[\text{PtCl}_3(\text{C}_2\text{H}_4)]$	- 2785 ¹¹⁵	CDCl_3 (280 K) ¹¹⁵
$\text{K}[\text{PtCl}_3(\text{C}_2\text{H}_4)]$	- 2743 ¹¹⁴	D_2O ^{114,114}
$(\text{NBu}_4)[\text{PtCl}_3(1\text{-butene})]$	- 2705	CD_2Cl_2 (295 K)
	- 2707	CDCl_3 (298 K)
	- 2683	d_6 -acetone (298 K)
$(\text{PPN})[(1\text{-C}_4\text{H}_8)\text{PtCl}_3]$	- 2707	CD_2Cl_2 (295 K)
$(\text{PPN})[(2\text{-C}_4\text{H}_8)\text{PtCl}_3]$	- 2639	d_6 -acetone (298 K)
	- 2663	CD_2Cl_2 (295 K)
$\text{K}[(2\text{-C}_4\text{H}_8)\text{PtCl}_3]$	- 2643	d_6 -acetone (298 K)

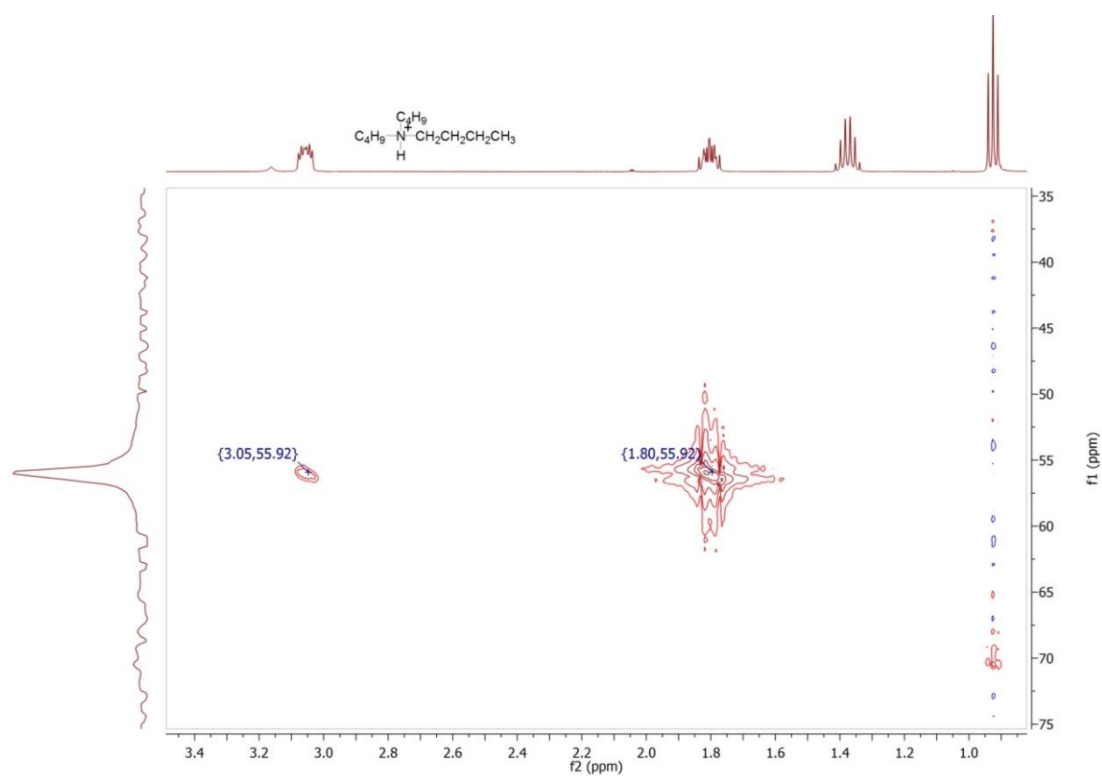
Appendix 2: The $^{195}\text{Pt}\{^1\text{H}\}$ NMR spectra (107 MHz) of $\text{K}_2[\text{PtCl}_6]$ in D_2O (top) and after one-hour irradiation (below).



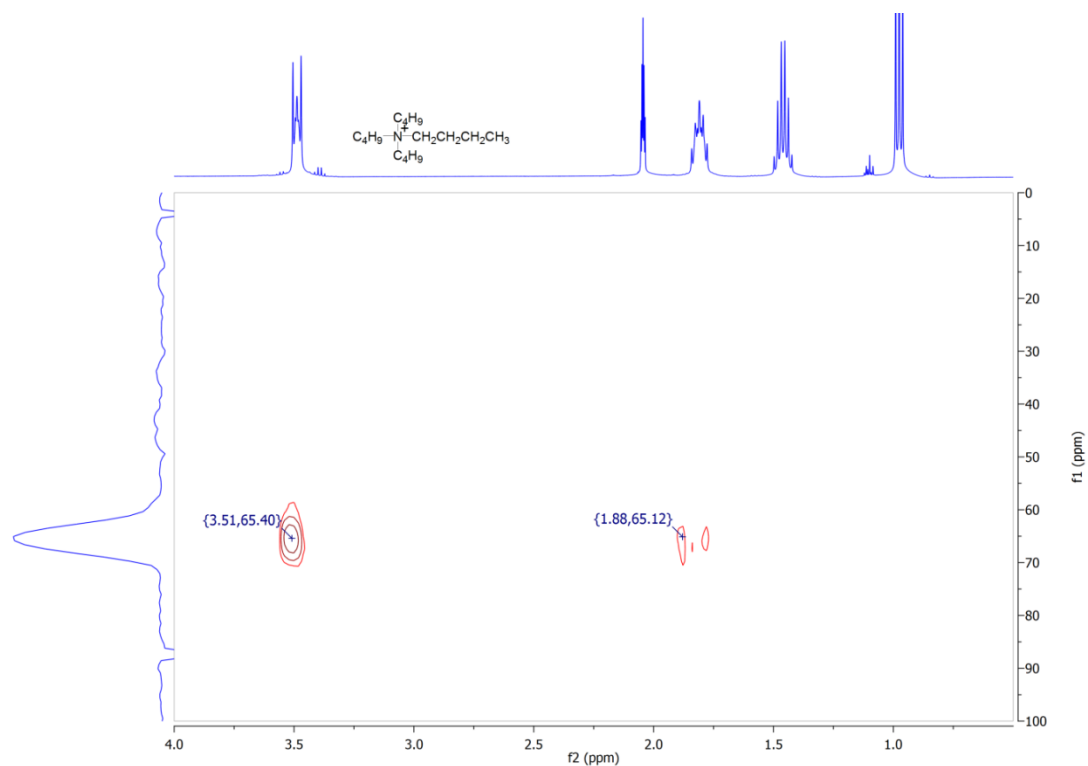
Appendix 3: The 2D (^{15}N - ^1H) NMR spectra (500 MHz for ^1H) of NBu_3



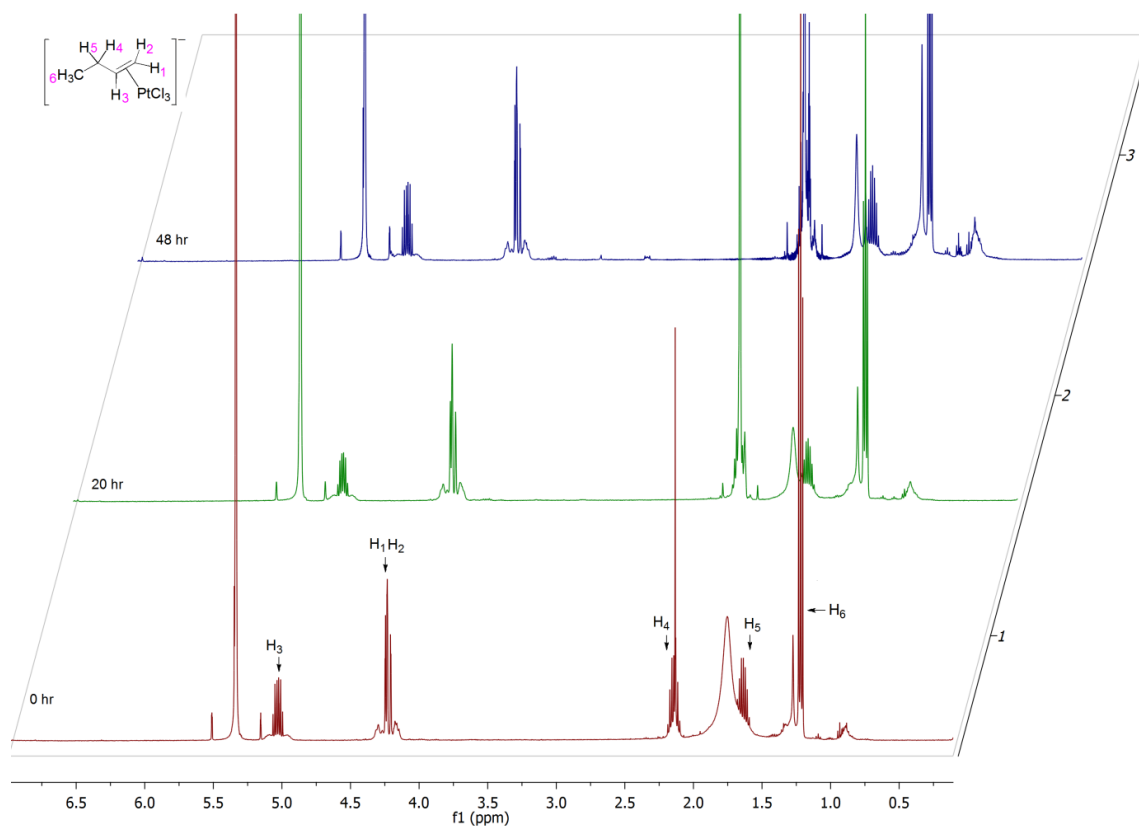
Appendix 4: The 2D (^{15}N - ^1H) NMR spectra (500 MHz for ^1H) of HNBU_3Cl in d_6 -acetone



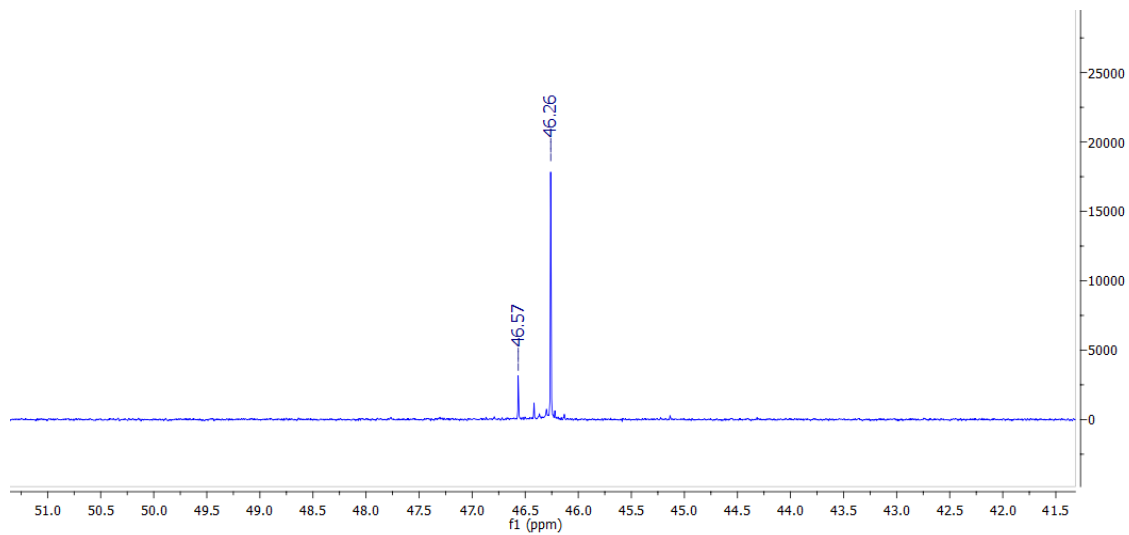
Appendix 5: The 2D (^{15}N - ^1H) NMR spectra (500 MHz for ^1H) of $(\text{NBu}_4)_2[\text{PtCl}_6]$ in d_6 -acetone



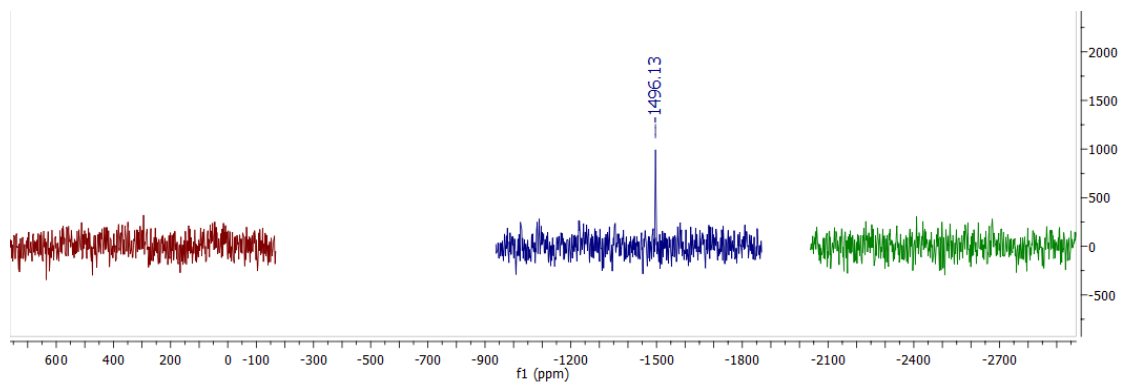
Appendix 6: The ^1H NMR spectra (500 MHz) of the mixture of $(\text{PPN})(\text{PtCl}_3(1\text{-butene}))$ and $(\text{PPN})_2[\text{PtCl}_6]$ in CD_2Cl_2 on the heating in the dark condition.

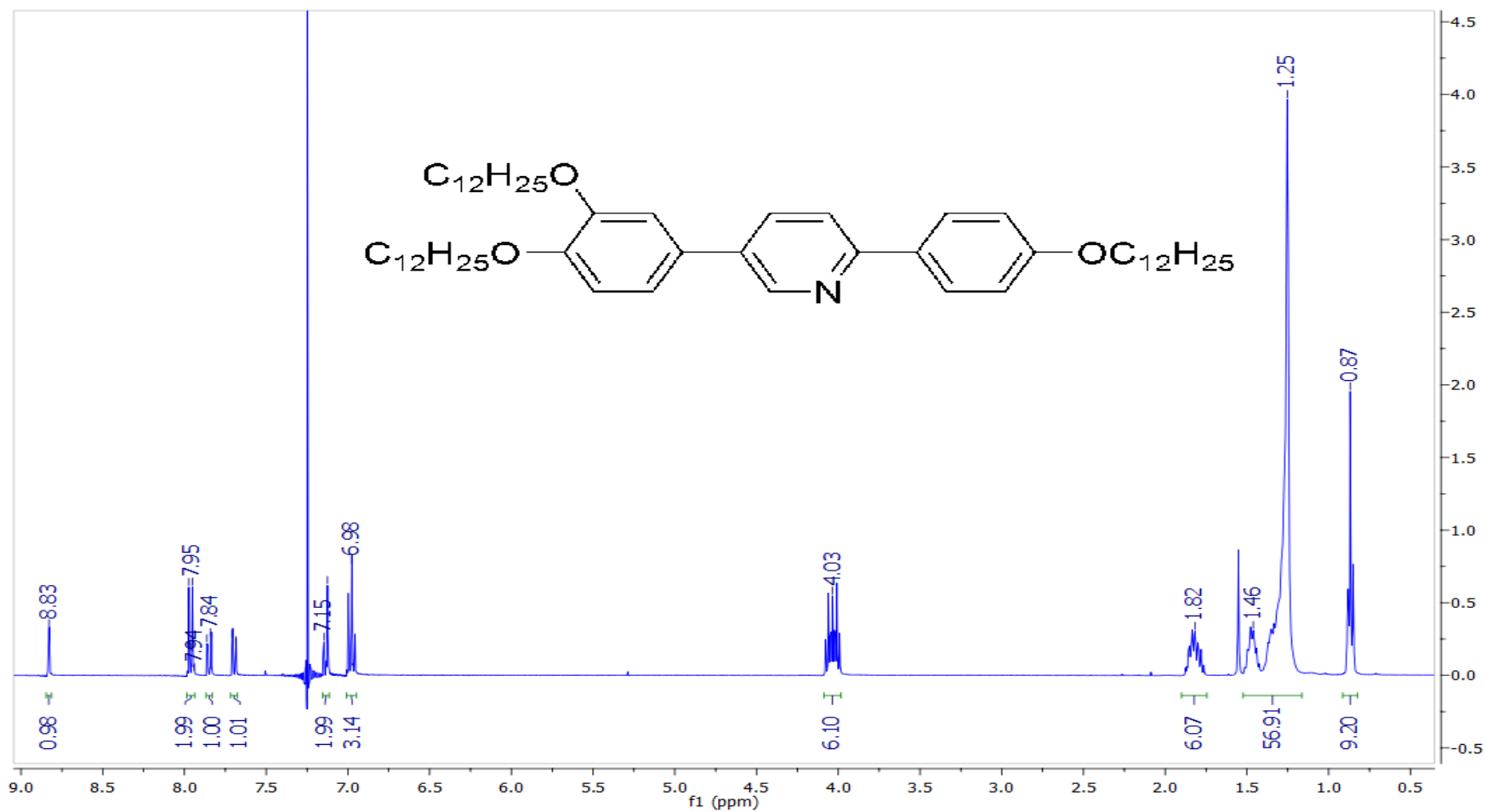


Appendix 7: The $^{31}\text{P}\{^1\text{H}\}$ NMR spectrum of photoreaction mixture of $(\text{PBU}_4)_2[\text{PtCl}_6]$ recorded in d_6 -acetone.

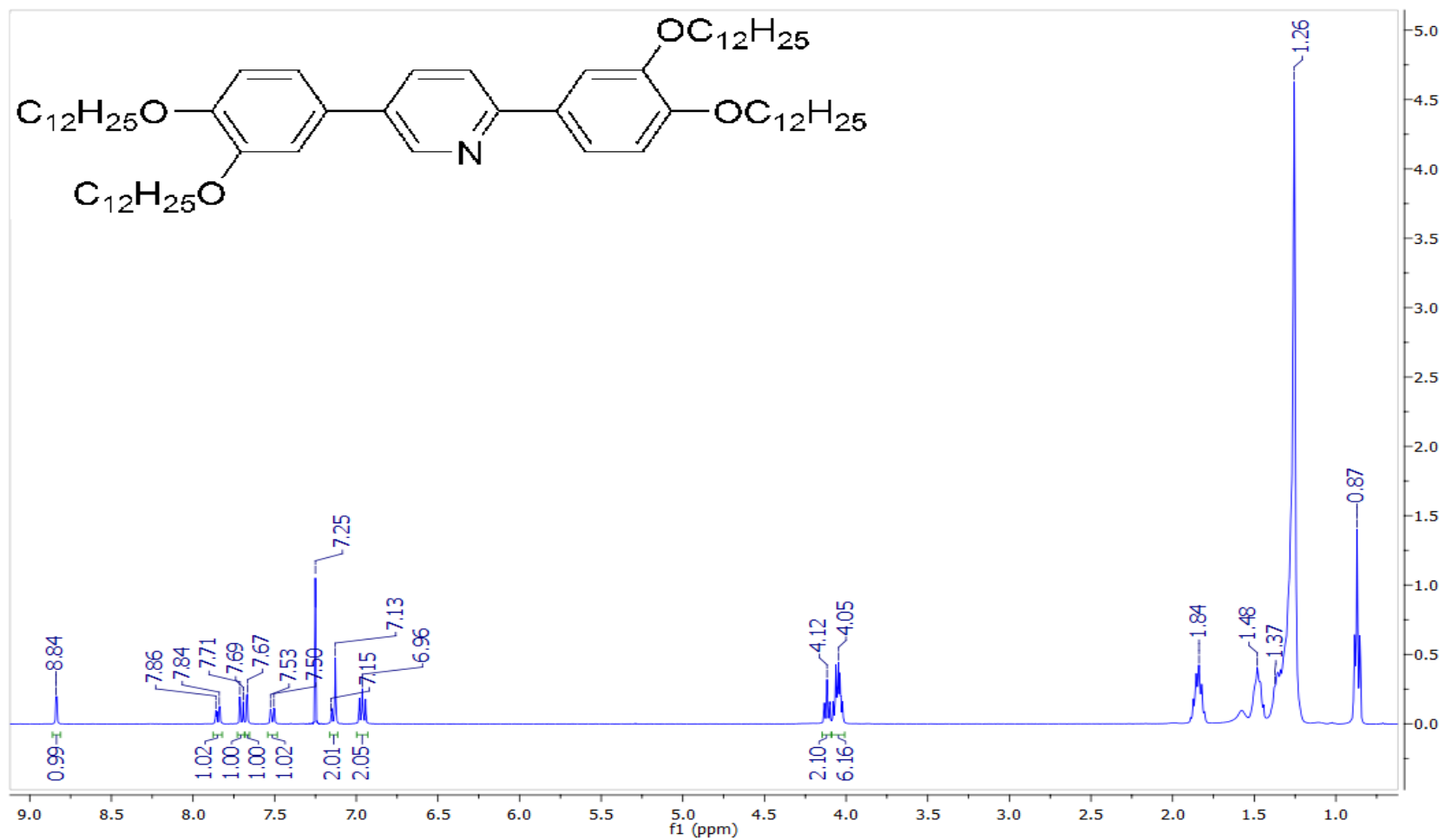


Appendix 8: The $^{195}\text{Pt}\{^1\text{H}\}$ NMR spectra (107 MHz) of photoreaction mixture of $(\text{PBU}_4)_2[\text{PtCl}_6]$ recorded in d_6 -acetone.

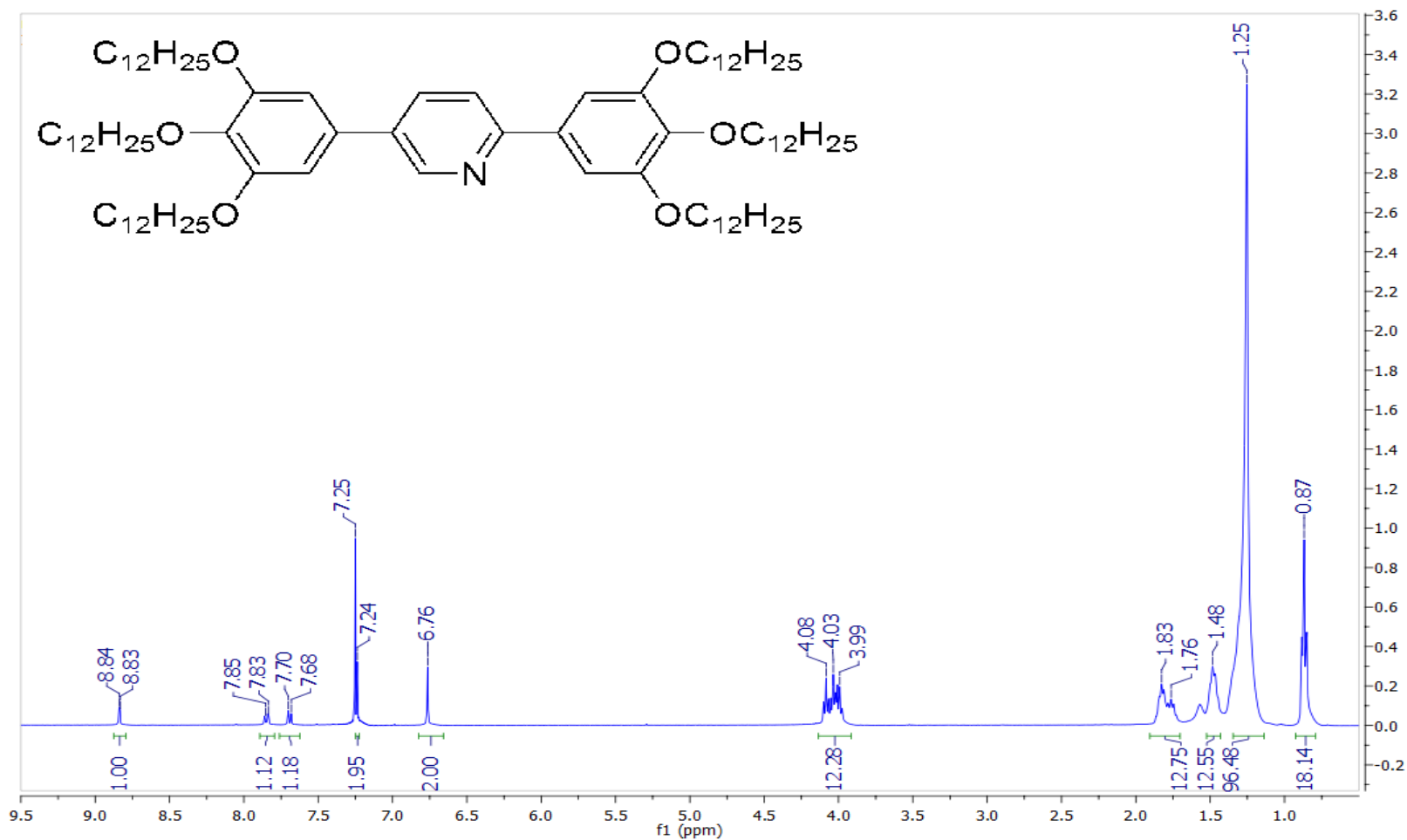




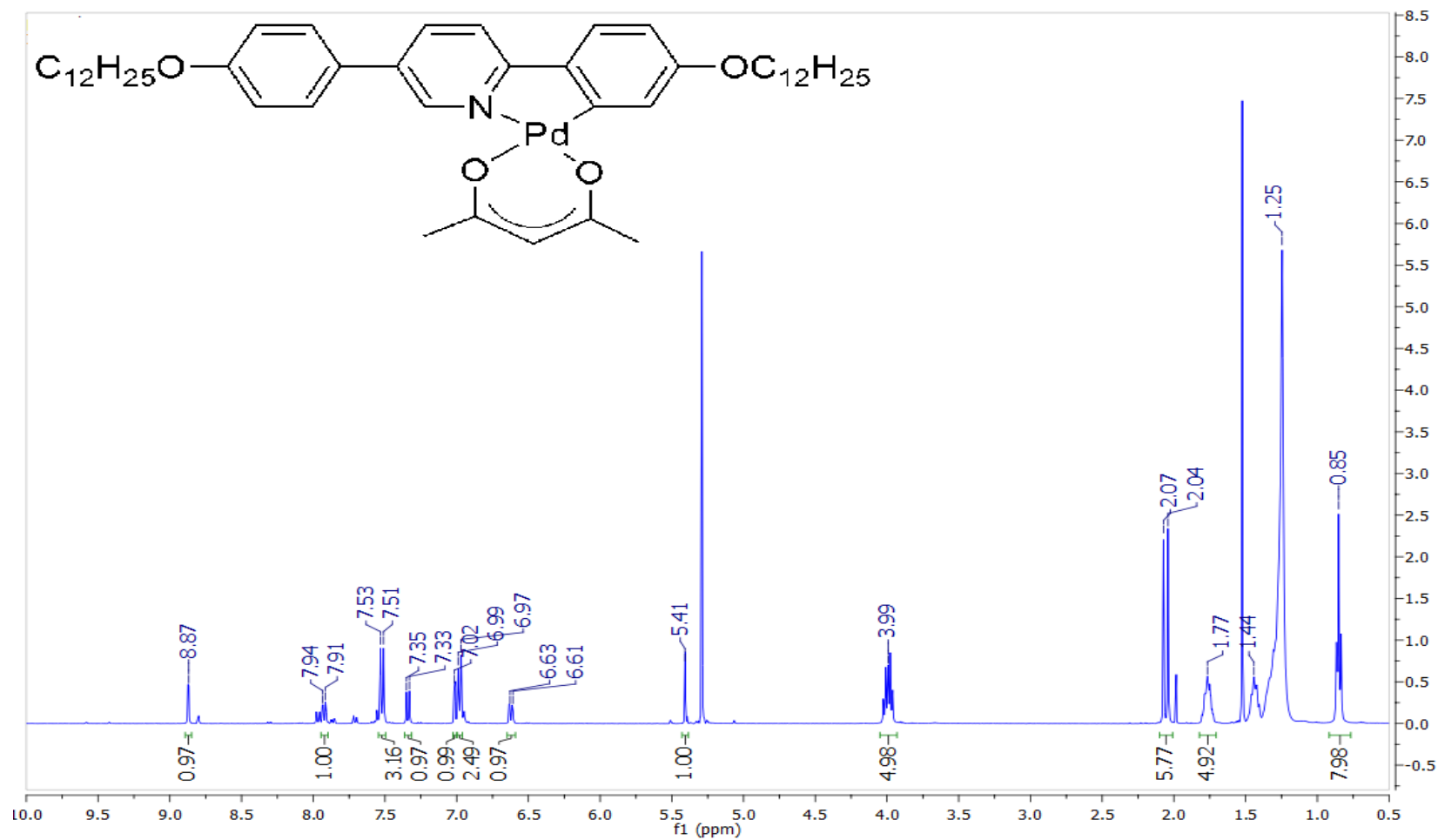
Appendix 9: ¹H NMR spectrum (400 MHz) of 2-(4-dodecyloxyphenyl)-5-(3,4-didodecyloxyphenyl)pyridine, V (2), in CDCl₃.



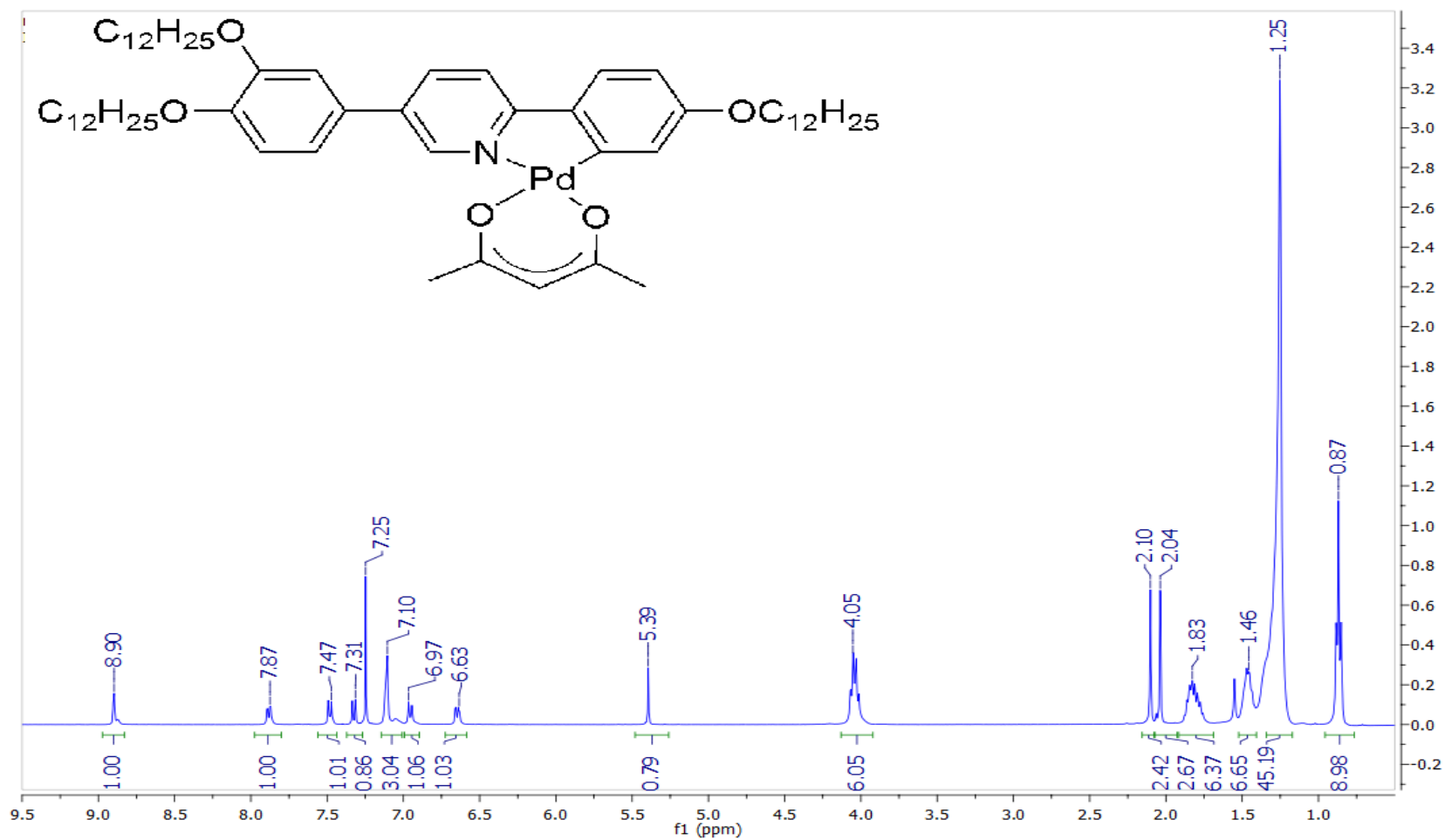
Appendix 10: ¹H NMR spectrum (400 MHz) of 2,5-Bis(3,4-bis(dodecyloxyphenyl)pyridine, **V** (3), in CDCl₃.



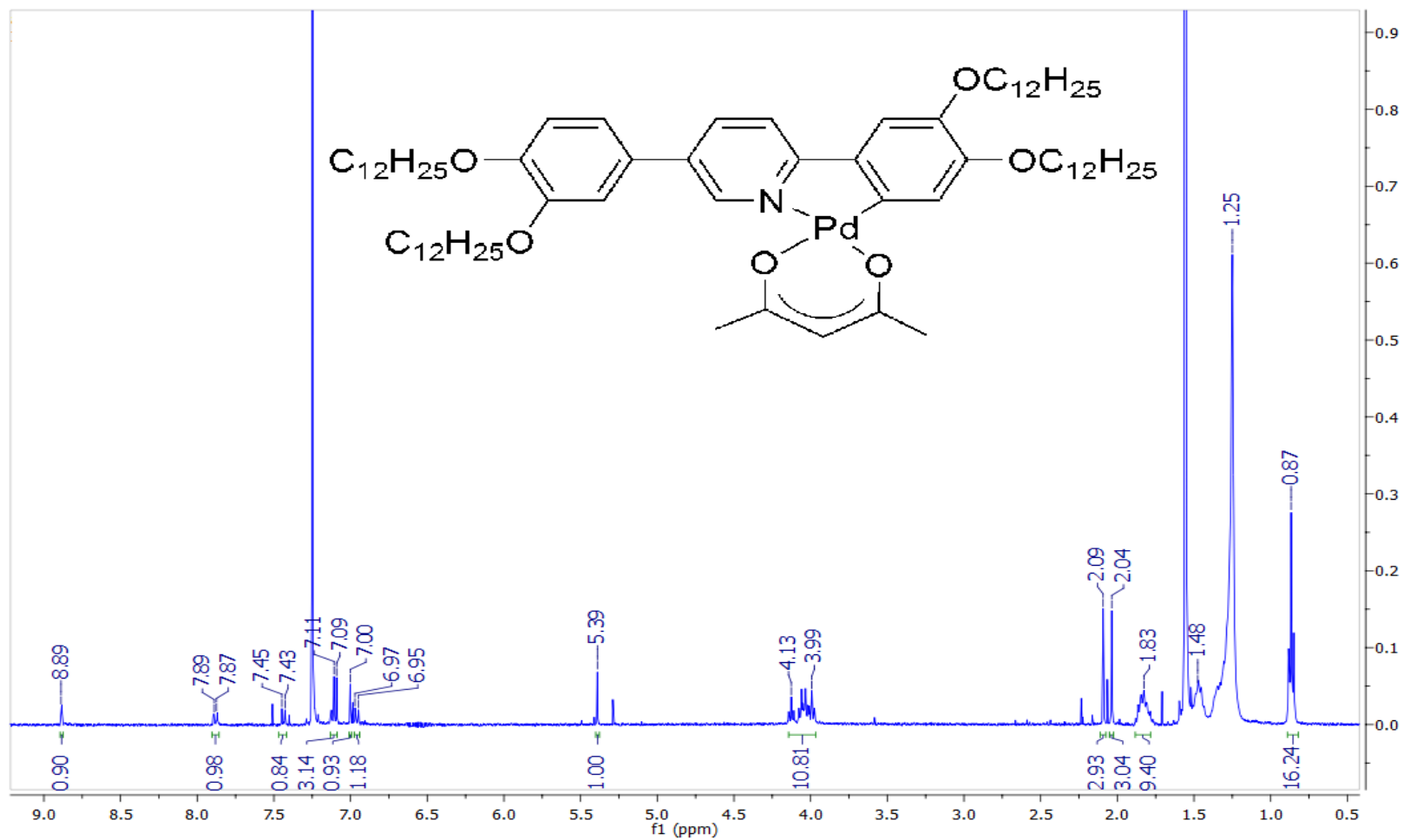
Appendix 11: ¹H NMR spectrum (400 MHz) of 2,5-Bis(3,4,5-tris(dodecyloxyphenyl)pyridine, **V** (4), in CDCl₃.



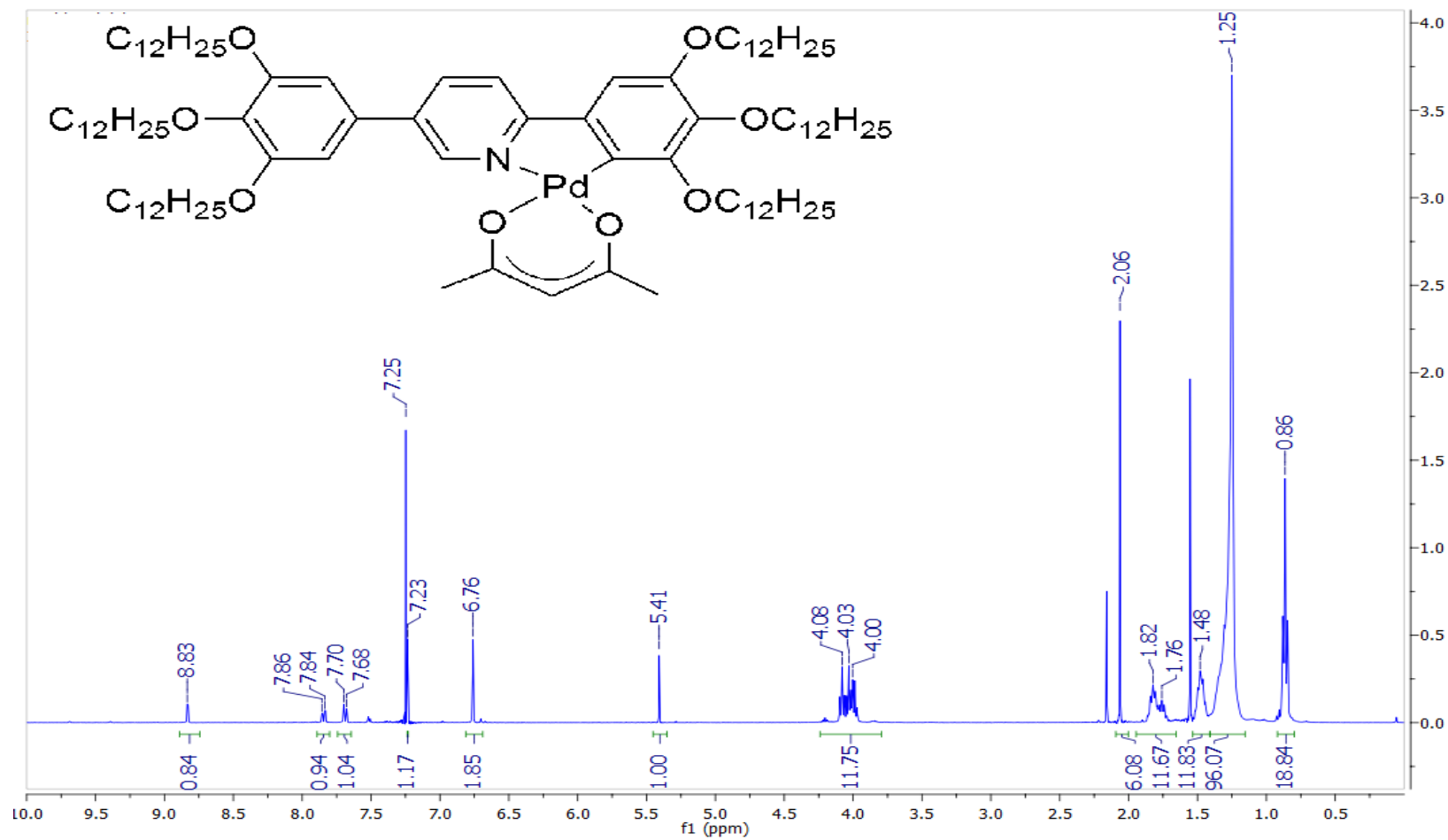
Appendix 12: ¹H NMR spectrum (400 MHz) of complex XIV (1) in CD₂Cl₂.



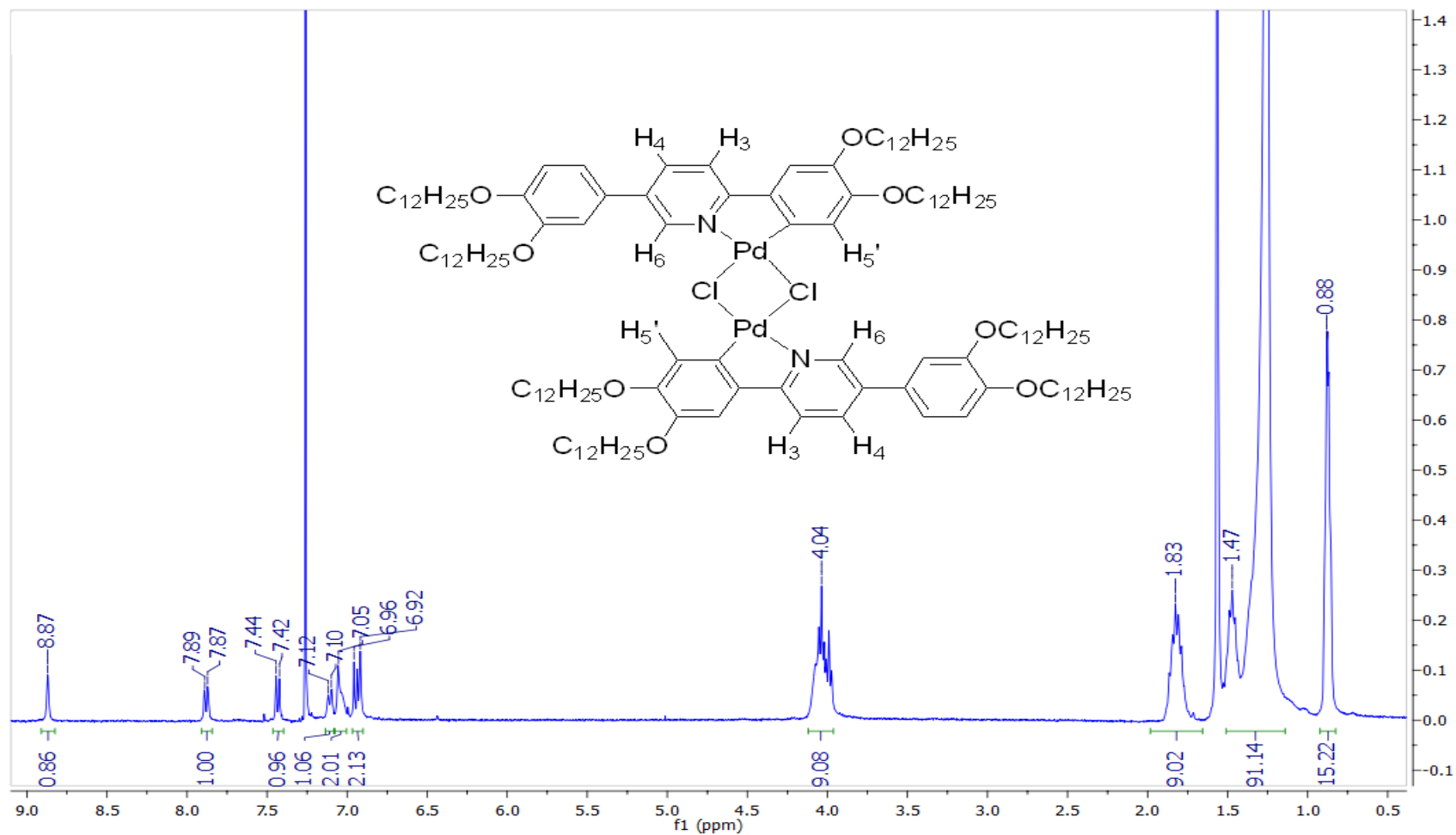
Appendix 13: ¹H NMR spectrum (400 MHz) of complex XIV (2) in CDCl₃.



Appendix 14: ¹H NMR spectrum (400 MHz) of complex XIV (3) in CDCl₃.



Appendix 15: ¹H NMR spectrum (400 MHz) of complex XIV (4) in CDCl₃.



Appendix 16: ^1H NMR spectrum (400 MHz) of the chloro-bridged dimer palladium complex, (XIII (3)) in CDCl_3 .

Abbreviations

acac	acetylacetonate
Ar	aryl
atm	atmosphere
ATR	attenuated total reflectance
BQ	benzoquinone
Bu	butyl
bpym	2,2'-bipyrimidine
CHN	elemental analysis for carbon, hydrogen and nitrogen, %
cif	crystallographic information framework
cnst2	constant two, coupling constant used in two dimensional correlation nuclear magnetic resonance spectroscopy
cod	cyclooctadiene
COSY	correlation spectroscopy
d	doublet
DCM	dichloromethane
dd	doublet of doublets
DFT	density functional theory
DMF	dimethylformamide
DMSO	dimethyl sulfoxide
dppe	1,2-bis(diphenylphosphino)ethane
dpy	diphenylpyridine
ECP	electron core potential
EI	electron ionisation, also known as electron impact ionisation
EPR	electron paramagnetic resonance
ESI-MS	electrospray ionisation-mass spectrometry
FG	functional group
FID	flame ionisation detector
FT-IR	fourier transform infrared spectroscopy
GC	gas chromatography
GC-MS	gas chromatography-mass spectrometry
HMQC	heteronuclear multiple quantum coherence
HOMO	highest occupied molecular orbital
HSAB	hard soft acid base
IR	infra-red
L	ligand
LIFDI-MS	liquid injection field desorption/ionisation-mass spectrometry

LMCT	ligand-to-metal charge transfer
LUMO	lowest unoccupied molecular orbital
m/z	mass-to-charge ratio
MCM-41	Mobil composition of matter no. 41: mesoporous material containing a hierarchical structure from a family of silicate and aluminosilicate solids, first developed by researchers at Mobil Oil corporation
MLCT	metal-to-ligand charge transfer
NHC	<i>N</i> -heterocyclic carbene
NMR	nuclear magnetic resonance
NMP	<i>N</i> -methylpyrrolidinone
NOE	nuclear Overhauser effect
OAc	acetate
OTf	trifluoromethanesulfonate, also known as triflate
Ph	phenyl
ppy	2-phenylpyridine
py	pyridine
RT	room temperature
SAXS	small-angle X-ray scattering
t	triplet
TCD	thermal conductivity detector
TDDFT	time-dependent density functional theory
TFA	trifluoroacetic acid
THF	tetrahydrofuran
TMEDA	tetramethylethylenediamine
Ts	tosyl
TsOH	<i>p</i> -toluenesulfonic acid
UV	ultraviolet
UV-Vis	ultraviolet and visible
XRD	X-ray diffraction

References

1. A. E. Shilov and G. B. Shul'pin, *Chem. Rev.*, 1997, **97**, 2879-2932.
2. J. A. Labinger and J. E. Bercaw, *Nature*, 2002, **417**, 507-514.
3. R. A. Periana, *J. Mol. Catal. A: Chem.*, 2004, **220**, 7-25.
4. B. G. Hashiguchi, S. M. Bischof, M. M. Konnick and R. A. Periana, *Acc. Chem. Res.*, 2012, **45**, 885-898.
5. F. Kakiuchi, T. Kochi and S. Murai, *Synlett*, 2014, **25**, 2390-2414.
6. N. G. Jonathan Clayden, and Stuart Warren, *Organic Chemistry*, Oxford University Press, Oxford, Second edn., 2012.
7. M. Lersch and M. Tilset, *Chem. Rev.*, 2005, **105**, 2471-2526.
8. R. H. Crabtree, *J. Organomet. Chem.*, 2015, **793**, 41-46.
9. J. Chatt and J. M. Davidson, *J. Chem. Soc.*, 1965, 843-855.
10. L. Vaska and J. W. DiLuzio, *J. Am. Chem. Soc.*, 1962, **84**, 679-680.
11. J. F. Young, J. A. Osborn, F. H. Jardine and G. Wilkinson, *Chem. Commun.*, 1965, 131-132.
12. A. E. Shilov and A. A. Shteinman, *Coord. Chem. Rev.*, 1977, **24**, 97-143.
13. R. G. Bergman, *Science*, 1984, **223**, 902-908.
14. R. H. Crabtree, *Chem. Rev.*, 1985, **85**, 245-269.
15. A. S. Goldman and K. I. Goldberg, in *Activation and Functionalization of C-H Bonds*, American Chemical Society, 2004, vol. 885, ch. 1, pp. 1-43.
16. R. G. Bergman, *Nature*, 2007, **446**, 391-393.
17. J. K. Hoyano and W. A. G. Graham, *J. Am. Chem. Soc.*, 1982, **104**, 3723-3725.
18. P. L. Watson, *J. Chem. Soc., Chem. Commun.*, 1983, 276-277.
19. S. Murai, F. Kakiuchi, S. Sekine, Y. Tanaka, A. Kamatani, M. Sonoda and N. Chatani, *Nature*, 1993, **366**, 529-531.
20. T. Matsubara, N. Koga, D. G. Musaev and K. Morokuma, *J. Am. Chem. Soc.*, 1998, **120**, 12692-12693.
21. T. Matsubara, N. Koga, D. G. Musaev and K. Morokuma, *Organometallics*, 2000, **19**, 2318-2329.
22. A. E. Shilov and A. A. Shteinman, *Coord. Chem. Rev.*, 1977, **24**, 97-143.
23. A. E. Shilov and G. B. Shul'pin, *Russ. Chem. Rev.*, 1987, **56**, 20.
24. R. A. Periana, D. J. Taube, S. Gamble, H. Taube, T. Satoh and H. Fujii, *Science*, 1998, **280**, 560-564.
25. J. A. Labinger and J. E. Bercaw, in *Higher Oxidation State Organopalladium and Platinum Chemistry*, ed. A. J. Canty, 2011, vol. 35, pp. 29-59.
26. K. I. Goldberg and A. S. Goldman, *Activation and Functionalization of C-H Bonds*, American Chemical Society, 2004.
27. G. A. Luinstra, L. Wang, S. S. Stahl, J. A. Labinger and J. E. Bercaw, *J. Organomet. Chem.*, 1995, **504**, 75-91.

28. B. G. Hashiguchi, M. M. Konnick, S. M. Bischof, S. J. Gustafson, D. Devarajan, N. Gunsalus, D. H. Ess and R. A. Periana, *Science*, 2014, **343**, 1232-1237.
29. D. García-Cuadrado, A. A. C. Braga, F. Maseras and A. M. Echavarren, *J. Am. Chem. Soc.*, 2006, **128**, 1066-1067.
30. D. García-Cuadrado, P. de Mendoza, A. A. C. Braga, F. Maseras and A. M. Echavarren, *J. Am. Chem. Soc.*, 2007, **129**, 6880-6886.
31. S. I. Gorelsky, D. Lapointe and K. Fagnou, *J. Am. Chem. Soc.*, 2008, **130**, 10848-10849.
32. D. Lapointe and K. Fagnou, *Chem. Lett.*, 2010, **39**, 1119-1126.
33. I. A. Sanhueza, A. M. Wagner, M. S. Sanford and F. Schoenebeck, *Chem. Sci.*, 2013, **4**, 2767-2775.
34. P. B. Arockiam, C. Bruneau and P. H. Dixneuf, *Chem. Rev.*, 2012, **112**, 5879-5918.
35. D. A. Colby, R. G. Bergman and J. A. Ellman, *Chem. Rev.*, 2010, **110**, 624-655.
36. V. Ritleng, C. Sirlin and M. Pfeffer, *Chem. Rev.*, 2002, **102**, 1731-1770.
37. F. Kakiuchi and S. Murai, in *Activation of Unreactive Bonds and Organic Synthesis*, eds. S. Murai, H. Alper, R. A. Gossage, V. V. Grushin, M. Hidai, Y. Ito, W. D. Jones, F. Kakiuchi, G. Koten, Y. S. Lin, Y. Mizobe, S. Murai, M. Murakami, T. G. Richmond, A. Sen, M. Suginome and A. Yamamoto, Springer Berlin Heidelberg, Berlin, Heidelberg, 1999, pp. 47-79.
38. G. Dyker, *Angew. Chem., Int. Ed.*, 1999, **38**, 1698-1712.
39. Y.-G. Lim, Y. H. Kim and J.-B. Kang, *J. Chem. Soc., Chem. Commun.*, 1994, 2267-2268.
40. Y.-G. Lim, J.-B. Kang and Y. H. Kim, *J. Chem. Soc., Perkin Trans. 1*, 1996, 2201-2206.
41. C.-H. Jun, J.-B. Hong, Y.-H. Kim and K.-Y. Chung, *Angew. Chem., Int. Ed.*, 2000, **39**, 3440-3442.
42. N. Fujii, F. Kakiuchi, N. Chatani and S. Murai, *Chem. Lett.*, 1996, **25**, 939-940.
43. T. Sakakura, T. Sodeyama and M. Tanaka, *Chem. Lett.*, 1988, **17**, 683-684.
44. S. Oi, S. Fukita, N. Hirata, N. Watanuki, S. Miyano and Y. Inoue, *Org. Lett.*, 2001, **3**, 2579-2581.
45. S. Oi, Y. Ogino, S. Fukita and Y. Inoue, *Org. Lett.*, 2002, **4**, 1783-1785.
46. S. Oi, R. Funayama, T. Hattori and Y. Inoue, *Tetrahedron*, 2008, **64**, 6051-6059.
47. S. Oi, H. Sasamoto, R. Funayama and Y. Inoue, *Chem. Lett.*, 2008, **37**, 994-995.
48. J. H. Teles, S. Brode and M. Chabanas, *Angew. Chem., Int. Ed.*, 1998, **37**, 1415-1418.
49. Y. Fukuda and K. Utimoto, *J. Org. Chem.*, 1991, **56**, 3729-3731.
50. J. Guenther, S. Mallet-Ladeira, L. Estevez, K. Miqueu, A. Amgoune and D. Bourissou, *J. Am. Chem. Soc.*, 2014, **136**, 1778-1781.

51. P. Gualco, S. Ladeira, K. Miqueu, A. Amgoune and D. Bourissou, *Angew. Chem., Int. Ed.*, 2011, **50**, 8320-8324.
52. P. Gualco, S. Ladeira, K. Miqueu, A. Amgoune and D. Bourissou, *Angew. Chem.*, 2011, **123**, 8470-8474.
53. J. H. Teles, *Angew. Chem., Int. Ed.*, 2015, **54**, 5556-5558.
54. C.-Y. Wu, T. Horibe, C. B. Jacobsen and F. D. Toste, *Nature*, 2015, **517**, 449-454.
55. D. M. Roe, P. M. Bailey, K. Moseley and P. M. Maitlis, *J. Chem. Soc., Chem. Commun.*, 1972, 1273-1274.
56. J. R. Chipperfield, in *Chemistry of the Platinum Group Metals*, ed. F. R. Hartley, Elsevier, Amsterdam, 1991, vol. 11, pp. 147-179.
57. I. Moritanl and Y. Fujiwara, *Tetrahedron Lett.*, 1967, **8**, 1119-1122.
58. T. Satoh, T. Tsuda, Y. Kushino, M. Miura and M. Nomura, *J. Org. Chem.*, 1996, **61**, 6476-6477.
59. T. Satoh, Y. Kawamura, M. Miura and M. Nomura, *Angew. Chem., Int. Ed. Engl.*, 1997, **36**, 1740-1742.
60. M. Miura, T. Tsuda, T. Satoh, S. Pivsa-Art and M. Nomura, *J. Org. Chem.*, 1998, **63**, 5211-5215.
61. X. Chen, K. M. Engle, D.-H. Wang and J.-Q. Yu, *Angew. Chem., Int. Ed.*, 2009, **48**, 5094-5115.
62. T. W. Lyons and M. S. Sanford, *Chem. Rev.*, 2010, **110**, 1147-1169.
63. J. L. Garnett and R. J. Hodges, *J. Am. Chem. Soc.*, 1967, **89**, 4546-4547.
64. R. H. Crabtree, *J. Organomet. Chem.*, 2004, **689**, 4083-4091.
65. M. M. Konnick, S. M. Bischof, M. Yousufuddin, B. G. Hashiguchi, D. H. Ess and R. A. Periana, *J. Am. Chem. Soc.*, 2014, **136**, 10085-10094.
66. R. G. P. Fred Basolo, *Mechanism of Inorganic Reactions: Study of Metal Complexes in Solution*, John Wiley & Sons Inc, 2nd edn., 1967.
67. R. L. Rich and H. Taube, *J. Am. Chem. Soc.*, 1954, **76**, 2608-2611.
68. R. E. Cameron and A. B. Bocarsly, *J. Am. Chem. Soc.*, 1985, **107**, 6116-6117.
69. R. E. Cameron and A. B. Bocarsly, *Inorg. Chem.*, 1986, **25**, 2910-2913.
70. P. E. Hoggard, *Coord. Chem. Rev.*, 1997, **159**, 235-243.
71. O. Monreal, T. Esmaeili and P. E. Hoggard, *Inorg. Chim. Acta*, 1997, **265**, 279-282.
72. P. E. Hoggard and A. Vogler, *Inorg. Chim. Acta*, 2003, **348**, 229-232.
73. P. E. Hoggard, A. J. Bridgeman, H. Kunkely and A. Vogler, *Inorg. Chim. Acta*, 2004, **357**, 639-643.
74. M. Chanon, *Acc. Chem. Res.*, 1987, **20**, 214-221.
75. G. B. Shulpin, G. V. Nizova and A. E. Shilov, *J. Chem. Soc., Chem. Commun.*, 1983, 671-672.
76. M. V. Serdobov, G. V. Nizova and G. B. Shulpin, *J. Organomet. Chem.*, 1984, **265**, C12-C14.
77. A. N. Kitaigorodskii, V. M. Nekipelov, A. T. Nikitaev and G. B. Shulpin, *J. Organomet. Chem.*, 1984, **275**, 295-301.

78. G. V. Nizova, M. V. Serdobov, A. T. Nikitaev and G. B. Shulpin, *J. Organomet. Chem.*, 1984, **275**, 139-144.
79. G. B. Shulpin, G. V. Nizova, A. N. Kitaigorodskii and M. V. Serdobov, *J. Organomet. Chem.*, 1984, **275**, 273-282.
80. R. P. Shibaeva, L. P. Rozenberg, R. M. Lobkovskaya, A. E. Shilov and G. B. Shulpin, *J. Organomet. Chem.*, 1981, **220**, 271-276.
81. G. B. Shulpin and G. V. Nizova, *J. Organomet. Chem.*, 1984, **276**, 109-114.
82. G. B. Shul'pin, *Dalton Trans.*, 2013, **42**, 12794-12818.
83. K. M. Harmon, I. Gennick, S. L. Madeira and D. L. Duffy, *J. Org. Chem.*, 1974, **39**, 2809-2810.
84. R. K. Sharma and J. L. Fry, *J. Org. Chem.*, 1983, **48**, 2112-2114.
85. M. Soulard, S. Bilger, H. Kessler and J. L. Guth, *Zeolites*, 1991, **11**, 107-115.
86. S. Bilger, M. Soulard, H. Kessler and J. L. Guth, *Zeolites*, 1991, **11**, 784-791.
87. M. Soulard, S. Bilger, H. Kessler and J. L. Guth, *Thermochim. Acta*, 1992, **204**, 167-178.
88. J. A. Davies and C. T. Eagle, *Organometallics*, 1986, **5**, 2149-2151.
89. A. Wrzyszczyński, M. Pietrzak, J. Bartoszewicz, H. Kozubek, G. L. Hug, B. Marciniak and J. Pączkowski, *J. Am. Chem. Soc.*, 2003, **125**, 11182-11183.
90. S. Erhardt, V. V. Grushin, A. H. Kilpatrick, S. A. Macgregor, W. J. Marshall and D. C. Roe, *J. Am. Chem. Soc.*, 2008, **130**, 4828-4845.
91. J. Chatt and R. G. Wilkins, *J. Chem. Soc.*, 1952, 2622-2626.
92. J. S. Anderson, *J. Chem. Soc.*, 1934, 971-974.
93. J. S. Anderson, *J. Chem. Soc.*, 1936, 1042-1049.
94. P. E. Slade and H. B. Jonassen, *J. Am. Chem. Soc.*, 1957, **79**, 1277-1279.
95. J. Chatt, N. P. Johnson and B. L. Shaw, *J. Chem. Soc.*, 1964, 1662-1666.
96. M. J. Grogan and K. Nakamoto, *J. Am. Chem. Soc.*, 1966, **88**, 5454-&
97. M. J. Grogan and K. Nakamoto, *Inorg. Chim. Acta*, 1967, **1**, 228.
98. V.C.Adam, J. A. J. Jarvis, B. T. Kilbourn and P. G. Owston, *Chem. Commun.*, 1971, 467.
99. J. R. Briggs, C. Crocker, W. S. McDonald and B. L. Shaw, *J. Chem. Soc., Dalton Trans.*, 1982, 457-463.
100. C. M. A. Parlett, D. W. Bruce, N. S. Hondow, A. F. Lee and K. Wilson, *ACS Catalysis*, 2011, **1**, 636-640.
101. C. M. A. Parlett, D. W. Bruce, N. S. Hondow, M. A. Newton, A. F. Lee and K. Wilson, *ChemCatChem*, 2013, **5**, 939-950.
102. N. C. King, R. A. Blackley, M. L. Wears, D. M. Newman, W. Zhou and D. W. Bruce, *Chem. Commun.*, 2006, 3414-3416.
103. N. K. Sethi, A. C. Whitwood and D. W. Bruce, *Eur. J. Inorg. Chem.*, 2013, 2078-2082.
104. N. K. Sethi, PhD Thesis, University of York, 2013.
105. M. R. Plutino, S. Otto, A. Roodt and L. I. Elding, *Inorg. Chem.*, 1999, **38**, 1233-1238.

106. A. Koenig, M. Bette, C. Bruhn and D. Steinborn, *Eur. J. Inorg. Chem.*, 2012, 5881-5895.
107. F. Mohr, ed., *Gold Chemistry: Applications and Future Directions in the Life Sciences*, WILEY-VCH, Weinheim, 2009.
108. D. T. Richens, *Chem. Rev.*, 2005, **105**, 1961-2002.
109. W. J. Gerber, P. Murray and K. R. Koch, *Dalton Trans.*, 2008, 4113-4117.
110. A. L. Segre, L. Zetta and A. Di Corato, *J. Mol. Spectrosc.*, 1969, **32**, 296-308.
111. B. C. Terence N. Mitchell, *NMR - From Spectra to Structure An Experimental Approach*, Springer, New York, 2nd edn., 2007.
112. P. S. Pregosin, *Coord. Chem. Rev.*, 1982, **44**, 247-291.
113. B. E. M. J.W. Akitt, *NMR and Chemistry: An introduction to modern NMR spectroscopy*, Chapman & Hall, United Kingdom, Fourth edn., 2000.
114. P. S. Pregosin and L. M. Venanzi, *Helv. Chim. Acta*, 1975, **58**, 1548-1551.
115. P. L. Goggin, R. J. Goodfellow, S. R. Haddock, B. F. Taylor and I. R. H. Marshall, *J. Chem. Soc., Dalton Trans.*, 1976, 459-467.
116. G. W. T. M. J. Frisch, H. B. Schlegel, G. E. Scuseria, , J. R. C. M. A. Robb, G. Scalmani, V. Barone, B. Mennucci, , H. N. G. A. Petersson, M. Caricato, X. Li, H. P. Hratchian, , J. B. A. F. Izmaylov, G. Zheng, J. L. Sonnenberg, M. Hada, , K. T. M. Ehara, R. Fukuda, J. Hasegawa, M. Ishida, T. Nakajima, , O. K. Y. Honda, H. Nakai, T. Vreven, J. A. Montgomery, Jr., , F. O. J. E. Peralta, M. Bearpark, J. J. Heyd, E. Brothers, , V. N. S. K. N. Kudin, T. Keith, R. Kobayashi, J. Normand, , A. R. K. Raghavachari, J. C. Burant, S. S. Iyengar, J. Tomasi, , N. R. M. Cossi, J. M. Millam, M. Klene, J. E. Knox, J. B. Cross, , C. A. V. Bakken, J. Jaramillo, R. Gomperts, R. E. Stratmann, , A. J. A. O. Yazyev, R. Cammi, C. Pomelli, J. W. Ochterski, , K. M. R. L. Martin, V. G. Zakrzewski, G. A. Voth, , J. J. D. P. Salvador, S. Dapprich, A. D. Daniels, , J. B. F. O. Farkas, J. V. Ortiz, J. Cioslowski, and G. and D. J. Fox, *Gaussian 09, Revision D.01*, Gaussian, Inc., Wallingford CT, 2013.
117. F. Weigend and R. Ahlrichs, *Phys. Chem. Chem. Phys.*, 2005, **7**, 3297-3305.
118. F. Weigend, *Phys. Chem. Chem. Phys.*, 2006, **8**, 1057-1065.
119. D. Andrae, U. Häußermann, M. Dolg, H. Stoll and H. Preuß, *Theor. Chim. Acta*, 1990, **77**, 123-141.
120. U. Belluco, B. Crociani, R. Pietropaolo and P. Uguagliati, *Inorg. Chim. Acta Rev.*, 1969, **3**, 19-54.
121. O. Monreal and P. E. Hoggard, *Abstr. Pap. Am. Chem. Soc.*, 1997, **213**, 454.
122. A. Schäfer, H. Horn and R. Ahlrichs, *J. Chem. Phys.*, 1992, **97**, 2571-2577.
123. S. Sinnecker, A. Rajendran, A. Klamt, M. Diedenhofen and F. Neese, *J. Phys. Chem. A*, 2006, **110**, 2235-2245.
124. S. H. Kaufman, J. M. Weber and M. Pernpointner, *J. Chem. Phys.*, 2013, **139**.
125. G. W. Eastland, D. N. R. Rao and M. C. R. Symons, *J. Chem. Soc., Perkin Trans. 2*, 1984, 1551-1557.
126. T. Krigas and M. T. Rogers, *J. Chem. Phys.*, 1971, **55**, 3035-&.
127. W. Levason and D. Pletcher, *Platinum Metals Rev.*, 1993, **37**, 17-23.
128. R. A. Ogg, *J. Chem. Phys.*, 1954, **22**, 560.
129. R. A. O. Jr., J. D. Ray and M. Y., *J. Chem. Phys.*, 1957, **26**, 1339-1340.

130. E. Matthews, A. Sen, N. Yoshikawa, E. Bergstrom and C. E. H. Dessent, *Phys. Chem. Chem. Phys.*, 2016, **18**, 15143-15152.
131. A. E. Shilov and G. B. Shul'pin, *Chem. Rev.*, 1997, **97**, 2879-2932.
132. B. E. Mann, B. L. Shaw and G. Shaw, *J. Chem. Soc. A*, 1971, 3536.
133. G. Bandoli, A. Dolmella, F. P. Fanizzi, N. G. Di Masi, L. Maresca and G. Natile, *Organometallics*, 2001, **20**, 805-807.
134. R. B. Cundall and T. F. Palmer, *Trans. Faraday Soc.*, 1960, **56**, 1211-1224.
135. J. P. Chesick, *J. Chem. Phys.*, 1966, **45**.
136. D. M. Adams and D. J. Hills, *J. Mol. Struct.*, 1991, **247**, 335-342.
137. R. K. Blundell and P. Licence, *Phys. Chem. Chem. Phys.*, 2014, **16**, 15278-15288.
138. B. Donnio and D. W. Bruce, in *Liquid Crystals II*, ed. D. M. P. Mingos, Springer Berlin Heidelberg, Berlin, Heidelberg, 1999, pp. 193-247.
139. J. Torroba and D. W. Bruce, in *Compr. Inorg. Chem. II*, ed. J. R. Poeppelemeier, Elsevier, Amsterdam, 2013, pp. 837-917.
140. P. J. C. a. M. Hird, *Introduction to Liquid Crystals Chemistry and Physics*, Taylor and Francis, London and New York, 1997.
141. K. Binnemans, *J. Mater. Chem.*, 2009, **19**, 448-453.
142. Y. Wang, J. Shi, J. Chen, W. Zhu and E. Baranoff, *J. Mater. Chem. C*, 2015, **3**, 7993-8005.
143. S. A. Hudson and P. M. Maitlis, *Chem. Rev.*, 1993, **93**, 861-885.
144. S. Chandrasekhar, B. K. Sadashiva and K. A. Suresh, *Pramana*, 1977, **9**, 471-480.
145. I. W. Tobias Wohrle, Jochen Kirres, Antonia Kostidou, Nadia Kapernaum, Juri Litterscheidt, Johannes Christian Haenle, Peter Staffeld, Angelika Baro, Frank Giesselmann and Sabine Laschat, *Chem. Rev.*, 2016, **116**, 103.
146. D. Fazio, C. Mongin, B. Donnio, Y. Galerne, D. Guillon and D. W. Bruce, *J. Mater. Chem.*, 2001, **11**, 2852-2863.
147. B. Donnio, B. Heinrich, H. Allouchi, J. Kain, S. Diele, D. Guillon and D. W. Bruce, *J. Am. Chem. Soc.*, 2004, **126**, 15258-15268.
148. H.-T. Nguyen, C. Destrade and J. Malthécte, *Adv. Mater. (Weinheim, Ger.)*, 1997, **9**, 375-388.
149. V. N. Kozhevnikov, B. Donnio and D. W. Bruce, *Angew. Chem., Int. Ed.*, 2008, **47**, 6286-6289.
150. A. Santoro, A. C. Whitwood, J. A. G. Williams, V. N. Kozhevnikov and D. W. Bruce, *Chem. Mater.*, 2009, **21**, 3871-3882.
151. D. N. Kozhevnikov, V. N. Kozhevnikov, M. Z. Shafikov, A. M. Prokhorov, D. W. Bruce and J. A. G. Williams, *Inorg. Chem.*, 2011, **50**, 3804-3815.
152. A. Santoro, A. M. Prokhorov, V. N. Kozhevnikov, A. C. Whitwood, B. Donnio, J. A. G. Williams and D. W. Bruce, *J. Am. Chem. Soc.*, 2011, **133**, 5248-5251.
153. A. M. Prokhorov, A. Santoro, J. A. G. Williams and D. W. Bruce, *Angew. Chem., Int. Ed.*, 2012, **51**, 95-98.
154. D. Pucci and B. Donnio, in *Handbook of Liquid Crystals*, Wiley-VCH Verlag GmbH & Co. KGaA, 2014.

155. J. A. Gareth Williams, S. Develay, D. L. Rochester and L. Murphy, *Coord. Chem. Rev.*, 2008, **252**, 2596-2611.
156. T. Hegmann, J. Kain, S. Diele, B. Schubert, H. Bogel and C. Tschierske, *J. Mater. Chem.*, 2003, **13**, 991-1003.
157. M. Spencer, A. Santoro, G. R. Freeman, A. Diez, P. R. Murray, J. Torroba, A. C. Whitwood, L. J. Yellowlees, J. A. G. Williams and D. W. Bruce, *Dalton Trans.*, 2012, **41**, 14244-14256.
158. Y. Wang, Y. Liu, J. Luo, H. Qi, X. Li, M. Nin, M. Liu, D. Shi, W. Zhu and Y. Cao, *Dalton Trans.*, 2011, **40**, 5046-5051.
159. S. J. Farley, D. L. Rochester, A. L. Thompson, J. A. K. Howard and J. A. G. Williams, *Inorg. Chem.*, 2005, **44**, 9690-9703.
160. C.-T. Liao, H.-H. Chen, H.-F. Hsu, A. Poloek, H.-H. Yeh, Y. Chi, K.-W. Wang, C.-H. Lai, G.-H. Lee, C.-W. Shih and P.-T. Chou, *Chem. - Eur. J.*, 2011, **17**, 546-556.
161. C. Cuerva, J. A. Campo, M. Cano and C. Lodeiro, *Chem. - Eur. J.*, 2016, **22**, 10168-10178.
162. H.-Y. Ku, B. Tong, Y. Chi, H.-C. Kao, C.-C. Yeh, C.-H. Chang and G.-H. Lee, *Dalton Trans.*, 2015, **44**, 8552-8563.
163. F. Camerel, R. Ziessel, B. Donnio, C. Bourgogne, D. Guillon, M. Schmutz, C. Iacovita and J.-P. Bucher, *Angew. Chem., Int. Ed.*, 2007, **46**, 2659-2662.
164. M. L. Deda, M. Ghedini, I. Aiello, T. Pugliese, F. Barigelletti and G. Accorsi, *J. Organomet. Chem.*, 2005, **690**, 857-861.
165. M. Ghedini, D. Pucci, A. Crispini, A. Bellusci, M. L. Deda, I. Aiello and T. Pugliese, *Inorg. Chem. Commun.*, 2007, **10**, 243-246.
166. M. J. Mayoral, P. Ovejero, J. A. Campo, J. V. Heras, E. Oliveira, B. Pedras, C. Lodeiro and M. Cano, *J. Mater. Chem.*, 2011, **21**, 1255-1263.
167. A. S. Mocanu, M. Iliş, F. Dumitraşcu, M. Ilie and V. Cîrcu, *Inorg. Chim. Acta*, 2010, **363**, 729-736.
168. M. Micutz, M. Ilis, T. Staicu, F. Dumitrascu, I. Pasuk, Y. Molard, T. Roisnel and V. Cîrcu, *Dalton Trans.*, 2014, **43**, 1151-1161.
169. A. Prokorov, unpublished work.
170. A. R. Chianese, S. J. Lee and M. R. Gagné, *Angew. Chem., Int. Ed.*, 2007, **46**, 4042-4059.
171. T. Ishii, S. Tsuboi, G. Sakane, M. Yamashita and B. K. Breedlove, *Dalton Trans.*, 2009, 680-687.
172. V. N. Kozhevnikov, S. J. Cowling, P. B. Karadakov and D. W. Bruce, *J. Mater. Chem.*, 2008, **18**, 1703-1710.
173. S.-I. Sugita, S. Toda, T. Yoshiyasu, T. Teraji, A. Murayama and M. Ishikawa, *Molecular Crystals and Liquid Crystals Science and Technology. Section A. Molecular Crystals and Liquid Crystals*, 1993, **237**, 319-328.
174. J. D. a. M. Pfeffer, ed., *Palladacycles: Synthesis, Characterization and Applications*, Wiley-VCH, Germany, 2008.
175. I. P. Smoliakova, K. J. Keuseman, D. C. Haagenson, D. M. Wellmann, P. B. Colligan, N. A. Kataeva, A. V. Churakov, L. G. Kuz'mina and V. V. Dunina, *J. Organomet. Chem.*, 2000, **603**, 86-97.
176. R. L. Burwell, *Chem. Rev.*, 1954, **54**, 615-685.

